APPENDIX O

HYDRODYNAMIC AND SEDIMENT TRANSPORT ANALYSIS FOR THE ROCKAWAY DELIVERY LATERAL PROJECT

HYDRODYNAMIC AND SEDIMENT TRANSPORT ANALYSES FOR ROCKAWAY DELIVERY LATERAL PROJECT

Prepared for:

Ecology and Environment, Inc.
368 Pleasant View Drive
Lancaster, New York

Prepared by:

HDR|HydroQual
1200 MacArthur Boulevard
Mahwah, New Jersey

April 30, 2013

Table of Contents

1. INTRODUCTION

This report was developed as part of the Rockaway Delivery Lateral Project (Project). The Project involves offshore construction of a 26-inch diameter natural gas pipeline (Rockaway Delivery Lateral). Rockaway Delivery Lateral would extend approximately 3.20 miles from a proposed offshore interconnect with Transco's existing 26-inch diameter Lower New York Bay Lateral (LNYBL) in the Atlantic Ocean to an onshore delivery point for the National Grid pipeline system on the Rockaway Peninsula in Queens County, New York. Hydrodynamic and sediment transport simulations were developed to help assess potential impacts of project construction.

The ECOM (Estuarine, Coastal, and Ocean Model) framework was used to develop a hydrodynamic and sediment transport model to evaluate potential impacts of pipeline installation and burial in the seabed along the preferred route. When used with its integrated sediment transport module (SEDZLJ), ECOM is also known as ECOMSED. ECOM has a long history of development and application to the New York Bight area and has been used to support regulatory decision-making. Previous ECOM applications with hydrodynamic and sediment transport simulations in the area of the proposed pipeline route include the System-Wide Eutrophication Model (SWEM) (HQI, 1999a-f; HQI, 2002), Contaminant Assessment and Reduction Project (CARP) (HQI, 2007), Harbor Toxics and Nutrients Total Maximum Daily Load (TMDL) efforts and Lower Passaic River/Newark Bay (LPR/NB) Superfund efforts for the U.S. Environmental Protection Agency (USEPA).[1] Each of these models includes the New York (Mid-Atlantic) Bight area around Long Island as well as New York-New Jersey Harbor because of complex flow interactions that occur as freshwater from the Hudson River, Raritan River and other sources, mix and are influenced by ocean currents and tides.

Model parameters (e.g., bottom roughness, sediment grain size distributions, particle diameters, etc.) were assigned or calibrated based on field measurements and other site data. Model results were compared to site data to assess model reliability. Potential impacts of pipeline installation along the proposed route were evaluated by simulating sediment releases during construction and determining:

- sediment plume areal extent in the water column and duration over time;
- areal extent and depth of sediment deposition attributable to construction;
- anticipated rate of pipeline burial by periodic sediment transport processes.

[1] Harbor Toxics and Nutrient TMDL and LPR/NB efforts are ongoing projects and reports related to those efforts are not yet publically available.

Modeling efforts examine sediment releases from construction activities and alternatives that include:

(1) hydraulic jetting of sediments along the pipeline route (jet sled) for "worst case" conditions;
(2) hydraulic jetting of sediments along the pipeline route (jet sled) for "typical" conditions;
(3) mechanical plowing of sediments along the pipeline route (mechanical plow) for "worst case" conditions;
(4) mechanical plowing of sediments along the pipeline route (mechanical plow) for typical conditions;
(5) mechanical (clamshell) dredging of sediments along the pipeline route;
(6) hand jetting of sediments at the site where the existing main will be tapped to connect to submarine portion of the lateral;
(7) mechanical (clamshell) dredging at the site of a pit where the submarine portion of the pipeline will connect to pipeline sections that will be installed by horizontal directional drilling (HDD);

2. HYDRODYNAMIC AND SEDIMENT TRANSPORT MODEL THEORY

A three-dimensional (3-D) hydrodynamic model for the Rockway pipeline areas was constructed using the ECOM (Estuarine, Coastal, and Ocean Model) framework (HQI, 2010). ECOM is the hydrodynamic module of the framework and SEDZLJ (Jones and Lick, 2001; James et al. 2010) is its integrated sediment transport module. When used with its sediment transport module, ECOM is also known as ECOMSED. For simplicity, the acronym ECOM is used hereafter to describe the model and its hydrodynamic and sediment transport modules.

ECOM has been successfully applied to rivers, lakes, estuaries, coastal and ocean areas worldwide and its predictive capabilities have been assessed through extensive comparisons with data to demonstrate that the model represents the predominant physics of different water bodies in a realistic manner. These applications include: Delaware River, Delaware Bay, and adjacent continental shelf (Galperin and Mellor, 1990a,b,c), South Atlantic Bight (Blumberg and Mellor, 1983), Hudson-Raritan estuary (Oey et al., 1985a,b), Gulf of Mexico (Blumberg and Mellor, 1985), Chesapeake Bay (Blumberg and Goodrich 1990), Massachusetts Bay (Blumberg et al., 1993), St. Andrew Bay (Blumberg and Kim, 2000), New York Harbor and Bight (Blumberg et al., 1999), Onondaga Lake (Ahsan and Blumberg, 1999), Lake Michigan (Schwab et al., 1999), Lake Pontchartrain (Signell and List, 1997), Green Bay (HQI, 2001), and Lake Ontario (HQI, 2005 and 2008).

ECOM uses a conformal curvilinear coordinate system with variable grid resolution. Fine spatial (horizontal) resolution can be achieved by using a smaller model grid size in areas of special interest or concern. In the vertical direction, the model uses a transformed σ-coordinate system, which allows it to follow changes in bottom topography and surface elevation and to resolve associated vertical currents. The model solves coupled three-dimensional advection-diffusion equations for water mass, momentum, heat, and salinity and employs a two-equation turbulent-closure scheme (Blumberg and Mellor, 1987; Galerpin et al., 1988; Mellor and Yamada, 1982) to provide realistic representation of vertical mixing processes. ECOM can be used as a stand-alone hydrodynamic model or in conjunction with its integrated sediment transport model to simulate erosion, deposition, and transport of cohesive and non-cohesive sediments.

2.1. HYDRODYNAMICS

Currents and tides move water (fluid) and transport sediments in the water column and sediment bed. Water movement is also influenced by meteorological conditions and also temperature and salinity differences. As water flows, it is subject to frictional resistance (drag) along boundaries (surfaces) of all material it passes. The balance between gravity and drag forces along the flow path determines the velocity and depth of flow. The force

that flowing water exerts on the sediment bed is described in terms of the shear stress. The hydrodynamic module in ECOM is used to simulate water velocities, depths, and shear stresses. Velocities and shear stresses are used in sediment transport calculations to determine plume extents from pipeline installation.

The governing equations for hydrodynamics are:

Conservation of Mass (Continuity): Fluid

$$\frac{\partial U}{\partial x}+\frac{\partial V}{\partial y}+\frac{\partial W}{\partial z}=0 \tag{2-1}$$

Conservation of Momentum: Fluid

$$\frac{\partial U}{\partial t}+U\frac{\partial U}{\partial x}+V\frac{\partial U}{\partial y}+W\frac{\partial U}{\partial z}-fV=-\frac{1}{\rho_0}\frac{\partial P}{\partial x}+\frac{\partial}{\partial z}\left(K_M\frac{\partial U}{\partial z}\right)+F_x \tag{2-2}$$

$$\frac{\partial V}{\partial t}+V\frac{\partial V}{\partial x}+V\frac{\partial V}{\partial y}+W\frac{\partial V}{\partial z}-fU=-\frac{1}{\rho_0}\frac{\partial P}{\partial y}+\frac{\partial}{\partial z}\left(K_M\frac{\partial V}{\partial z}\right)+F_y \tag{2-3}$$

$$\rho g=-\frac{\partial P}{\partial z} \tag{2-4}$$

Conservation of Mass (Continuity): Temperature

$$\frac{\partial T}{\partial t}+U\frac{\partial T}{\partial x}+V\frac{\partial T}{\partial y}+W\frac{\partial T}{\partial z}=\frac{\partial}{\partial z}\left(K_H\frac{\partial T}{\partial z}\right)+F_T \tag{2-5}$$

Conservation of Mass (Continuity): Salinity

$$\frac{\partial S}{\partial t}+U\frac{\partial S}{\partial x}+V\frac{\partial S}{\partial y}+W\frac{\partial S}{\partial z}=\frac{\partial}{\partial z}\left(K_H\frac{\partial S}{\partial z}\right)+F_S \tag{2-6}$$

where:

U, V, W = mean (Reynolds-average) velocities in the x, y, and z directions, respectively [L T^{-1}]

T = temperature [θ] [2]

S = salinity [dimensionless] (e.g., parts per thousand)

ρ_0 = reference density of water [M L^{-3}]

ρ = local density of water [M L^{-3}]

g = gravitational acceleration [L T^{-2}]

f = Coriolis parameter [T^{-1}];

P = pressure [M L^{-1} T^{-2}]

K_M = vertical eddy viscosity for fluid [L^2 T^{-1}]

K_H = vertical eddy diffusivity for temperature and salinity [L^2 T^{-1}]

F_x, F_y = horizontal diffusion of momentum in the x- and y-directions, respectively [L^2 T^{-1}]

F_T, F_S = horizontal diffusion of temperature and salinity, respectively [θ T^{-1}, T^{-1}]

Horizontal diffusion terms represent small (sub-grid) scale processes not directly resolved by the model grid and are expressed in a form analogous to molecular diffusion:

$$F_x = \frac{\partial}{\partial x}\left(2A_M \frac{\partial U}{\partial x}\right) + \frac{\partial}{\partial y}\left[A_M\left(\frac{\partial U}{\partial y} + \frac{\partial V}{\partial x}\right)\right] \quad (2\text{-}7)$$

$$F_y = \frac{\partial}{\partial y}\left(2A_M \frac{\partial V}{\partial y}\right) + \frac{\partial}{\partial x}\left[A_M\left(\frac{\partial U}{\partial y} + \frac{\partial V}{\partial x}\right)\right] \quad (2\text{-}8)$$

$$F_T = \frac{\partial}{\partial x}\left(A_H \frac{\partial T}{\partial x}\right) + \frac{\partial}{\partial y}\left[A_H\left(\frac{\partial T}{\partial y}\right)\right] \quad (2\text{-}9)$$

$$F_S = \frac{\partial}{\partial x}\left(A_H \frac{\partial S}{\partial x}\right) + \frac{\partial}{\partial y}\left[A_H\left(\frac{\partial S}{\partial y}\right)\right] \quad (2\text{-}10)$$

where:

A_M = horizontal eddy viscosity [L^2 T^{-1}]

A_H = horizontal eddy diffusivity [L^2 T^{-1}]

[2] The symbol θ is used to represent fundamental units of temperature in the LTMθ system (see Dingman, 2002). θ indicates degree and θ^{-1} indicates degree^{-1}.

In developing these equations, two simplifying assumptions were made: (1) the weight of the fluid identically balances the pressure (hydrostatic pressure assumption); and (2) density differences are negligible unless those differences are multiplied by the gravitational acceleration (Boussinesq approximation). As implemented in the model, these equations are transformed into a terrain-following, sigma (σ)-level coordinate system in the vertical direction and an orthogonal, curvilinear coordinate system in the horizontal direction as described by HQI (2010).

The governing equations contain Reynolds stress and flux terms that account for turbulent diffusion of momentum as expressed by eddy viscosity. The turbulence closure approach of Mellor and Yamada (1982) is used to solve these equations. Turbulent mixing terms (K_M) in the governing equations also occur in relationships between velocity gradients (∂U/∂z and ∂V/∂z) and shear stresses at the air-water and sediment-water interfaces (boundaries conditions). Shear stress at the sediment-water interface depends on a drag coefficient that relates surface roughness to velocity gradients at the bottom of the water column. Drag coefficients are determined using a logarithmic velocity profile to describe how velocities change near a boundary using the following relationship:

$$C_D = \left[\frac{1}{\kappa} \ln\left(\frac{z}{z_0} \right) \right]^{-2} \qquad (2\text{-}11)$$

where:

C_D = coefficient of drag [dimensionless]

κ = von Karman constant = 0.4 [dimensionless]

z = height above the sediment bed [L]

z_0 = hydrodynamic roughness height of the sediment bed [L]

The height above the sediment bed (z) used in the logarithmic velocity profile is termed the matching height. Operationally, the matching height is equal one half the thickness of the bottom layer of water in the model. When 10 sigma-layers are used in the model, each water column layer is one tenth (10%) of the total water depth and the matching height is one twentieth (5%) of the water depth. As total water depth increases, hydrodynamic drag on the water column will decrease to a minimum value ($C_{D,min}$). Operationally, the minimum drag coefficient is in the range of 0.0025 to 0.003 and is used as a floor function (i.e., C_D can never be less than $C_{D,min}$). If the drag coefficient value calculated using Equation 2-11 is less than $C_{D,min}$, C_D is set equal to the minimum value. In practical terms, drag coefficients will be set equal to minimum values when water depth is greater than approximately 1.5 meters (5 feet).

Using this approach, the primary model calibration parameters for hydrodynamics are hydrodynamic roughness height, z_0, and minimum coefficient of drag ($C_{D,min}$). Principal outputs of the hydrodynamic model are water velocities in the x, y, and z directions, water depths (water surface elevations), and total hydrodynamic shear stresses at the sediment-water interface. Further descriptions of shear stress are provided in the description of the sediment transport model and Appendix A.

2.2. SEDIMENT TRANSPORT

In the water column, particles are transported by advection (movement with currents) and can be exchanged between the sediment bed and water column by erosion and deposition. Particles may be transported as suspended load (fully entrained in the water column) or as bedload (in contact with the bed). Sediment behavior can be classified across a continuum from cohesive to non-cohesive. Cohesive sediments are typically described in terms of aggregate properties (i.e., properties of the sediment as a whole) because of the tendency of individual sediment grains to aggregate and flocculate in the water column and exhibit erosional resistance in the sediment bed. Non-cohesive sediments are described in terms of the properties of individual grains because the individual grains comprising the sediment mixture do not flocculate in the water column and do not exhibit erosional resistance beyond that attributable to individual grains. For application to Rockaway pipeline, model development focuses on non-cohesive sediment because the seabed along the proposed pipeline route is largely comprised of sands with a small amount of silt.

2.2.1. Shear Stress Partitioning and Surface Drag

The shear stress at the sediment–water interface generated by water flowing over the bed surface is a primary determinant of the extent to which materials settling out of the water column are deposited on the bed or are eroded from it and whether particles in motion are transported as suspended load or bed load. Near the bed, vertical velocity gradients exist because water velocities decrease and typically diminish to zero at the sediment-water interface. Vertical velocity gradients generate shear stresses that act on the bed. Very close to the bed, at scales that typically range from a few particle diameters to the length of bedforms (e.g., ripples and dunes), the total (hydrodynamic) bed shear stress can be separated (partitioned) into two components: (1) surface drag, and (2) form drag. The relationship between total shear stress and its components is:

$$\tau_b = \tau_g + \tau_f \qquad (2\text{-}12)$$

where:

τ_b = total (hydrodynamic) bed shear stress [M L^{-1} T^{-2}]

τ_g = surface drag ("grain-related") shear stress [M L^{-1} T^{-2}]

τ_f = form drag shear stress [M L^{-1} T^{-2}]

Surface drag acts to initiate particle movement off the bed surface, through the bottom boundary layer, and into the main body of the flow. The surface drag component of total bed shear stress is often termed "grain-related" or "grain" shear stress or "skin friction". A more detailed description of the process used to separate total hydrodynamic shear stress into surface drag and form drag components is presented in Appendix A.

2.2.2. Erosion

Erosion is the process by which particles at rest in the sediment bed are set into motion. Rates at which sediments erode vary widely because sediment characteristics vary by location and also with depth in the sediment bed. Erosion rates for cohesive sediments are highly variable and generally must be determined from site-specific flume studies. Rates for non-cohesive sediment vary with composition (i.e., grain size distribution) and can be estimated from tabulated results of laboratory flume studies. SEDZLJ (Jones and Lick, 2001; Scott et. al. 2010) is designed to use erosion rate measurements performed using the SEDFLUME device. SEDFLUME measurements for cohesive sediments are illustrated by McNeil et al. (1996) and Jepsen et al. (1997, 2000). SEDFLUME and similar measurements for non-cohesive sediments are illustrated by Roberts et al. (1998, 2003).

With the SEDZLJ framework, erosion rates at known shear stress levels and depths in the sediment bed are tabulated based on SEDFLUME measurements. Erosion rates at shear stresses and depths between measured values are estimated by interpolating between pairs of measured values as follows:

$$E\left(\tau_g\right)=\left(\frac{\tau_{m+1}-\tau_g}{\tau_{m+1}-\tau_m}\right)E_m+\left(\frac{\tau_g-\tau_m}{\tau_{m+1}-\tau_m}\right)E_{m+1} \tag{2-13}$$

$$\ln\left[E(D)\right]=\left(\frac{{D_0}^n-D}{{D_0}^n}\right)\ln\left[E^n\right]+\left(\frac{D}{{D_0}^n}\right)\ln\left[E^{n+1}\right] \tag{2-14}$$

where:

$E(\tau_g)$ = erosion at a grain-related shear stress equal to τ_g [L T^{-1}]

τ_g = grain-related shear stress [M L^{-1} T^{-2}]

τ_{m+1} = measured grain-related shear stress greater than τ_g [M L^{-1} T^{-2}]

τ_m = measured grain-related shear stress less than τ_g [M L^{-1} T^{-2}]

E_m = measured erosion at a measured grain-related shear stress τ_m [L T^{-1}]

E_{m+1} = measured erosion at a measured grain-related shear stress τ_{m+1} [L T^{-1}]

$E(D)$ = erosion rate at a depth in the sediment bed equal to D [L T^{-1}]

D = depth in the sediment bed within sediment layer n [L]

D_0^n = initial thickness of sediment layer n prior to erosion [L]

E^n = measured erosion at the top of sediment layer n [L T^{-1}]

E^{n+1} = measured erosion at the top of sediment layer $n+1$ (i.e., measured rate at the bottom of sediment layer n) [L T^{-1}]

Equations (2-13) and (2-14) are used to express erosion rate variation as a function of both shear stress and depth in the sediment bed.

Erosion occurs when grain shear stress at the sediment surface exceeds the critical shear stress for erosion (i.e. the incipient motion threshold), τ_{ce}. For cohesive sediments, τ_{ce} is generally determined from site-specific measurements. For non-cohesive sediments, τ_{ce} can be estimated from grain size using the Shields (1936) curve as described in standard references (see Julien, 1998). Formulae by van Rijn (1984a), Soulsby (1997), or Guo (2002) provide algebraic approximations to the Shields curve. The formula of Guo (2002) is:

$$\tau_{ce} = \left(G_p - 1\right)\rho_w g d_p \left(\frac{0.23}{d_*} + 0.054\left[1 - \exp\left(-\frac{d_*^{0.85}}{23} \right) \right] \right) \tag{2-15}$$

$$d_* = d_p \left[\frac{\left(G_p - 1\right)g}{\nu^2} \right]^{-1/3} \tag{2-16}$$

where:

τ_{ce} = critical shear stress for erosion [M L^{-1} T^{-2}]

G_p = sediment particle specific gravity ≈ 2.65 [dimensionless]

ρ_w = fluid density ≈ 1000 kg/m^3 (≈ 1025 kg/m^3 for seawater) [M L^{-3}]

g = gravitational acceleration = 9.81 m/s [L T^{-2}]

d_p = sediment particle diameter [L]

d_* = dimensionless particle diameter [dimensionless]

ν = kinematic viscosity [L^2 T^{-1}]

Equation (2-15) is applicable to non-cohesive sediments and the subscript p is used to denote properties of individual types of grains (particles) in the sediment bed. When

using SEDFLUME measurements, the onset of erosion is operationally defined as the shear stress at which erosion occurs at a rate of 10^{-4} cm/s.

2.2.3. Bedload and Suspended Load Transport

Two distinct modes of sediment transport occur: (i) bedload, and (ii) suspended load. During bedload transport, particles move by rolling, sliding, or saltation in a thin layer in contact with the bed surface. During suspended transport, particles are fully entrained in the water column and do not have contact with the bed. Cohesive particles are not typically transported as bedload because they are often very small in size and readily entrained into the water column. Non-cohesive sediments usually span a wide range of particle sizes and can be transported as bedload, suspended load, or a combination of the two.

When shear stresses acting on the bed surface are less than the critical shear stress for erosion (τ_{ce}), sediment particles on the bed surface will be stationary. When shear stresses on the bed exceed the critical shear stress for erosion (τ_{ce}) but are less than the critical shear stress for suspension (τ_{cs}), sediment particles will be transported as bedload. When shear stresses on the bed exceed the critical shear stress for suspension, some or all of the sediment in motion will be entrained and transported as suspended load. The fraction of sediment transported as bedload or suspended load are determined as (van Rijn, 1984a-c; van Rijn, 1993; Jones and Lick, 2001; James et al. 2010):

$$f_{BL} = \begin{cases} 0 & for \quad \tau_g \le \tau_{ce} \\ 1 - f_{SL} & for \quad \tau_g > \tau_{cs} \end{cases} \tag{2-17}$$

$$f_{SL} = \begin{cases} 0 & for \quad \tau_g \le \tau_{cs} \\ \dfrac{\ln\left(u_*/w_s\right) - \ln\left(\sqrt{\tau_{cs}/\rho_w}/w_s\right)}{\ln(4) - \ln\left(\sqrt{\tau_{cs}/\rho_w}/w_s\right)} & for \quad \tau_g > \tau_{cs} \quad and \quad u_*/w_s < 4 \\ 1 & for \quad \tau_g > \tau_{cs} \quad and \quad u_*/w_s \ge 4 \end{cases} \tag{2-18}$$

$$\tau_{cs} = \begin{cases} \rho_w \left(\dfrac{4w_s}{d_*}\right)^2 & for \quad d_p \le 400\,\mu m \\ \rho_w \left(0.4 w_s\right)^2 & for \quad d_p > 400\,\mu m \end{cases} \tag{2-19}$$

where:

f_{BL} = fraction of sediment transported as bedload [dimensionless]

f_{SL} = fraction of sediment transported as suspended load [dimensionless]

τ_g = surface drag (grain-related) component of total shear stress

τ_{ce} = critical shear stress for erosion [M L^{-1} T^{-2}]

τ_{cs} = critical shear stress for suspension [M L^{-1} T^{-2}]

u_{*g} = surface drag (grain-related) component of total shear velocity [L T^{-1}]

w_s = particle settling velocity [L T^{-1}]

ρ_w = fluid density ≈ 1000 kg/m^3 (≈ 1025 kg/m^3 for seawater) [M L^{-3}]

d_* = dimensionless particle diameter [dimensionless]

d_p = sediment particle diameter [L]

For non-cohesive sediments, Equations (2-17) through (2-19) are used for each particle type in combination with the particle grain size distribution to express the erosion flux of sediment by grain size that is transported by bedload and suspended load as a function of the bottom shear stress.

2.2.4. Settling and Deposition

Sediment particles in the water column move downward (i.e., settle) under the force of gravity and may be deposited on the bed surface depending on shear stress conditions. The effective setting velocity of a particle is a function of its settling characteristics under quiescent conditions and probability of deposition (i.e., likelihood that a particle will come to rest on the bed surface). Cohesive and non-cohesive particles types have different setting and deposition characteristics. Descriptions of cohesive sediment behavior are presented by HQI (2010), and other references (e.g., van Rijn, 1993; Winterwerp and van Kesteren, 2004). The model development that follows focuses on non-cohesive sediment because the seabed along the proposed route for Rockaway pipeline is largely comprised of non-cohesive sands with a small amount of silt.

The effective settling velocity of a particle is computed as:

$$w_{se} = w_{sq} P_{dep} \tag{2-20}$$

where:

w_{se} = effective settling velocity [L T^{-1}]

w_{sq} = quiescent settling velocity [L T^{-1}]

P_{dep} = probability of deposition [dimensionless]

For natural non-cohesive particles, quiescent settling velocities are determined using the formula of Cheng (1997):

$$w_{sq} = \frac{\nu}{d_p}\left[\left(25 + 1.2d_*^{\,2}\right)^{0.5} - 5\right]^{-1.5} \tag{2-21}$$

where:

w_{sq} = quiescent settling velocity [L T^{-1}]

ν = kinematic viscosity of water [L^2 T^{-1}]

d_p = sediment particle diameter [L]

d_* = dimensionless particle diameter [dimensionless]

As a result of turbulence and other factors, not all particles settling through a column of flowing water necessarily reach the sediment-water interface or are incorporated into the bed. The effective settling velocity of a particle is described as a reduction in the quiescent settling velocity by a probability of deposition. Probability of deposition varies with particle size and shear stress near the sediment bed. As particle size decreases or shear stress increases, probability of deposition decreases. For non-cohesive particles, probability of deposition has been described as a function of bottom shear stress and critical shear stress for deposition (Gessler, 1965; Gessler 1967; Gessler, 1971):

$$P_{dep} = P = \frac{1}{\sqrt{2\pi}}\int_{-\infty}^{Y} e^{-0.5x^2}\,dx \tag{2-22}$$

$$Y = \frac{1}{\sigma}\left(\frac{\tau_{cd}}{\tau} - 1\right) \tag{2-23}$$

where:

P = probability integral for the Gaussian distribution

σ = experimentally determined constant = 0.57

τ_g = surface (grain-related) component of total shear stress [M L^{-1} T^{-2}]

τ_{cd} = critical shear stress for deposition, defined as the shear stress at which 50% of particles deposit (or erode) = τ_{ce} [M L^{-1} T^{-2}]

For non-cohesive particles, the definition of critical shear stress for deposition is the point at which 50% of particles of a specified type will deposit to the bed (with the other 50% remaining in transport. For all practical purposes, this is identical to the definition of

critical shear stress for erosion, which is the shear stress at which 50% of particles will start to move, with the other 50% remaining at rest on the bed surface. Thus, τ_{cd} equals τ_{ce}.

3. MODEL APPLICATION FOR ROCKAWAY PIPELINE

The ECOM framework was applied to the coastal ocean area of the New York Bight in the region of the proposed Rockaway pipeline south of Long Island. The model includes the area near the proposed pipeline route as well as large portions of the New York-New Jersey Harbor because of complex flow interactions that occur as freshwater from the Hudson River, Raritan River and other sources, mix and are influenced by ocean currents and tides. ECOM was used to perform hydrodynamic and sediment transport calculations to simulate anticipated changes in environmental conditions generated by trenching operations during pipeline installation. Model results were used to evaluate:

- Suspended sediment concentrations, spatial extent, and temporal duration of plumes generated during pipeline construction;
- Deposited sediment spatial extent and depth of accumulation on the sea bed following pipeline construction;
- Natural rates of sediment accumulation in the construction area and expected time required to bury the pipeline.

Model results are expected to provide reliable estimates of site conditions because model set-up and parameterization are based on site-specific information and fundamental, principles such conservation of mass and other physically-based constraints. In addition, ECOM has a long history of development and application to the New York Bight area and has been used to support regulatory decision-making. Previous ECOM applications with hydrodynamic and sediment transport simulations in the area of the proposed pipeline route include the System-Wide Eutrophication Model (SWEM) (HQI, 1999a-f; HQI, 2002), Contaminant Assessment and Reduction Project (CARP) (HQI, 2007), Harbor Toxics and Nutrients Total Maximum Daily Load (TMDL) efforts and Lower Passaic River/Newark Bay (LPR/NB) Superfund efforts for the U.S. Environmental Protection Agency (USEPA). Model set-up and parameterization for the application to Rockaway pipeline was derived from the most recent generation of modeling work performed for USEPA as part of LPR/NB Superfund efforts.

3.1. MODEL GRID

Three-dimensional (3D) hydrodynamic and sediment transport simulations were performed for a wide area surrounding the pipeline preferred route. Model calculations for these simulations were performed using a spatially-variable network of segments (i.e., "grid cells"). The collection of grid cells representing the study area around the pipeline route is termed the model grid. The area represented by the model grid is termed the model domain. Cells comprising the grid are larger in distant areas and gradually become much smaller so that individual grid are approximately 150 meters long (parallel to the

pipeline) and 50 meters wide (perpendicular to the pipeline) in the area near the pipeline. The model grid used for the pipeline project was derived from ongoing efforts to model hydrodynamics, sediment transport, and contaminant transport and fate for LPR/NB Superfund efforts for USEPA. The pipeline evaluation model grid is "nested down" to a much finer scale than the LPR/NB model grid. An overview of the pipeline model grid is presented in Figure 1.

3.2. MODEL SET-UP AND CALIBRATION

Model set-up and calibration was performed for a 60 day period during July-August, 2009. This timeframe was selected because site-specific data for the pipeline area and other portions of the model domain were collected during this period. Measurements used for model set-up and calibration include current velocities, water surface elevations (depth), water temperature, salinity, freshwater inflows, and meteorological conditions. Model initial conditions and inputs for open ocean boundaries along the southern and eastern edges of the pipeline model domain were obtained from results of LPR/NB model simulations performed for USEPA for the July-August 2009 period.

Water surface elevations along open ocean boundaries in the model were calculated using the inverted Reid and Bodine option (HQI, 2010). This option improves model stability by allowing long waves to pass through model boundaries (i.e., it minimizes the potential for uncertainty in specified boundary conditions to generate unrealistic water surface elevations and cause numerical instability). Parameters for minimum coefficient of drag ($C_{D,min}$) and hydrodynamic roughness height of the sediment bed (z_0) were calibrated to achieve the best agreement between model results and site-specific measurements. Values for these parameters were set equal to their values as assigned in LPR/NB model a efforts. As part of calibration, a series of exploratory simulations were performed to evaluate model response to a range of values for $C_{D,min}$ and z_0. These simulations show that model results are not materially affected by changes in z_0 because water depths in nearly all the model domain exceed the depth where the model uses the minimum drag coefficient value to perform calculations (i.e., nearly all water surface calculations in the model end up being calculated using $C_{D,min}$ rather than z_0). Values for $C_{D,min}$ were incrementally varied from a low of 0.002 to a high of 0.006. A summary of hydrodynamic model parameters is presented in Table 1.

The National Oceanic and Atmospheric Administration (NOAA) Sandy Hook tide gage (Station 8531680) is located within the model domain. Water surface elevations and water temperatures are routinely measured at this station. Current velocities, water surface elevations, water temperatures, and salinity were also measured by an Acoustic Doppler Current Profiler (ADCP) and other instruments deployed at a point near the south end of the proposed pipeline during July and August, 2009. Data from these two sources were compared to model outputs to determine if the hydrodynamic model calibration was reasonable. Graphical comparisons of agreement between model results and field

measurements indicate that a $C_{D,min}$ value of 0.003 and a z_0 value of 0.4 mm successfully reproduce salient characteristics of hydrodynamic conditions (e.g. amplitude and timing of tides, velocities, etc.) at the Sandy Hook tide gage (Figure 2). Model results also reproduced water temperatures at the Sandy Hook gage (Figure 3). Simulated water temperatures tend to be 1-2 °C cooler than measured values. This difference is attributable to uncertainty in water temperatures assigned along open ocean boundaries of the model. However, such small temperature differences are not expected to affect sediment transport simulations because water affected by construction will be at or near ambient water temperatures (e.g., hydraulic jets will not be buoyant, mechanical dredging will not alter temperatures, etc.).

Near the proposed pipeline route, model results reproduce ranges and patterns of velocities measured at different water column depths as well as temperature and salinity patterns (Figures 4-8). However, model results exhibit a consistent shift in the timing between velocity peaks in the tidal cycle. These differences in timing may be attributable to unresolved differences in the time zone in which data were reported. For example, ADCP data were reported in Coordinated Universal Time (UTC) but may have been recorded in Greenwich Mean Time (GMT). During summer months when daylight saving time is in use, there is a one hour time difference between UTC and GMT. It should be noted that differences in the timing of peak velocities during a tidal cycle does not impact the model's ability to simulate sediment transport for proposed pipeline installation because potential impacts of trenching operations such as the extent of a plume are influenced by the magnitudes tidal velocities rather than an absolute date or time of day.

Sediment transport parameters in the model were based on site-specific measurements of grain size distributions and non-cohesive sediment erosion rate measurements reported in peer-reviewed scientific literature. Grain size was measured in samples collected from the seabed along the proposed pipeline route (Figure 9-10). Those data were used to determine the number of particle size classes needed to represent sediment transport in the model as well as mean diameters for each particle class. Erosion rate measurements for non-cohesive sediments are summarized by Roberts et al. (1998) and are specifically designed to provide data in the form needed for the SEDZLJ sediment transport module integrated within the ECOM framework. Sediment specific gravity was assumed to be 2,650 kg/m3, representative of quartz particles. Dry bulk density was assumed to be 1,495 kg/m^3, corresponding to a sediment bed porosity of 0.44. All remaining sediment transport parameters in the model (e.g. critical shear stresses for erosion and suspension, settling velocities, etc.) are defined based on particle diameter. A total of five particle size classes were defined. Particle diameters for these size classes range from 0.031 mm (silt) to 2.25 mm (very fine gravel), with the bulk of all particles being 0.078 mm (very fine sand). Critical shear stresses for erosion (τ_{ce}) were calculated using Equation (2-14). Critical shear stresses for suspension (τ_{cs}) were calculated using Equation (2-18). Quiescent setting velocities (w_{sq}) were calculated using Equation (2-20). A summary of sediment transport parameters is presented in Table 2.

3.3. MODEL APPLICATION FOR PIPELINE INSTALLATION

The submarine portion of the proposed pipeline is 1.95 miles (3,138 meters) long. In the model, the pipeline extends along 30 model grid cells (i.e., a portion of the pipeline is in each of 30 cells). The calibrated model was used to perform a series of simulations to evaluate potential impacts of pipeline construction. These simulations examine sediment releases from construction activities that include:

(1) hydraulic jetting of sediments along the pipeline route (jet sled) for "worst case" conditions;
(2) hydraulic jetting of sediments along the pipeline route (jet sled) for "typical" conditions;
(3) mechanical plowing of sediments along the pipeline route (mechanical plow) for "worst case" conditions;
(4) mechanical plowing of sediments along the pipeline route (mechanical plow) for "typical" conditions;
(5) mechanical (clamshell) dredging of sediments along the pipeline route;
(6) hand jetting of sediments at the site where the existing main will be tapped to connect to submarine portion of the lateral;
(7) mechanical (clamshell) dredging at the site of a pit where the submarine portion of the pipeline will connect to pipeline sections that will be installed by horizontal directional drilling (HDD).

3.3.1. General Description of Model Set-up

To simplify model set-up, sediment releases from construction activities were simulated as point sources to the water column. When simulating trenching with a jet sled, sediment is uniformly released into the bottom three layers of the water column (i.e., between the sediment-water interface and a height of approximately 3 meters above the bed) with releases occurring into each model grid cell where trenching occurs. When simulating trenching with a mechanical plow, sediment is released into the bottom-most layer of the water column with releases into each cell where trenching occurs. When simulating hand jetting of sediments at the hot tap site, sediment is released into the bottom-most layer of the water column with the release occurring into a single model cell at the seaward end of the pipeline. When simulating mechanical dredging at the HDD pit site, sediment is released into the bottom three layers of the water column with the release occurring into a single cell at the shoreward end of the pipeline. In all cases, the grain size distribution of sediments released by construction was assumed to equal the distribution of sediment in the bed along the pipeline route (see Figure 9).

The model was set up so that sediments from point sources representing construction were the only transportable source of sediment to distinguish sediments released during construction activities from ambient sources. Using this approach, simulated sediment

concentrations represent levels above ambient conditions. To interpret model results, simulated solids concentrations must be added to representative ambient solids concentrations. Measurements collected in support of pipeline permitting efforts during Fall 2010 indicate that ambient total suspended solids (TSS) levels along the proposed pipeline route averaged approximately 6 mg/L and ranged from 1.4 to 18 mg/L. Ambient turbidity at those TSS levels averaged 2.2 NTU and ranged from 0 to 9.4 NTU. For reference, those water column TSS and turbidity data are summarized in Table 3.

HDD pit construction and hand trenching at the hot tap site are scheduled to begin in a February to early March timeframe. Trenching is scheduled to begin in an early May timeframe. Because differences in tidal and meteorological conditions can affect currents over time, statistical analyses were performed to select representative conditions during construction. As part of modeling efforts completed for USEPA, a catalog of annual hydrodynamic simulations exists for the sixteen year period 1995-2010. Probability distributions of the volume flux ("flow") of water moving through the pipeline area in March and May of each year were compiled and graphically compared to the average condition for all 16 years. Conditions for March and May, 2010 were close to 16-year averages for those months and judged to be representative of hydrodynamic conditions during proposed construction periods (Figures 11-12). For simplicity, model initial and boundary conditions (e.g. starting water temperatures, water surface levels at open ocean boundaries, etc.) for HDD pit dredging and hand jetting at the hot tap site reflect March, 2010 conditions. For trenching, model initial and boundary conditions reflect May, 2010 conditions.

Simulations were performed for each type of construction activity. The model was run for 10 days for trenching, hot tap hand jetting, and HDD pit dredging scenarios, with construction releases beginning 24 hours after simulation start. The model was run for 35 days for the trench mechanical dredging scenario, with construction releases beginning 24 hours after simulation start, to account for its longer construction period. Water column results for each simulation were graphically summarized to present suspended solids concentrations and the spatial extent of plumes generated during construction for six timeframes:

- Just after the start of construction (~0% completion)
- 25% completion
- 50% completion
- 75% completion
- Just before the end of construction (~100% completion)
- 4 hours following the end of construction

Maximum suspended solids concentrations simulated in each water column (sigma) layer of the model were also graphically summarized to illustrate vertical distributions of solids released during construction. Sediment bed results were also graphically summarized to

present spatial distributions and depths (thickness) of sediment accumulation on the seabed following the end of construction. Note that the Rockaway reef area and locations of sonar targets are shown in white on all figures. Remaining scenario-specific details of sediment releases for each simulation are described below.

3.3.2. Trenching: Hydraulic Jetting "Worst Case" Conditions

Trenching is assumed to occur by means of a hydro-plow ("jet sled") that uses jets of water to displace sediments from the trench. Sediment releases during trenching were simulated as a point source to the bottom three layers of the water column (i.e. sediment is uniformly released into water between the sediment-water interface and a height approximately 3 meters above the bed). Releases occur in sequence into each of the 30 model grid cells, representing jet sled movement along the pipeline route. In this scenario, the trench has a length of 3,138 m (1.95 miles), a maximum depth of 2 m (6.5 ft), and a cross-sectional area of approximately 22.5 m^2 (243 ft^2). This scenario assumes that sediment from the entire disturbed footprint and along trench sidewalls will be jetted and displaced. Total sediment volume released during trenching equals approximately 78,600 m^3 (102,800 yd^3). This represents "worst case" conditions because sediment volume released equals 100% of all sediment from the maximum disturbed footprint (which includes an additional 10% contingency) and exceeds the sediment volume that would be displaced during trenching to construct the pipeline.

The duration (i.e. time) and rate (i.e. mass per time) of sediment releases to the water column are directly related to the rate of trenching. The duration of trenching is equal to trench length divided by trenching rate. For this set of "worst case" conditions, three trenching rate cases were simulated: (i) 366 meters per hour (1,200 feet per hour); (ii) 183 meters per hour (600 feet per hour); and (iii) 122 meters per hour (400 feet per hour). In all cases, the jet for trenching was assumed to discharge at a rate of 70 liters per minute (18.5 gallons per minute). A summary of trenching rates, durations, and other sediment release characteristics is presented in Table 4. Water column and sediment bed results for the 366 m/hr (1,200 ft/hr) trenching rate scenario are presented in Figures 13-21. Results for the 183 m/hr (600 ft/hr) scenario are presented in Figures 22-30. Results for the 122 m/hr (400 ft/hr) scenario are presented in Figures 31-39. In all cases, suspended solids concentrations are presented for the bottom layer of the water column, which is the depth where maximum concentrations occur. Simulated suspended solids concentrations for the surface layer of the water column for each trenching rate case are presented in Appendix B.

3.3.3. Trenching: Hydraulic Jetting "Typical" Conditions

Trenching is assumed to occur by means of a jet sled that uses jets of water to displace sediments from the trench. Sediment releases during trenching were simulated as a point source to the bottom three layers of the water column. Releases occur in sequence into

each of the 30 model grid cells where trenching occurs, representing jet sled movement along the pipeline route. In this scenario, the trench has a length of 3,138 m (1.95 miles), a depth of 2 m (6.5 ft), and a cross-sectional area of approximately 15.1 m^2 (162 ft^2). This scenario assumes trench sidewalls will be allowed to fall into the trench and reach stable side slopes and partially bury the pipeline. Total sediment volume released during trenching equals approximately 47,400 m^3 (62,000 yd^3). This represents more "typical" conditions because the sediment volume released more closely approximates the jet sled footprint. However, it is still an "upper bound" for jetting because it assumes the volume associated with the jet sled footprint exceeds the footprint needed to construct the pipeline (which includes an additional 10% contingency) and also assumes that 100% of jetted sediment is released into the water column.

For this "typical" case, a 183 meter per hour (600 feet per hour) trenching rate was simulated. The jet for trenching was assumed to discharge at a rate of 70 liters per minute (18.5 gallons per minute). A summary of trenching rates, durations, and other sediment release characteristics is presented in Table 4. Water column and sediment bed results for this 183 m/hr (600 ft/hr), "typical case" hydraulic jetting scenario are presented in Figures 40-48. Suspended solids concentrations are presented for the bottom layer of the water column, which is the depth level where maximum concentrations occur. Simulated suspended solids concentrations for the surface layer of the water column for this "typical" hydraulic jetting case are presented in Appendix C.

3.3.4. Trenching: Mechanical Plowing "Worst Case" Conditions

Trenching is assumed to occur by means of a mechanical plow that is pulled through the bed to displace sediments from the trench. Sediment releases during plowing were simulated as a point source to the bottom layer of the water column. Releases occur in sequence into each of the 30 model grid cells where trenching occurs, representing plow movement along the pipeline route. In this scenario, the trench has a length of 3,138 m (1.95 miles), a maximum depth of 2 m (6.5 ft), and a cross-sectional area of approximately 8.9 m^2 (96 ft^2). This scenario assumes that sediment along trench sidewalls will be disturbed until the sides are stable. Total sediment volume disturbed by plowing equals approximately 27,900 m^3 (36,500 yd^3) and the scenario assumes that 20% of this material, 5,580 m^3 (7,300 yd^3), is released into the water column, with the remainder falling back into the trench and partially burying the pipeline. This represents "worst case" conditions because the sediment volume displaced during trenching exceeds the minimum footprint needed to construct the pipeline (plus an additional 10% contingency) and includes material along trench sidewalls.

For this "worst" case, a 183 meter per hour (600 feet per hour) trenching rate was simulated. A summary of trenching rates, durations, and other sediment release characteristics is presented in Table 4. Water column and sediment bed results for this 183

m/hr (600 ft/hr), "typical case" hydraulic jetting scenario are presented in Figures 49-57. Suspended solids concentrations are presented for the bottom layer of the water column, which is the depth level where maximum concentrations occur. Simulated suspended solids concentrations for the surface layer of the water column for this "typical" hydraulic jetting case are presented in Appendix D.

3.3.5. Trenching: Mechanical Plowing "Typical" Conditions

Trenching is assumed to occur by means of a mechanical plow that is pulled through the bed to displace sediments from the trench. Sediment releases during plowing were simulated as a point source to the bottom layer of the water column. Releases occur in sequence into each of the 30 model grid cells where trenching occurs, representing plow movement along the pipeline route. In this scenario, the trench has a length of 3,138 m (1.95 miles), a maximum depth of 2 m (6.5 ft), and a cross-sectional area of approximately 8.9 m^2 (96 ft^2). This scenario assumes that sediment along trench sidewalls will be disturbed until the sides are stable. Total sediment volume disturbed by plowing equals approximately 27,900 m^3 (36,500 yd^3) (which includes an additional 10% contingency) and the scenario assumes that 15% of this material, 4,190 m^3 (5,475 yd^3), is released into the water column, with the remainder falling back into the trench and partially burying the pipeline. This represents more "typical" conditions because the sediment volume displaced during trenching more closely approximates the footprint needed to construct the pipeline.

For this "typical" case, a 183 meter per hour (600 feet per hour) trenching rate was simulated. A summary of trenching rates, durations, and other sediment release characteristics is presented in Table 4. Water column and sediment bed results for this 183 m/hr (600 ft/hr), "typical case" hydraulic jetting scenario are presented in Figures 58-66. Suspended solids concentrations are presented for the bottom layer of the water column, which is the depth level where maximum concentrations occur. Simulated suspended solids concentrations for the surface layer of the water column for this "typical" hydraulic jetting case are presented in Appendix E.

3.3.6. Trenching: Mechanical (Clamshell) Dredging

Trenching is assumed to occur by means of a mechanical, clamshell dredge to displace sediments from the trench. Dredged sediments will be lifted a short distance above the bed surface and then sidecast. Sediment releases during dredging were simulated as a point source to the bottom three layers of the water column. Releases occur in sequence into each of the 30 model grid cells where trenching occurs, representing dredge movement along the pipeline route. In this scenario, the trench has a length of 3,138 m (1.95 miles), a maximum depth of 2 m (6.5 ft), and a cross-sectional area of approximately 14.7 m^2 (158 ft^2). This scenario assumes that sediment along trench sidewalls will be disturbed until the sides are stable. Dredging is assumed to occur over a 746 hour period,

at a rate of 30 cycles per hour with a clamshell bucket capacity of 3 yd^3 per cycle. This is equivalent to a linear trenching rate of 4.2 m/hr (13.8 feet/hour). Total sediment volume disturbed by dredging equals approximately 51,300 m^3 (67,100 yd^3) (which includes an additional 10% contingency). The scenario assumes that 100% of this material is released into the water column, with 5% of the release occurring in each of the bottom two water column layers (representing sediment disturbance and loss from the clamshell during lifting), and 90% into the third layer above the bed (representing sidecasting).

A summary of trenching rates, durations, and other sediment release characteristics is presented in Table 4. Water column and sediment bed results for this trench dredging scenario are presented in Figures 67-75. Suspended solids concentrations are presented for the bottom layer of the water column, which is the depth level where maximum concentrations occur. Simulated suspended solids concentrations for the surface layer of the water column for this trench dredging case are presented in Appendix F.

3.3.7. Hand Jetting at Hot Tap Site

This construction activity is assumed to occur by means of diver-guided hydraulic ("hand") jets to displace sediments from the hot tap location. Sediment releases during jetting were simulated as a point source to the bottom layer of the water column. Releases occur in a single model grid cell at the seaward end of the pipeline where the lateral will be joined to the existing main. In this scenario, jetting occurs in four eight-hour pulses, with 16 hours between each pulse. Each pulse releases 5,960 m^3 (7,800 yd^3) from the hot tap site to clear sediments away from the existing main and construct the manifold, tap the main, and connect the new lateral. Total sediment volume displaced by hand jetting equals approximately 23,850 m^3 (31,200 yd^3) and the scenario assumes that 100% of this material is released into the water column.

A summary of jetting rates, durations, and other sediment release characteristics is presented in Table 4. Water column and sediment bed results for this hand jetting scenario are presented in Figures 76-84. Suspended solids concentrations are presented for the bottom layer of the water column, which is the depth level where maximum concentrations occur. Simulated suspended solids concentrations for the surface layer of the water column for this hand jetting case are presented in Appendix G.

3.3.8. Mechanical (Clamshell) Dredging from the HDD Pit

This construction activity is assumed to occur by means of mechanical, clamshell dredging to displace sediments from a pit that will be constructed to hold cuttings and drilling muds at the HDD exit site. Dredged sediments will be lifted a short distance above the bed surface and then sidecast. Sediment releases during dredging were simulated as a point source to the bottom three layers of the water column. Releases occur in a single model grid cell at the shoreward end of the pipeline where the lateral will be

joined to the pipeline segment constructed from shore. In this scenario, dredging is assumed to occur over a 170 hour period, at a rate of 30 cycles per hour with a clamshell bucket capacity of 3 yd^3 per cycle. Total sediment volume displaced by dredging equals approximately 11,700 m^3 (15,300 yd^3). The scenario assumes that 100% of this material is released into the water column, with 5% of the release occurring in each of the bottom two water column layers (representing sediment disturbance and loss from the clamshell during lifting), and 90% into the third layer above the bed (representing sidecasting).

A summary of dredging rates, durations, and other sediment release characteristics is presented in Table 4. Water column and sediment bed results for this dredging scenario are presented in Figures 85-93. Suspended solids concentrations are presented for the bottom layer of the water column, which is the depth level where maximum concentrations occur. Simulated suspended solids concentrations for the surface layer of the water column for this mechanical dredging case are presented in Appendix H.

3.4. ANTICIPATED RATE OF TRENCH INFILL BY AMBIENT SEDIMENT TRANSPORT PROCESSES

Previous modeling studies of the New York Bight area have estimated long-term average net deposition of solids to be approximately 0.25 cm/year (HQI, 1999a-f, HQI, 2002). Other studies of sediment disposal sites suggest that sediment transport and dispersion rates in the area vary in response to combined effects of tidal currents and surface waves (Clarke et al. 1982, 1983). Analysis of site-specific ADCP velocity and sediment grain size data suggest that rates of trench infill by sediment transport from currents that occur along the pipeline route is expected to be relatively slow. However, surface waves can induce oscillatory near-bed currents with boundary shear stresses that exceed critical shear stresses for sediment erosion. The potential magnitude of wave-induced sediment transport for trench infilling was assessed using oceanographic data for a 40-m deep site located approximately 2.8 miles offshore Rockaway Beach, NY (42.52343° N, 73.86120° W) as detailed in a report prepared by A.H. Glenn and Associates Services (2011).

3.4.1. Method to Calculate Sediment Transport by Wave Action

Wave characteristics and their potential for sediment transport change as waves progress from deeper to shallower water. Fenton (1988, 2012) describes an approach to determine wave characteristics by approximating the nonlinear equations for surface-gravity waves with a Fourier series. This method is advantageous because it is applicable to deep-, intermediate-, and shallow-water waves of nearly any wave height that is less than the wave-breaking limit. The FOURIER software package (Fenton, 2012) was used to solve wave equations to estimate wave velocities, shear stresses, and net sediment transport as bedload. These calculations are summarized as follows:

1. For water depth (h) and wave period (T_w), use FOURIER program to determine wavelength (λ) and horizontal orbital velocity near the seabed $\left(U_w\right)$ under the wave crest $\left(U_{w\,\text{crest}}\right)$ and trough $\left(U_{w\,\text{trough}}\right)$:

$$U_w = -\bar{u}_1 + \sqrt{\frac{g}{k}}\sum_{j=1}^{N} jB_j \frac{\cos\left[jk\left(x-ct\right)\right]}{\cosh\left(jkh\right)} \tag{3-1}$$

$$k = \frac{2\pi}{\lambda} \tag{3-2}$$

$$\omega = \frac{2\pi}{T_w} \tag{3-3}$$

$$c = \frac{\omega}{k} \tag{3-4}$$

where:

h	=	water depth [L]
T_w	=	wave period [T]
$\bar{u}_1$	=	mean Eulerian current in direction of wave propagation (conservatively assumed to be zero for these calculations) [L T^{-1}]
g	=	acceleration of gravity = 9.81 m/s [L T^{-2}]
j	=	index for terms in Fourier series
B_j	=	j^{th} coefficient of Fourier series (solved by FOURIER software package)
x	=	position (of crest or trough) in the direction of wave propagation [L]
t	=	time [T]
λ	=	wavelength [L]
k	=	wave number [L^{-1}]
ω	=	wave angular frequency [T^{-1}]
c	=	wave celerity [L T^{-1}]

2. Determine rough-bed and smooth-bed wave friction factors under wave crest $\left(f_{w_{smooth}}, f_{w_{rough}}\right)_{crest}$ and trough $\left(f_{w_{smooth}}, f_{w_{rough}}\right)_{trough}$ and select the larger (maximum) of the two factors $\left(f_{w,\max_{cresth}}, f_{w,\max_{troughh}}\right)$ in each case:

$$f_{w_{rough}} = 1.39\left(\frac{U_{w\,crest}}{\omega z_{0g}}\right)^{-0.52} \qquad f_{w_{rough}} = 1.39\left(\frac{U_{w\,trough}}{\omega z_{0g}}\right)^{-0.52} \tag{3-5}$$

$$f_{w_{smooth}} = BR_{w_{crest}}^{-N} \qquad f_{w_{smooth}} = BR_{w_{trough}}^{-N} \tag{3-6}$$

$$R_{w_{crest}} = U_{w_{crest}}^2 \big/ \omega\nu \qquad R_{w_{trough}} = U_{w_{trough}}^2 \big/ \omega\nu \tag{3-7}$$

$$z_{0g} = \frac{d_{50}}{15} \tag{3-9}$$

where:

R_w = wave Reynolds number (for crest or trough) [dimensionless]

ν = kinematic viscosity [$L^2\ T^{-1}$]

B = empirical coefficient $\left(= 2 \text{ for } R_w \le 5\times10^5;\ = 0.0521 \text{ for } R_w > 5\times10^5\right)$

N = empirical coefficient $\left(= 0.5 \text{ for } R_w \le 5\times10^5;\ = 0.187 \text{ for } R_w > 5\times10^5\right)$

z_{0g} = grain roughness height [L]

d_{50} = mean diameter of particles in sediment bed (≈ 0.078 mm) [L]

3. Calculate maximum wave shear stress (τ) under crest ($\tau_{w_{crest}}$) and trough ($\tau_{w_{trough}}$):

$$\tau_{w_{crest}} = 0.5\rho f_{w,\max\,crest} U_{w_{crest}}^2 \qquad \tau_{w_{trough}} = 0.5\rho f_{w,\max\,trough} U_{w_{trough}}^2 \tag{3-7}$$

where:

τ_w = wave shear stress (for crest or trough) [$M\ L^{-1}\ T^{-2}$]

ρ = fluid density (≈ 1025 kg/m³ for seawater) [$M\ L^{-3}$]

4. Calculate wave Shields parameter $\left(\theta_w\right)$ under crest $\left(\theta_{w_{crest}}\right)$ and trough $\left(\theta_{w_{trough}}\right)$:

$$\theta_{w_{crest}} = \frac{\rho\tau_{w_{crest}}}{g\left(G_p - 1\right)d_{50}} \qquad \theta_{w_{trough}} = \frac{\rho\tau_{w_{trough}}}{g\left(G_p - 1\right)d_{50}} \tag{3-8}$$

where:

θ_w = wave Shields parameter for erosion [dimensionless]

G_p = sediment particle specific gravity ≈ 2.65 [dimensionless]

5. Determine critical Shields parameter for erosion of noncohesive sediment:

$$\theta_{cr} = \frac{0.30}{1+1.2d_*} + 0.055\left[1 - e^{-0.02d_*}\right] \quad (3\text{-}9)$$

$$d_* = d_{50}\left[\frac{(G_p - 1)g}{\nu^2}\right]^{-1/3} \quad (3\text{-}10)$$

where:

θ_{cr} = critical Shields parameter for erosion [dimensionless]

d_* = dimensionless particle diameter [dimensionless]

6. If the Shields parameter under the wave crest exceeds the critical Shields parameter for erosion, calculate the half-cycle unit bedload transport rate in the direction of wave propagation:

$$q_{b\,crest} = 5.1(\theta_{w\,crest} - \theta_{cr})^{1.5}\sqrt{g(G_p - 1)d_{50}{}^3} \qquad for\ \ \theta_{w\,crest} > \theta_{cr} \quad (3\text{-}11)$$

where:

$q_{b\,crest}$ = half-cycle unit bedload transport rate under wave crest [$L^2\ T^{-1}$]

7. If the dimensionless Shields parameter under the wave trough exceeds the critical Shields parameter for erosion, then calculate the half-cycle bedload transport in the direction opposite to wave propagation:

$$q_{b\,trough} = 5.1(\theta_{w\,trough} - \theta_{cr})^{1.5}\sqrt{g(G_p - 1)d_{50}{}^3} \qquad for\ \ \theta_{w\,trough} > \theta_{cr} \quad (3\text{-}12)$$

where:

$q_{b\,trough}$ = half-cycle unit bedload transport rate under wave trough [$L^2\ T^{-1}$]

8. Calculate net unit bedload transport in direction of wave propagation:

$$q_{b\,net} = q_{b\,crest} - q_{b\,trough} \tag{3-13}$$

where:

$q_{b\,net}$ = net unit bedload transport rate [$L^2\ T^{-1}$]

9. Calculate net volumetric bedload transport rate:

$$Q_{b\,net} = q_{b\,net} L_{trench} \tag{3-14}$$

where:

$Q_{b\,net}$ = net volumetric bedload transport rate [$L^3\ T^{-1}$]

L_{trench} = projected trench length normal to direction of wave propagation [L]

The trench infill rate is calculated by multiplying the net volumetric bedload transport rate (i.e., the particle volume entering the trench over time, with fundamental dimensions of [$L^3\ T^{-1}$]) by particle density (i.e., particle mass per particle volume) and then expressed in terms of in-situ volume by dividing by sediment bulk density (i.e., particle mass per total volume of particles and pore space in the bed). In this case, particle density is 2,650 kg/m^3 and sediment bulk density is 1,495 kg/m^3.

3.4.2. Sediment Transport for Annual Wave Event Conditions

On an annual basis, in 40-ft deep water, significant wave heights in the range of 4.0–5.9 feet occurred 12.5% of the time, and significant wave heights in the range of 6.0–7.9 feet occurred 5.7% of the time (A.H. Glenn and Associates Services, 2011). As a broad average, a significant wave height of 6 ft occurs approximately 18% of this time (i.e., 66 days per year). Waves larger than this have a greater sediment transport potential but occur much less frequently. Conversely, waves smaller than this are more frequent but have a much lower potential to transport sediment.

A significant wave height of 6.0 ft, was used to estimate sediment transport for annual wave conditions. The A.H. Glenn and Associates Services (2011) wave report did not provide the wave periods corresponding to these wave heights, so a value of 12 seconds was selected. A 12 second wave period was judged to be characteristic of long-period coastal waves based on the A.H. Glenn and Associates Services (2011) wave report. At the seaward end of the pipeline, where water depths are approximately 10-15 m (32-49 ft), the net unit bedload transport rate is estimated to be 0.39 m^2/day. Assuming that the project pipeline length normal (i.e. perpendicular) to the direction of wave propagation is approximately 800 m (2640 ft; 0.5 miles), the annual rate of trench infill by wave-induced

bedload would be approximately 36,500 m^3/year (47,800 yd^3/year). At the shoreward end of the pipeline, where water depths are approximately 5-10 m (16-32 ft), the net unit bedload transport rate is estimated to be 2.8 m^2/day. This corresponds to an infill rate of approximately 262,400 m^3/year (343,100 yd^3/year). These estimated infill rates suggest that annual wave events could transport appreciable amounts of sediment back into the trench but that the seaward end of the pipeline could require several years for annual wind-driven sediment transport event to return the trench to its original grade.

3.4.3. Sediment Transport for a 5-Year Wave Event Conditions

Storms that generate larger waves are expected to generate greater sediment transport rates. However, large storms are also associated with storm surges where water levels increase. For a five-year wave event, the still-water depth was estimated to be 50.5 ft (i.e. 40 ft base depth plus an additional 10.5 ft storm surge) with a significant wave height of 23.7 ft and a wave period of 11.3 seconds (A.H. Glenn and Associates Services, 2011). These wave characteristics represent conditions that cause the greatest forces normal to pipeline route (A.H. Glenn and Associates Services, 2011), indicating that bedload transport would occur over the entire length of the trench. For these conditions, the net unit bedload transport rate is estimated to be approximately 13.1 m^2/day. The duration of the 5-year wave event was not specified in the A.H. Glenn and Associates Services (2011) wave report. As a conservative approximation, this 5-year event was assumed to occur over an eight hour period. With this short duration, the unit bedload transport rate corresponds to trench infill of 24,300 m3 (31,800 yd^3). If the 5-year wave event had a 24-hour duration, trench infill would be three times greater. These values are representative of conditions for the seaward end of the trench. Infill rates for the shoreward end of the trench would be greater.

4. INTERPRETATION OF SEDIMENT TRANSPORT SIMULATION RESULTS

Sediment transport simulation results for each sediment release scenario provide a means to assess potential impacts of pipeline construction on the water column and sediment bed. The "worst case" jet trenching scenarios are illustrative because the total mass of sediment released to the water column is identical for each trenching rate case. Simulated suspended solids plumes and patterns of deposition differ between each case as a function of trenching rate, which controls construction duration and the rate of sediment release.

As trenching rates increase, the time over which a plume exists is shorter because construction duration is shorter. For the 366 m/hr (1,200 ft/hr) jet trenching case, construction duration is roughly 9 hours and is completed is less than one tidal cycle. However, plume extent is larger because the sediment mass released per unit time is larger and higher concentrations of suspended solids occur at greater distances from the trench. During peak tidal currents, water column bottom layer solids concentrations in the range of 50-100 mg/L can occur at distances of 4 kilometers (2.5 miles) from the trench. The water column plume dissipates within 4 hours following the end of construction. Including time for construction, a plume would occur over a 13-hour period. Solids deposition to the sediment bed greater than 0.3 cm (~0.1 inches) occurs in a roughly 630 meter (~0.4 mile) corridor adjacent to the trench. However, deposition is largely limited to one side (the west side) of the trench as controlled by tidal flows that occur in a single tidal cycle. It should be noted that sediment deposition on the west side of the trench is a reflection of conditions where tidal currents begin moving from east to west during the construction period. If construction were timed to occur when tidal currents were moving from west to east, sediment deposition would occur on the east side of the trench.

As trenching rates decrease, the time a water column plume exists is longer because construction duration is longer. For the 122 m/hr (400 ft/hr) jet trenching case, construction duration is roughly 26 hours and occurs over two tidal cycles. Plume extent is smaller because the sediment mass released per unit time is smaller. High suspended solids concentrations only occur at shorter distances from the trenching. During peak tidal currents, water column bottom layer solids concentrations in the range of 50-100 mg/L occurred at distances of 1.7 kilometers (~1.1 mile) from the trench. The water column plume dissipates within 4 hours following the end of construction. Including time for construction, a plume would occur over a 30 hour period for this case. Solids deposition to the sediment bed greater than 0.3 cm (~0.1 inches) occurs in a roughly 750 meter (~0.5 mile) corridor adjacent to the trench. However, deposition occurs on both sides of the trench in a sinusoidal pattern as controlled by the flood and ebb of tidal currents over roughly two tidal cycles.

Plume extent and sediment deposition patterns for the 183 m/hr (600 ft/hr) jet trenching case are intermediate between the other cases. Construction duration is just over 17 hours. During peak tidal currents, water column bottom layer solids concentrations in the range of 50-100 mg/L can occur at distances of 2.7 kilometers (1.7 miles) from the trenching site. As with the other two cases, the water column plume dissipates within 4 hours following the end of construction. Including time for construction, a plume would occur over a 21 hour period. Sediment deposition greater than 0.3 cm (~0.1 inches) occurs in a roughly 720 meter (~0.45 mile) corridor on both sides of the trench in a sinusoidal pattern as controlled by changing tidal currents over time. However, deposition patterns are less sinuous than occur for the 122 m/hr scenario because construction is completed in less two tidal cycles.

Plume extent and sediment deposition patterns for more typical jetting and both mechanical plowing scenarios exhibit patterns similar to the "worst case" jetting cases. However, the magnitude of plume suspended solids levels and as well as the depth of sediment accumulation on the bed are reduced because the total mass of sediment released during construction for these cases is reduced. Spatial extents of plumes and areas of sediment accumulation are also reduced. Those reductions occur in proportion to total sediment release. Water column plumes for these scenarios dissipate within 4 hours following the end of construction.

Trench construction by mechanical (clamshell) dredging differs from any jetting or plowing case. In this case, construction occurs over a period of just over 31 days. Near bed suspended solids concentrations are lower but occur over a much longer period compared to other cases. Sediment accumulation on the bed surface is somewhat lower than for other trenching cases but is spread more uniformly on either side of the trench because construction occurs over many more tidal cycles. Nonetheless, water column plumes dissipate within four hours following the end of construction.

Results for hand jetting at the hot tap site and clamshell dredging at the HDD exit pit are also similar in that the extent and magnitude of plumes is a reflection of the total mass of sediment released and the rate at which that release occurs. Patterns of sediment accumulation for these scenarios differ because hand trenching at the hot tap site has a duration of only 8 hours per pulse. In contrast, sediment accumulation for clamshell dredging at the HDD pit is spread over a wider area because dredging occurs over a much long period of time and subject to a wider range of transport conditions including flood and ebb tide cycles.

Uncertainties in wave conditions and estimated bedload transport influence trench infill rates. Significant wave height estimates for a 40-ft deep water column were used to drive bedload calculations. As waves move into shallow water, sediment transport rates will increase. Noting that bedload transport is nonlinear (because rates are based on shear stress exponentiated to the 1.5 power), the combined impact of currents and waves may

lead to larger trench infill rates. However, infilling would be controlled by the frequency, duration, and direction of wave events.

It must also be recognized that fine-scale hydrodynamic factors may also affect trench infill rates. At scales on the order of 0.1-1 m, vortices near the sediment bed can develop when currents flow around seabed obstructions like pipelines and other obstacles. These three-dimensional flow features can act to scour material away from any obstruction. The scale of such flow features is much finer than the spatial resolution of the hydrodynamic model grid and cannot be directly resolved. However, seabed images transmitted during a remotely operated vehicle survey of the pipeline route do not show evidence that scour holes occur around obstructions under typical conditions (Figure 94).

5. DISCUSSION

New York State Department of Environmental Conservation (NYSDEC) personnel and representatives of other agencies requested information and posed a series of questions regarding Rockaway delivery lateral hydrodynamic and sediment transport analysis. This section of the report groups those questions and information requests by topic to facilitate communication of hydrodynamic and sediment transport analysis results to reviewers.

5.1. DOCUMENTATION OF MODEL CONDITIONS AND ASSUMPTIONS

NYSDEC and others requested that assumptions be fully documented in the report. This request was accommodated by providing descriptions of:

- Model equations to document controlling parameters for hydrodynamics (Section 2.1) and sediment transport (Section 2.2);
- Site-specific measurement use for model set-up and calibration for the July-August 2009 ADCP deployment period at the site (Sections 3.1 and 3.2, Figures 1-10, Tables 1-2). Parameterizations for both hydrodynamics and sediment transport are described in those report sections. Grain size data used to drive sediment transport simulations were based on measurements from sediment grab samples collected along the pipeline route. Tables 1-2 also provide notes describing the basis for assigning each model parameter;
- Details of model application for pipeline installation tasks (Section 3.3.1) with specific details for each of the seven scenarios evaluated (Sections 3.3.2-3.3.8). Sediment releases in all scenarios were simulated as point sources to the water column. These point sources move from cell to cell along the pipeline route in the model over time. The grain size distribution of sediments released by the point sources is identical to sediments. The sediment volume released in each scenario is summarized in Table 4.

5.2. COEFFICIENT OF DRAG, MODEL SIMULATION TIMEFRAMES, AND SEASONALITY

As noted in Sections 2.1 and 3.2 and Table 1, the principle model calibration parameter is the coefficient of drag (C_D). This parameter affects momentum loss as water moves over the seabed and interacts with the shoreline. Based on comparisons to measurements for the July-August 2009 period at the Sandy Hook tide gage and ADCP deployment site, the minimum drag coefficient ($C_{D,min}$) was set to a value of 0.003 and is constrained by the roughness and composition of material on the seabed surface. For this area of the ocean in the New York Bight Apex, the drag coefficient is not expected to vary by season. This expectation is borne out by simulations conducted using the regional model prepared for

USEPA as part of LPR/NB Superfund efforts. The regional model was used to perform simulations for a 16-year period (1995-2010) and the best match of hourly water surface elevations and other conditions was achieved when $C_{D,min}$ = 0.003. This drag coefficient parameterization is also consistent with literature values for a smooth, fine sand bed that is largely planar (bedform heights on the order of 1 cm) (see Soulsby, 1997).

Model sensitivity to changes in the minimum drag coefficient depends how boundary conditions are represented. In ECOM, two general classes of boundary conditions can be specified, clamped (non-radiative) or radiative. When clamped boundary conditions are specified, amplitudes of simulated tidal elevations tend to decrease, velocities increase, and time between peaks decrease as $C_{D,min}$ decreases. Conversely, amplitudes of simulated tidal elevations tend to increase, velocities decrease, and time between peaks tends to increase as $C_{D,min}$ increases when using clamped boundary conditions. When radiative boundary conditions are specified, the model is less sensitive to $C_{D,min}$ because waves generated within the model domain can more readily move across open boundaries. Open ocean boundary conditions represent water surface elevations determined from the LPR/NB regional model developed for USEPA. Water surface elevations from the LPR/NB model were themselves derived from NOAA tide gage measurements for the region.

Initial hydrodynamic simulations for Rockaway Delivery Lateral Project were performed using clamped boundary conditions and $C_{D,min}$ values very varied between 0.002 to 0.006. Based on graphical comparisons, best fit between measured and simulated conditions was achieved when $C_{D,min}$ was 0.003. Given that a $C_{D,min}$ value of 0.003 was also consistent with parameterization of the regional model used for LPR/NB Superfund efforts, and which was used to simulate 16 years (1995-2010) with all tidal cycles, including spring tides and neap tides), this model parameterization was considered to be reasonable. Subsequent simulations for the Rockaway Delivery Lateral Project were performed using the Inverted Reid and Bodine radiative boundary condition (see p. 13 of HydroQual, 2010) at open ocean boundaries to improve model numerical stability. As a consequence of using radiative boundary conditions, hydrodynamic and sediment transport simulation results presented in this report are not very sensitive variation of the minimum drag coefficient.

Model calibration was performed for a July-August, 2009 timeframe because that period includes measurements for the NOAA Sandy Hook tide gage and also site-specific ADCP measurements collected at a point near the south end of the proposed pipeline. However, the model simulate other timeframes because $C_{D,min}$ depends on bed composition and is not expected to vary over time. For example, seabed composition is not expected to very widely over time, changing from fine sand to gravel and cobbles and back to sand. Although bed composition is expected to be constant, it is possible for bedforms such as ripples or dunes to develop over time in response to changes in tides and meteorological conditions. Bedforms can impact sediment transport simulations and the model accounts for these types of variations using the shear stress partitioning approach described in Appendix A.

It is important to recognize that hydrodynamic and sediment transport simulations are performed using tidal and meteorological conditions applicable to the timeframe for each simulation. The calibration period was July-August, 2009 and tidal and meteorological conditions in that simulation are those that were measured for that period. Pipeline site preparation and construction activities are scheduled for early March and early May timeframes. Representative tidal and meteorological conditions for those simulations were selected based on review of 16 years of results from the LPR/NB regional model for March and May periods. For the Rockaway Delivery Lateral Project, conditions for March and May, 2010 were judged to be representative of long-term conditions for those months. Tidal and meteorological conditions for March and May, 2010 were used in preference to long-term averages so that simulations reflected measurements and also so that timings of features such as spring tides and neap tides would be retained in each simulation.

The March and May 2010 timeframes both begin shortly after the new moon (i.e. just after spring tide) and follow the sequence of conditions as they were measured at those times. Jet sled or mechanical plow trenching scenarios have durations of 10 days, with sediment releases from construction completed in 2 days. The mechanical dredge trenching scenario has a duration of 30 days, with all sediment releases completed in 28 days. The hot tap hand jetting scenario has a duration of 10 days, with sediment releases occurring in three 8-hour pulses over a period of 3 days. The HDD exit pit mechanical dredging scenario has a duration of 10 days, with sediment releases occurring over a period of approximately 7 days.

5.3. WORST CASE CONDITIONS FOR JET SLED SCENARIOS

Sediment transport simulation results for jet sled scenarios are expected to overstate the extent of water column and sediment impacts from construction. The "worst case" jet sled scenario represents the maximum possible upper bound for any sediment release because the sediment volume released to the water column is equal to 100% of the volume of all sediment disturbed (plus an additional 10% contingency), with a trench cross-sectional area that far exceeds the likely footprint needed be displaced to install the pipeline package. Even the "typical" jet sled scenario is expected to be an upper bound for typical conditions because the sediment volume released still exceeds the likely footprint of sediment needed to be displaced to install the pipeline package. In contrast, mechanical plowing scenarios assume that only 15-20% the disturbed sediment volume would be released to the water column. However, the reliability of this assumption could not be directly verified in peer-reviewed literature or other publications. It is important to note that differences between simulations would be smaller if the sediment volumes released were more similar.

5.4. ANTICIPATED RATES OF TRENCH INFILL

Rates of trench infill are estimates. Under ambient conditions, little sediment transport is expected because shear stresses acting on the sediment grains on the bed surface are generally below critical shear stresses for erosion (incipient motion threshold). This is consistent with nearly plane bed conditions observed during remotely operated vehicle surveys of the pipeline route. This is also consistent with the occurrence of clam dredge scars observed during seabed surveys. However, the occurrence of small, tightly spaced ripples on the bed surface also suggest that waves interact with the bed. The combined effect of waves and currents could readily mobilize bed sediments and transport them as bedload. Sediments moving as bedload would be intercepted by the open trench until the trench returned to grade or close to it.

Bedload is nonlinear. A doubling of near-bed velocities would more than double shear stresses on particles and generate substantial bedload transport. Annual wave events may generate substantial trench infill rates, particularly at the shoreward area of the pipeline route. Larger waves are reasonably expected to transport more sediment over the entire length of the trench. Although such storms with large waves are infrequent, it might only take one event to return the trench to grade.

Apart from infill by bedload transport, it should be recognized that a considerable portion of the sediments disturbed during trenching may fall back into the trench. This would at least partially bury the pipeline at the time of construction. For example, jetted or plowed sediments are likely to slump into the trench until sediment comprising trench walls reach a stable angle of repose.

6. REFERENCES

A. H. Glenn and Associates Services. 2011. Selected Meteorological And Oceanographic Data at a Location Offshore Rockaway Beach, New York. A. H. Glenn and Associates Services, Metairie, Louisiana. 22 p.

Ahsan, A. K. M. Q., and Blumberg, A. F. 1999. A three-dimensional hydrothermal model of Onondaga Lake, New York. Journal of Hydraulic Engineering, 125(9):912-923.

Blumberg, A. F. and Mellor, G. L. 1983. Diagnostic and prognostic numerical circulation studies of the South Atlantic Bight. Journal of Geophysical Research, 88:4579-4592.

Blumberg, A. F. and Mellor, G. L. 1985. A simulation of the circulation in the Gulf of Mexico. Israel Journal of Earth Sciences, 34:122-144.

Blumberg, A. F., and Mellor, G. L. 1987. A description of a three-dimensional coastal ocean circulation model. In: Three-Dimensional Coastal Ocean Models. N.S. Heaps (ed.) American Geophysical Union, Washington DC. pp. 1-16.

Blumberg, A. F., and Goodrich, D. M. 1990. Modeling of wind-Induced destratification in Chesapeake Bay. Estuaries, 13:1236-1249.

Blumberg, A. F., Signell, R. P., and Jenter, H. L. 1993. Modeling transport processes in the coastal ocean. Journal of Marine Environmental Engineering, 1:3-52.

Blumberg, A. F., Khan, L. A., and St. John, J. P. 1999. Three-dimensional hydrodynamic model of New York Harbor Region. Journal of Hydraulic Engineering, 125:799-816.

Blumberg, A. F., and Kim, B. N. 2000. Flow balances in St. Andrew Bay revealed through hydrodynamic simulations. Estuaries, 23:21-33.

Cheng, N. S. 1997. Simplified settling velocity formula for sediment particle. Journal of Hydraulic Engineering, 123(2):149-152.

Clarke, T. L., Swift, D. J. P., and Young, R. A. 1982. A numerical model of fine sediment transport on the continental shelf. Environmental Geology, 4(2):117-129.

Clarke, T. L., Swift, D. J. P., and Young, R. A. 1983. A stochastic modeling approach to the fine sediment budget of the New York Bight. Journal of Geophysical Research, 88(C14):9653-9660.

Fenton, J. D. 1988. The numerical solution of steady water wave problems. Computers and Geosciences, 14:357-368.

Fenton, J. D. 2012. Use of the program FOURIER for steady waves. http://johndfenton.com/Steady-waves/Instructions.pdf. (Accessed on April 30, 2013.)

Galerpin, G., Kantha, L. H., Hassid, S., and Rosati, A. 1988. A quasi-equilibrium turbulent energy model for geophysical flows. Journal of Atmospheric Science, 45:55-62.

Galperin, B., and Mellor, G. L. 1990a. A time-dependent, three-dimensional model of the Delaware Bay and River System, part 1: description of the model and tidal analysis. Estuarine and Coastal Shelf Science, 31:231-253.

Galperin, B., and Mellor, G. L. 1990b. A time-dependent, three-dimensional model of the Delaware Bay and River System, part 2: three-dimensional flow fields and residual circulations. Estuarine and Coastal Shelf Science, 31:255-281.

Galperin, B., and Mellor, G. L. 1990c. Salinity intrusion and residual circulation in Delaware Bay during the drought of 1984. In: Residual Currents and Long-Term Transport (Coastal and Estuarine Studies, Volume 38). Cheng, R. T., ed. Springer-Verlag, Inc., New York. p. 469-480.

Gessler, J. 1965. The Beginning of Bedload Movement of Mixtures Investigated as Natural Armouring in Channels. Technical report No. 69, The Laboratory of Hydraulic Research and Soil Mechanics, Swiss Federal Institute of Technology, Zurich (translation by W. M. Keck Laboratory of Hydraulics and Water Resources, California Institute of Technology, Pasadena, California).

Gessler, J. 1967. The beginning of bedload movement of mixtures investigated as natural armoring in channels. California Institute of Technology, Pasadena, California. 89pp.

Gessler, J. 1971. Beginning and ceasing of sediment motion. In: River Mechanics, Shen, H.W., ed. Fort Collins, Colorado. pp. 7:1–7:22.

Guo, J. 2002. Hunter Rouse and Shields diagram. Proceedings of the 13th International Association of Hydraulic Research Asian and Pacific Division Congress, Singapore, Malaysia, August 6-8.

HQI. 1999a. Newton Creek Water Pollution Control Project East River Water Quality Plan, Report to NYCDEP. Task 10.0 System-Wide Eutrophication Model (SWEM) Sub-task 10.1 Construct SWEM. Prepared under subcontract to Greeley and Hansen, New York, NY. HydroQual, Inc., Mahwah, New Jersey.

HQI. 1999b. Newton Creek Water Pollution Control Project East River Water Quality Plan, Report to NYCDEP. Task 10.0 System-Wide Eutrophication Model (SWEM) Sub-

task 10.2 Obtain and Reduce Loading/Water Quality Data. Prepared under subcontract to Greeley and Hansen, New York, NY. HydroQual, Inc., Mahwah, New Jersey.

HQI. 1999c. Newton Creek Water Pollution Control Project East River Water Quality Plan, Report to NYCDEP. Task 10.0 System-Wide Eutrophication Model (SWEM) Sub-task 10.4 Calibrate SWEM Water Quality. Prepared under subcontract to Greeley and Hansen, New York, NY. HydroQual, Inc., Mahwah, New Jersey.

HQI. 1999d. Newton Creek Water Pollution Control Project East River Water Quality Plan, Report to NYCDEP. Task 10.0 System-Wide Eutrophication Model (SWEM) Sub-task 10.5 Apply SWEM for Preliminary Facility Design. Prepared under subcontract to Greeley and Hansen, New York, NY. HydroQual, Inc., Mahwah, New Jersey.

HQI. 1999e. Newton Creek Water Pollution Control Project East River Water Quality Plan, Report to NYCDEP. Task 10.0 System-Wide Eutrophication Model (SWEM) Sub-task 10.6 Validate SWEM Hydrodynamics. Prepared under subcontract to Greeley and Hansen, New York, NY. HydroQual, Inc., Mahwah, New Jersey.

HQI. 1999f. Newton Creek Water Pollution Control Project East River Water Quality Plan, Report to NYCDEP. Task 10.0 System-Wide Eutrophication Model (SWEM) Sub-task 10.7 Final Facility Design. Prepared under subcontract to Greeley and Hansen, New York, NY. HydroQual, Inc., Mahwah, New Jersey.

HQI. 2001. Enhancement and application of a PCB fate and transport model for Green Bay. HydroQual, Inc., Mahwah, New Jersey. 100 p.

HQI. 2002. Calibration Enhancement of the System-Wide Eutrophication Model (SWEM) in the New Jersey Tributaries, Report to NJDEP. Final Technical Report April 23, 2001 through July 31, 2002. Prepared under subcontract to Passaic Valley Sewerage Commissioners, Newark, NJ. HydroQual, Inc., Mahwah, New Jersey.

HQI. 2005. Near field and far field study for the R.E. Ginna Nuclear Power Plant, Constellation Energy. HydroQual, Inc., Mahwah, New Jersey.

HQI. 2007. A model for the evaluation and management of contaminants of concern in water, sediment and biota in the NY/NJ Harbor Estuary: Contaminant fate & transport & bioaccumulation sub-models. Prepared for the Contamination Assessment and Reduction Project (CARP) Management Committee. HydroQual, Inc., Mahwah, New Jersey.

HQI. 2008. Near Field and Far Field Thermal Modeling Study for the Nine Mile Point Nuclear Power Plant, Constellation Energy. HydroQual, Inc., Mahwah, New Jersey.

HQI. 2010. A Primer for ECOMSED (Version 1.4-LPR): Users Manual. HydroQual, Inc., Mahwah, New Jersey. 218 p. (Release Date: March 5, 2010.)

James, S. C., Jones, C. A., Grace M. D., and Roberts, J. D. 2010. Advanced in sediment transport modeling. Journal of Hydraulic Research, 48(6):754-763.

Jepsen, R., Roberts, J., and Lick, W. 1997. Effects of bulk density on sediment erosion rates. Water, Air, and Soil Pollution, 99(1-4): 21-31.

Jepsen, R., McNeil, J., and Lick, W. 2000. Effects of gas generation on the density and erosion of sediments from the Grand River. Journal of Great Lakes Research, 26(2):209-219.

Jones, C. A., and Lick, W. 2001. Contaminant flux due to sediment erosion. Proceedings of the 7th International Conference: Estuarine and Coastal Modeling, 280–293.

Julien, P. Y. 1998. Erosion and Sedimentation (First Paperback Edition). Cambridge University Press, Cambridge, UK. 280 p.

McNeil, J., Taylor, C., and Lick, W. 1996. Measurement of erosion of undisturbed bottom sediments with depth. Journal of Hydraulic Engineering, 122(6): 316-324.

Mellor, G. L., and Yamada, T. 1982. Development of a turbulence closure model for geophysical fluid problems. Reviews of Geophysics and Space Physics. 20:851-875.

Middleton, G. V. 1984. Mechanics of Sediment Movement. Second Edition. Society of Economic Paleontologists and Mineralogists, Tulsa, OK. 401 pp.

Oey, L. Y., Mellor, G. L., and Hires, R. I. 1985a. A three dimensional simulation of the Hudson-Raritan Estuary, part I: description of the model and model simulations, Journal of Physical Oceanography, 15:1676-1692.

Oey, L. Y., Mellor, G. L., and Hires, R. I. 1985b. A three dimensional simulation of the Hudson-Raritan Estuary, part II: comparison with observations. Journal of Physical Oceanography, 15:1693-1709.

Roberts, J. D., Jepsen, R., Gotthard, D., and Lick, W. 1998. Effect of particle size and bulk density on erosion of quartz particles. Journal of Hydraulic Engineering, 124(12):1261-1267.

Roberts, J.; Jepsen, R., and James, S. 2003. Measurement of sediment erosion and transport with the Adjustable Shear Stress Erosion and Transport flume. Journal of Hydraulic Engineering. 129(11): 862-871.

Shields, A. 1936. Anwendung der aenlichkeitsmechanik und der turbulenzforschung auf die geschiebebewegung. Mitteilungen der Preussischen Versuchsanstalt fur Wasserbau und Schiffbau, Berlin, Germany (translation by W. P. Ott and J. C. van Uchelen, California Institute of Technology, Pasadena, California).

Signell, R., and List, J. 1997. Modeling waves and circulation in Lake Pontchartrain. Gulf Coast Association of Geological Societies Transactions, 47:529-532.

Soulsby, R. 1997. Dynamics of Marine Sands. Thomas Telford Publications, London, UK. 249 pp.

van Rijn, L. C. 1984a. Sediment transport, part I: bed load transport. Journal of Hydraulic Engineering, 110(10):1431-1456.

van Rijn, L. C. 1984b. Sediment transport, part II: suspended load transport. Journal of Hydraulic Engineering, 110(11):1612-1638.

van Rijn, L. C. 1984c. Sediment transport, part III: bed forms and alluvial roughness. Journal of Hydraulic Engineering, 110(12):1733-1754.

van Rijn, L. C. 1993. Principles of sediment transport in rivers, estuaries and coastal seas. Aqua Publications, Amsterdam, Netherlands.

Winterwerp, J. C., and Van Kesteren, W. G. M. 2004. Introduction to the Physics of Cohesive Sediment in the Marine Environment. Elsevier B.V., Amsterdam, Netherlands. 466 p.

TABLES

Table 1. Summary of hydrodynamic model parameter values.

Parameter	*Value*	*Description*	*Notes*
$C_{D,min}$	0.003	minimum coefficient of drag	Primary control on simulated currents; value confirmed by calibration; calibrated value equals value used in other model applications to the area
z_o	0.4 mm	hydrodynamic roughness height of bed	Secondary control on simulated currents, used for calculations in shallow water (depth < 1.5 m); model results in area of proposed pipeline do not depend on z0 because water depth exceeds 1.5 m; assigned value equal value used in other model applications to the area

Table 2. Summary of sediment transport model parameter values.

Sediment Transport Model						
Parameter	*Size Class*					*Source/Notes*
	1	*2*	*3*	*4*	*5*	
d_p (mm)	0.031	0.078	0.188	0.375	2.225	Defined from field data
Bed GSD (%)	2.6	86.2	6.1	2.6	2.5	Defined from field data
d_* (dimensionless)	0.78	1.97	4.75	9.48	56.9	Equation (2-15)
τ_{ce} (Pa), τ_{cd} (Pa)	0.05	0.13	0.15	0.19	1.46	Equation (2-14)
τ_{cs} (Pa)	0.05	0.19	0.24	0.49	5.46	Equation (2-18)
$w_{s,q}$ (cm/s)	0.064	0.383	1.759	4.448	19.39	Equation (2-20)

Notes: GSD = grain size distribution.

Table 3. Summary of surface water turbidity and TSS measurements collected from sites near the proposed pipeline route during Fall 2010.

Station	***Turbidity (NTU)***	***TSS (mg/L)***	***Sample Type***
9-DS-9W	2.4	4	Surface
9-DM-9W	2.8	4	Middle
9-DB-0W	3.3	4	Bottom
11-DS-11W	1.4	1.4	Surface
11-DM-11W	2.9	2.9	Middle
11-DB-11W	2.6	2.6	Bottom
13-DS-13W	0	4	Surface
13-DM-13W	0	4	Middle
13-DB-13W	1.2	16	Bottom
15-DS-15W	0	5	Surface
15-DM-15W	0	4	Middle
15-DB-15W	9.4	18	Bottom
Average	2.2	5.8	
Standard Deviation	2.6	5.3	
Minimum	0.0	1.4	
Maximum	9.4	18.0	

Notes: Samples were collected near the surface, middle and bottom of the water column. Statistical summary values were computed for all depth intervals at all sites. Samples from the bottom depth could be higher than exist under ambient conditions as a consequence of sediment disturbance during sampling.

Table 4. Simulated trenching rates, durations, and sediment release characteristics.

Construction Rate (m/hr or as noted)	***Duration (hrs)***	***Sediment Release Rate (MT/hr)*** *(1)*	***Total Sediment Volume Released (m³)*** *(2)*
Hydraulic Jetting: "Worst" Case			
366 (1200 ft/hr)	8.6	13,695	78,600 (102,800 yd³)
183 (600 ft/hr)	17.2	6,847	
122 (400 ft/hr)	25.8	4,564	
Hydraulic Jetting: "Typical" Case			
183 (600 ft/hr)	17.2	4,127	47,400 (62,000 yd³)
Mechanical Plowing: "Worst" Case			
183 (600 ft/hr)	17.2	486	5,580 (7,300 yd³)
Mechanical Plowing: "Typical" Case			
183 (600 ft/hr)	17.2	364	4,190 (5,475 yd³)
Mechanical (Clamshell) Trenching			
4.2 (13.8 ft/hr) 30 cycles/hr	745.6	103	51,300 (67,100 yd³)
Hand Jetting at Hot Tap Site			
4 pulses	8 (per pulse)	1,114 (per 8-hour pulse)	23,850 (31,200 yd³) (for 4 pulses)
Mechanical Dredging at HDD Pit			
30 cycles/hr	170	103	11,700 (15,300 yd³)

Notes: (1) MT = metric ton; 1 MT = 1,000 kg. (2) Total sediment volume released is in situ volume; sediments are assumed to have a dry bulk density of 1,495 kg/m³.

FIGURES

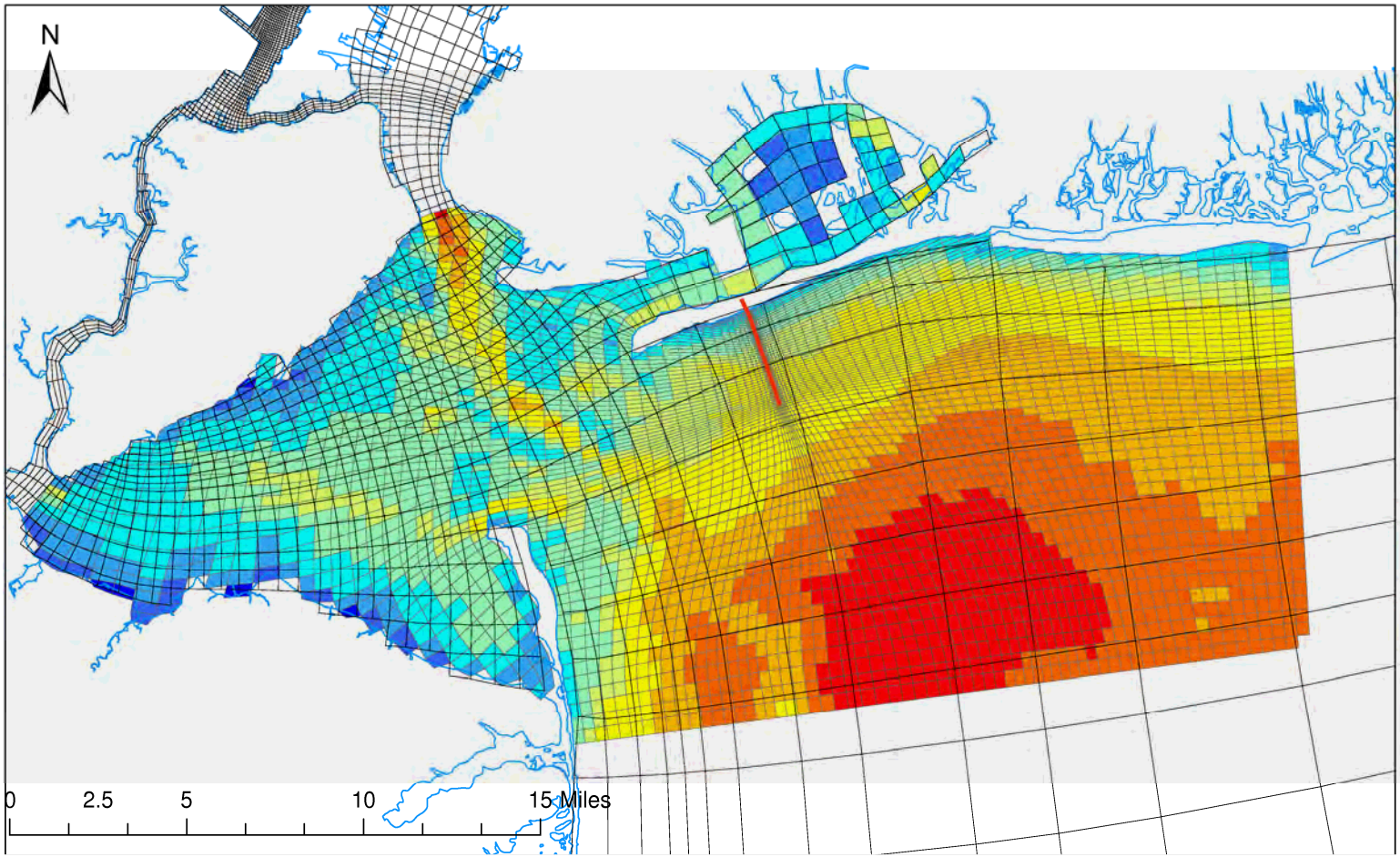

Notes: Pipeline model grid cells are shown as colored rectangles. The color applied to each cell indicates water depth at mean low low water (MLLW) level. Blues represent shallow water, greens and yellows intermediate water depths, and oranges and reds represent deeper water. Water depths in the area range from roughly 1 meter to 30 meters. The pipeline preferred route is shown by the thick red line near the center of the figure. Grid cells from the coarser-scale LPR/NB modeling efforts are shown as larger, uncolored rectangles overlaid on the pipeline model grid cells.

Figure 1. Overview of model grid used for pipeline evaluation efforts.

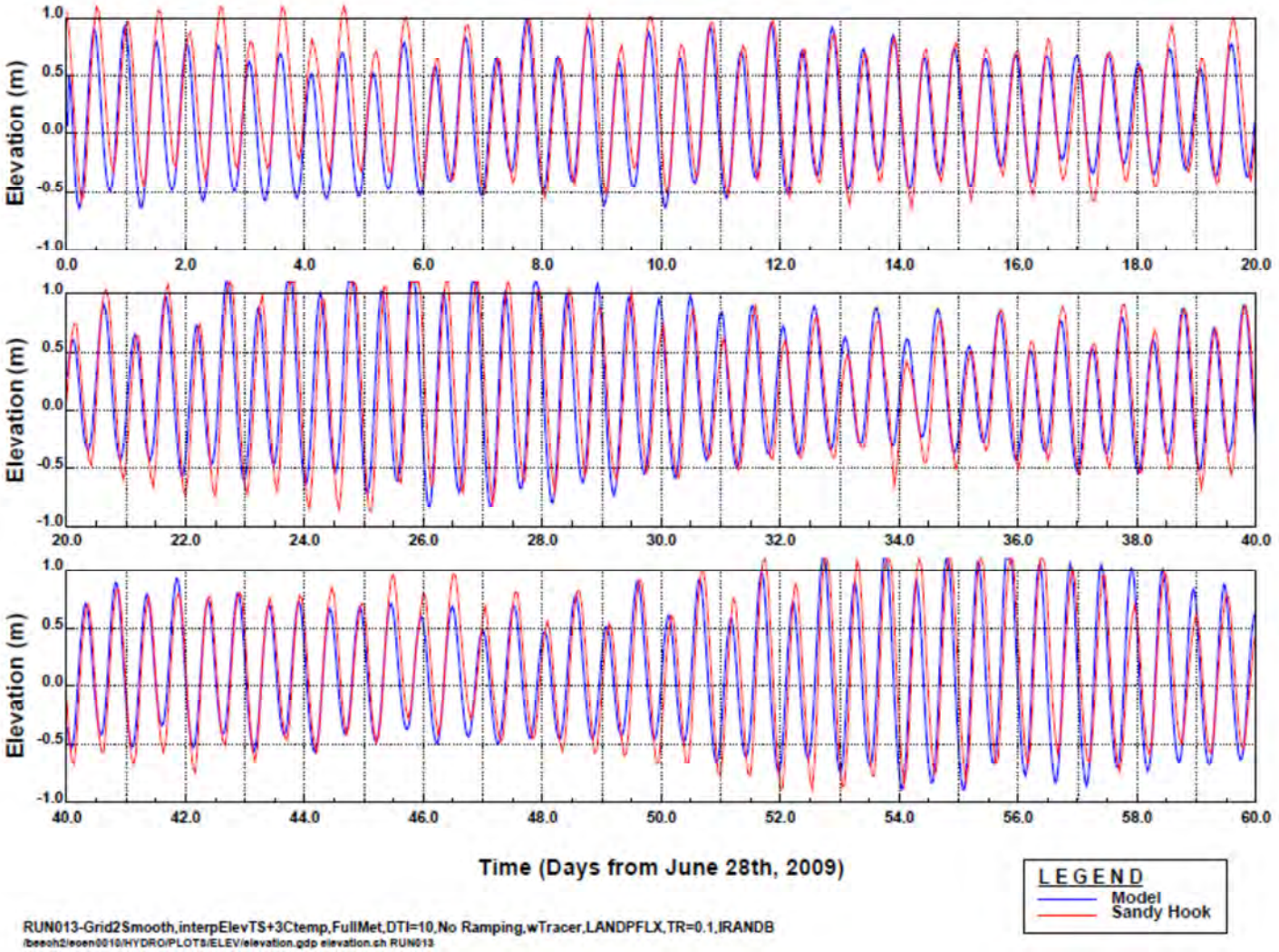

Note: Elevations indicate distance above (+) or below (-) mean sea level (0.0).

Figure 2. Simulated and measured water surface elevations at the Sandy Hook tide gage: July-August, 2009 calibration period.

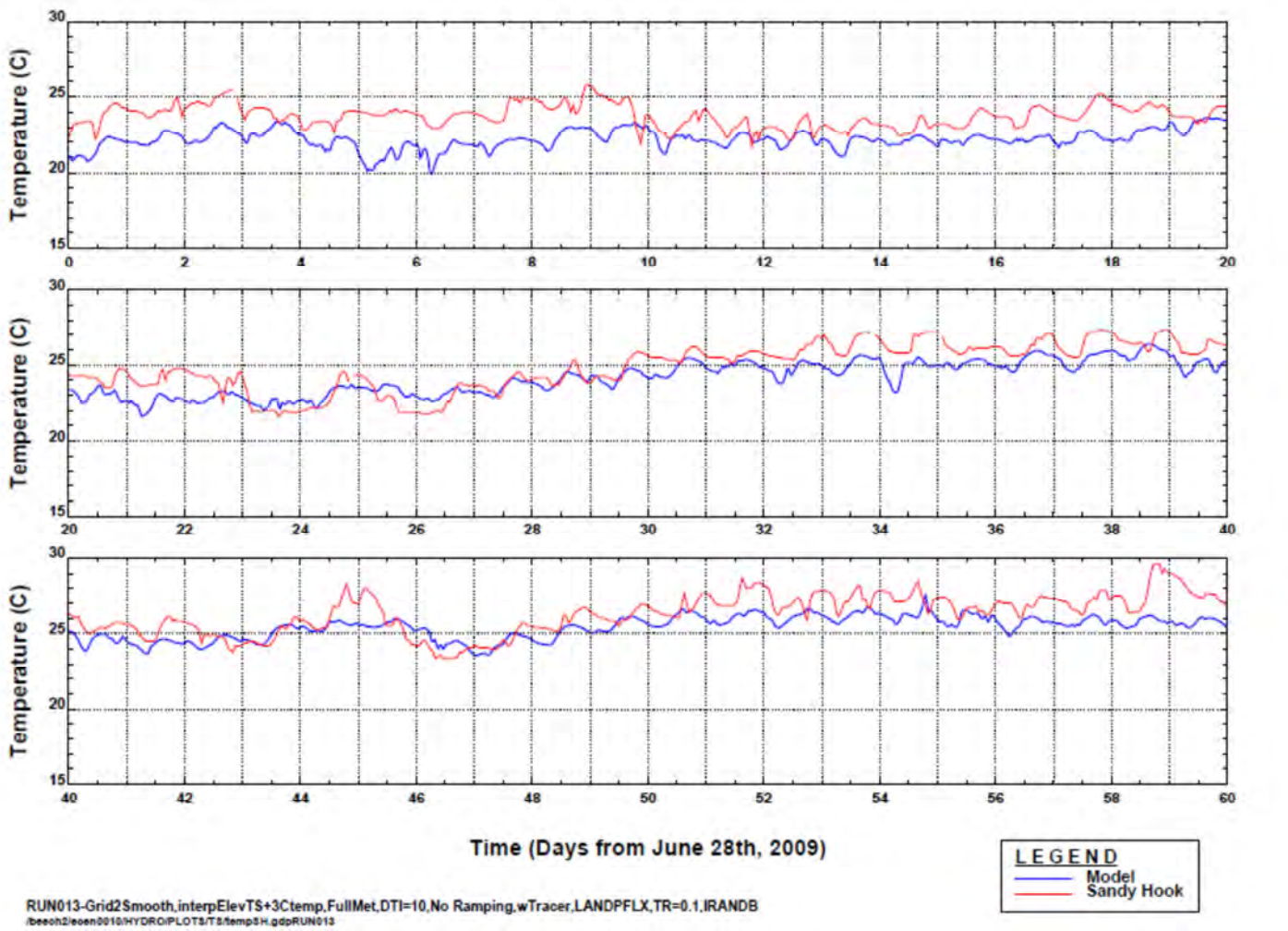

Note: Differences between simulated and measured temperatures during the first 10 days of simulation reflect uncertainty in assigning model initial conditions.

Figure 3. Simulated and measured water temperatures at the Sandy Hook tide gage: July-August, 2009 calibration period.

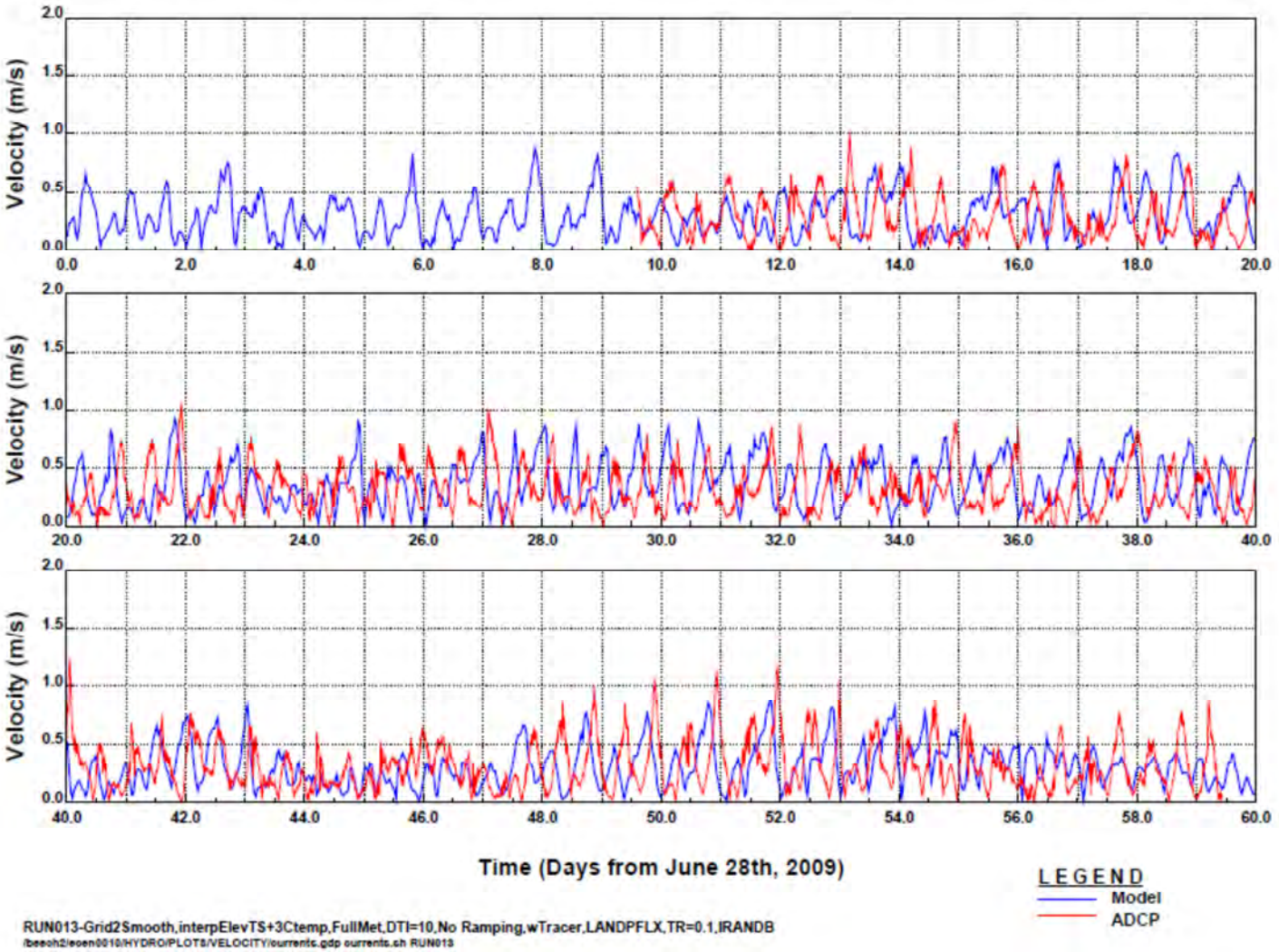

Figure 4. Simulated and measured current velocities in the upper portion of the water column at the ADCP deployment site near the proposed pipeline route: July-August, 2009 calibration period.

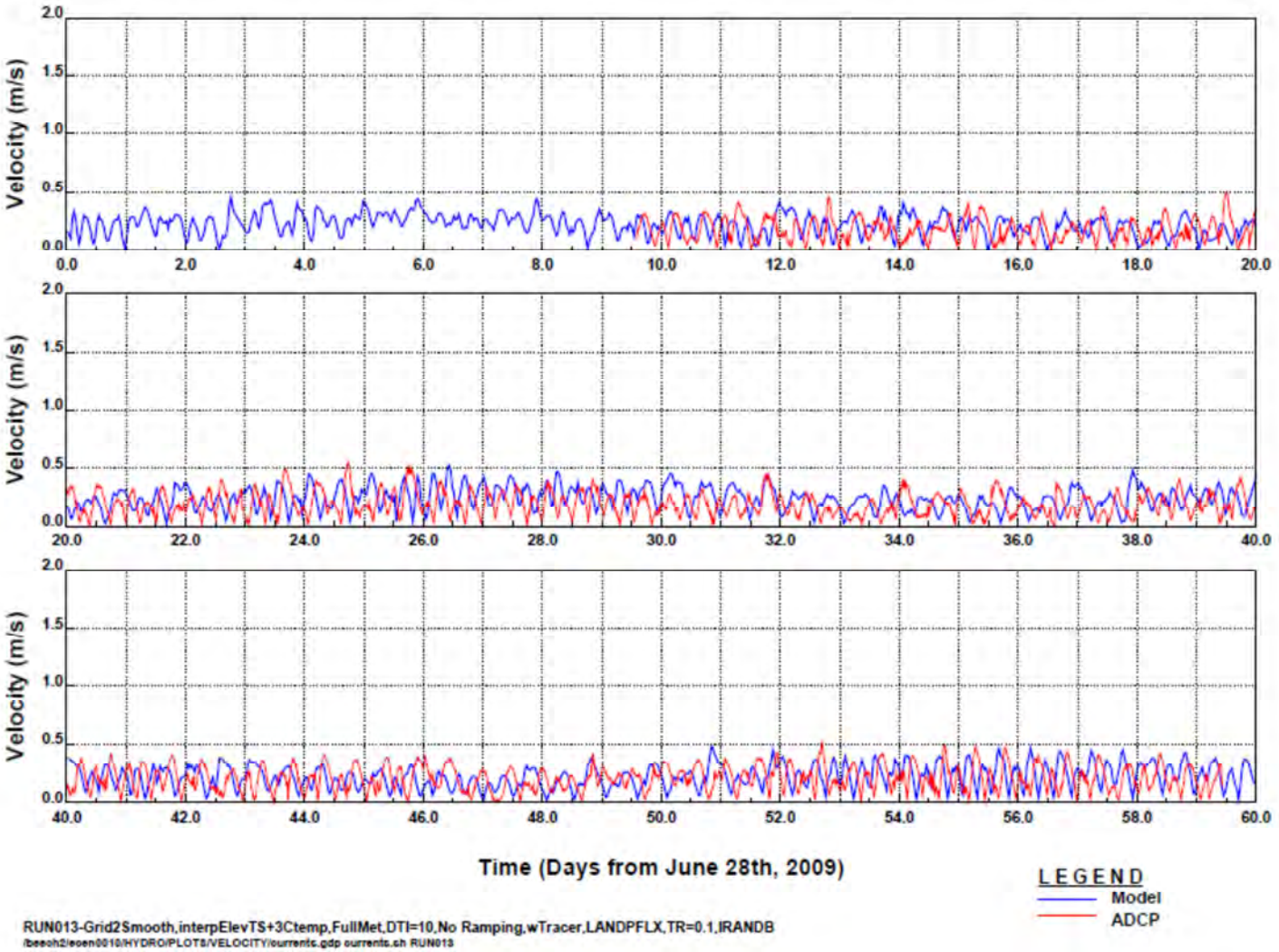

Figure 5. Simulated and measured current velocities in the mid-depth portion of the water column at the ADCP deployment site near the proposed pipeline route: July-August, 2009 calibration period.

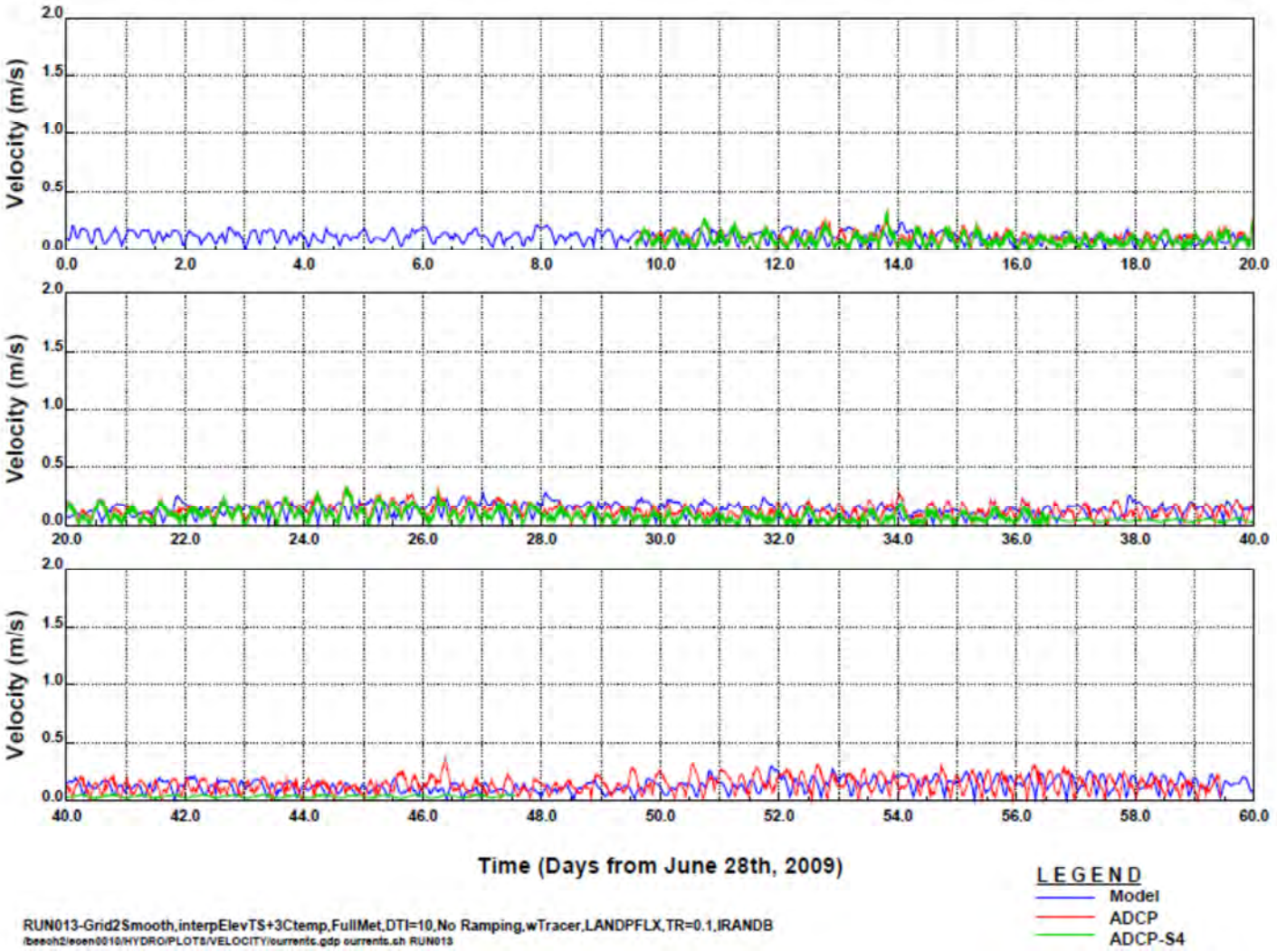

Figure 6. Simulated and measured current velocities in the bottom portion of the water column at the ADCP deployment site near the proposed pipeline route (includes secondary measurements collected using an S4 probe): July-August, 2009 calibration period.

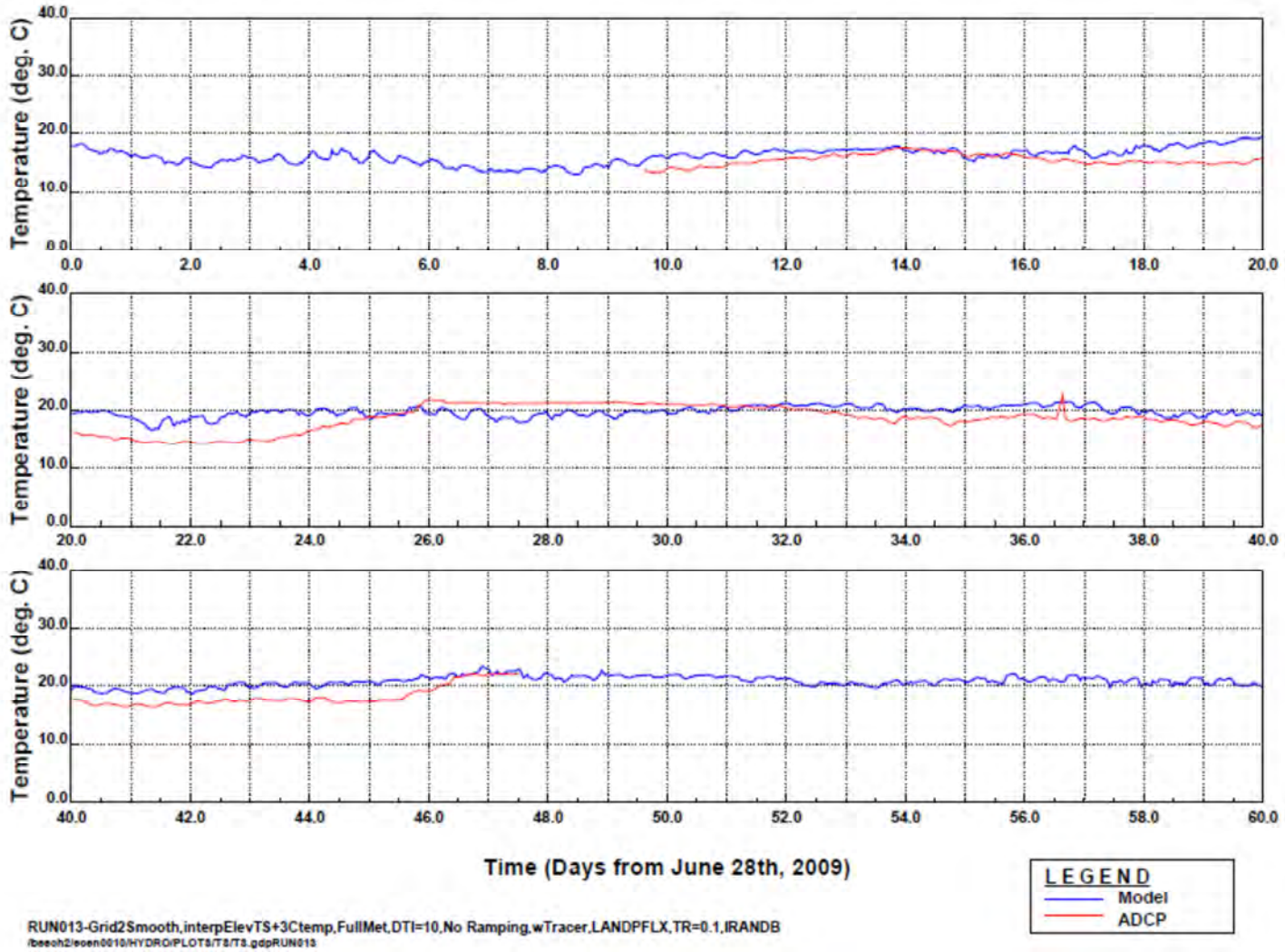

Figure 7. Simulated and measured temperatures in the bottom portion of the water column at the ADCP deployment site near the proposed pipeline route (measurements collected using an S4 probe): July-August, 2009 calibration period.

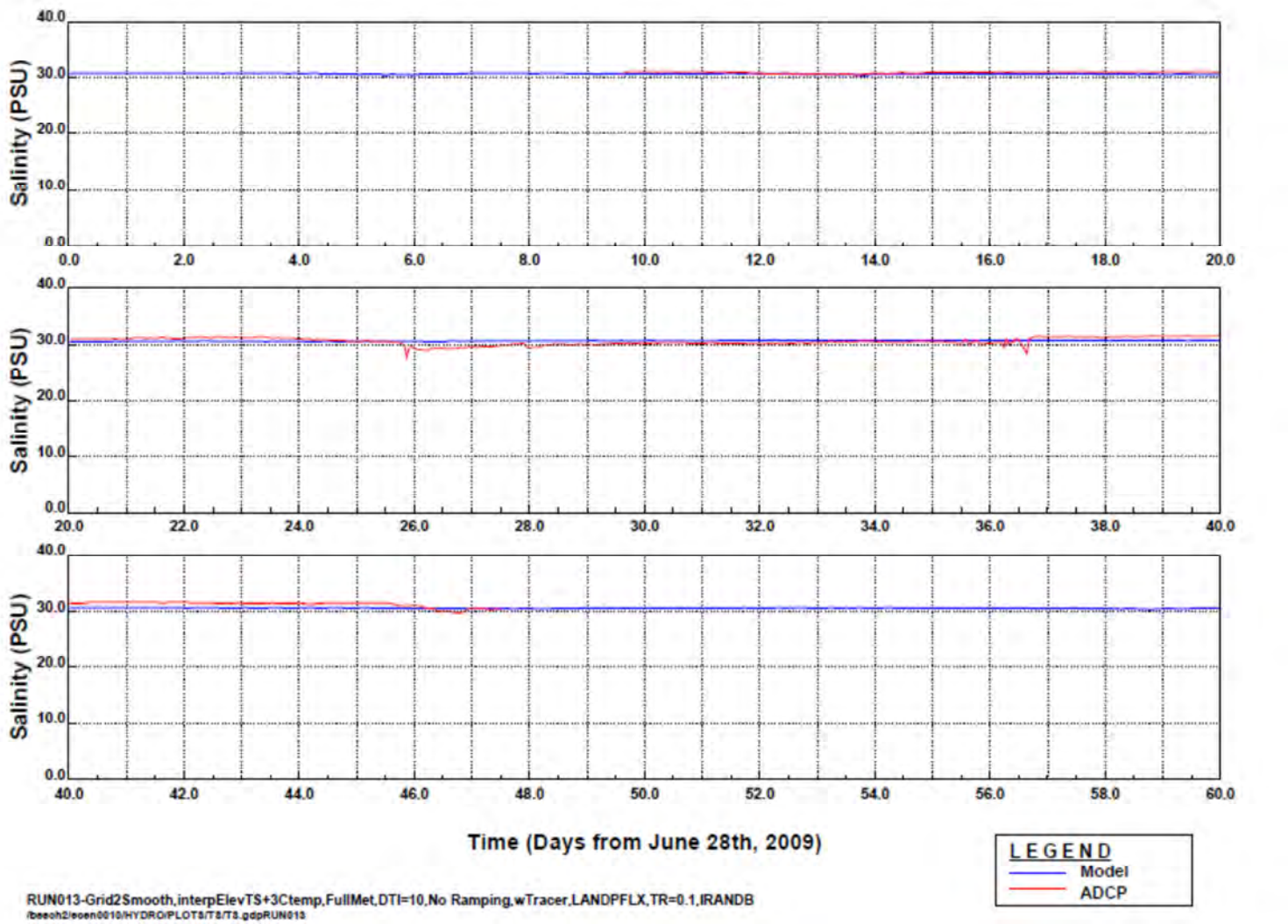

Figure 8. Simulated and measured salinities in the bottom portion of the water column at the ADCP deployment site near the proposed pipeline route (measurements collected using an S4 probe): July-August, 2009 calibration period.

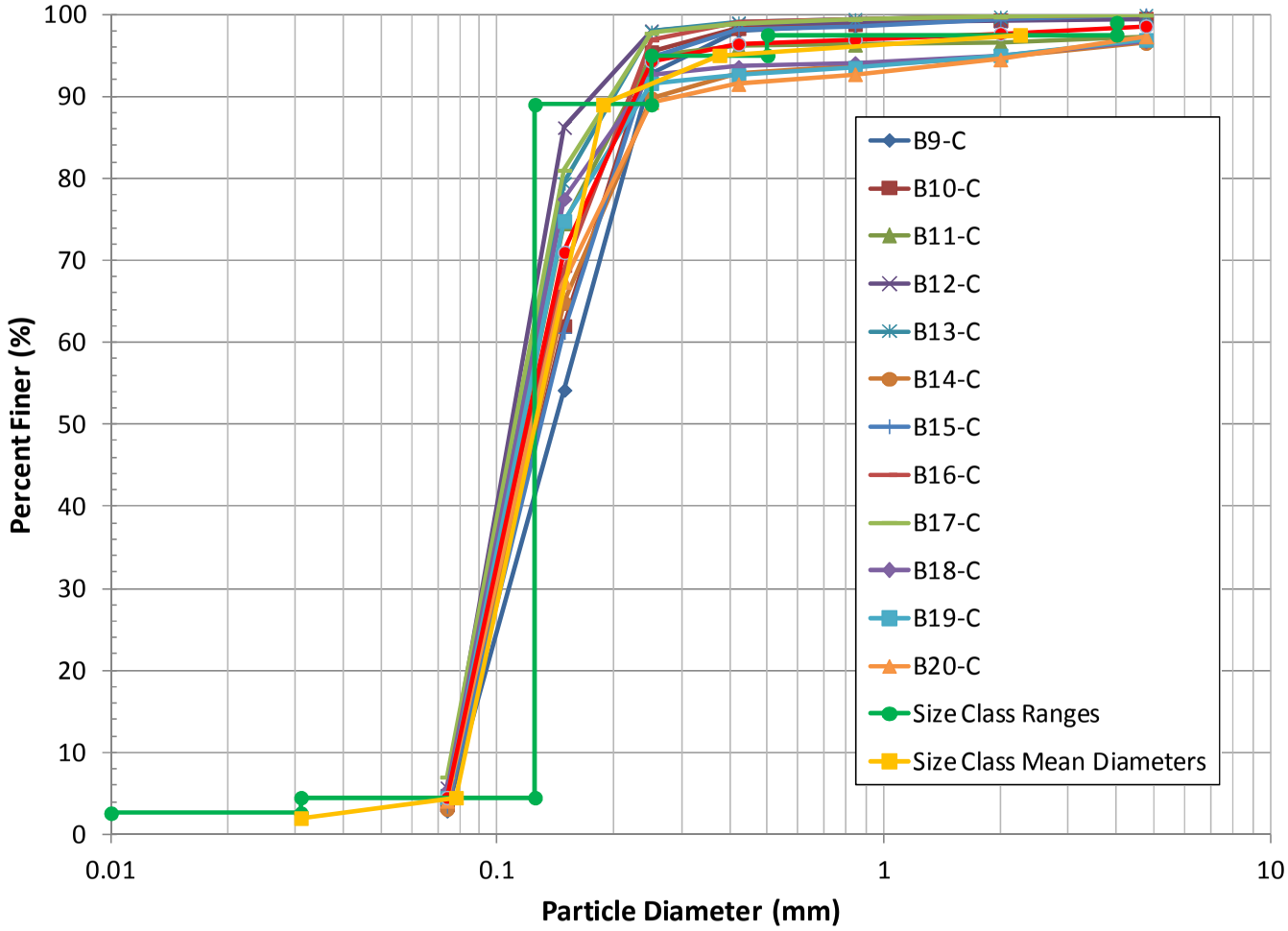

Note: Samples B9-C through B20-C indicate sediment cores collected from the bed along the proposed pipeline route. Those data were used to define size ranges and mean diameters for each particle size class in the sediment transport model.

Figure 9. Grain size distributions of sediments collected along the proposed pipeline route and modeled size classes.

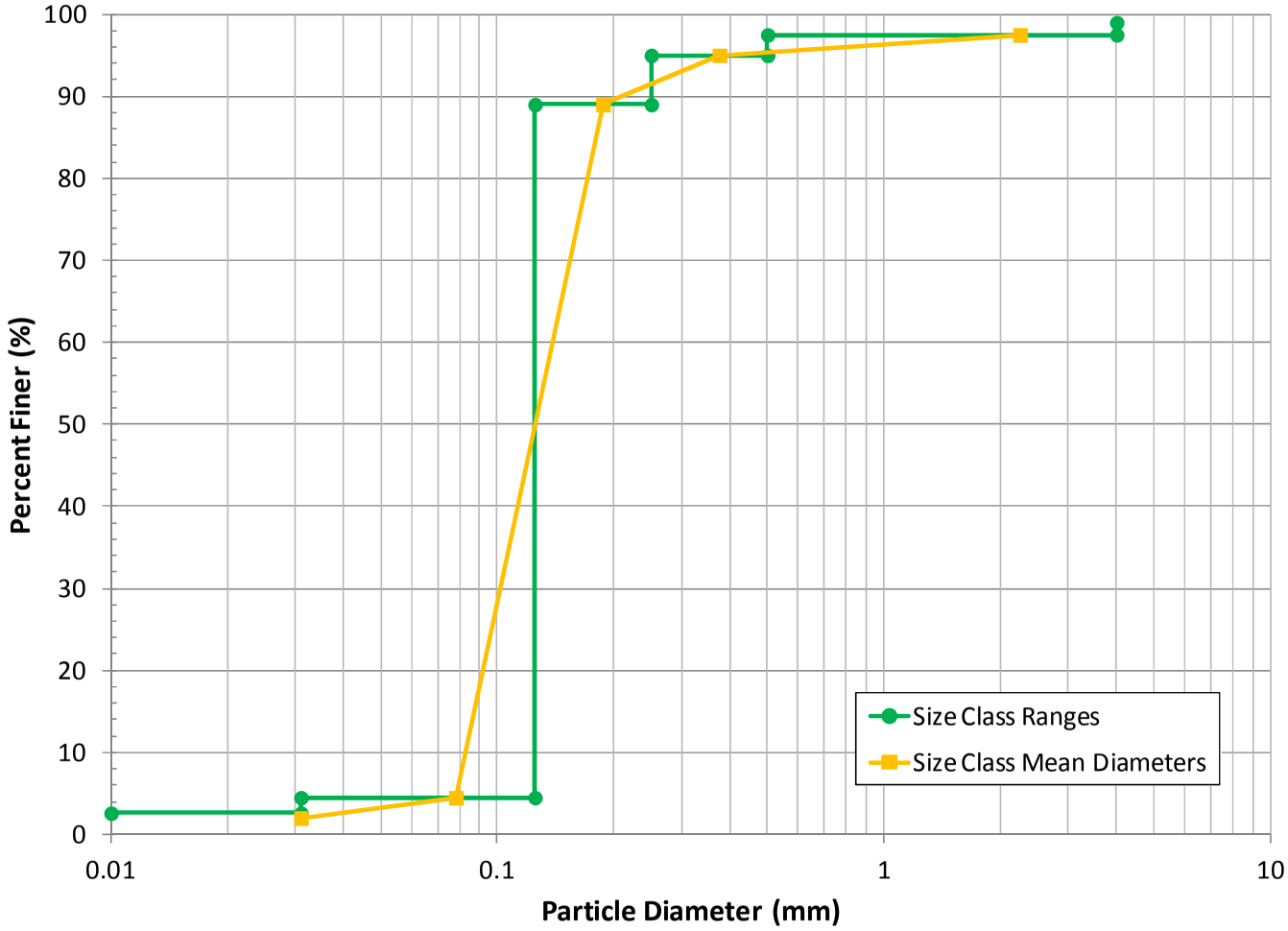

Note: Particle size class ranges and mean diameters in the sediment transport model. These are the same data as presented in Figure 9 with field measurements removed from the plot so that values used in the model are more clearly identifiable.

Figure 10. Particle size class grain size distribution ranges and mean diameters used in the sediment transport model.

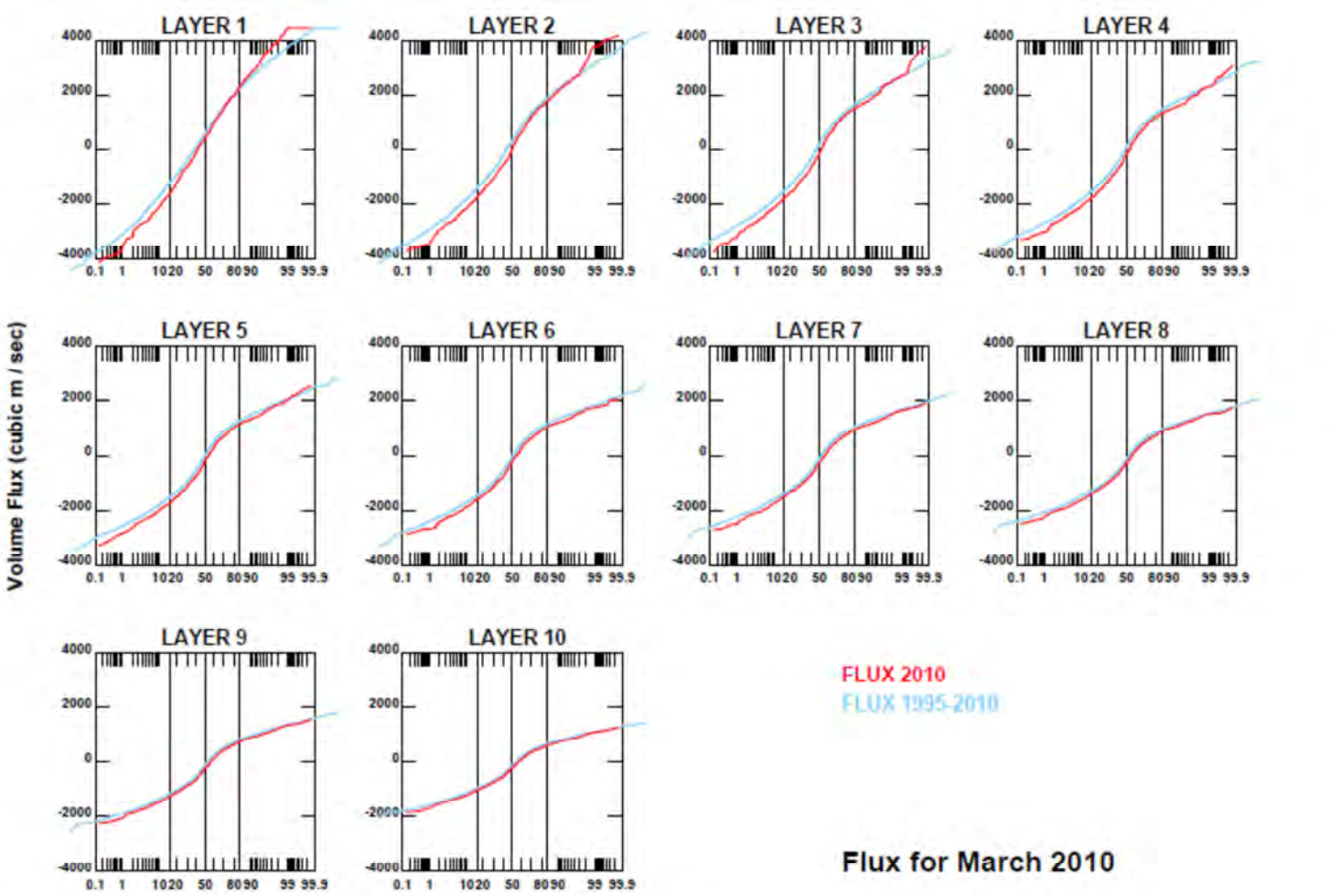

Note: Fluxes for March, 2010 shown in red. Long-term average fluxes (1995-2010) for March shown in blue. Similarity between 2010 and long-term average fluxes in each layer of the water column indicated that Match 2010 is representative of long-term conditions.

Figure 11. Probability distributions of volume fluxes in each water column layer passing proposed pipeline route: March, 2010.

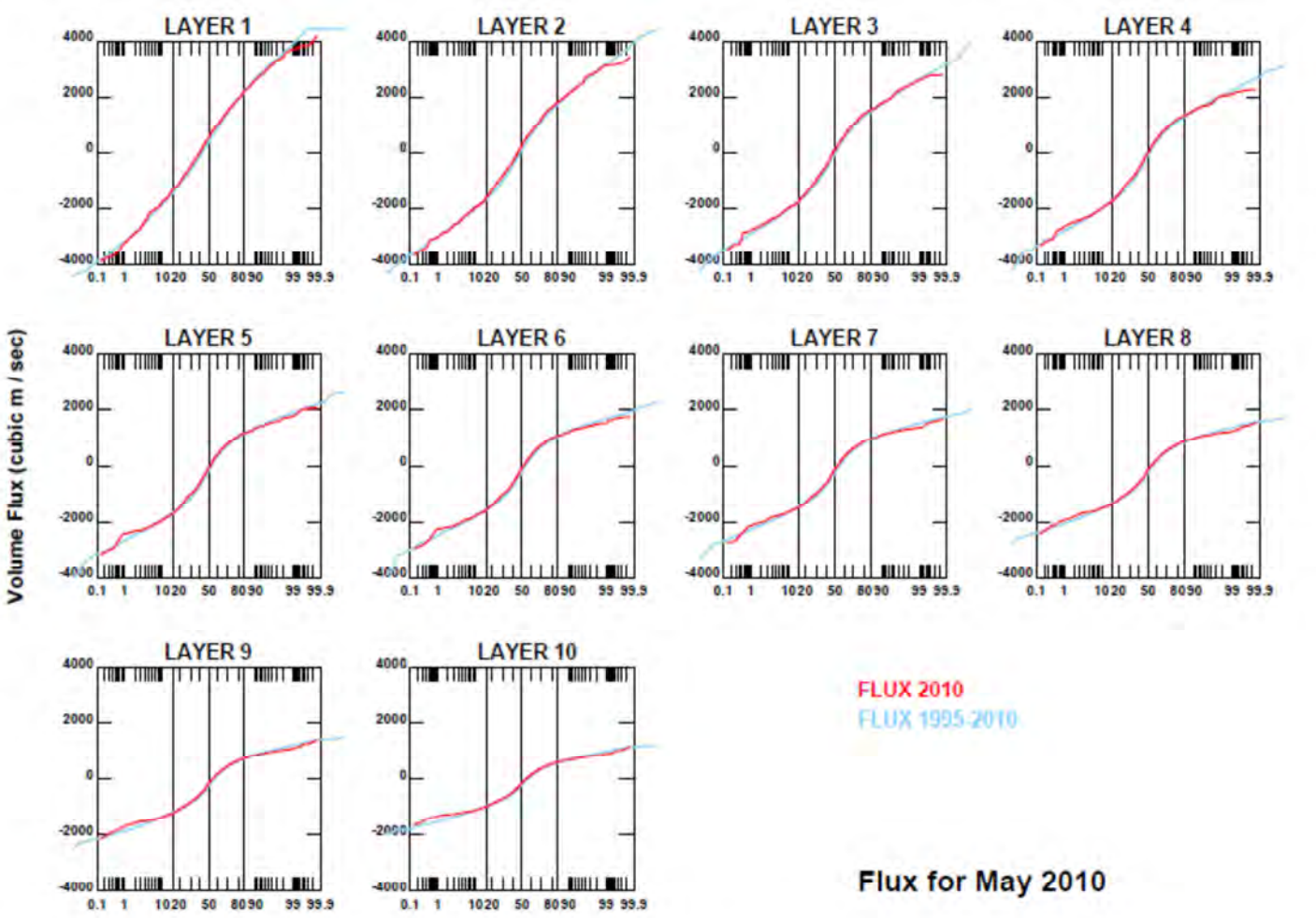

Note: Fluxes for May, 2010 shown in red. Long-term average fluxes (1995-2010) for May shown in blue. Similarity between 2010 and long-term average fluxes in each layer of the water column indicated that May 2010 is representative of long-term conditions.

Figure 12. Probability distributions of volume fluxes in each water column layer passing proposed pipeline route: May, 2010.

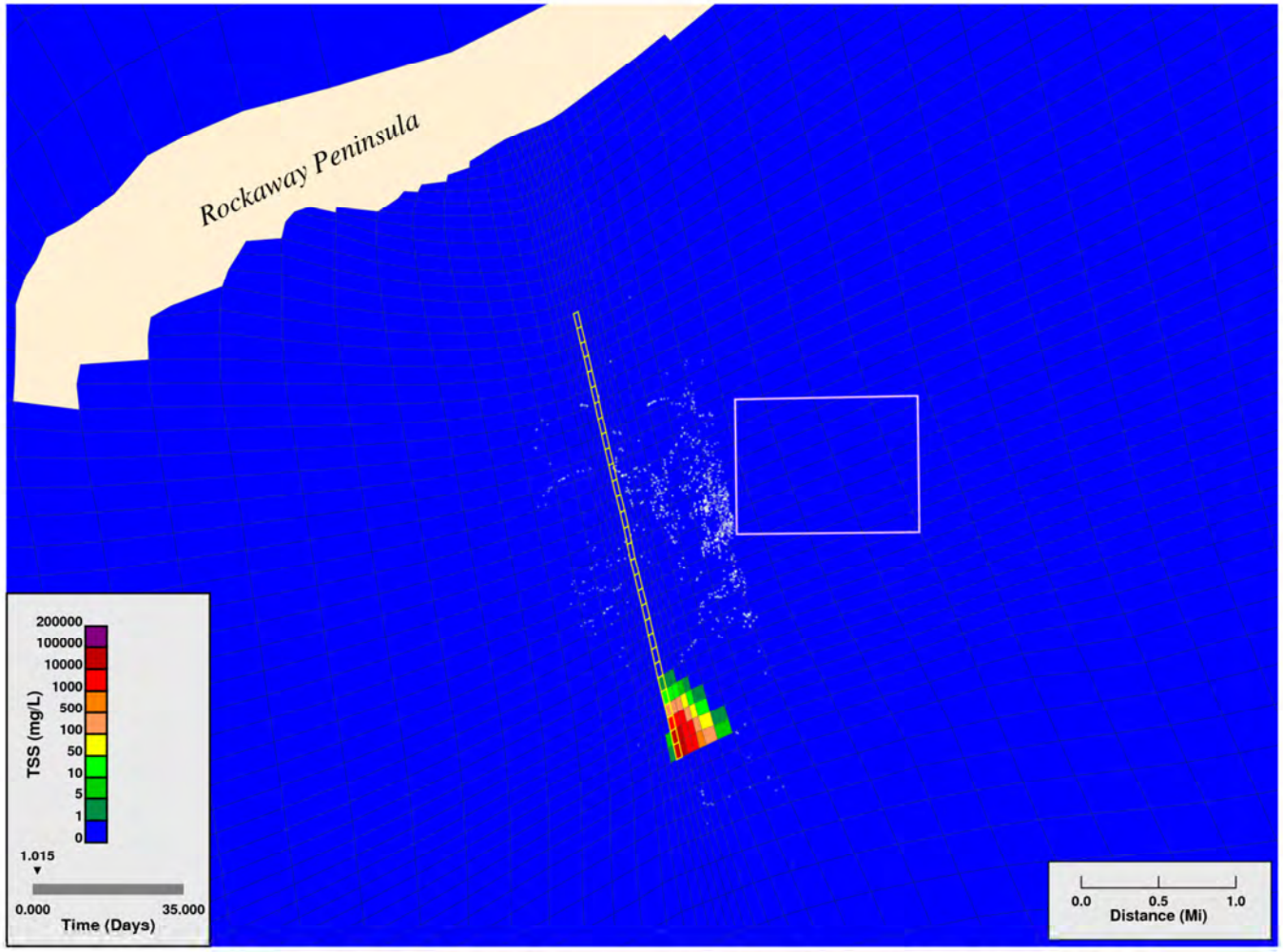

Figure 13. Worst case jetting: simulated suspended solids near water column bottom, start of trenching; rate = 366 m/hr.

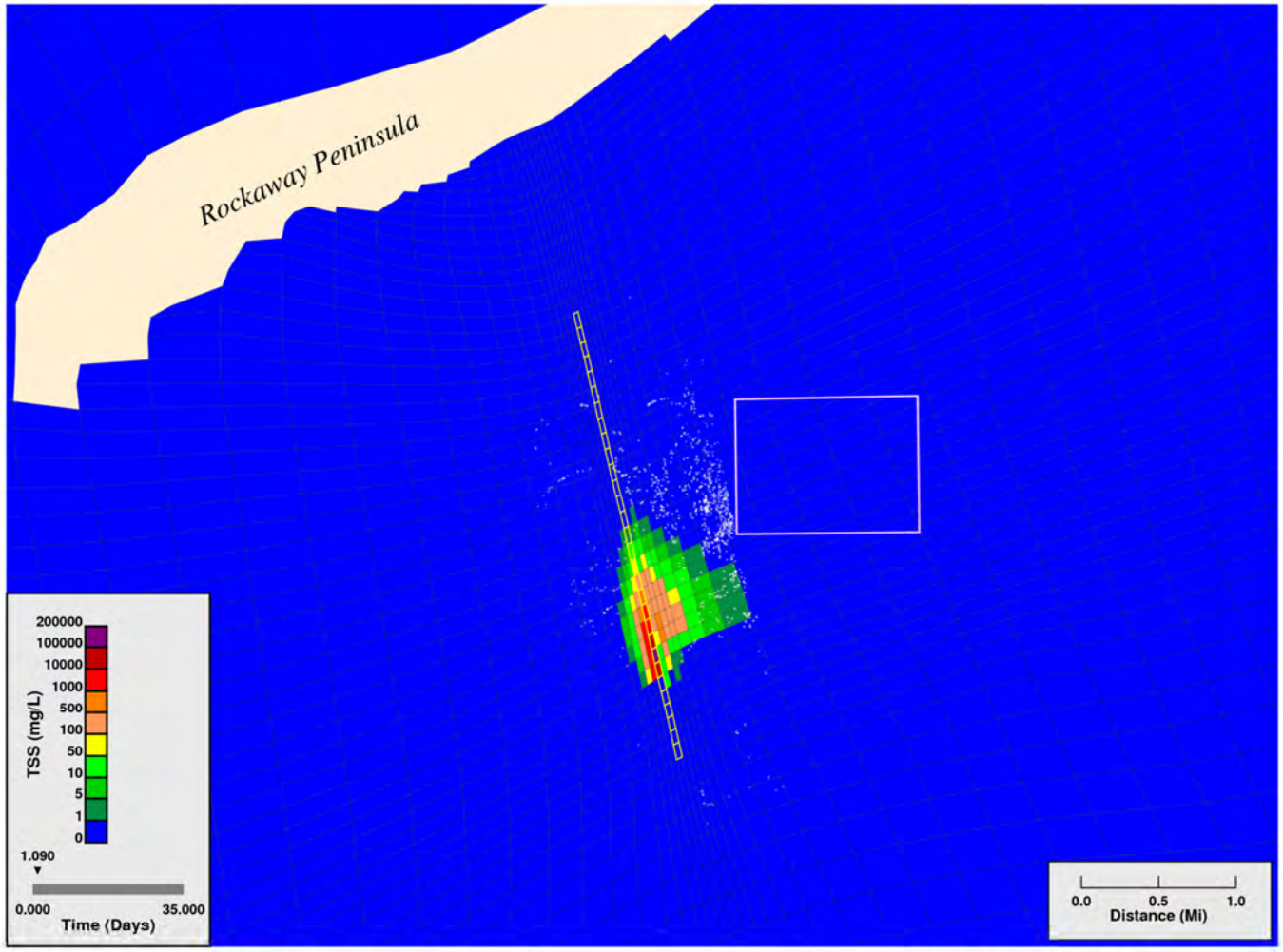

Figure 14. Worst case jetting: simulated suspended solids near water column bottom: Trenching 25% complete; rate = 366 m/hr.

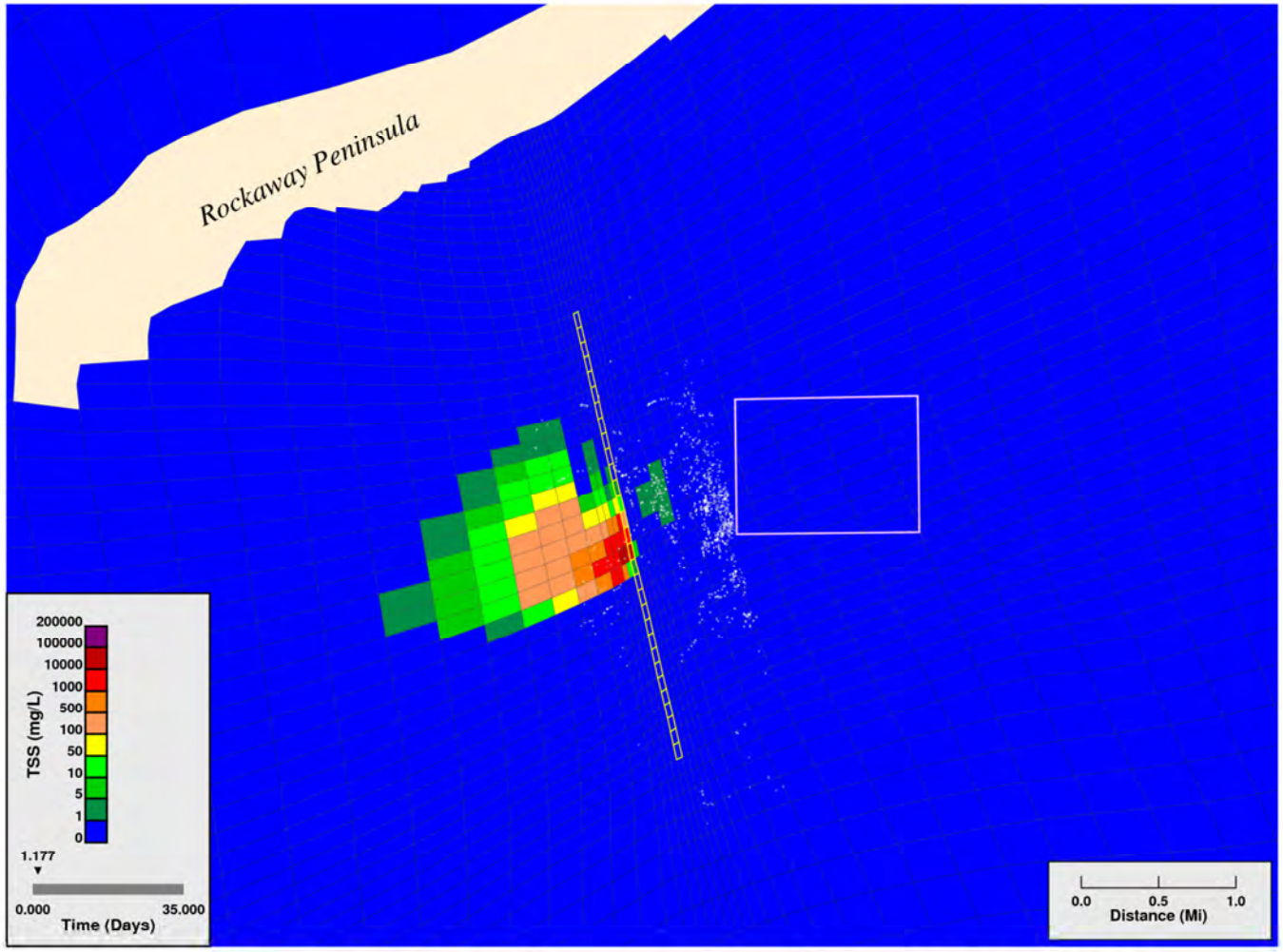

Bottom Layer Projected Solids Concentrations from Proposed Dredging, 1200 ft/hr

Figure 15. Worst case jetting: simulated suspended solids near water column bottom, trenching 50% complete, rate = 366 m/hr.

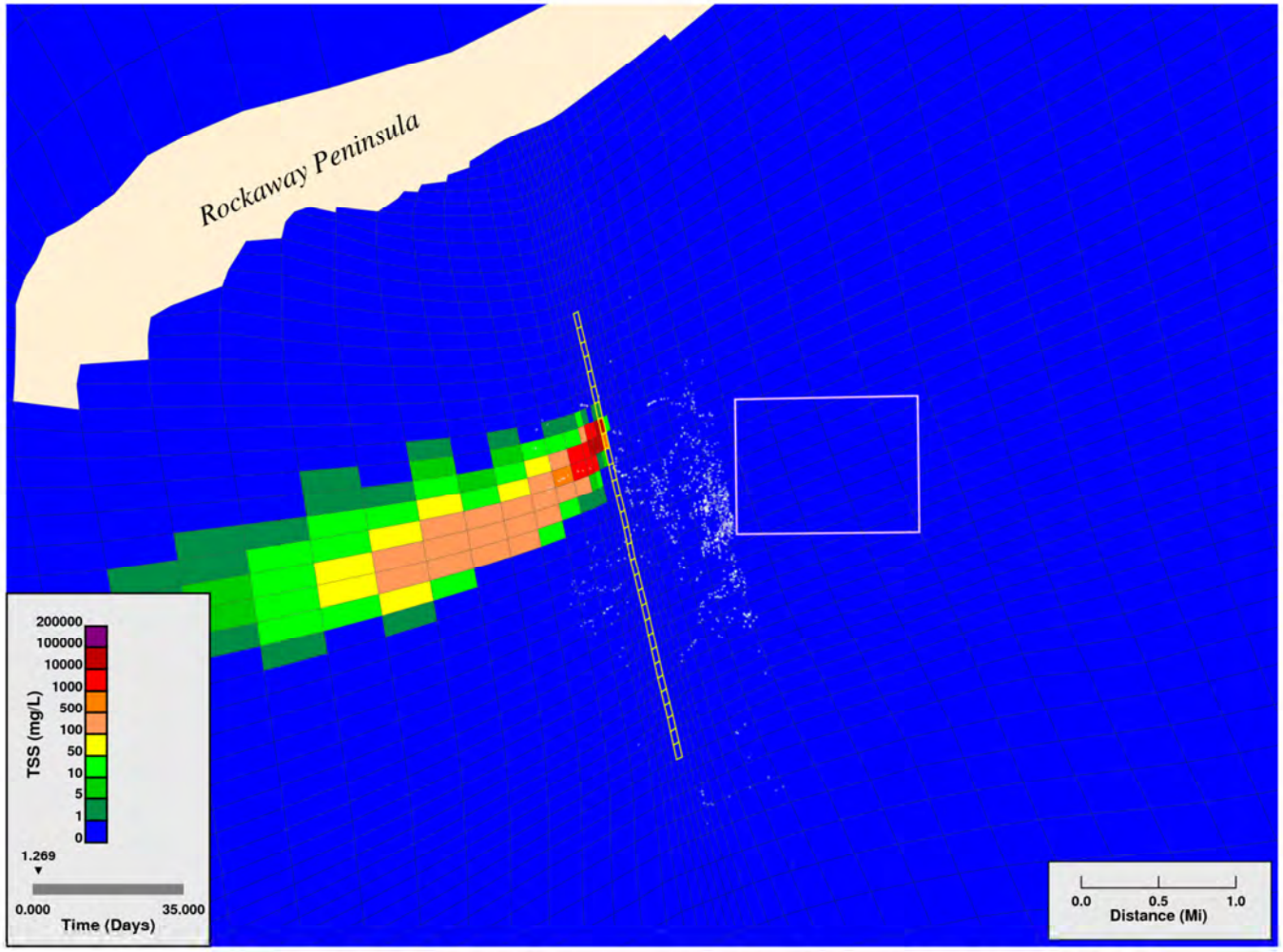

Figure 16. Worst case jetting: simulated suspended solids near water column bottom, trenching 75% complete; rate = 366 m/hr.

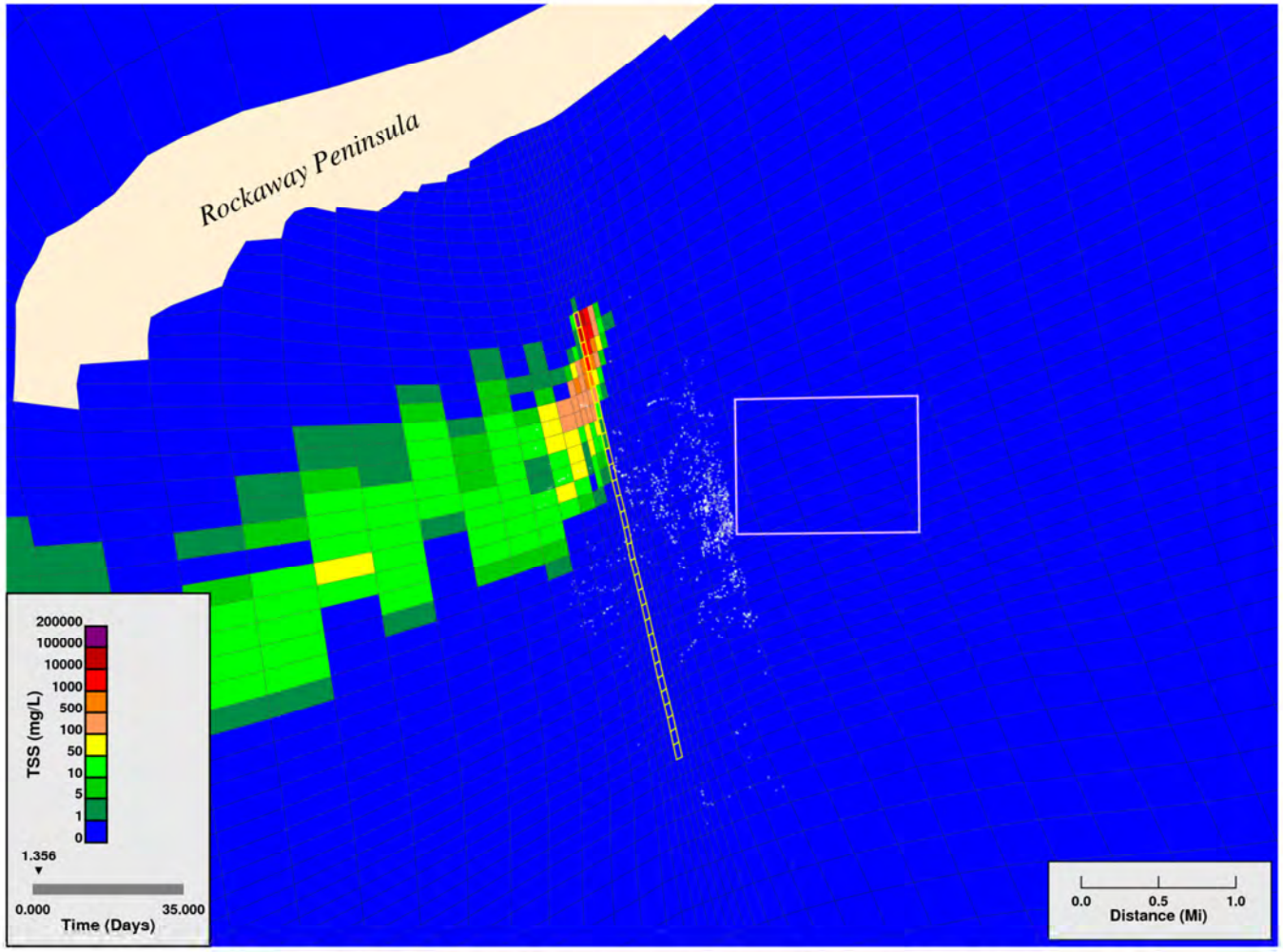

Figure 17. Worst case jetting: simulated suspended solids near water column bottom, end of trenching, rate = 366 m/hr.

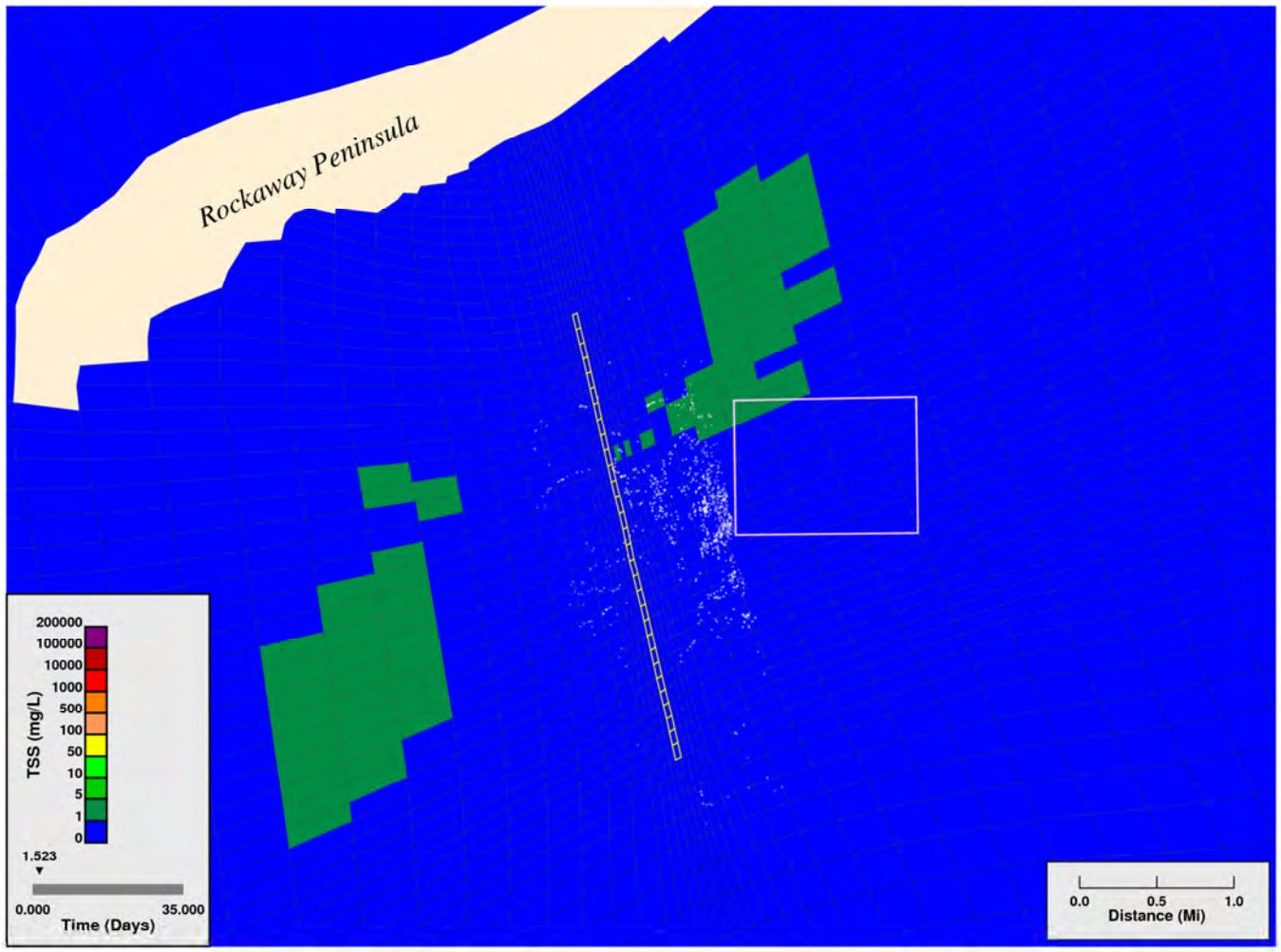

Figure 18. Worst case jetting: simulated suspended solids near water column bottom: 4 hrs after end of trenching, rate = 366 m/hr.

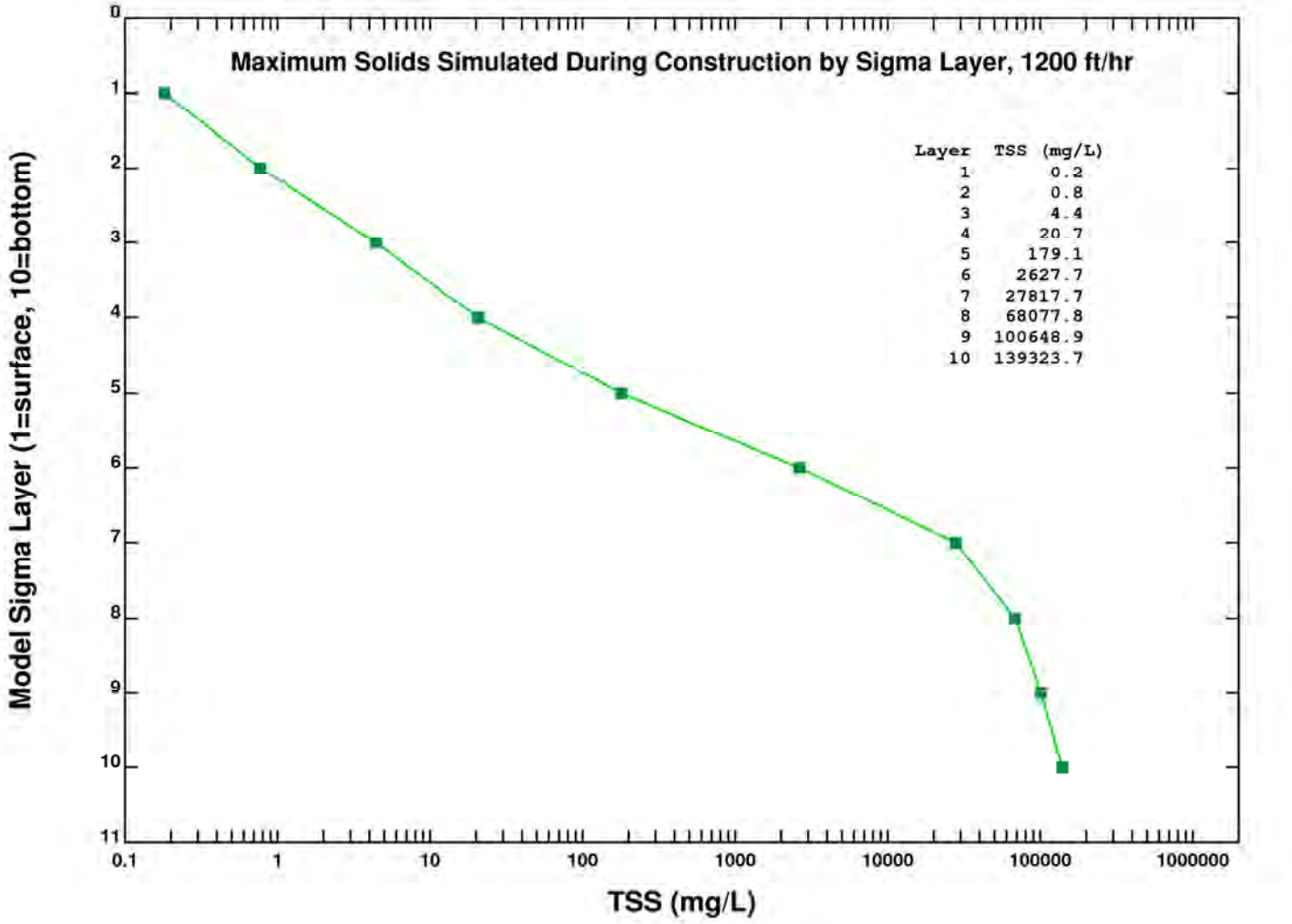

Figure 19. Worst case jetting: maximum simulated suspended solids in any cell of each water column sigma layer, rate = 366 m/hr.

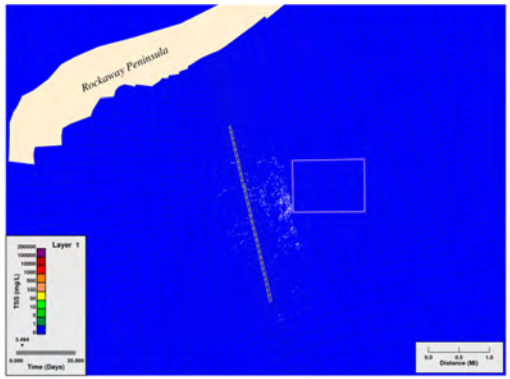

a) surface water layer

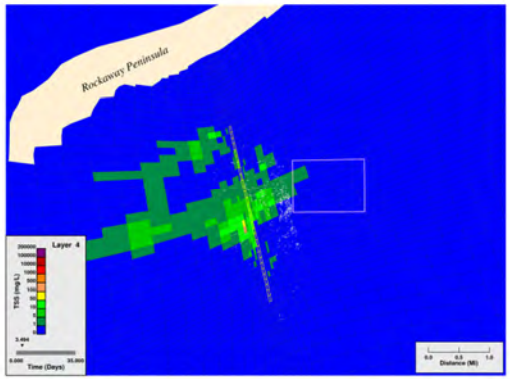

40% of water depth

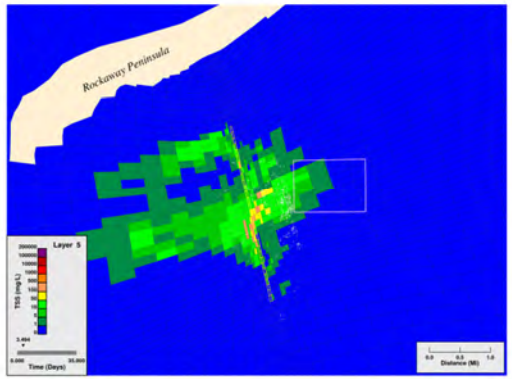

c) 50% of water depth

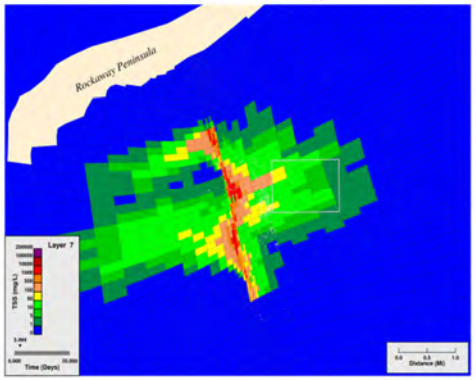

d) 70% of water depth

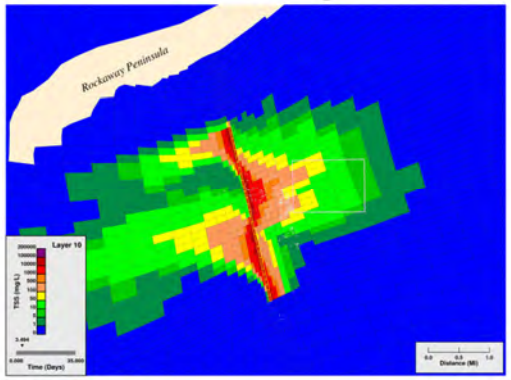

e) bottom water layer

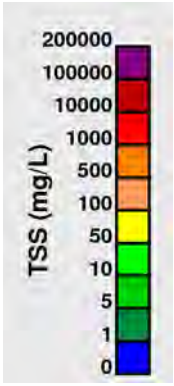

Notes: Values indicate the maximum solids concentration that occurred in each model grid at any time during the simulation. It should be noted the concentrations are elevated near the point of construction and rapidly decrease over time as a consequence of the relatively high settling velocities of sediment grains. Plumes clear the water column within 4 hours following the end of construction.

Figure 20. Worst case jetting: maximum simulated suspended solids extent in selected water column sigma layers, rate = 366 m/hr.

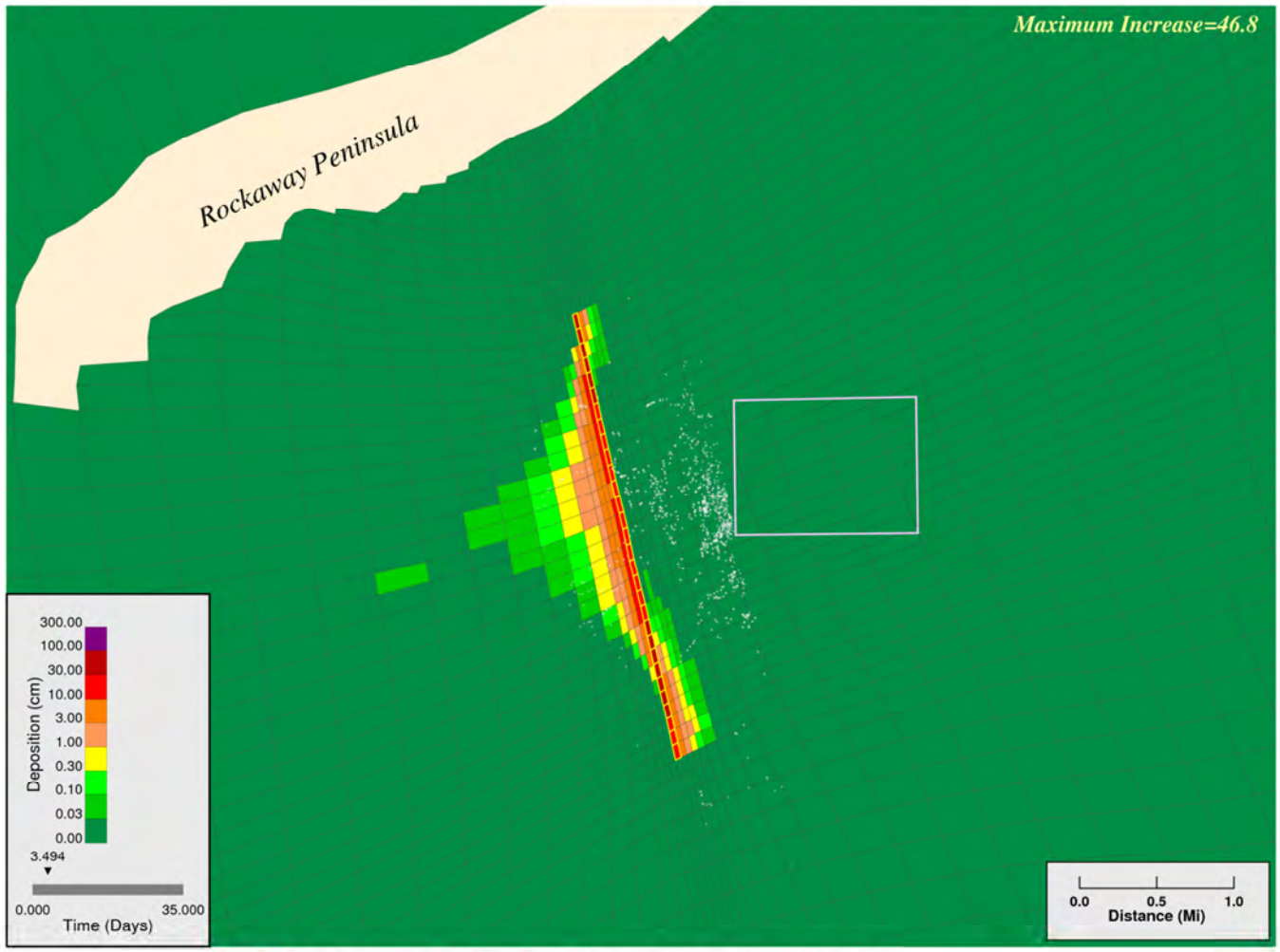

Figure 21. Worst case jetting: simulated thickness of deposited solids on bed surface following trenching, rate = 366 m/hr.

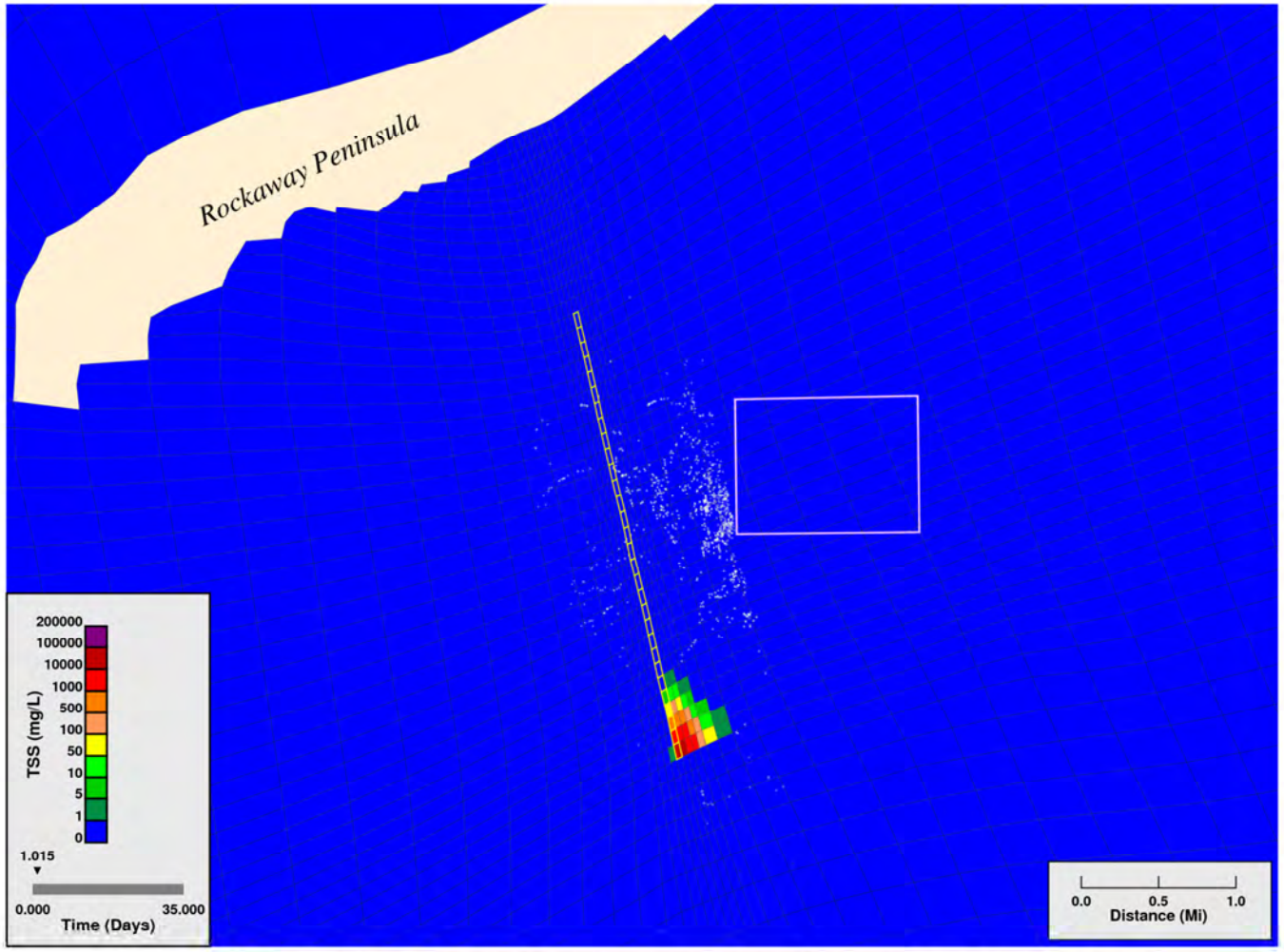

Figure 22. Worst case jetting: simulated suspended solids near water column bottom, start of trenching, rate = 183 m/hr.

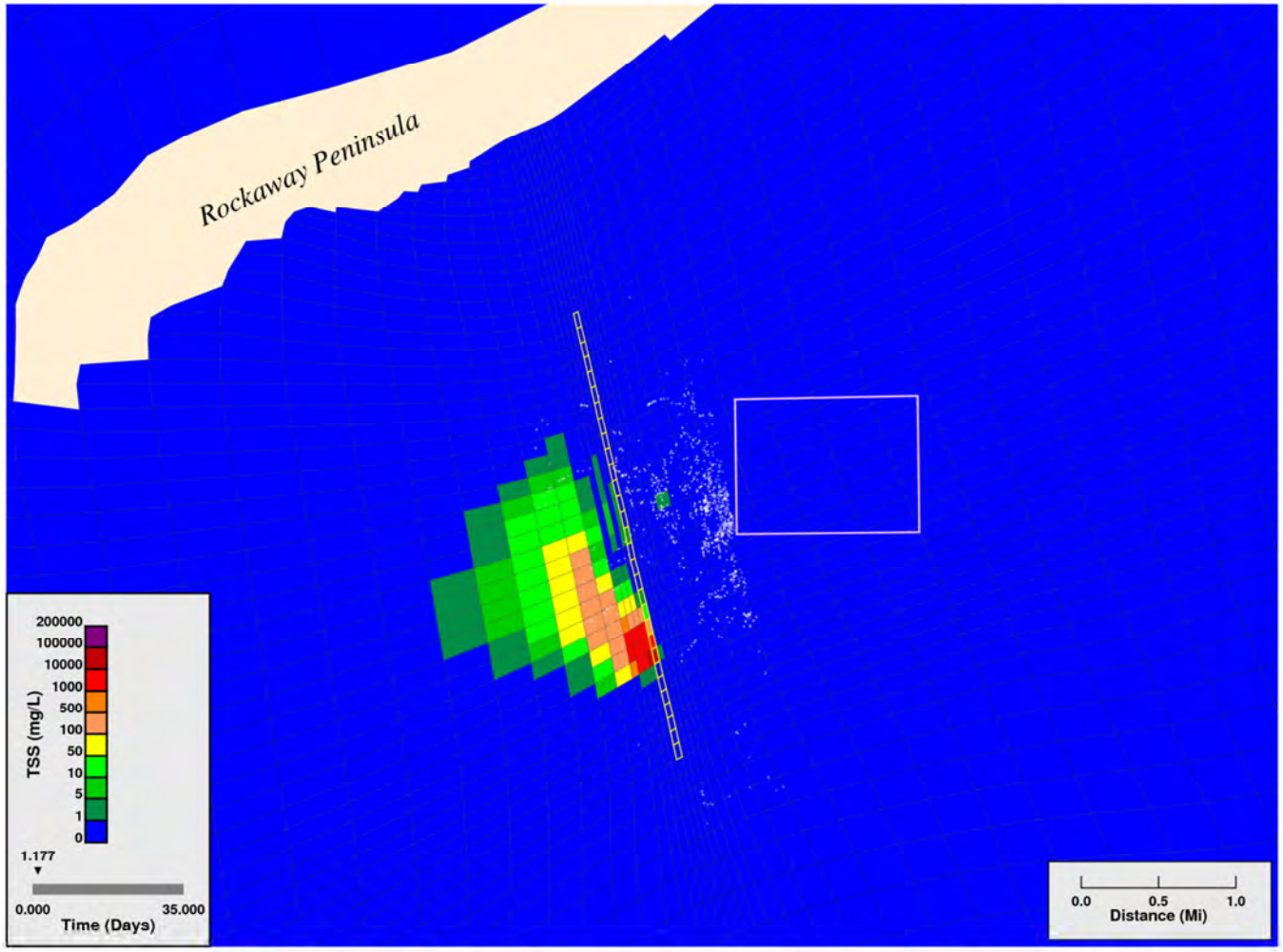

Bottom Layer Projected Solids Concentrations from Proposed Dredging, 600 ft/hr

Figure 23. Worst case jetting: simulated suspended solids near water column bottom, trenching 25% complete, rate = 183 m/hr.

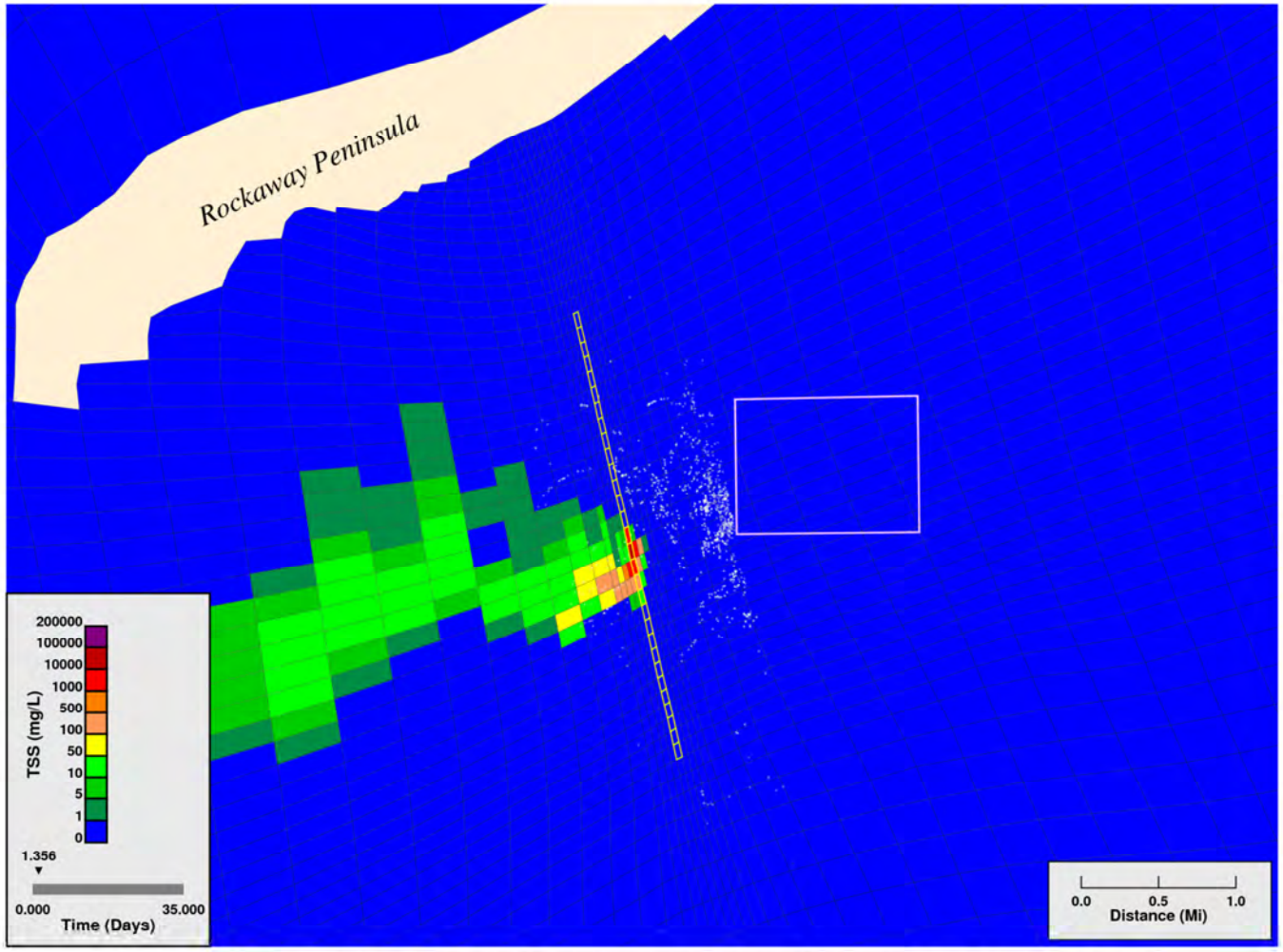

Figure 24. Worst case jetting: simulated suspended solids near water column bottom, trenching 50% complete; rate = 183 m/hr.

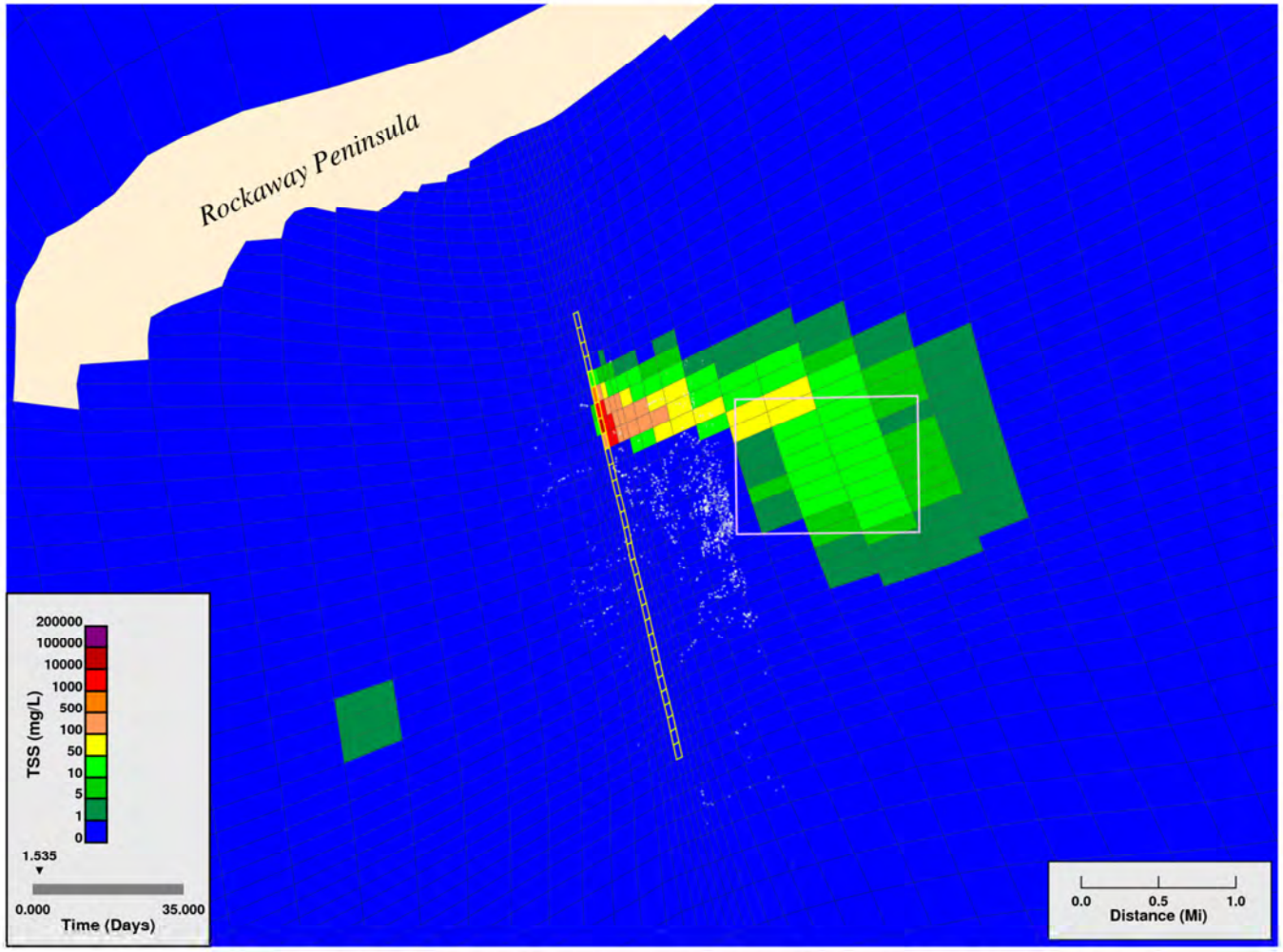

Bottom Layer Projected Solids Concentrations from Proposed Dredging, 600 ft/hr

Figure 25. Worst case jetting: simulated suspended solids near water column bottom, trenching 75% complete, rate = 183 m/hr.

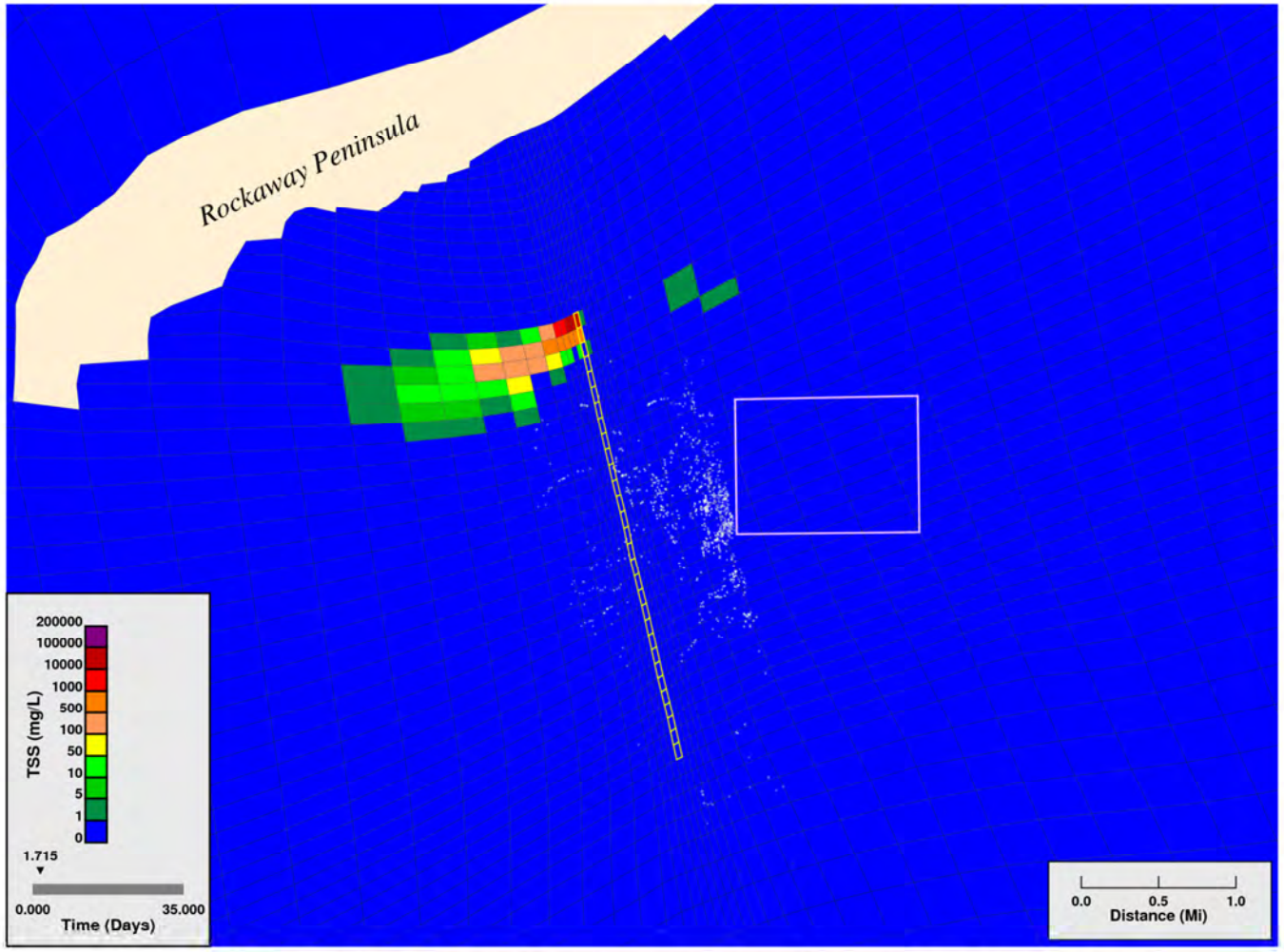

Figure 26. Worst case jetting: simulated suspended solids near water column bottom, end of trenching, rate = 183 m/hr.

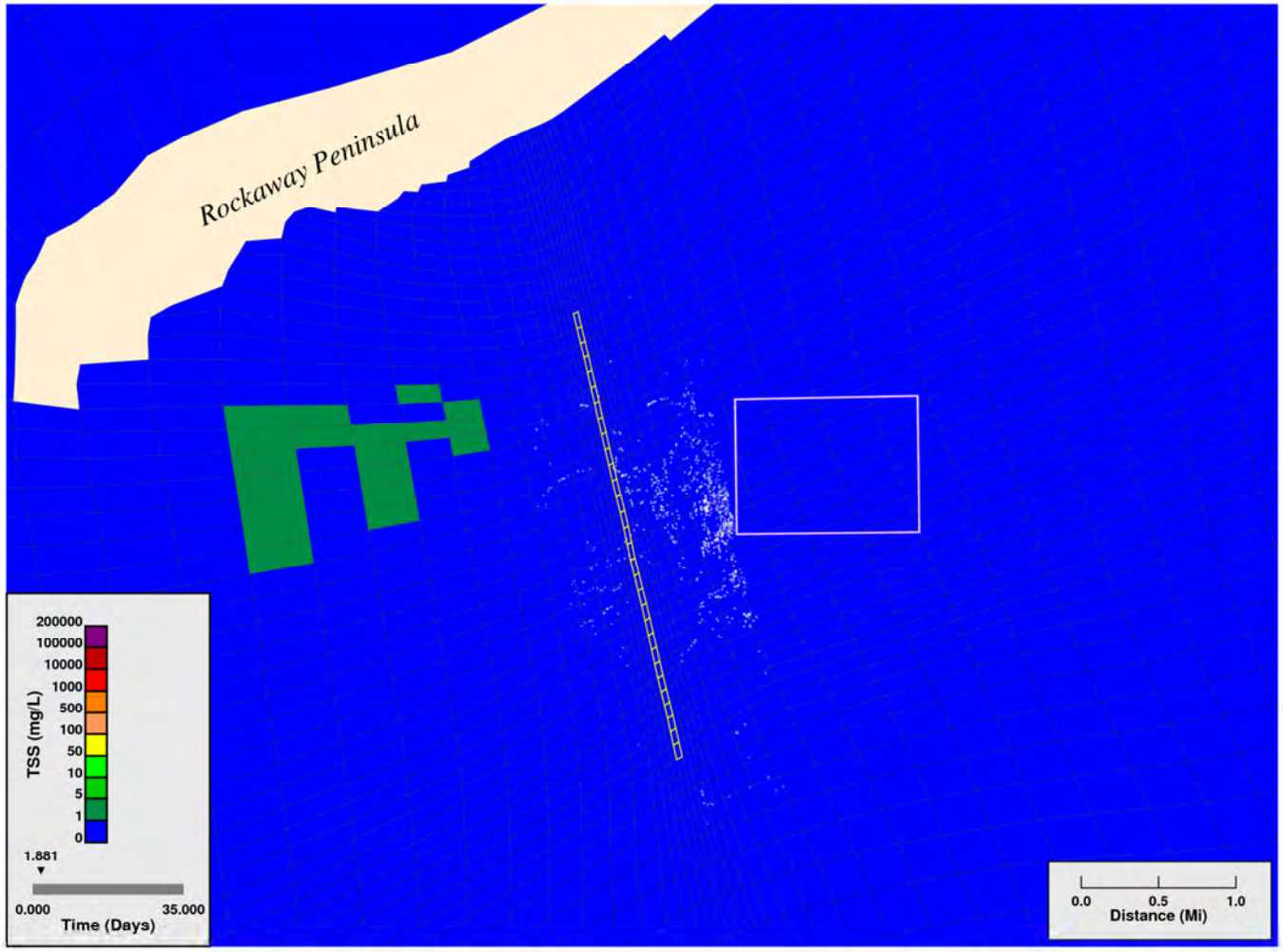

Bottom Layer Projected Solids Concentrations from Proposed Dredging, 600 ft/hr

Figure 27. Worst case jetting: simulated suspended solids near water column bottom: 4 hrs after end of trenching, rate = 183 m/hr.

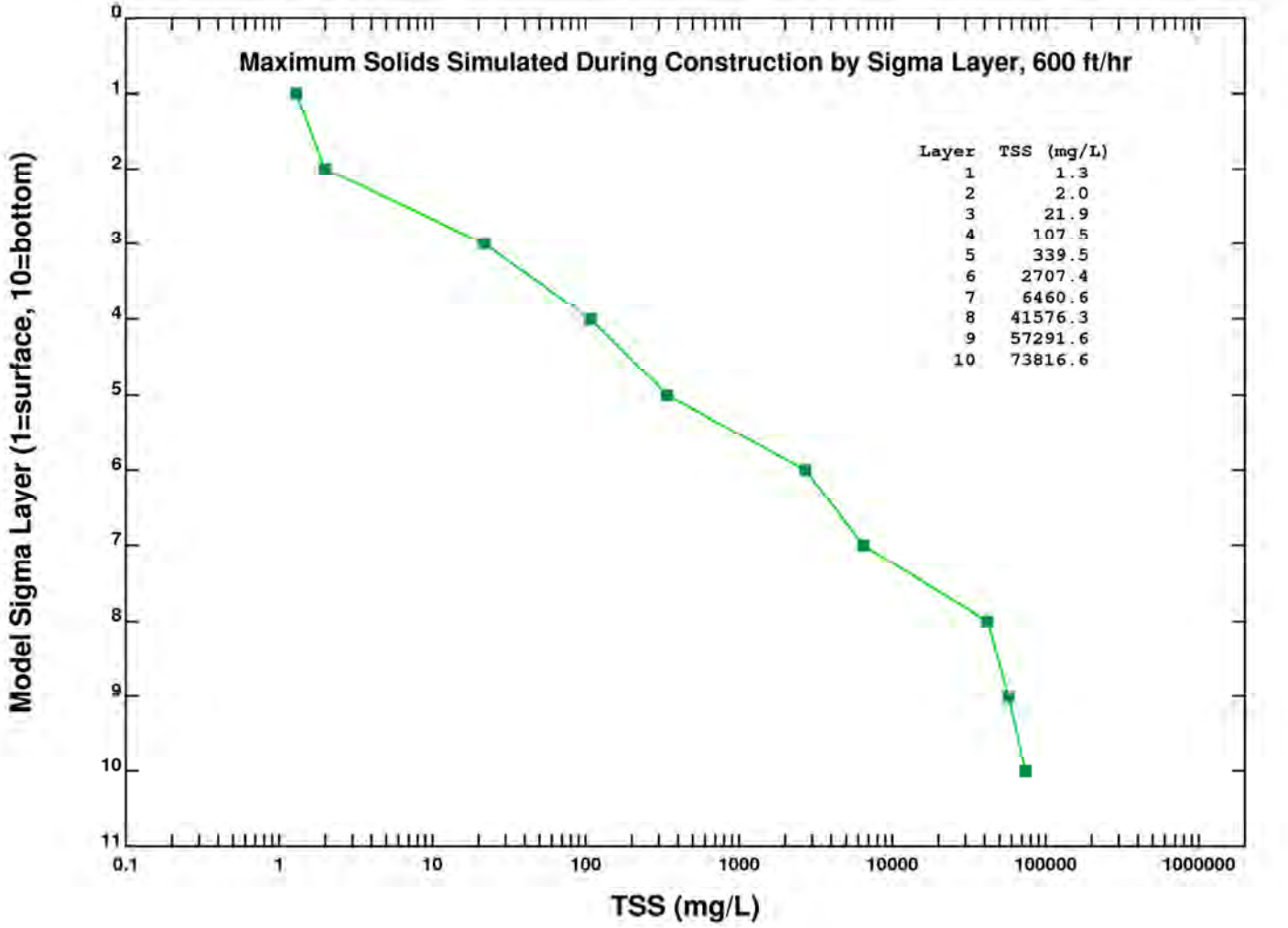

Figure 28. Worst case jetting: maximum simulated suspended solids in any cell of each water column sigma layer, rate = 183 m/hr.

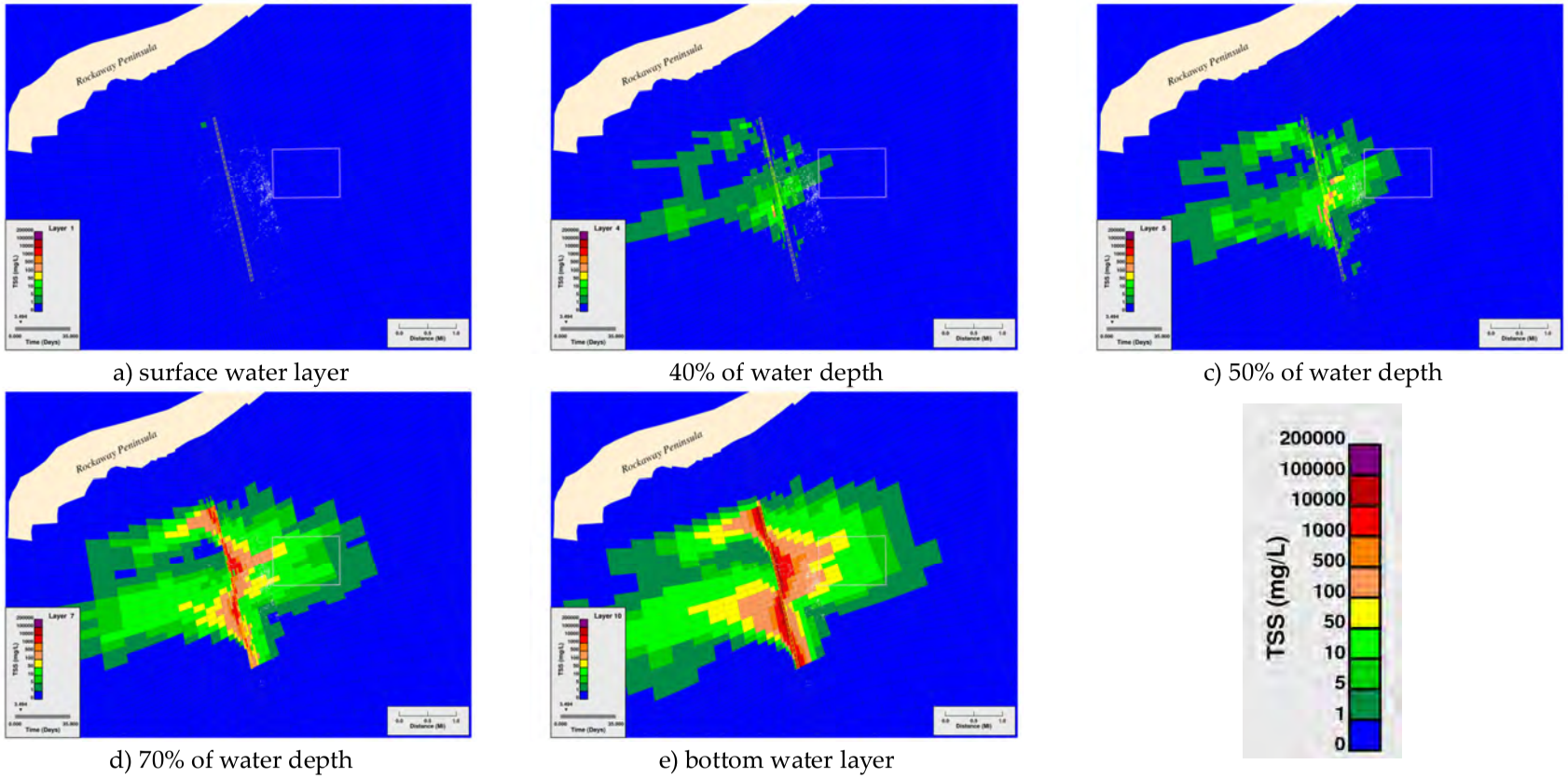

a) surface water layer

40% of water depth

c) 50% of water depth

d) 70% of water depth

e) bottom water layer

Notes: Values indicate the maximum solids concentration that occurred in each model grid at any time during the simulation. It should be noted the concentrations are elevated near the point of construction and rapidly decrease over time as a consequence of the relatively high settling velocities of sediment grains. Plumes clear the water column within 4 hours following the end of construction.

Figure 29. Worst case jetting: maximum simulated suspended solids extent in selected water column sigma layers, rate = 183 m/hr.

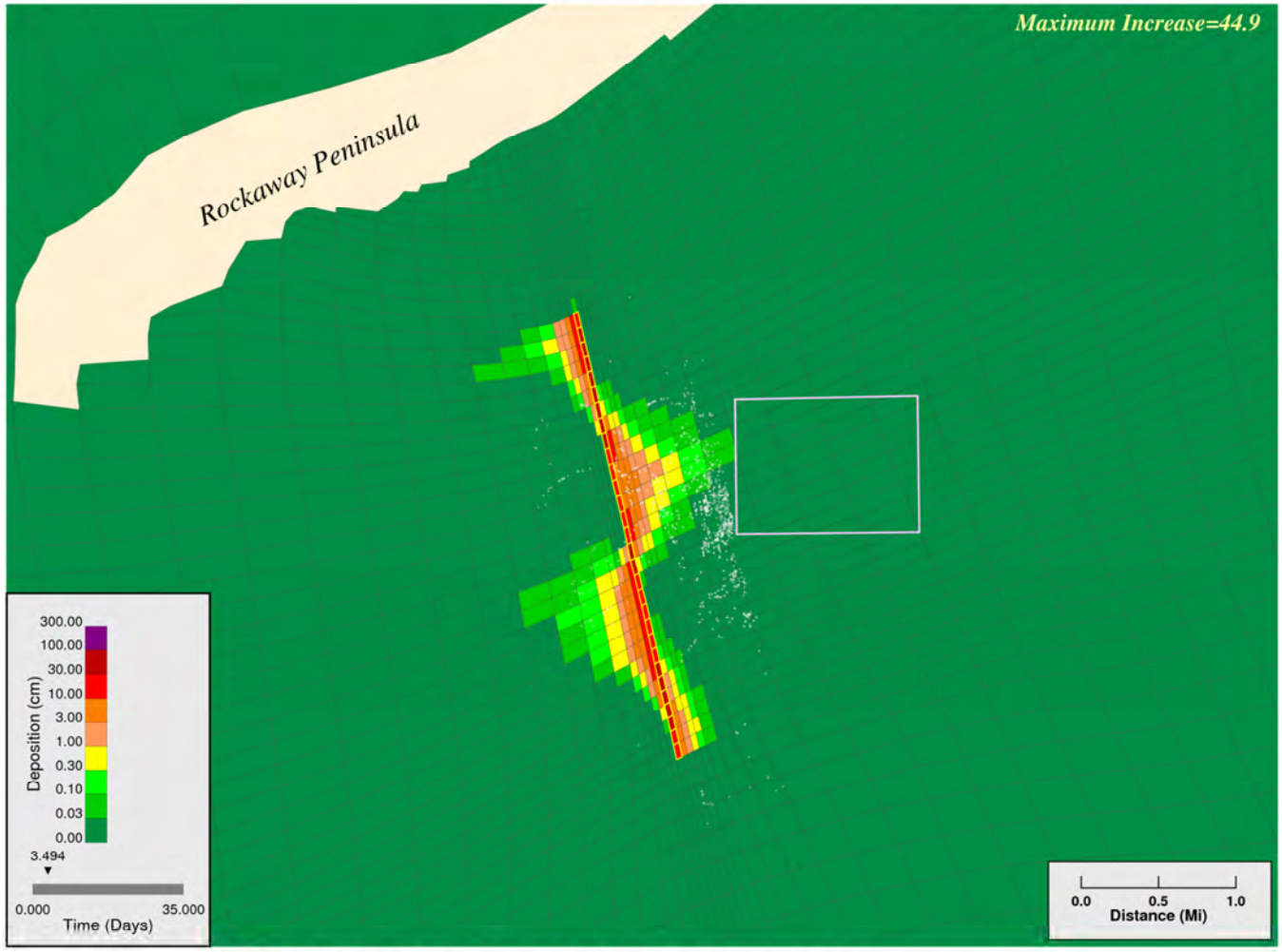

Figure 30. Worst case jetting: simulated thickness of deposited solids on bed surface following trenching, rate = 183 m/hr.

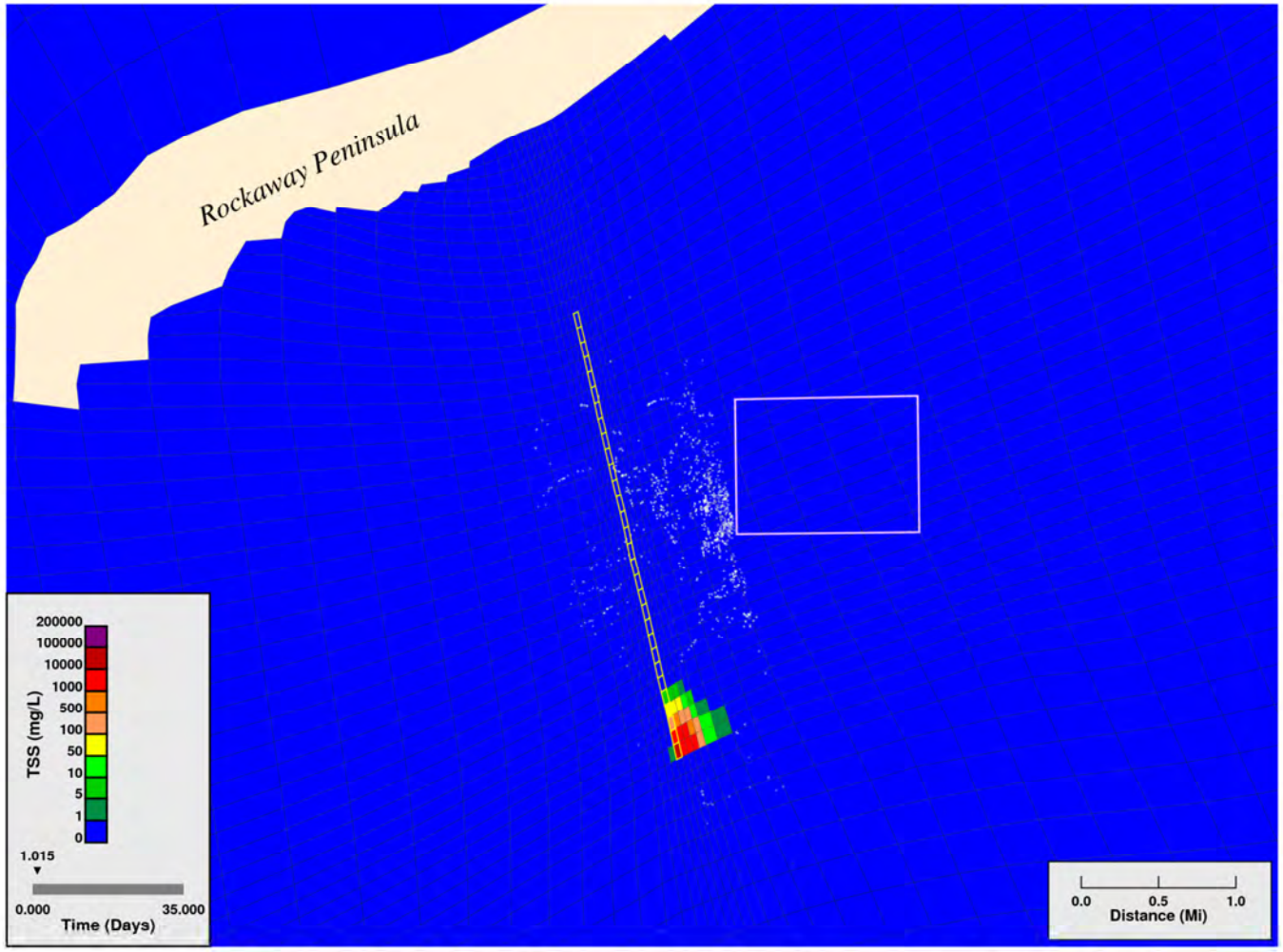

Figure 31. Worst case jetting: simulated suspended solids near water column bottom, start of trenching, rate = 122 m/hr.

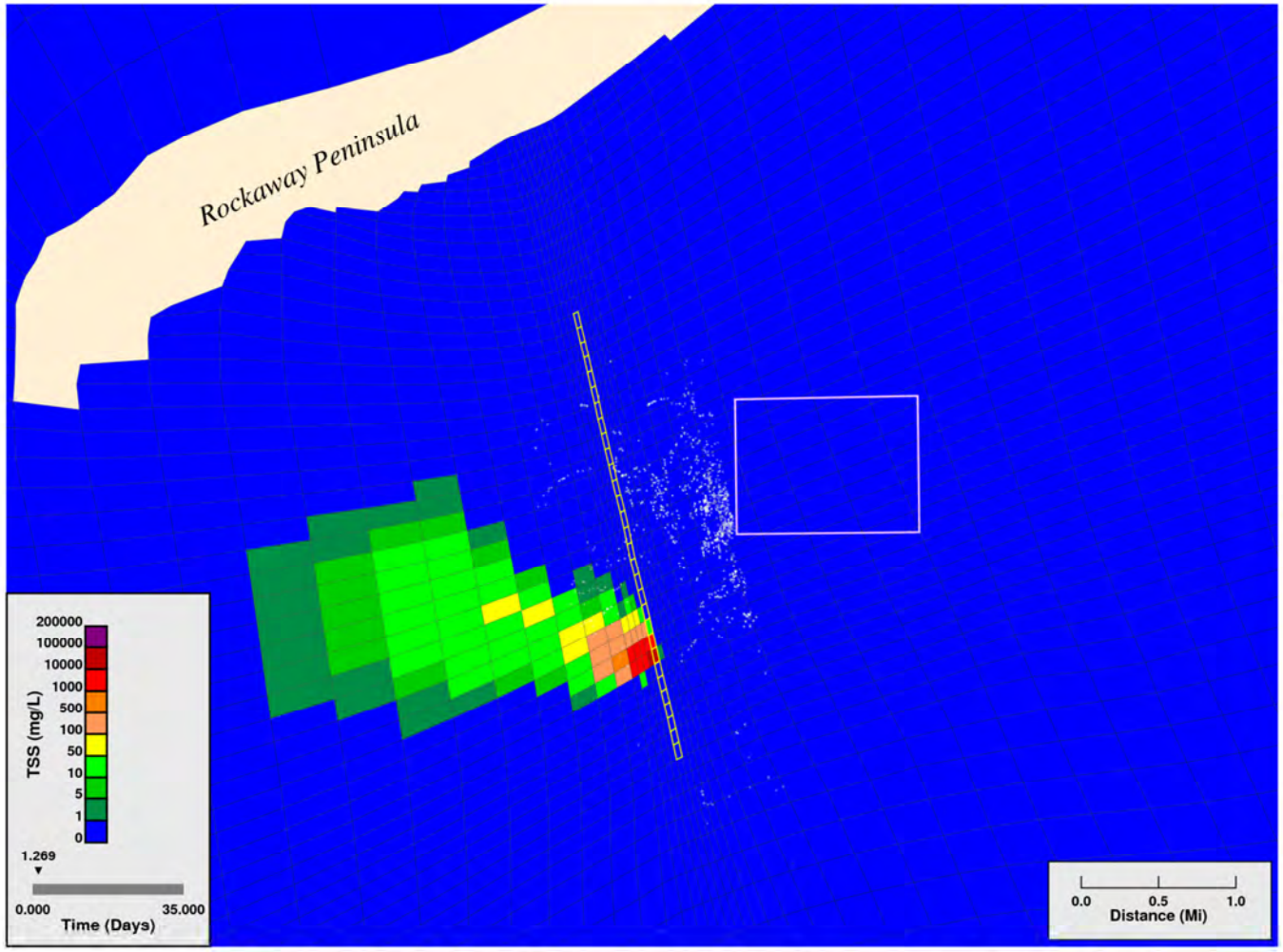

Figure 32. Worst case jetting: simulated suspended solids near water column bottom, trenching 25% complete, rate = 122 m/hr.

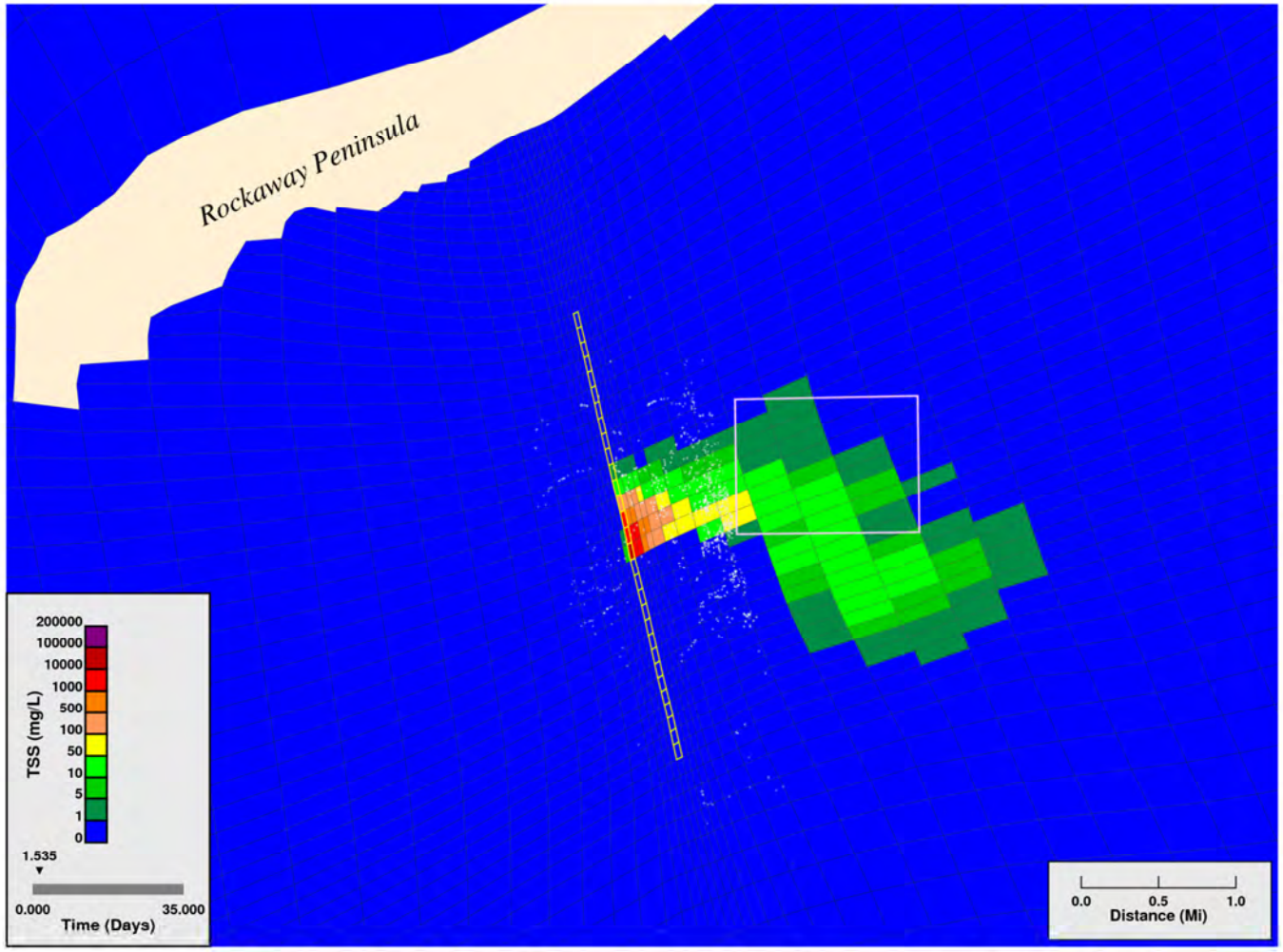

Figure 33. Worst case jetting: simulated suspended solids near water column bottom, trenching 50% complete, rate = 122 m/hr.

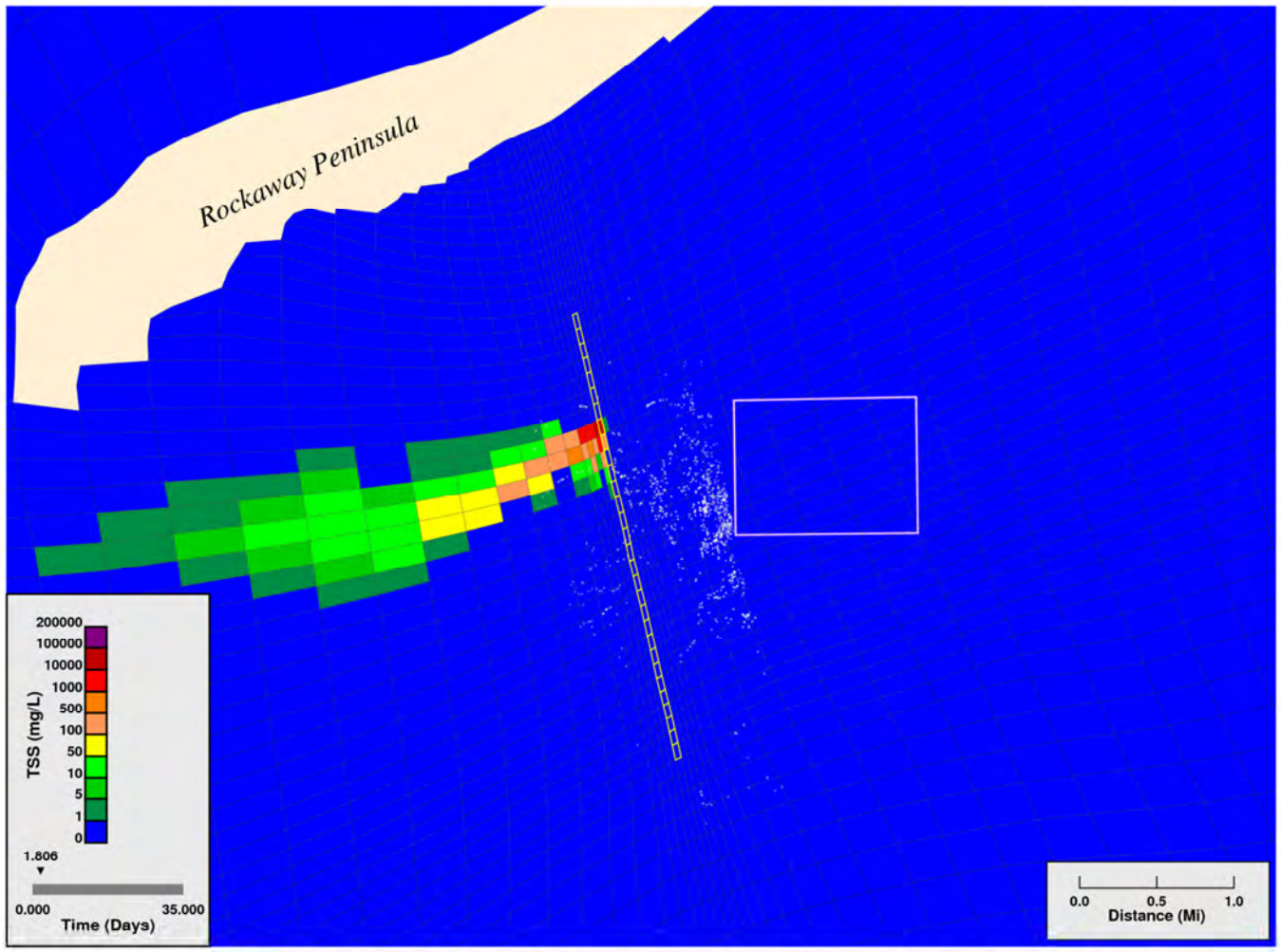

Figure 34. Worst case jetting: simulated suspended solids near water column bottom, trenching 75% complete, rate = 122 m/hr.

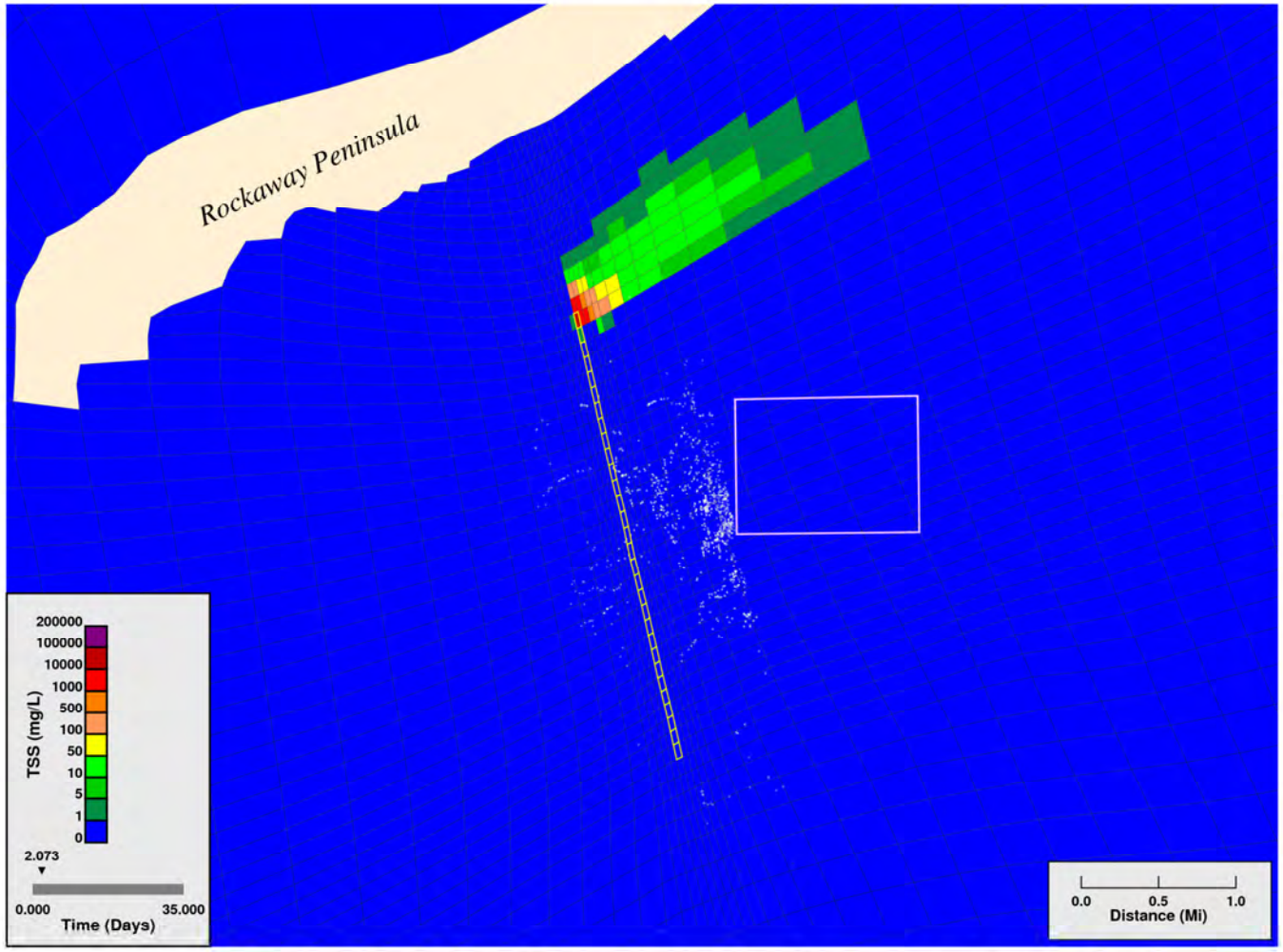

Figure 35. Worst case jetting: simulated suspended solids near water column bottom, end of trenching, rate = 122 m/hr.

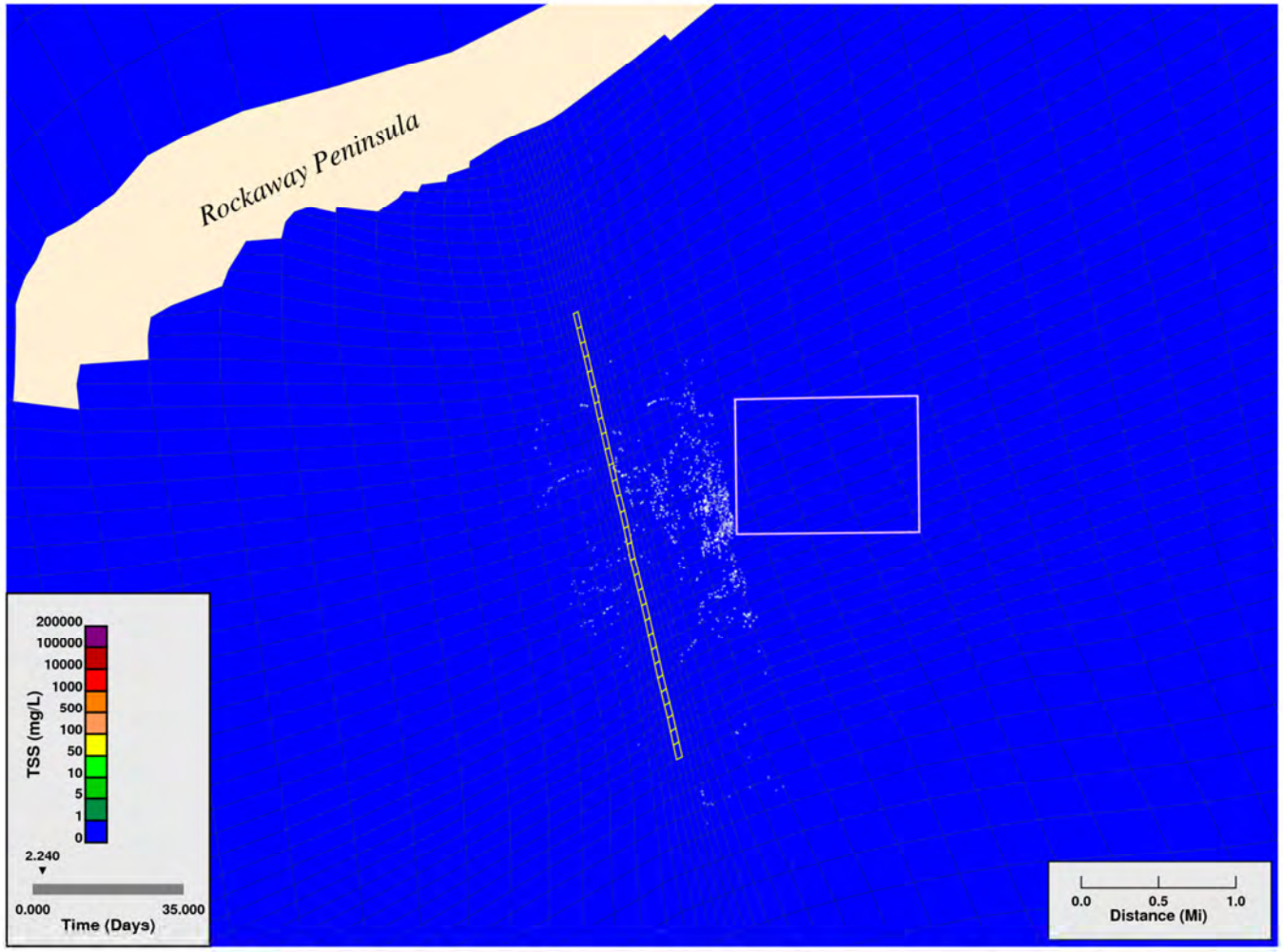

Bottom Layer Projected Solids Concentrations from Proposed Dredging, 400 ft/hr

Figure 36. Worst case jetting: simulated suspended solids near water column bottom: 4 hrs after end of trenching, rate = 122 m/hr.

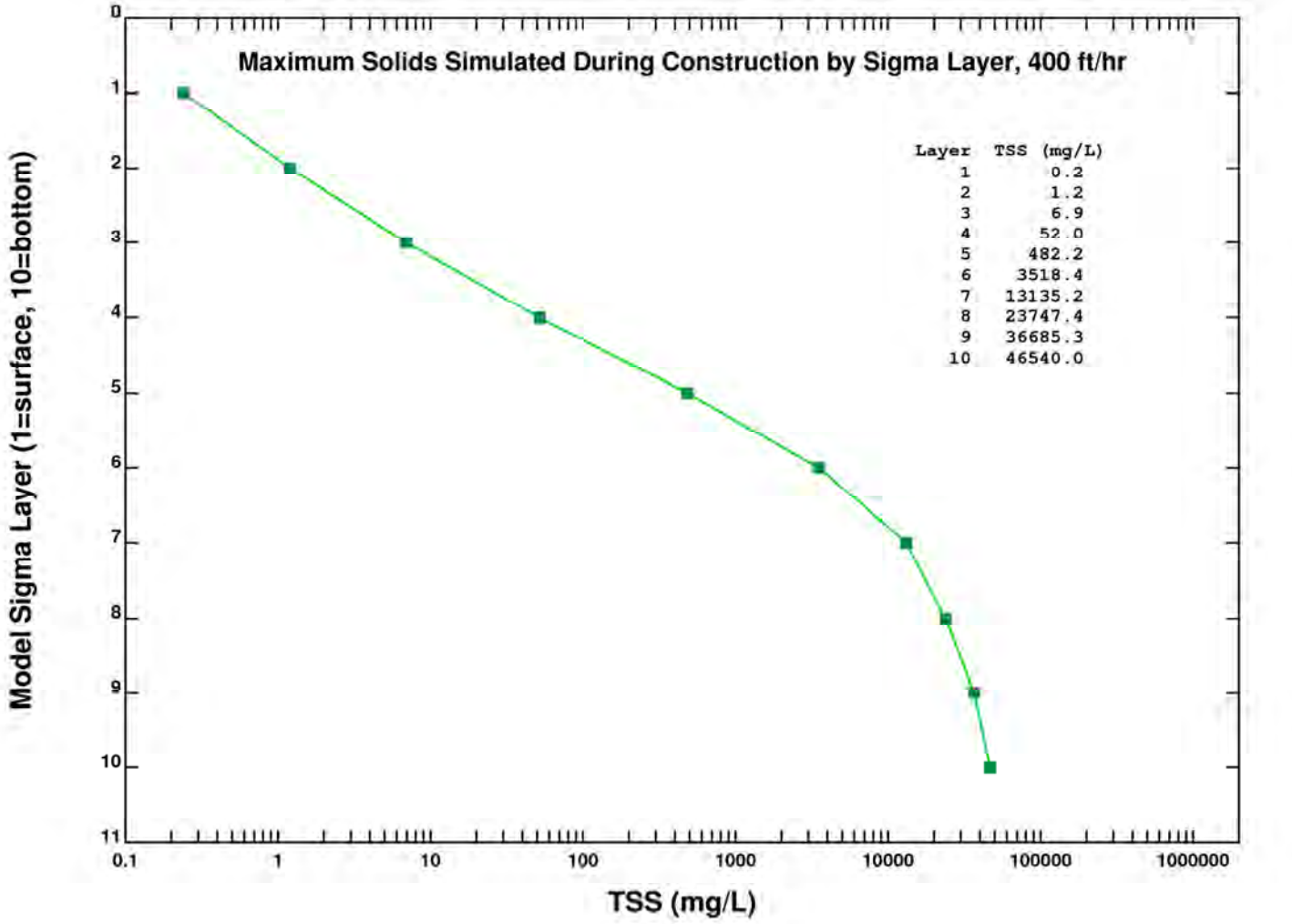

Figure 37. Worst case jetting: maximum simulated suspended solids in any cell of each water column sigma layer, rate = 122 m/hr.

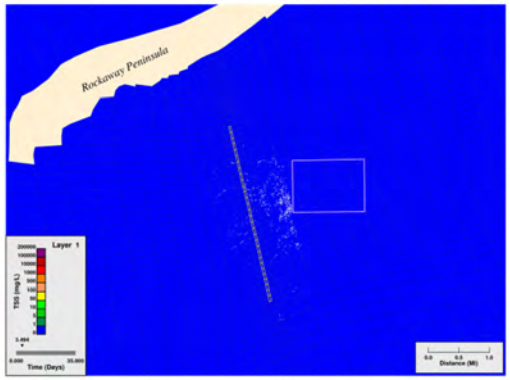

a) surface water layer

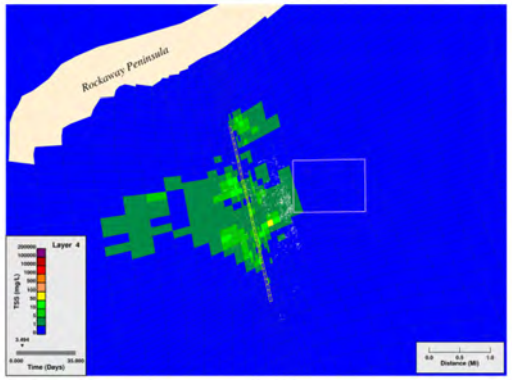

40% of water depth

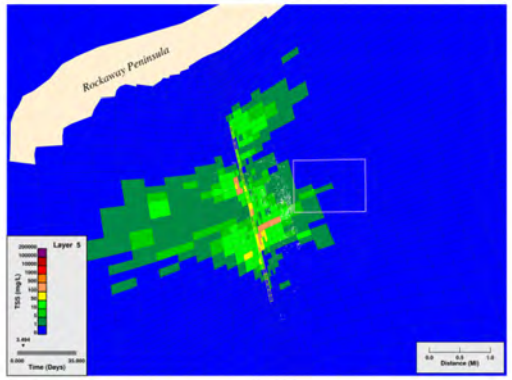

c) 50% of water depth

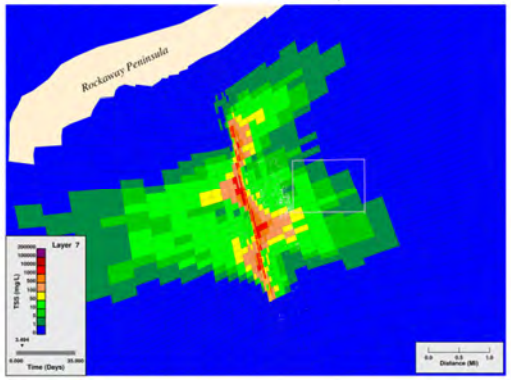

d) 70% of water depth

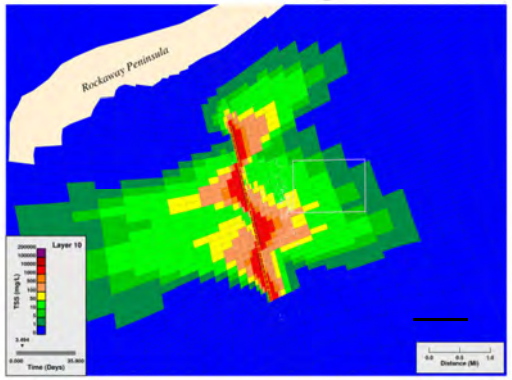

e) bottom water layer

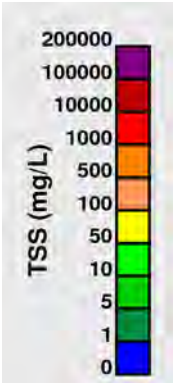

Notes: Values indicate the maximum solids concentration that occurred in each model grid at any time during the simulation. It should be noted the concentrations are elevated near the point of construction and rapidly decrease over time as a consequence of the relatively high settling velocities of sediment grains. Plumes clear the water column within 4 hours following the end of construction.

Figure 38. Worst case jetting: maximum simulated suspended solids extent in selected water column sigma layers, rate = 122 m/hr.

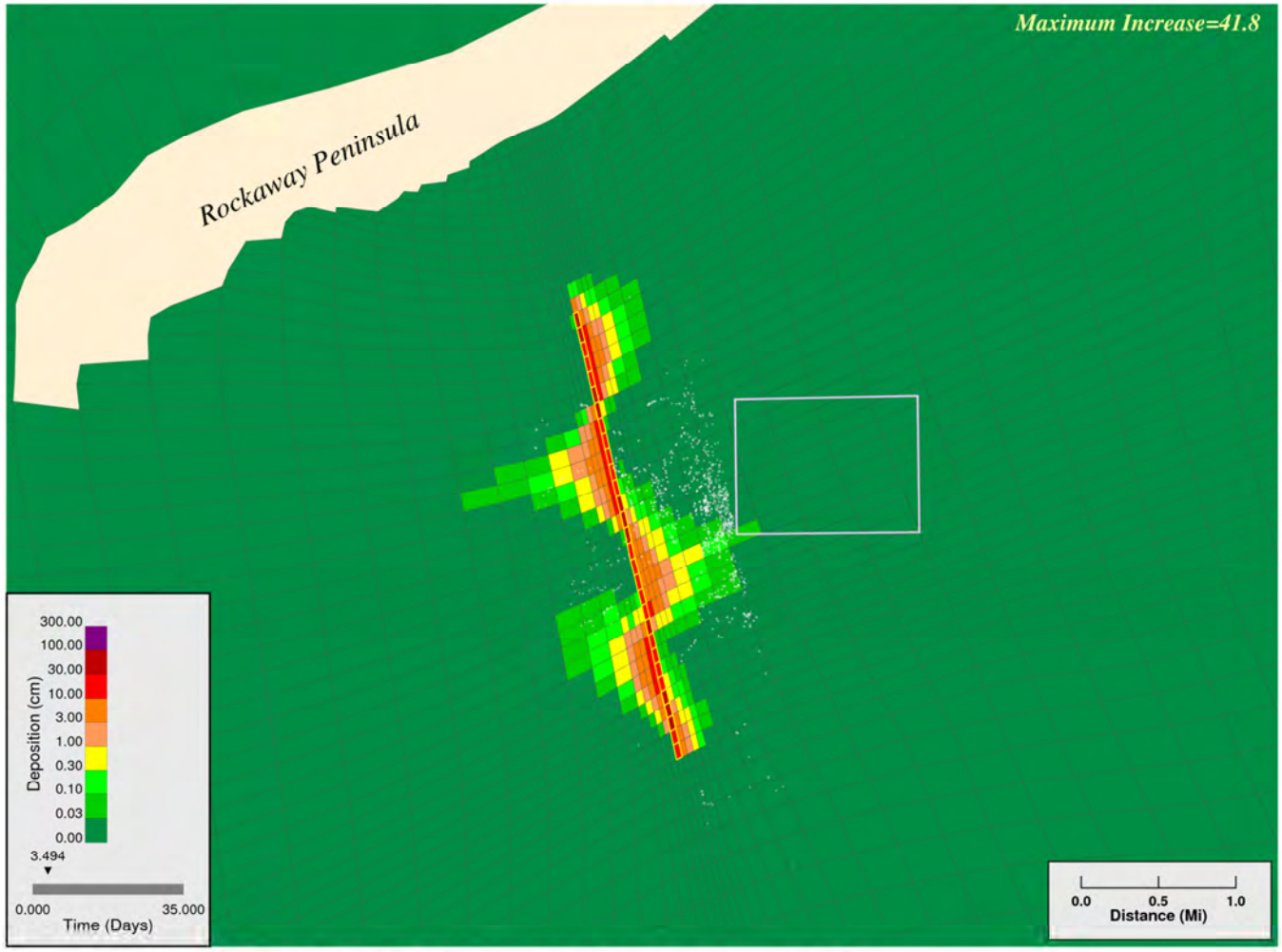

Figure 39. Worst case jetting: simulated thickness of deposited solids on bed surface following trenching, rate = 122 m/hr.

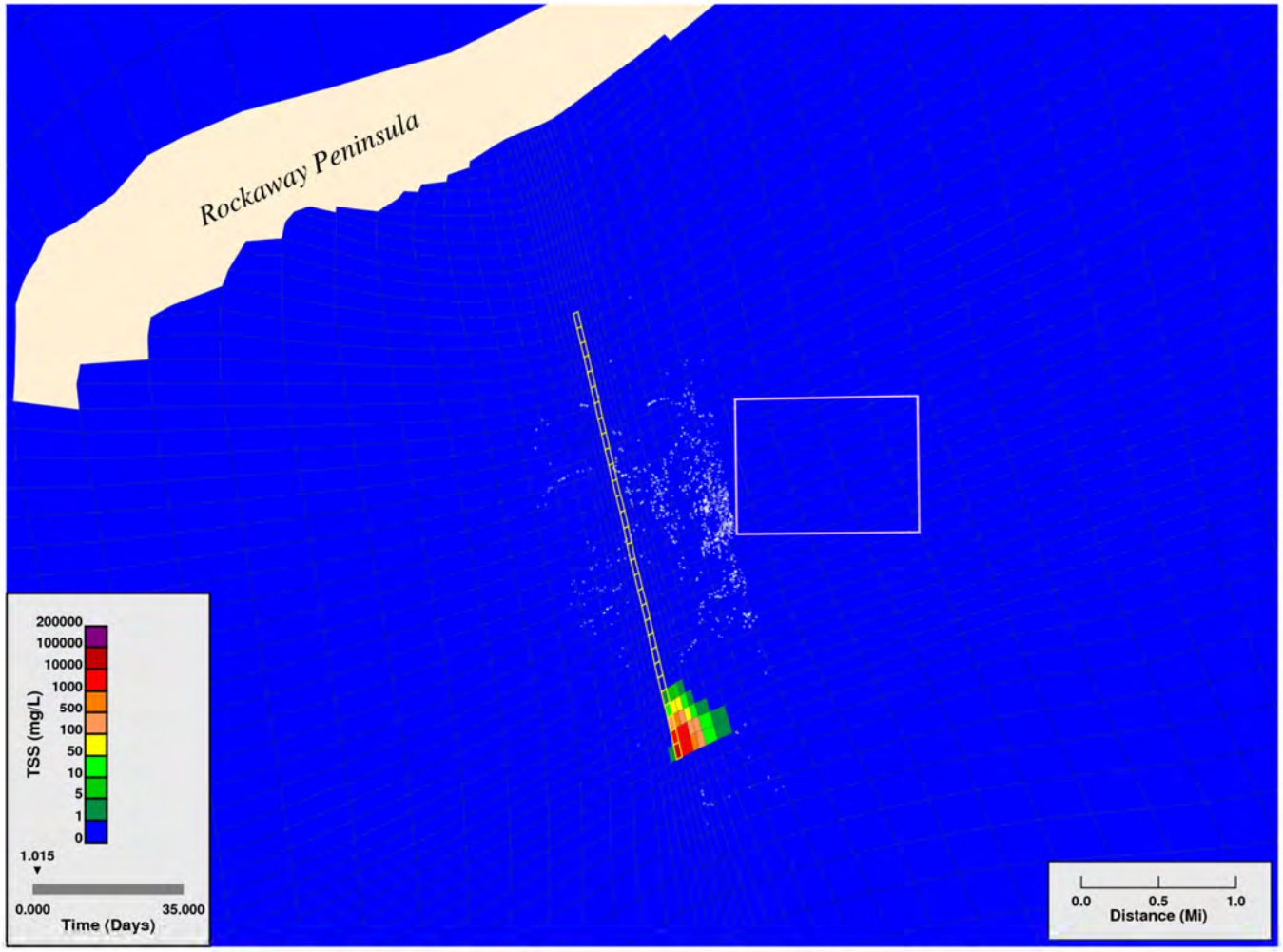

Figure 40. Typical jetting: simulated suspended solids near water column bottom, start of trenching, rate = 183 m/hr.

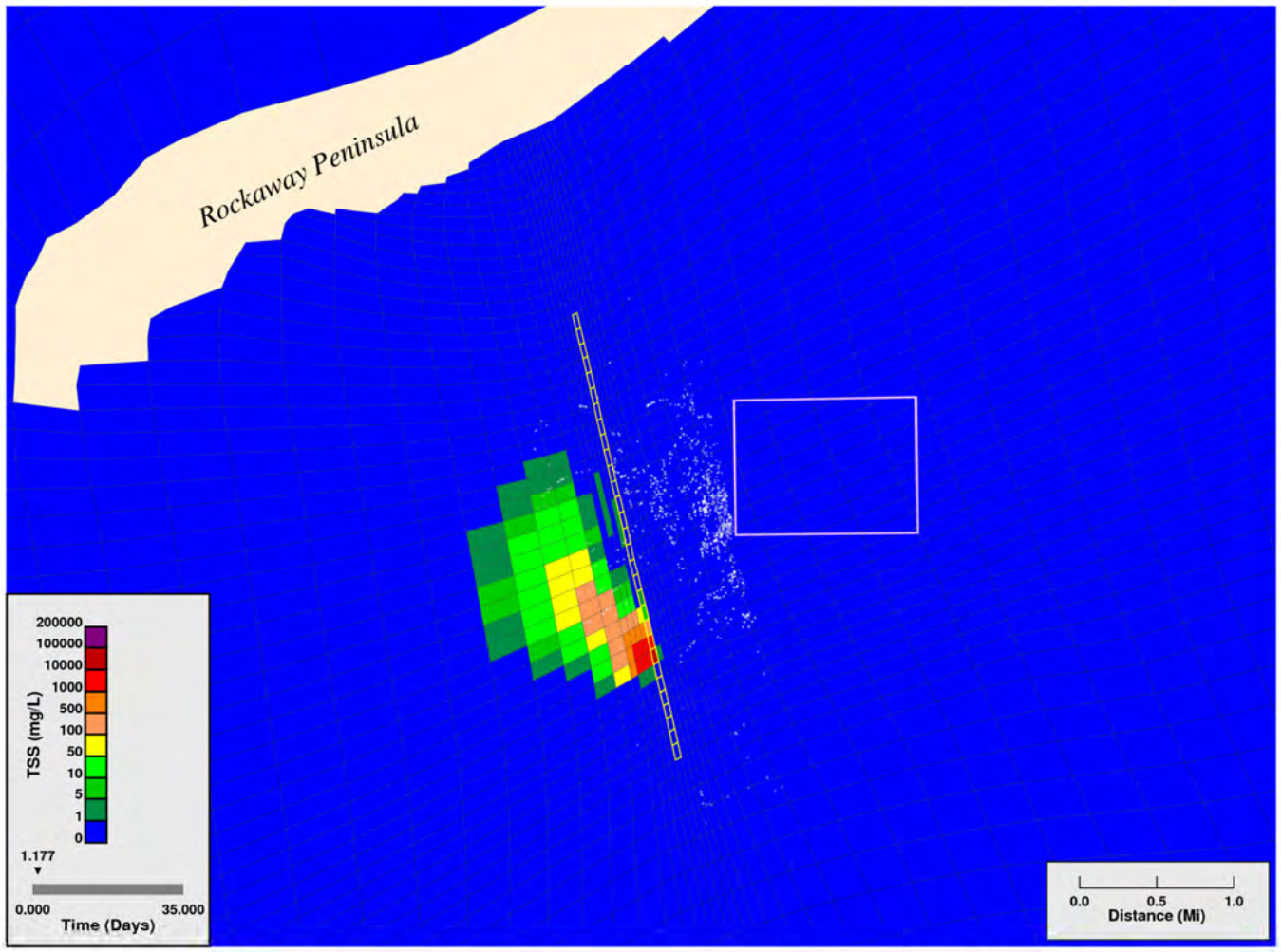

Figure 41. Typical jetting: simulated suspended solids near water column bottom, trenching 25% complete, rate = 183 m/hr.

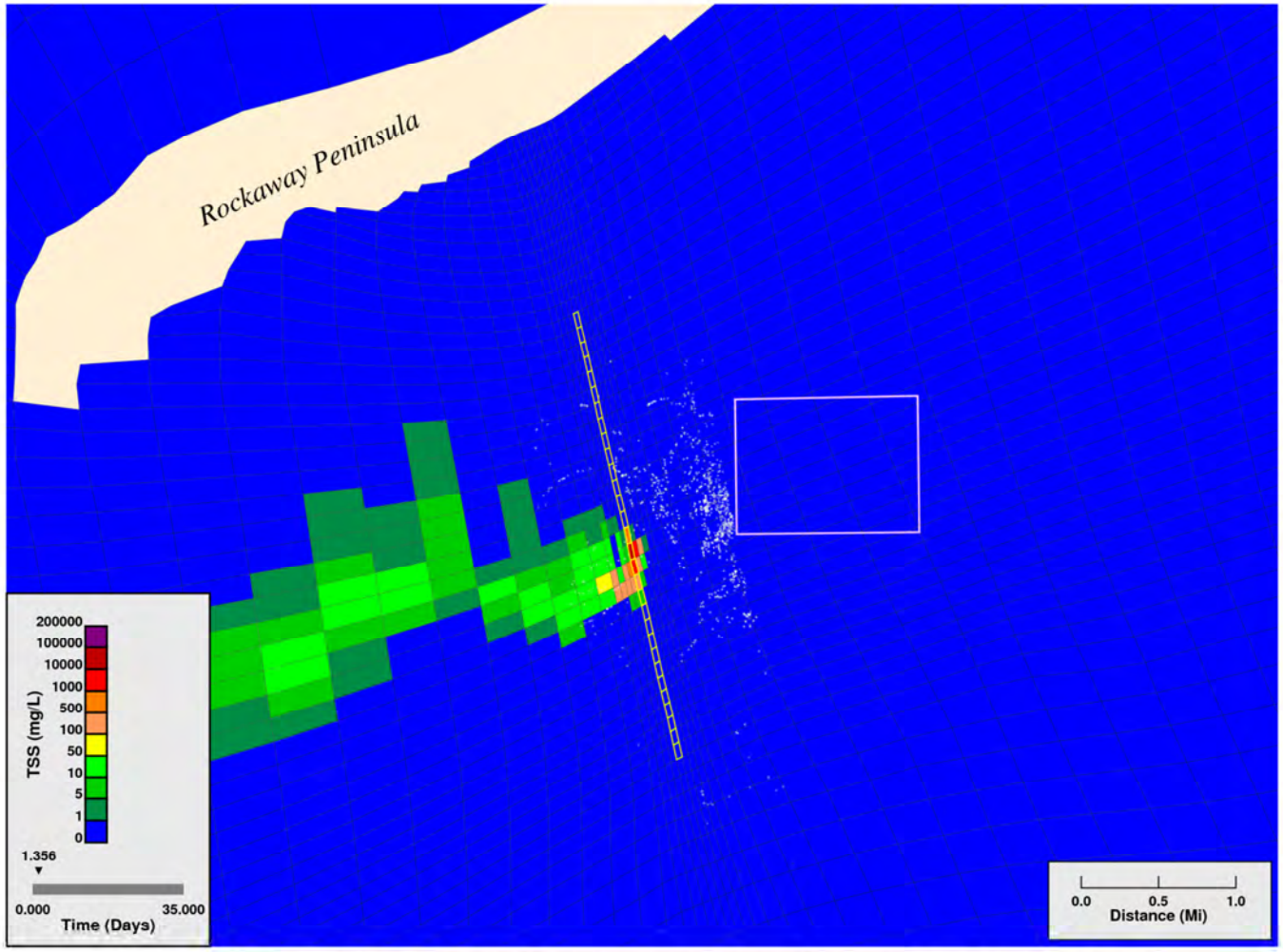

Figure 42. Typical jetting: simulated suspended solids near water column bottom, trenching 50% complete, rate = 183 m/hr.

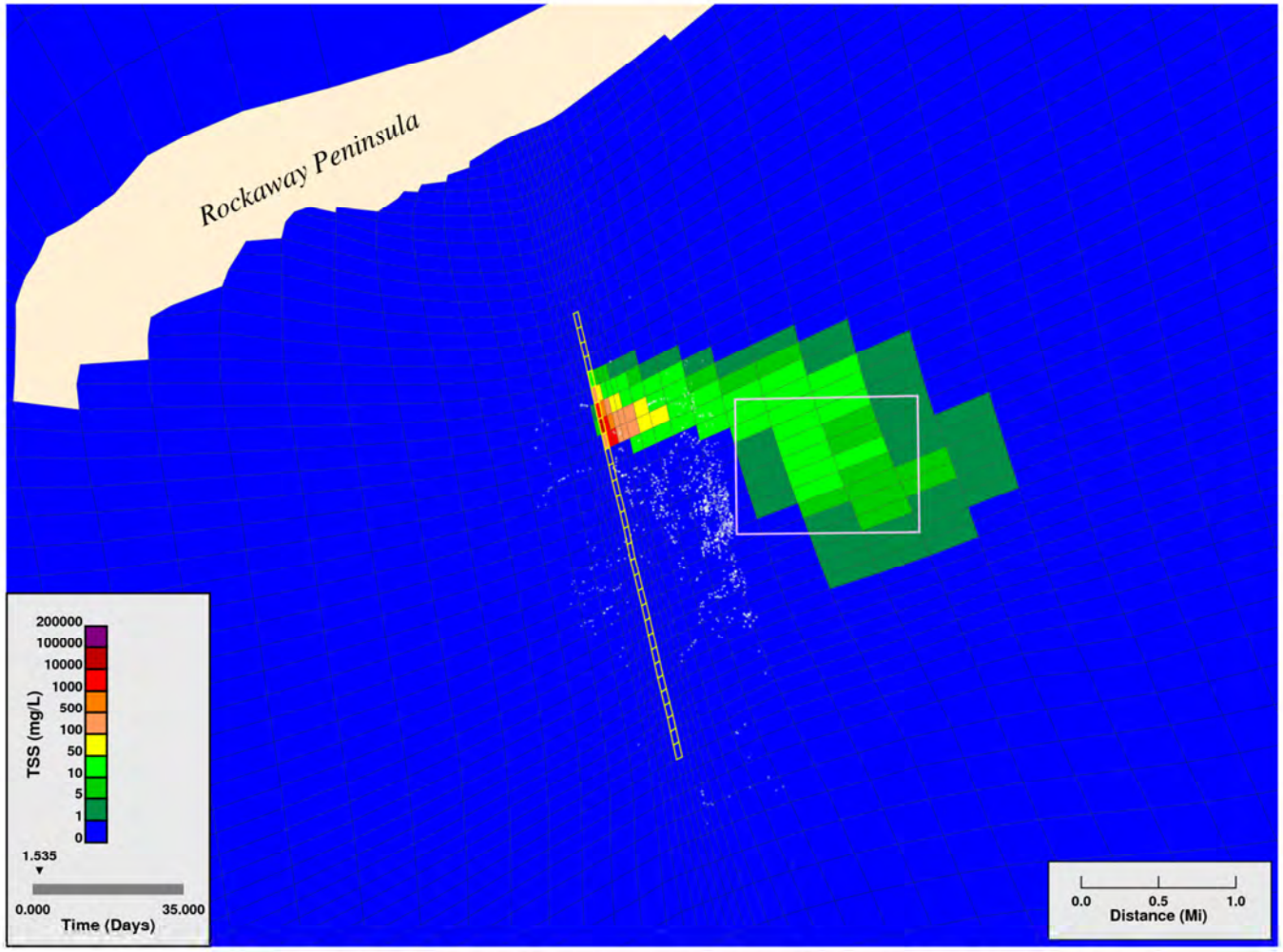

Figure 43. Typical jetting: simulated suspended solids near water column bottom, trenching 75% complete, rate = 183 m/hr.

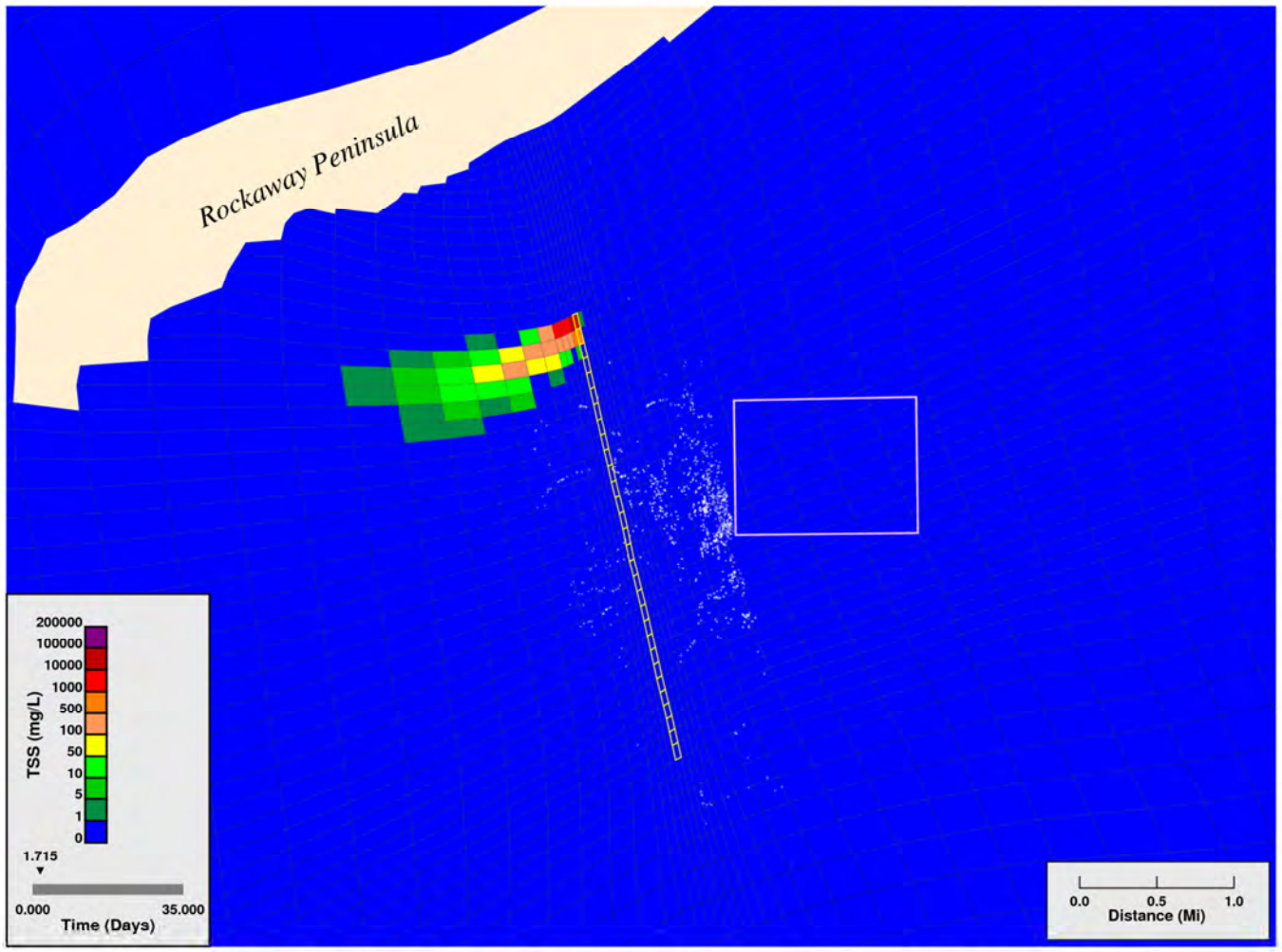

Figure 44. Typical jetting: simulated suspended solids near water column bottom, end of trenching, rate = 183 m/hr.

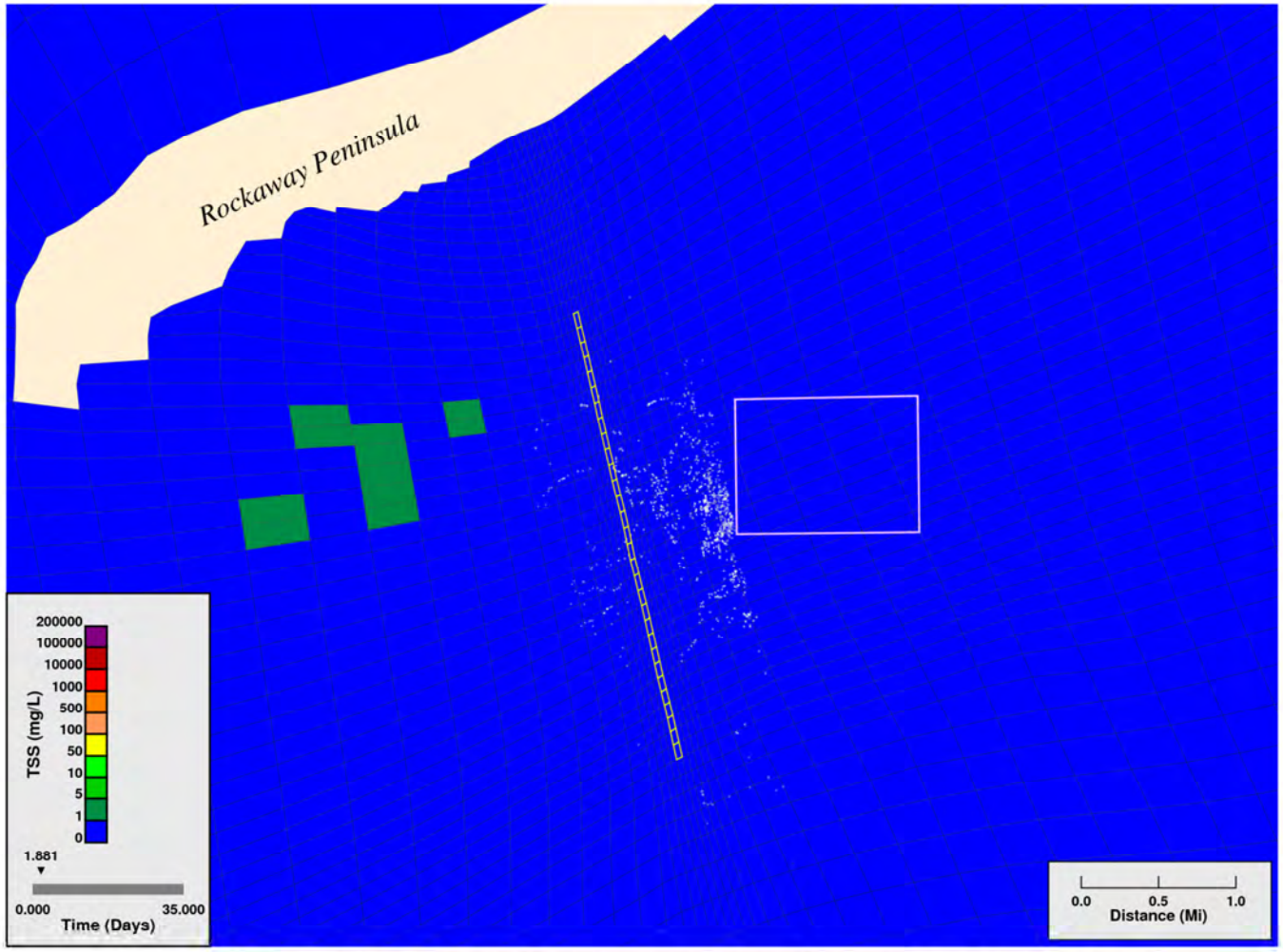

Figure 45. Typical jetting: simulated suspended solids near water column bottom: 4 hrs after end of trenching, rate = 183 m/hr.

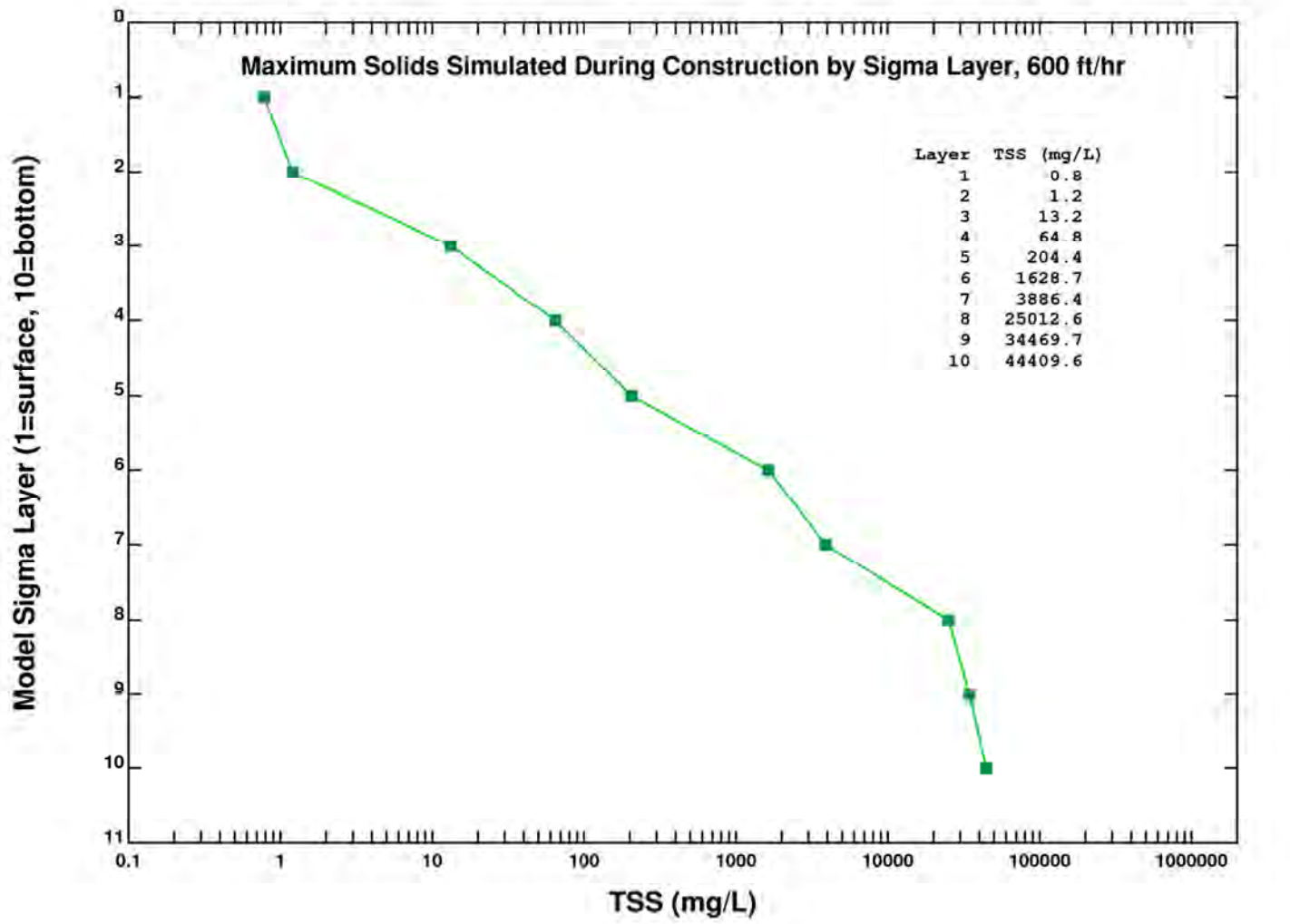

Figure 46. Typical jetting: maximum simulated suspended solids in any cell of each water column layer of model, rate = 183 m/hr.

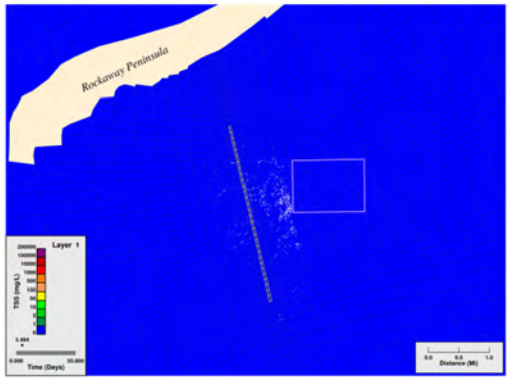

a) surface water layer

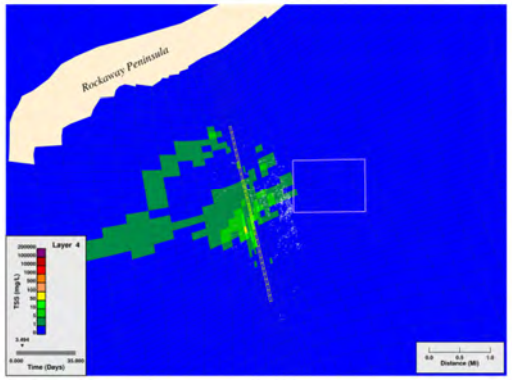

40% of water depth

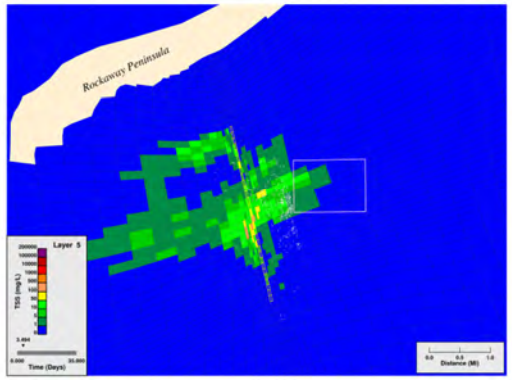

c) 50% of water depth

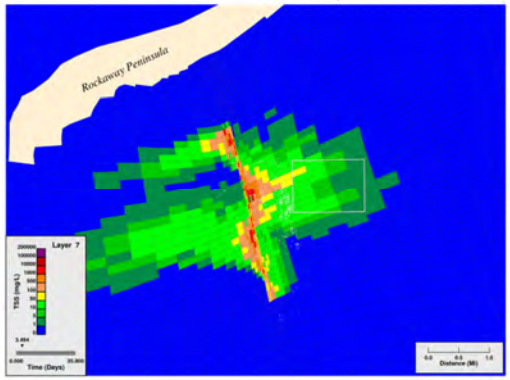

d) 70% of water depth

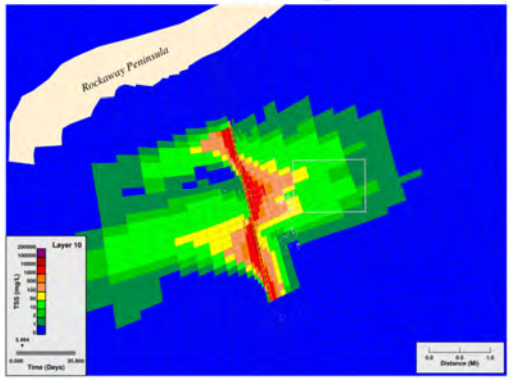

e) bottom water layer

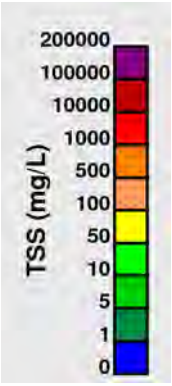

Notes: Values indicate the maximum solids concentration that occurred in each model grid at any time during the simulation. It should be noted the concentrations are elevated near the point of construction and rapidly decrease over time as a consequence of the relatively high settling velocities of sediment grains. Plumes clear the water column within 4 hours following the end of construction.

Figure 47. Typical jetting: maximum simulated suspended solids extent in selected water column sigma layers, rate = 183 m/hr.

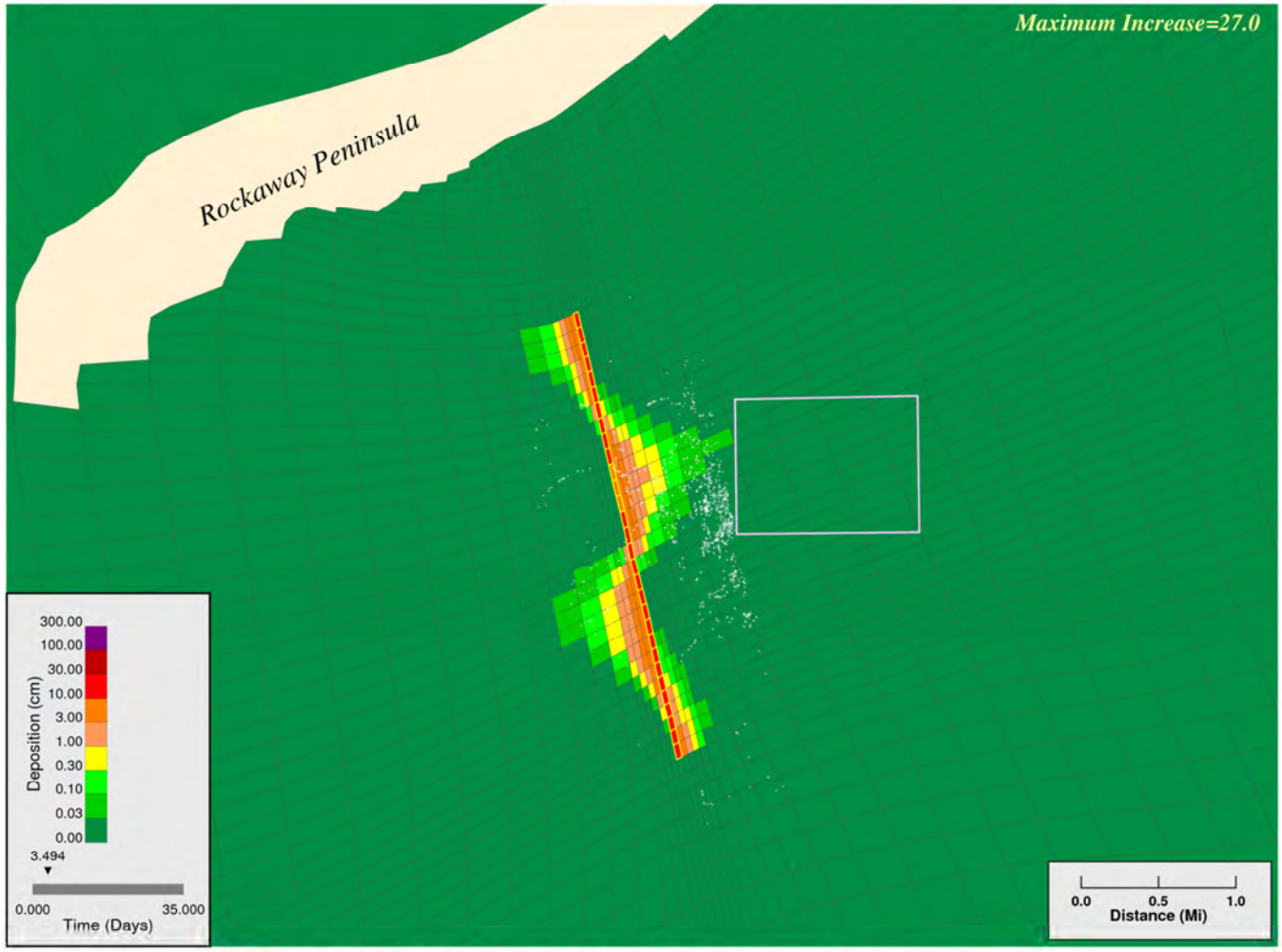

Figure 48. Typical jetting: simulated thickness of deposited solids on bed surface following trenching, rate = 183 m/hr.

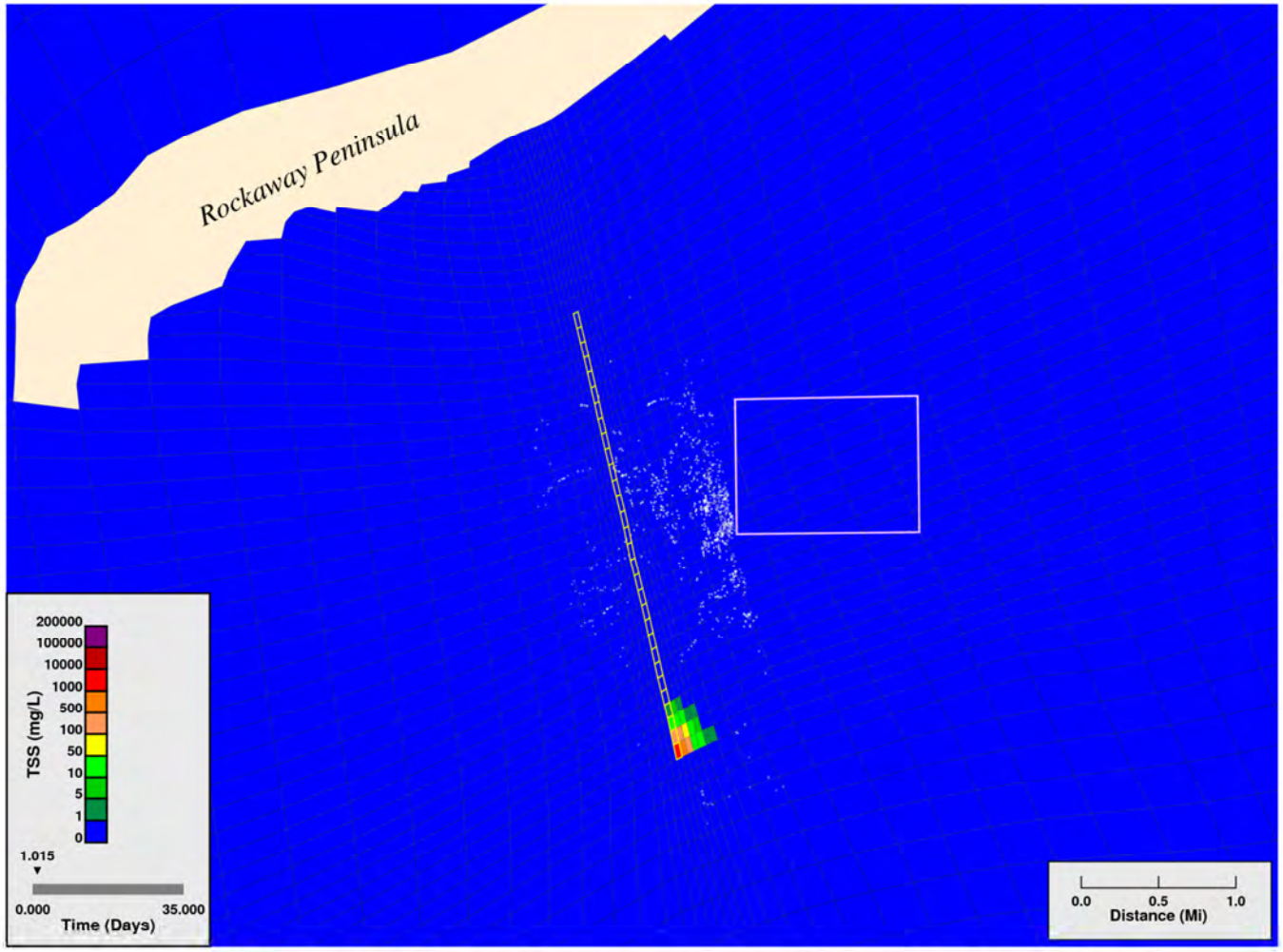

Figure 49. Worst case plowing: simulated suspended solids near water column bottom, start of trenching, rate = 183 m/hr.

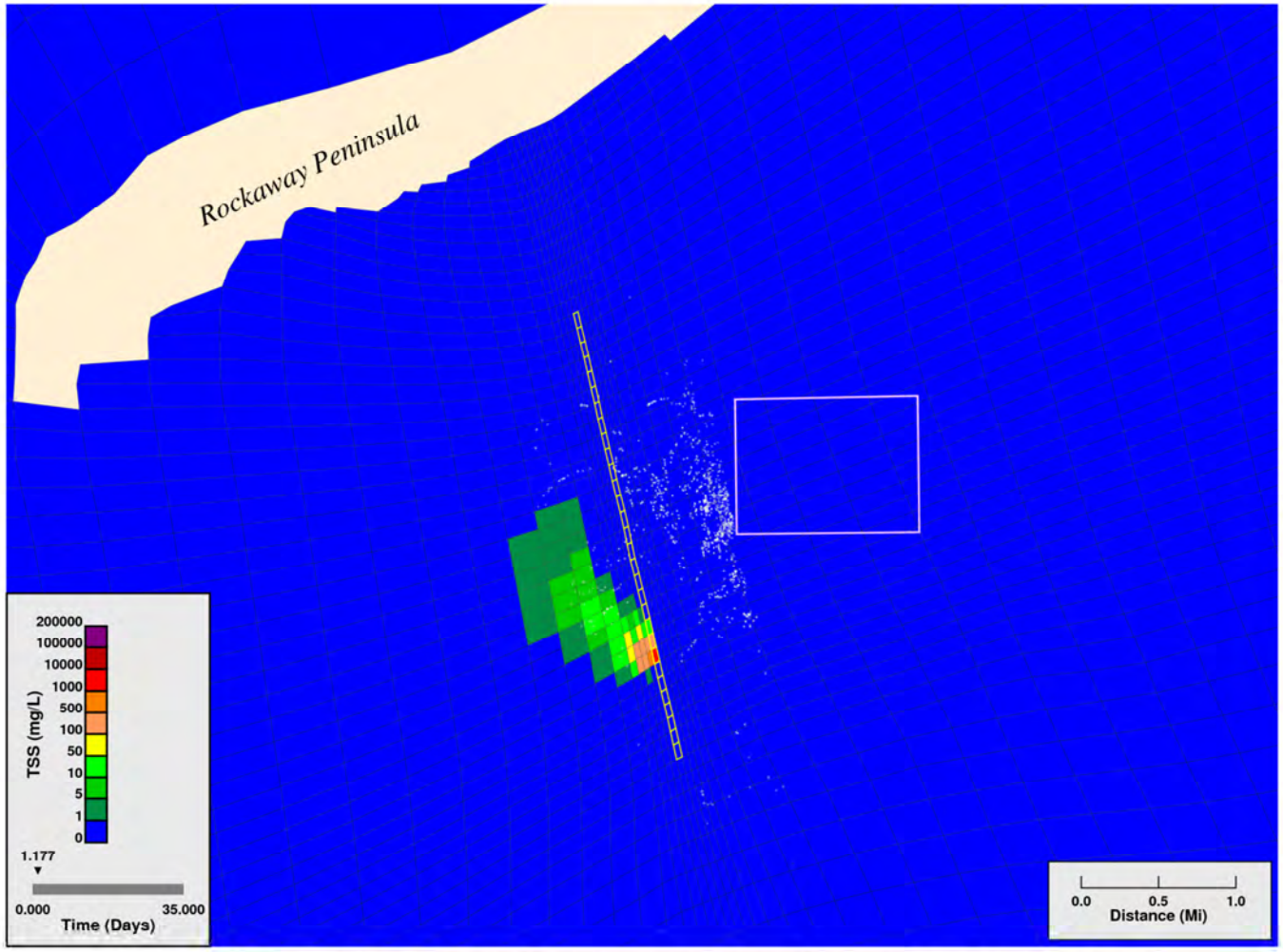

Bottom Layer Projected Solids Concentrations from Proposed Dredging, 600 ft/hr

Figure 50. Worst case plowing: simulated suspended solids near water column bottom, trenching 25% complete, rate = 183 m/hr.

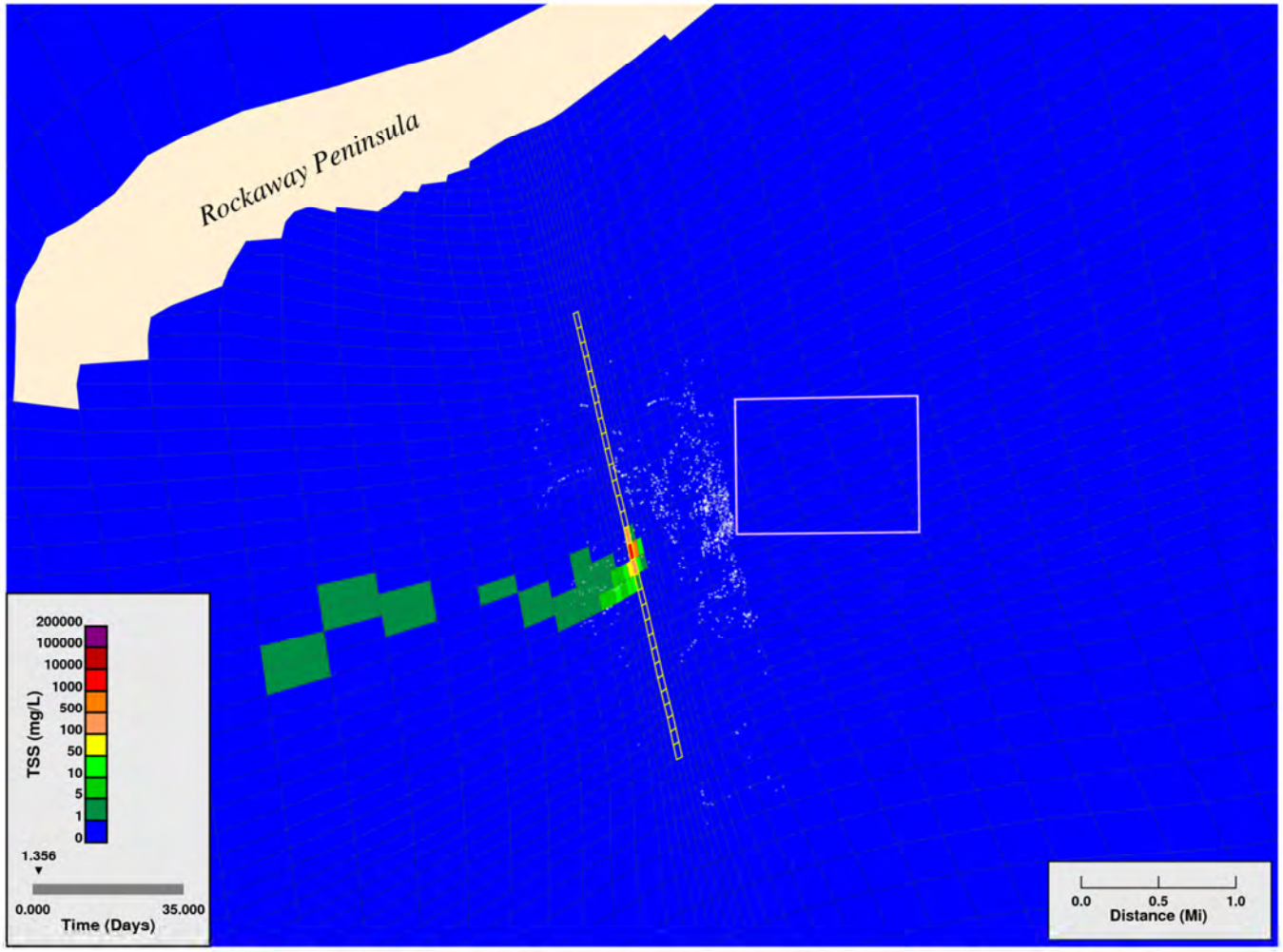

Bottom Layer Projected Solids Concentrations from Proposed Dredging, 600 ft/hr

Figure 51. Worst case plowing: simulated suspended solids near water column bottom, trenching 50% complete, rate = 183 m/hr.

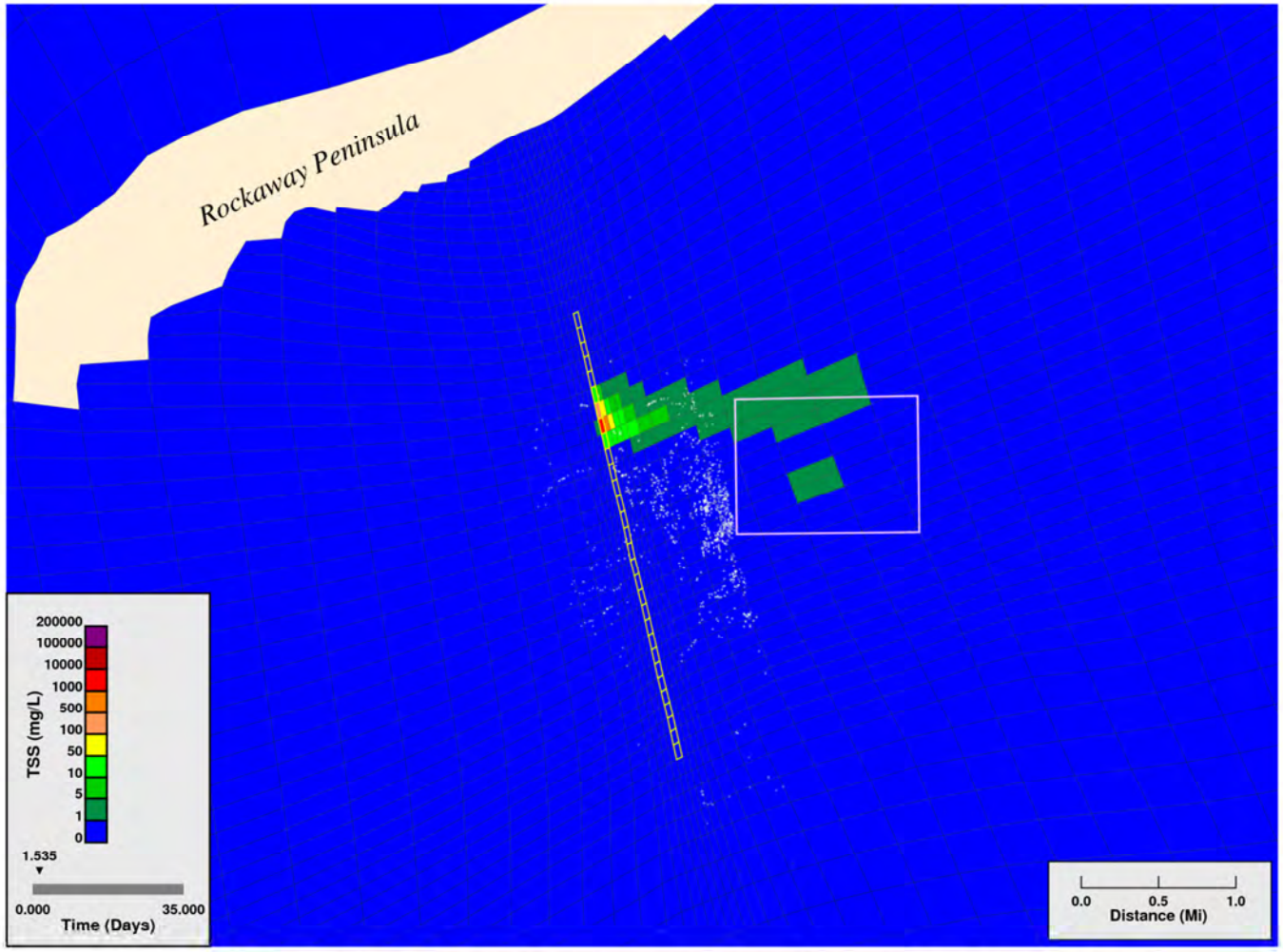

Figure 52. Worst case plowing: simulated suspended solids near water column bottom, trenching 75% complete, rate = 183 m/hr.

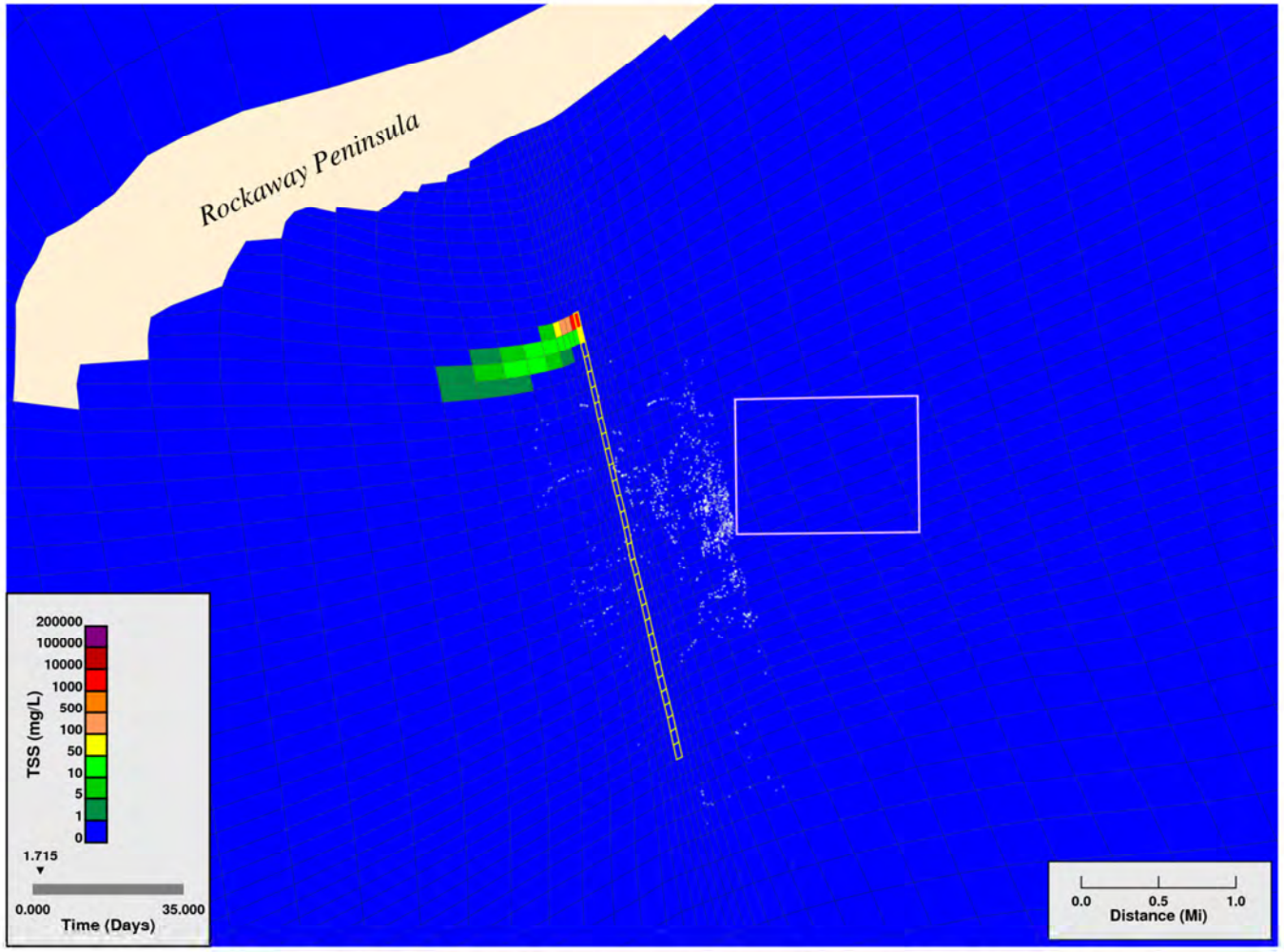

Figure 53. Worst case plowing: simulated suspended solids near water column bottom, end of trenching, rate = 183 m/hr.

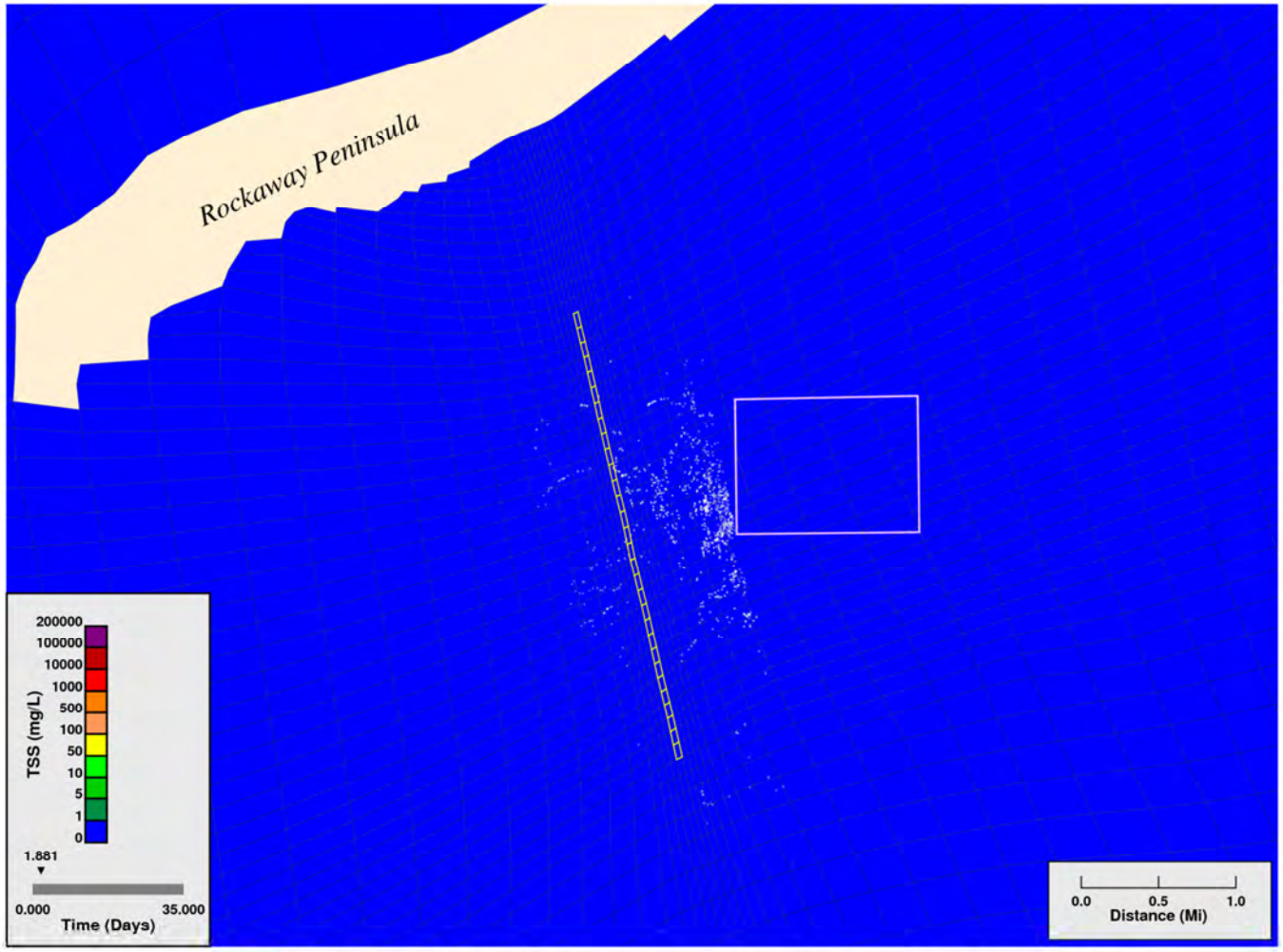

Bottom Layer Projected Solids Concentrations from Proposed Dredging, 600 ft/hr

Figure 54. Worst case plowing: simulated suspended solids near water column bottom: 4 hrs after end of trenching, rate = 183 m/hr.

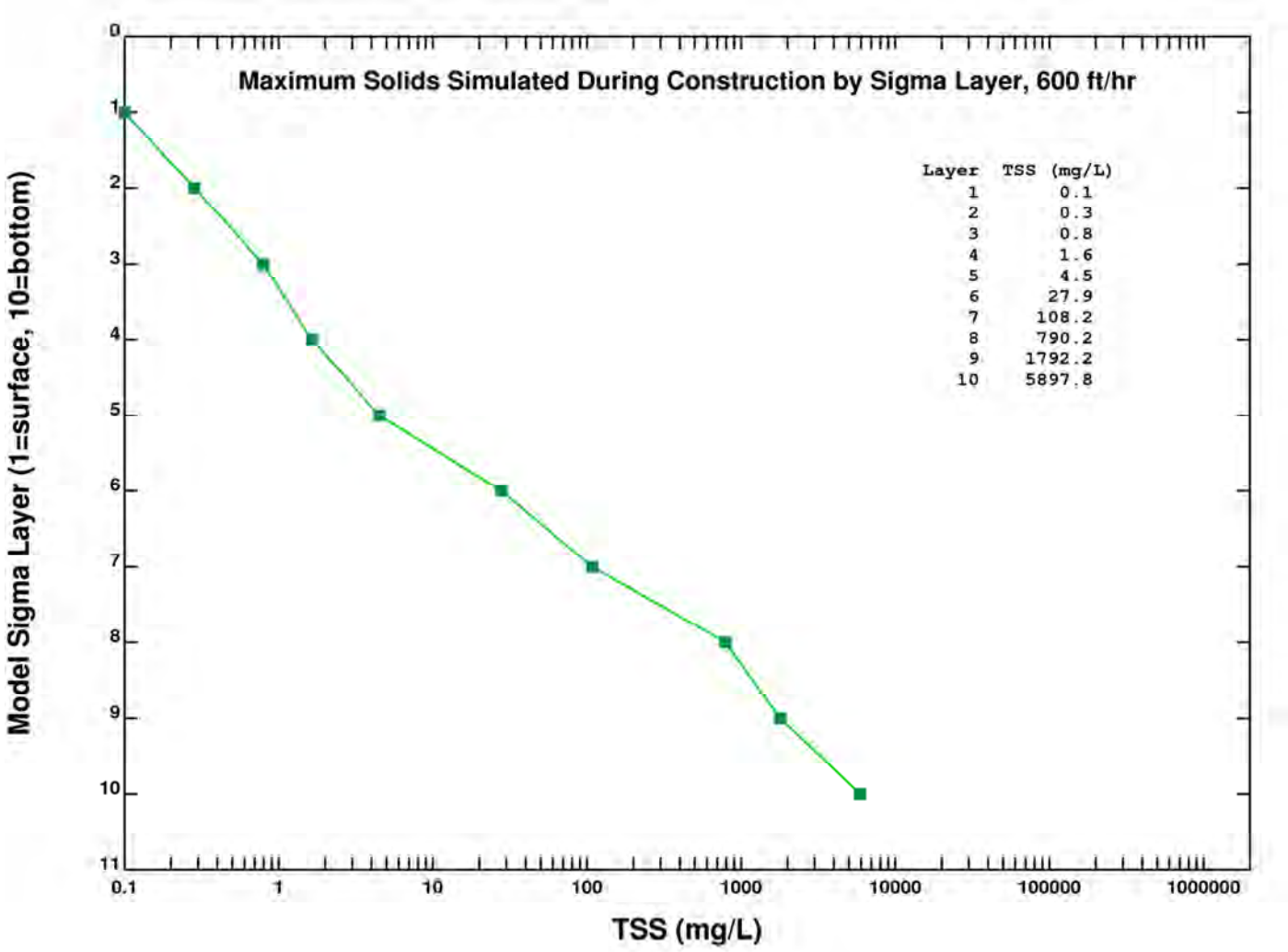

Figure 55. Worst case plowing: maximum simulated suspended solids in any cell of each water column layer of model, rate = 183 m/hr.

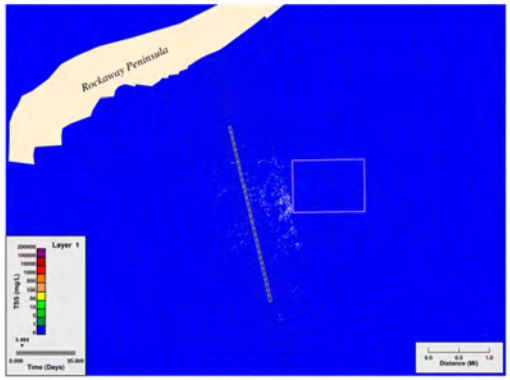

a) surface water layer

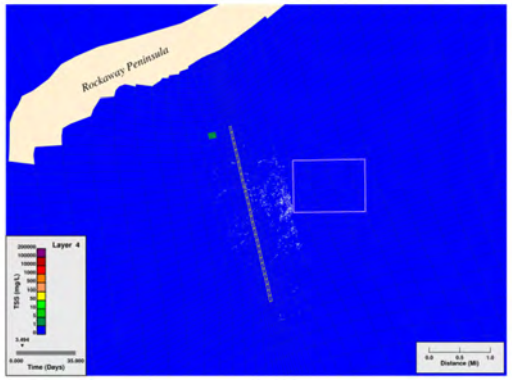

40% of water depth

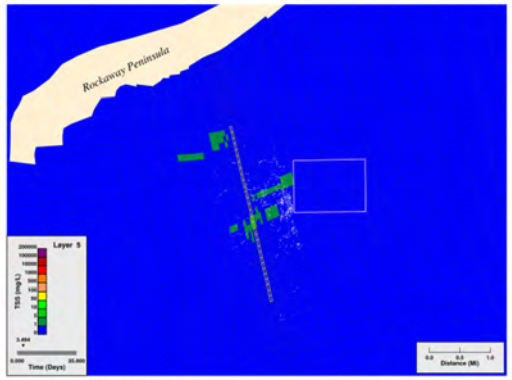

c) 50% of water depth

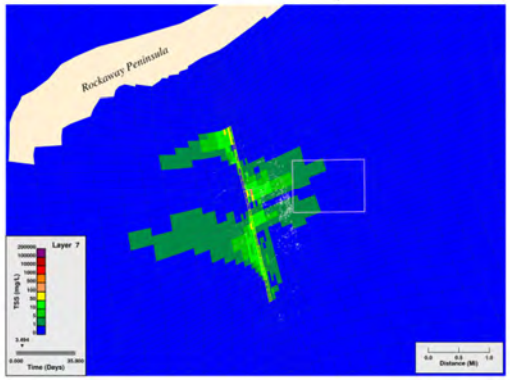

d) 70% of water depth

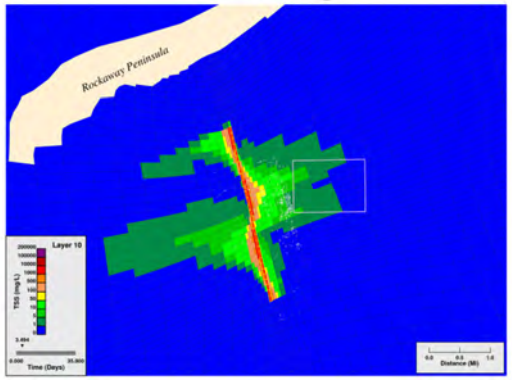

e) bottom water layer

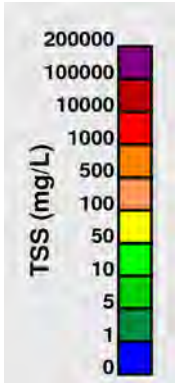

Notes: Values indicate the maximum solids concentration that occurred in each model grid at any time during the simulation. It should be noted the concentrations are elevated near the point of construction and rapidly decrease over time as a consequence of the relatively high settling velocities of sediment grains. Plumes clear the water column within 4 hours following the end of construction.

Figure 56. Worst case plowing: maximum simulated suspended solids extent in selected water column sigma layers, rate = 183 m/hr.

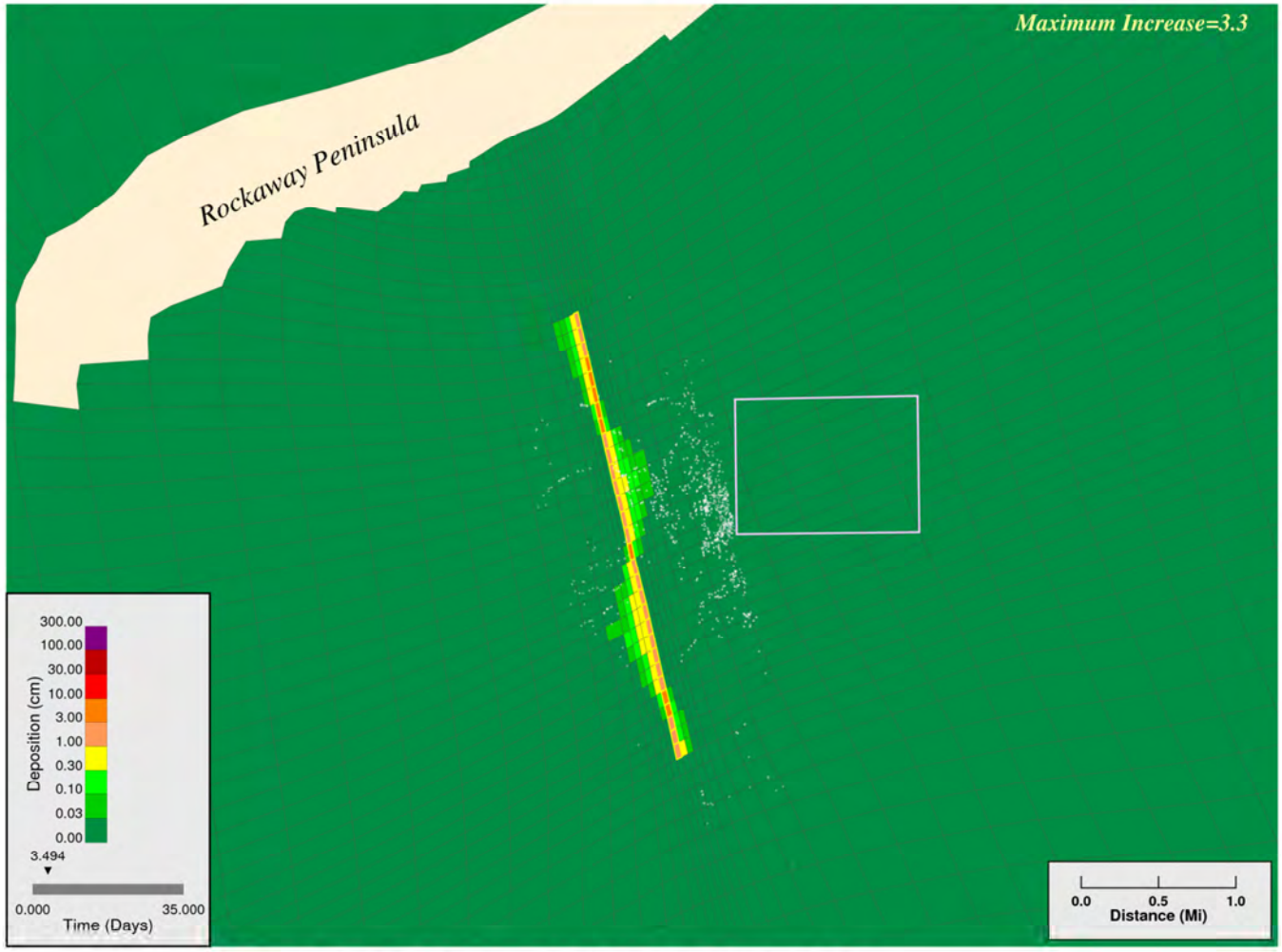

Figure 57. Worst case plowing: simulated thickness of deposited solids on bed surface following trenching, rate = 183 m/hr.

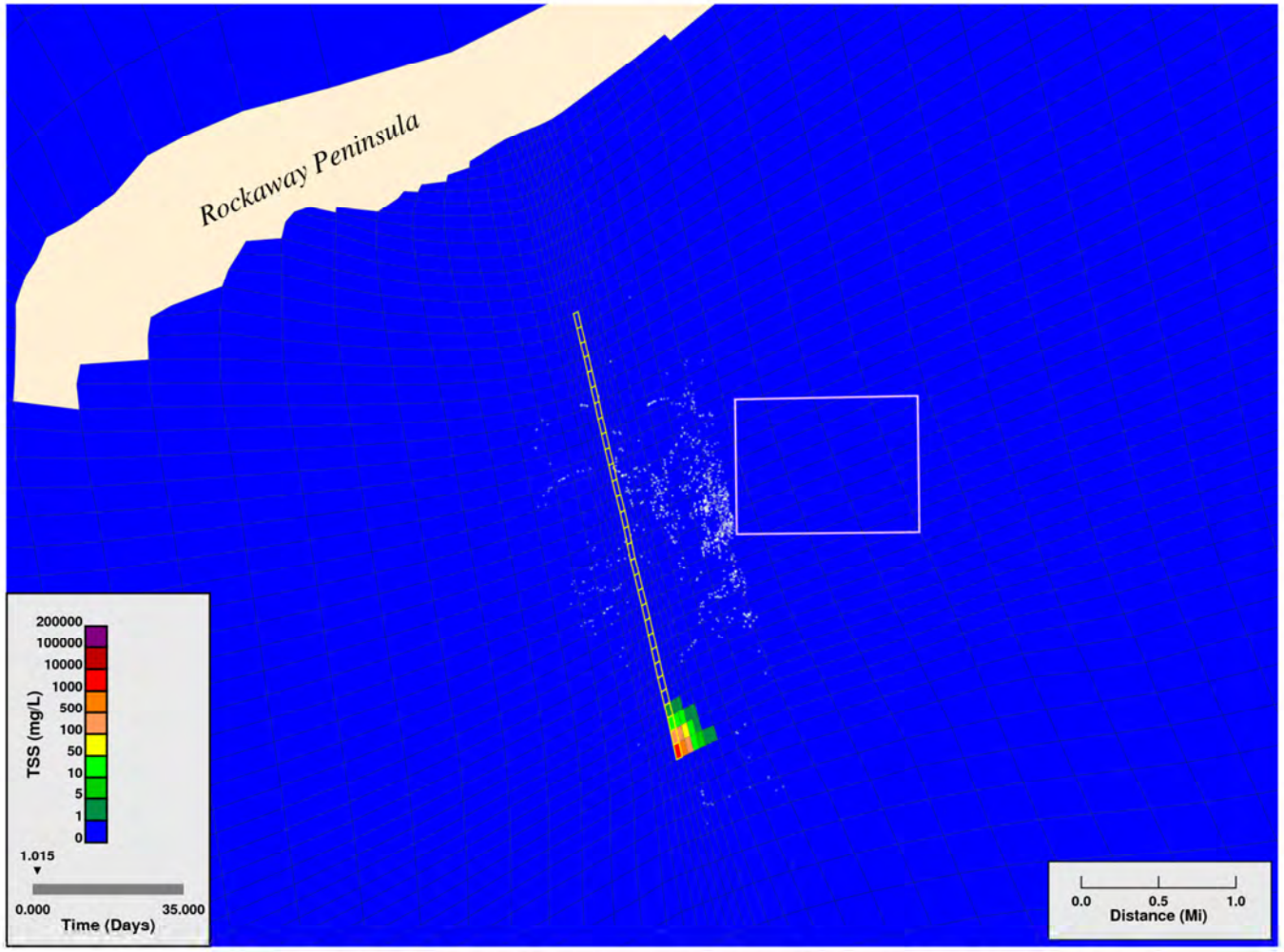

Figure 58. Typical plowing: simulated suspended solids near water column bottom, start of trenching, rate = 183 m/hr.

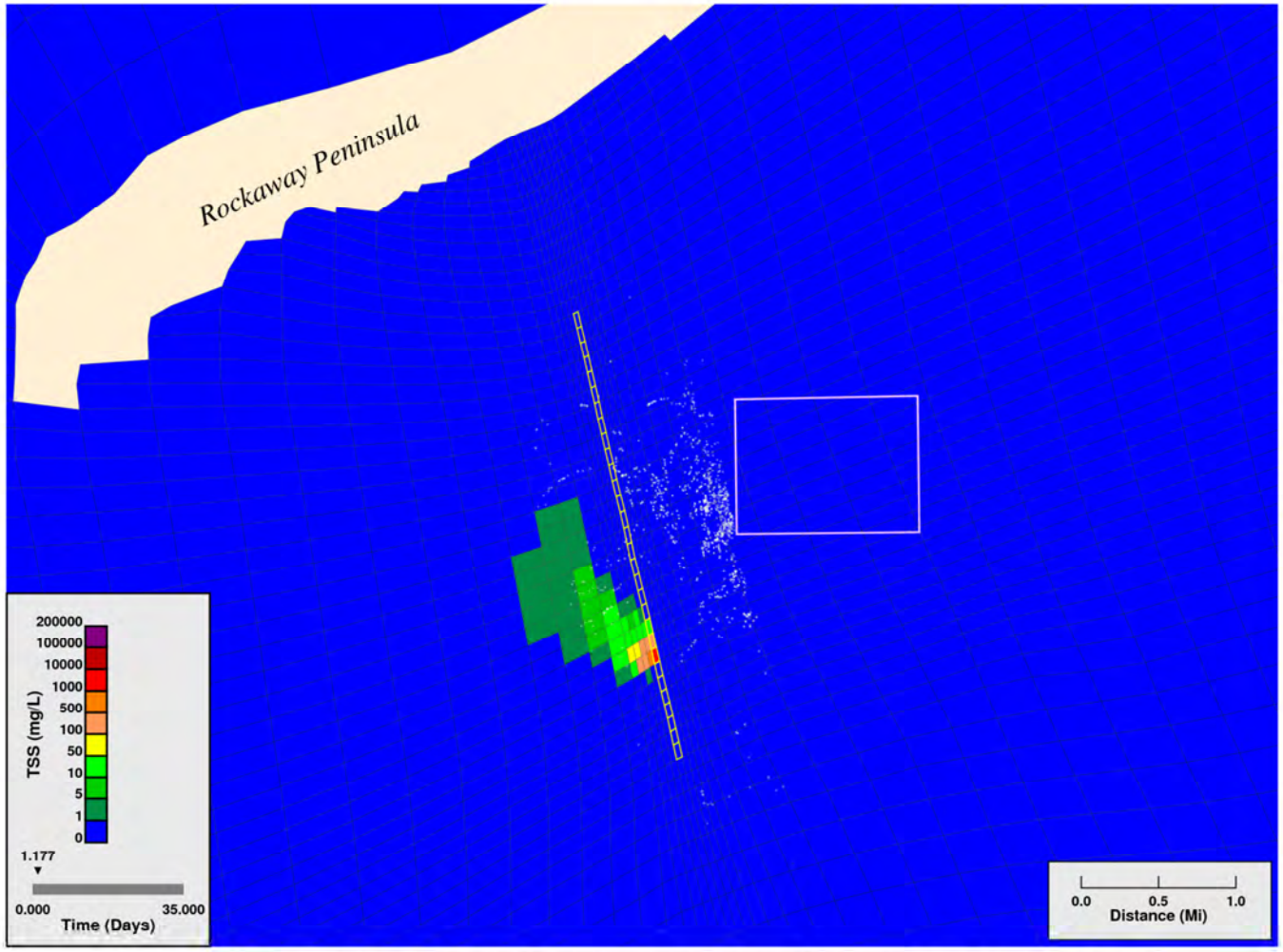

Bottom Layer Projected Solids Concentrations from Proposed Dredging, 600 ft/hr

Figure 59. Typical plowing: simulated suspended solids near water column bottom, trenching 25% complete, rate = 183 m/hr.

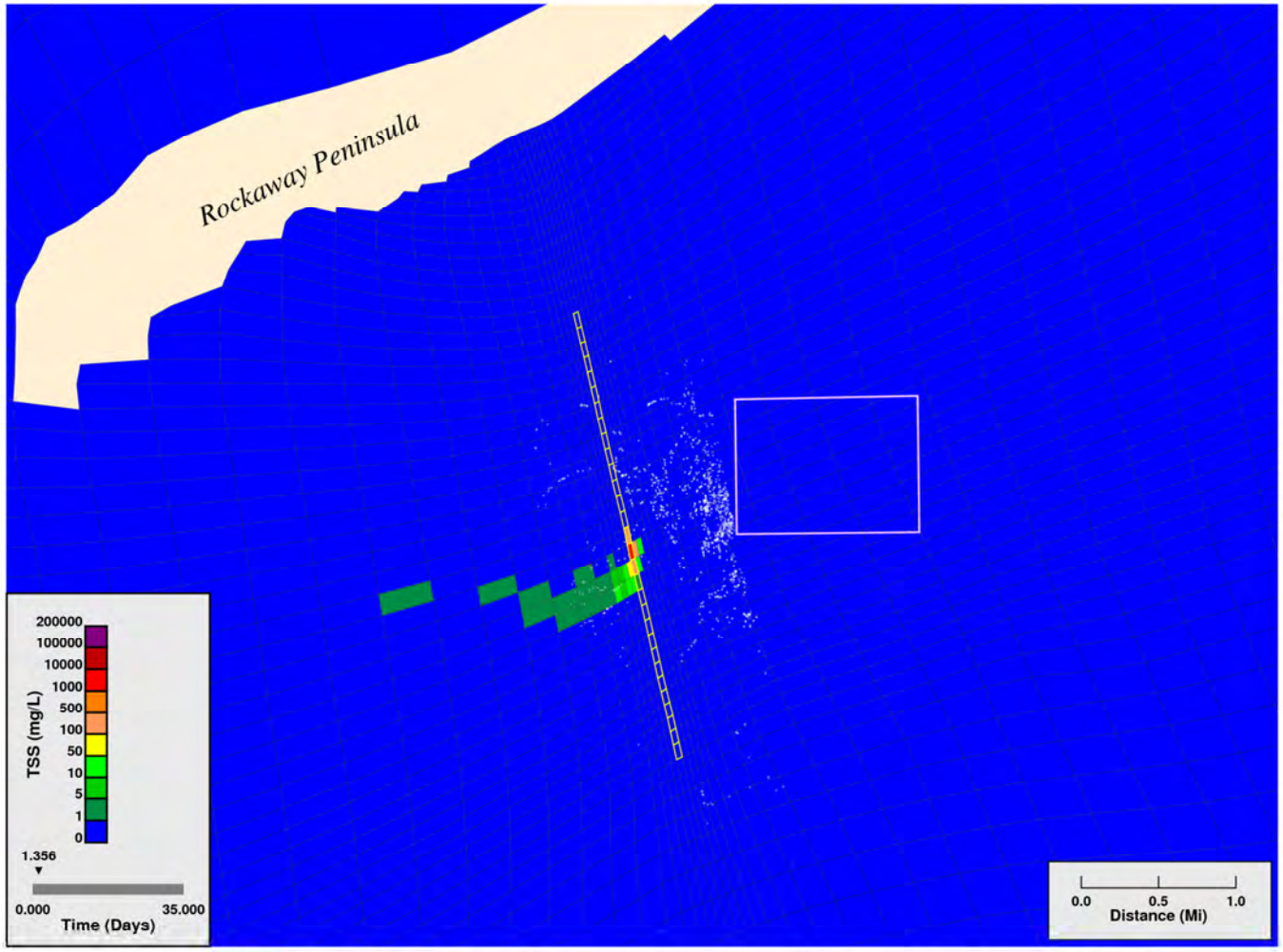

Figure 60. Typical plowing: simulated suspended solids near water column bottom, trenching 50% complete, rate = 183 m/hr.

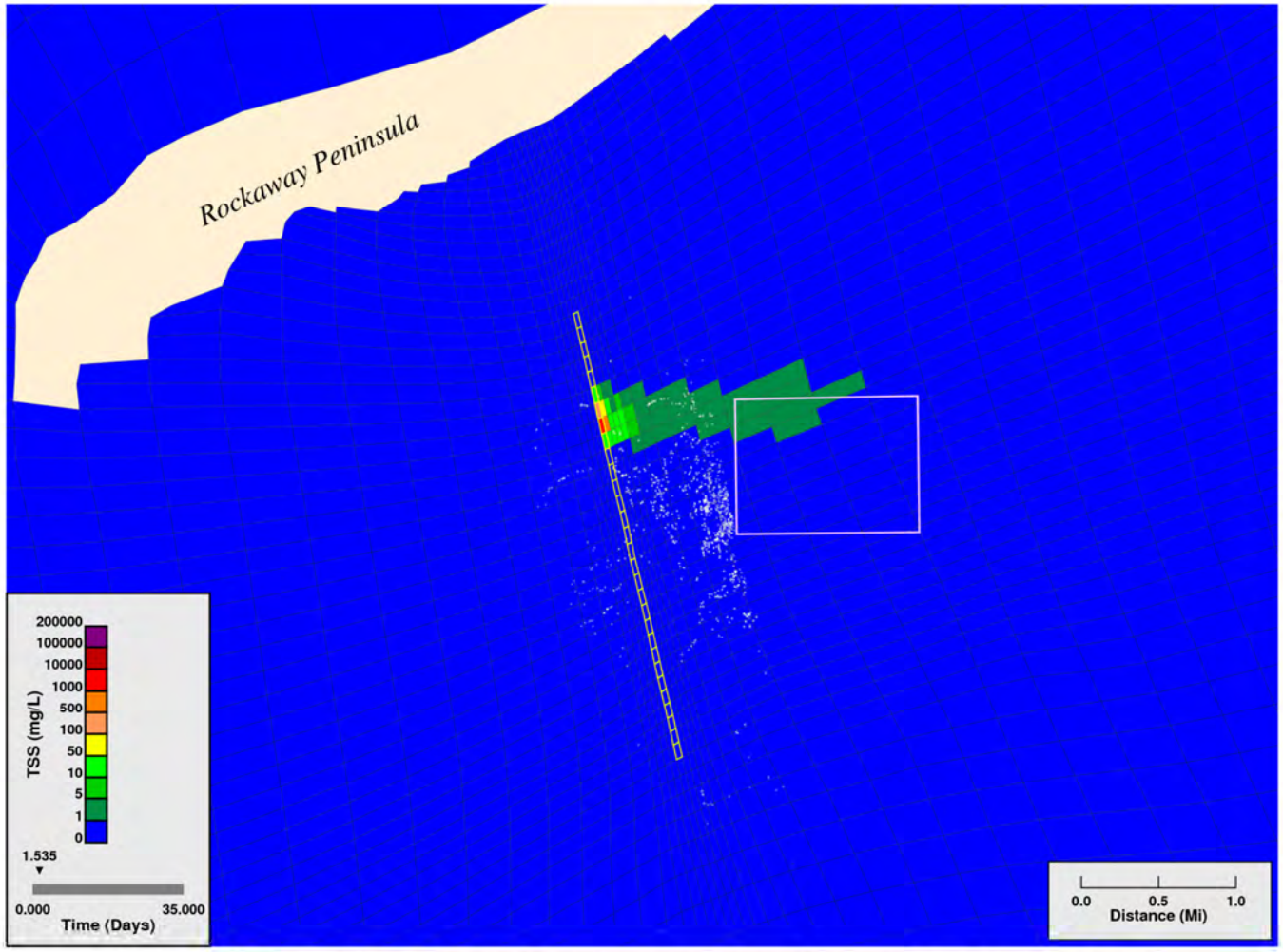

Figure 61. Typical plowing: simulated suspended solids near water column bottom, trenching 75% complete, rate = 183 m/hr.

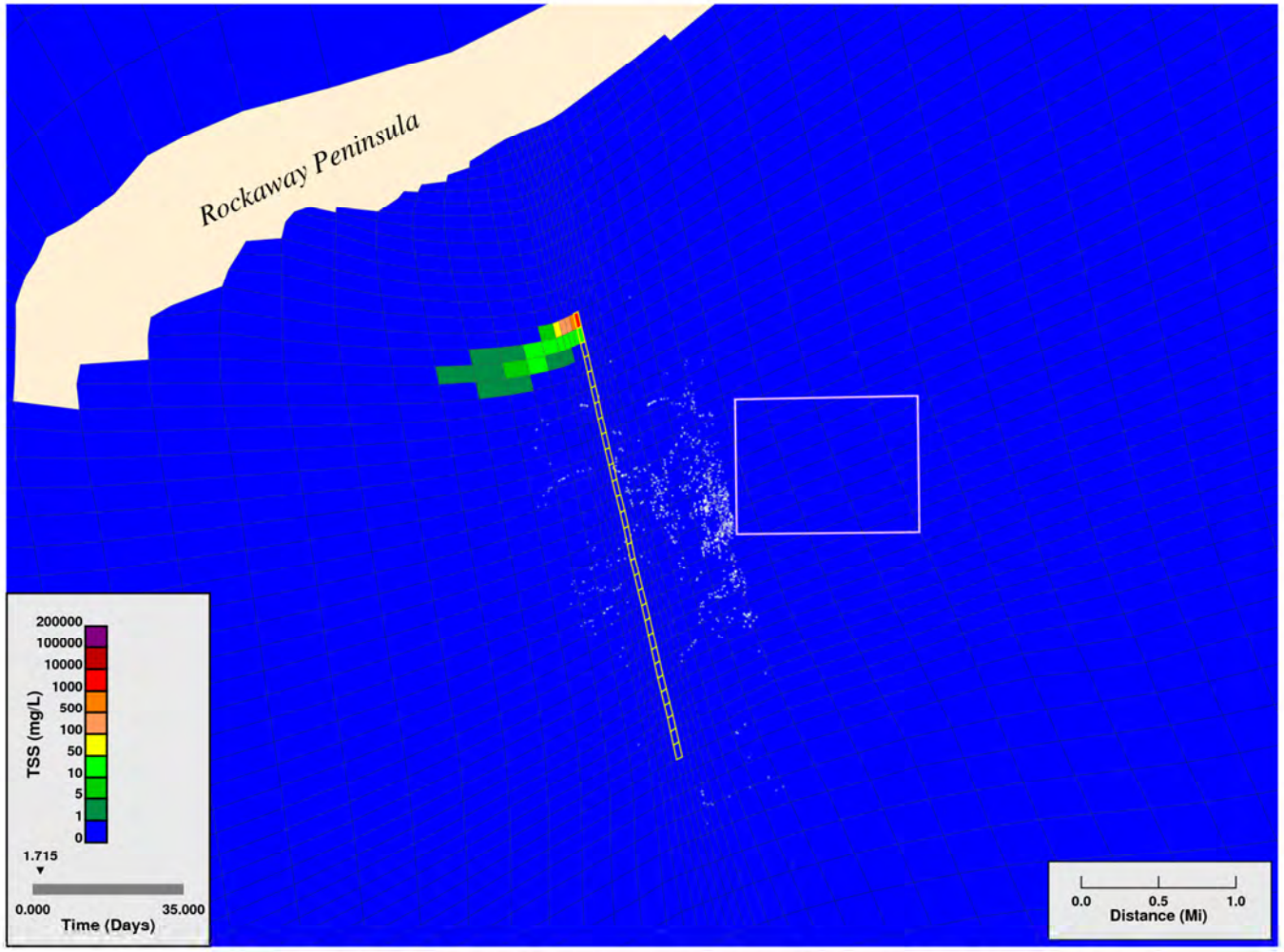

Figure 62. Typical plowing: simulated suspended solids near water column bottom, end of trenching, rate = 183 m/hr.

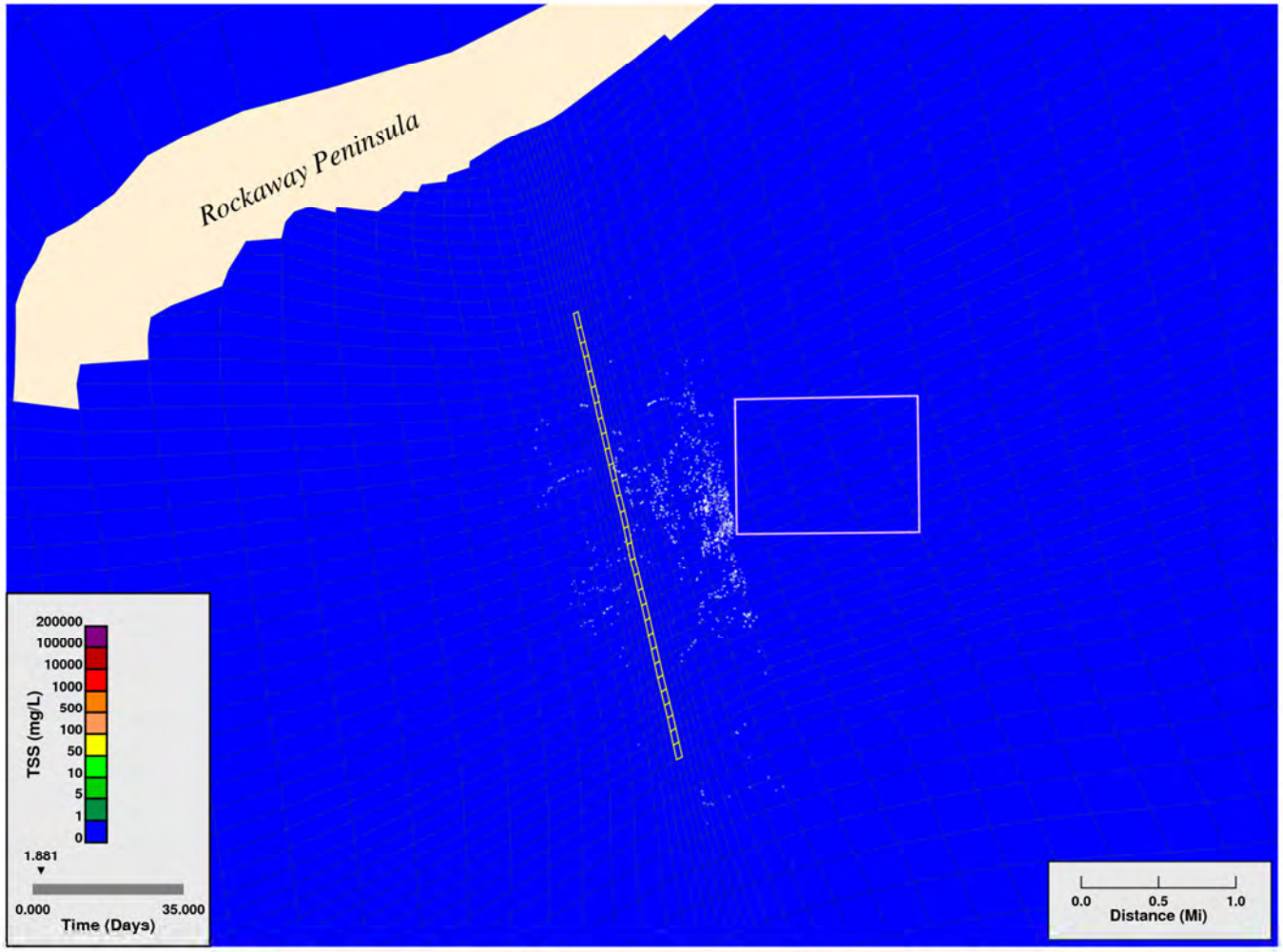

Figure 63. Typical plowing: simulated suspended solids near water column bottom: 4 hrs after end of trenching, rate = 183 m/hr.

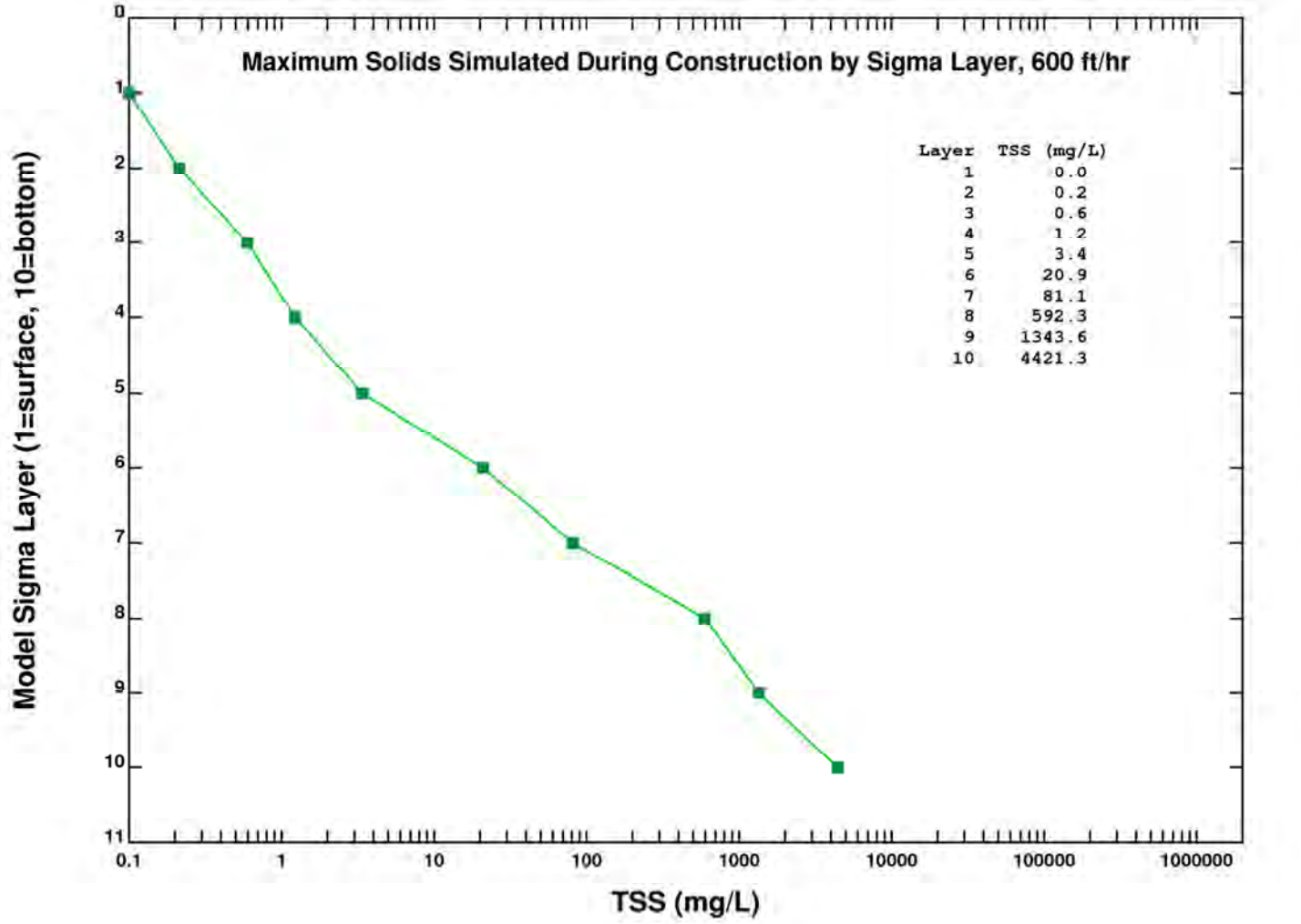

Figure 64. Typical plowing: maximum simulated suspended solids in each water column layer of model, rate = 183 m/hr.

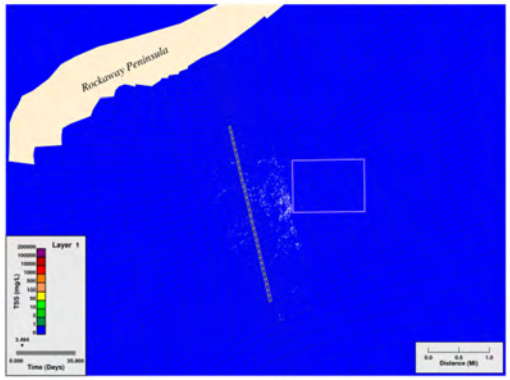

a) surface water layer

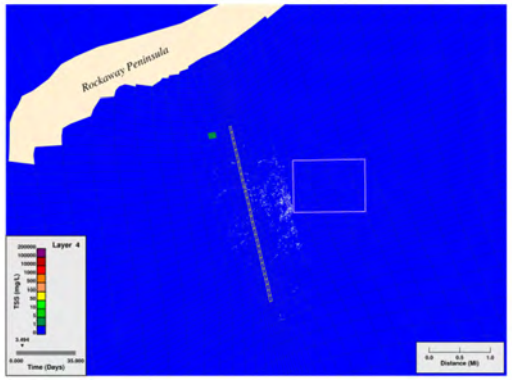

40% of water depth

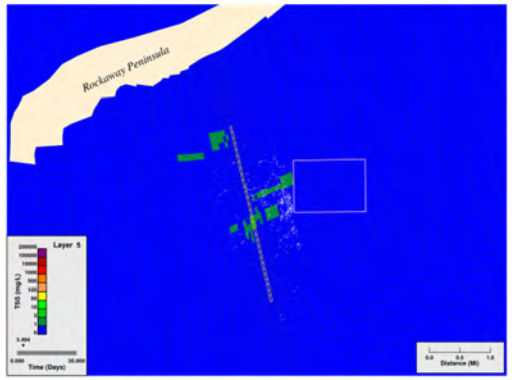

c) 50% of water depth

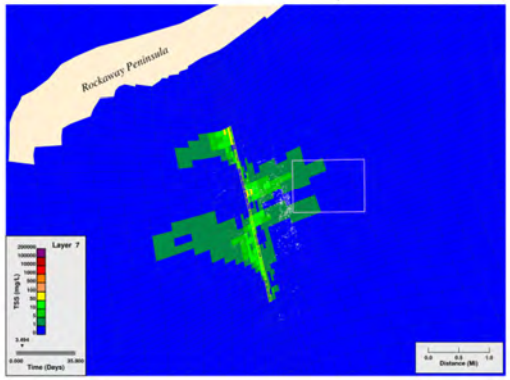

d) 70% of water depth

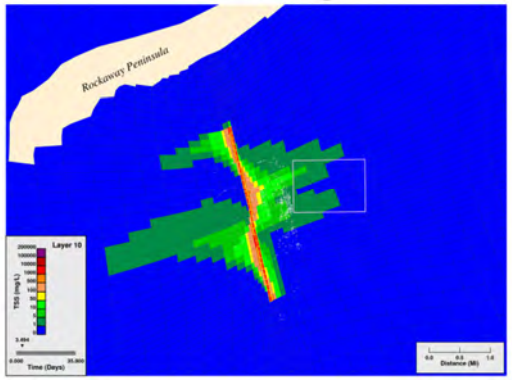

e) bottom water layer

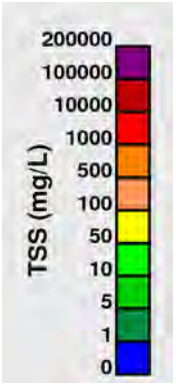

Notes: Values indicate the maximum solids concentration that occurred in each model grid at any time during the simulation. It should be noted the concentrations are elevated near the point of construction and rapidly decrease over time as a consequence of the relatively high settling velocities of sediment grains. Plumes clear the water column within 4 hours following the end of construction.

Figure 65. Typical plowing: maximum simulated suspended solids extent in selected water column sigma layers, rate = 183 m/hr.

Figure 66. Typical plowing: simulated thickness of deposited solids on bed surface following trenching, rate = 183 m/hr.

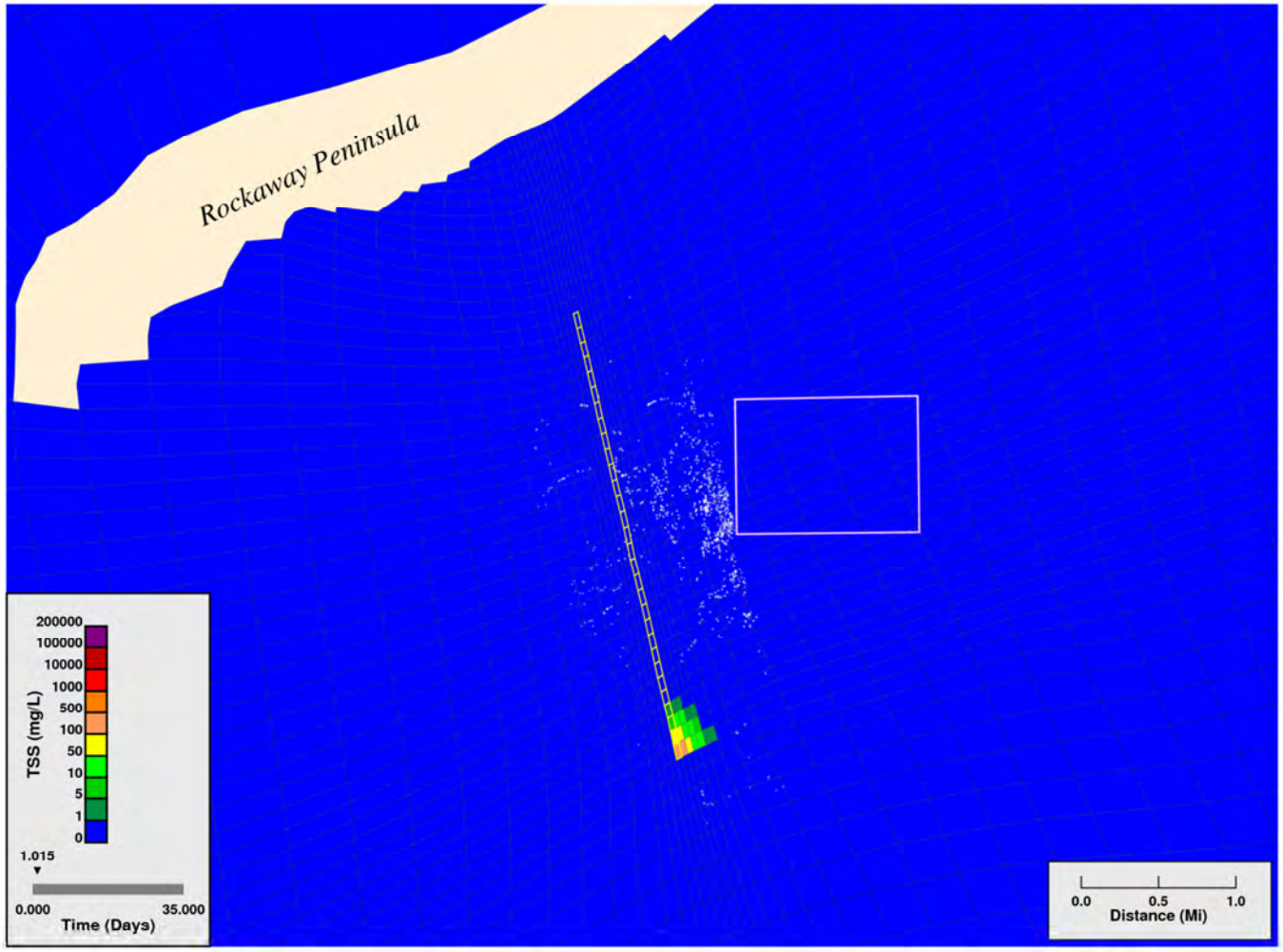

Bottom Layer Projected Solids Concentrations from Proposed Dredging, 13.8 ft/hr

Figure 67. Mechanical trenching: simulated suspended solids near water column bottom, start of dredging, rate = 4.2 m/hr.

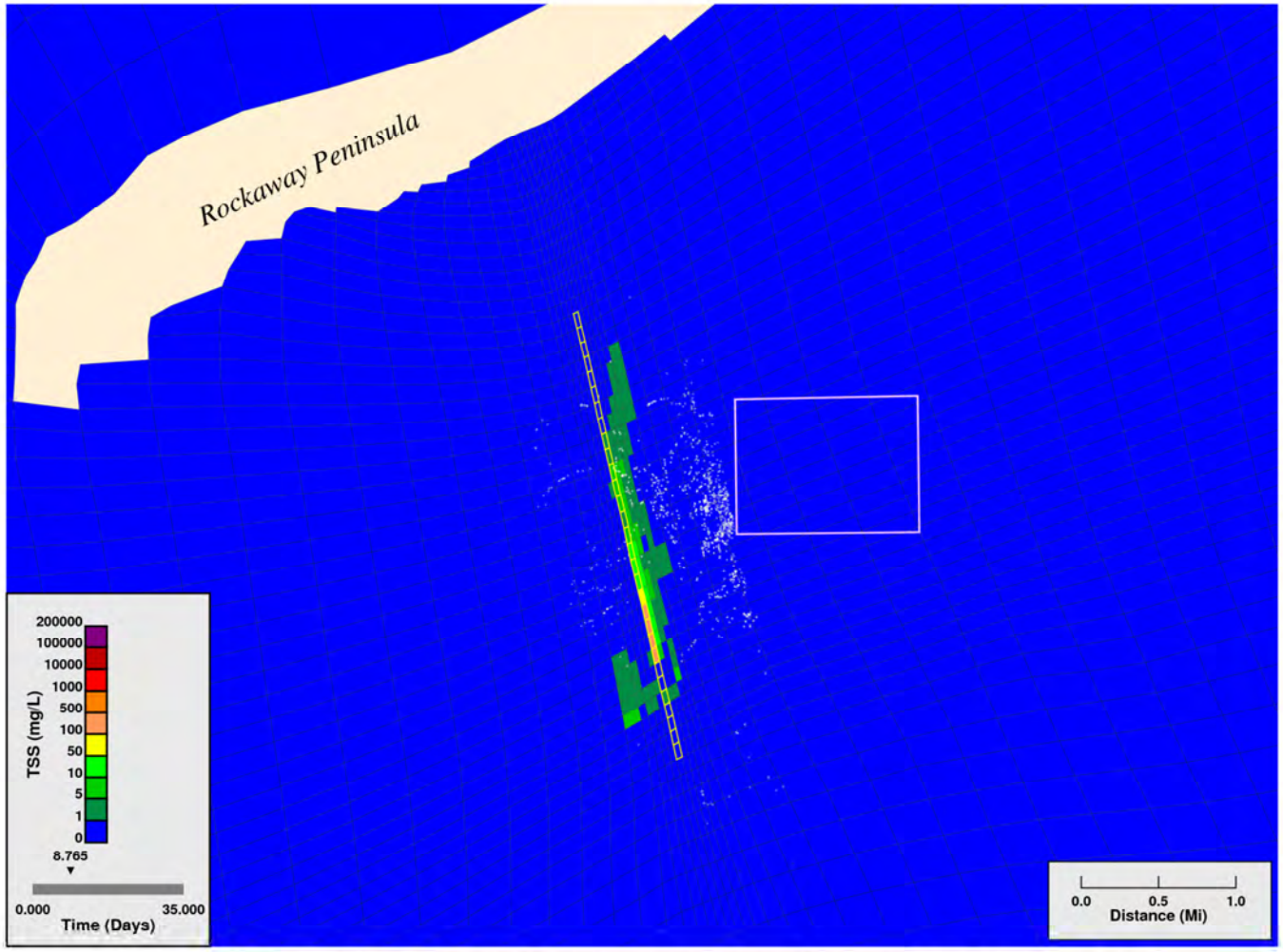

Figure 68. Mechanical trenching: simulated suspended solids near water column bottom, dredging 25% complete, rate = 4.2 m/hr.

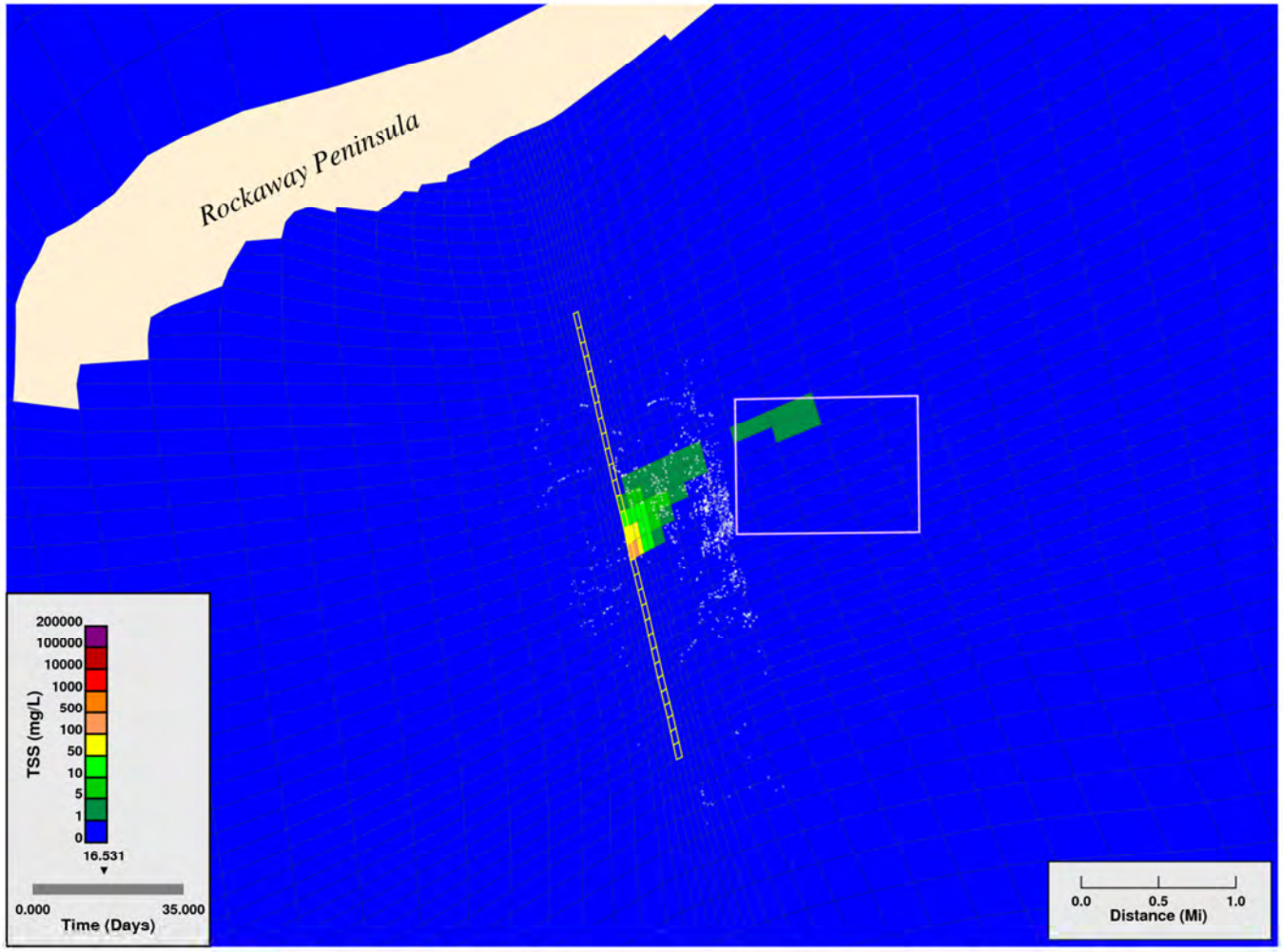

Figure 69. Mechanical trenching: simulated suspended solids near water column bottom, dredging 50% complete, rate = 4.2 m/hr.

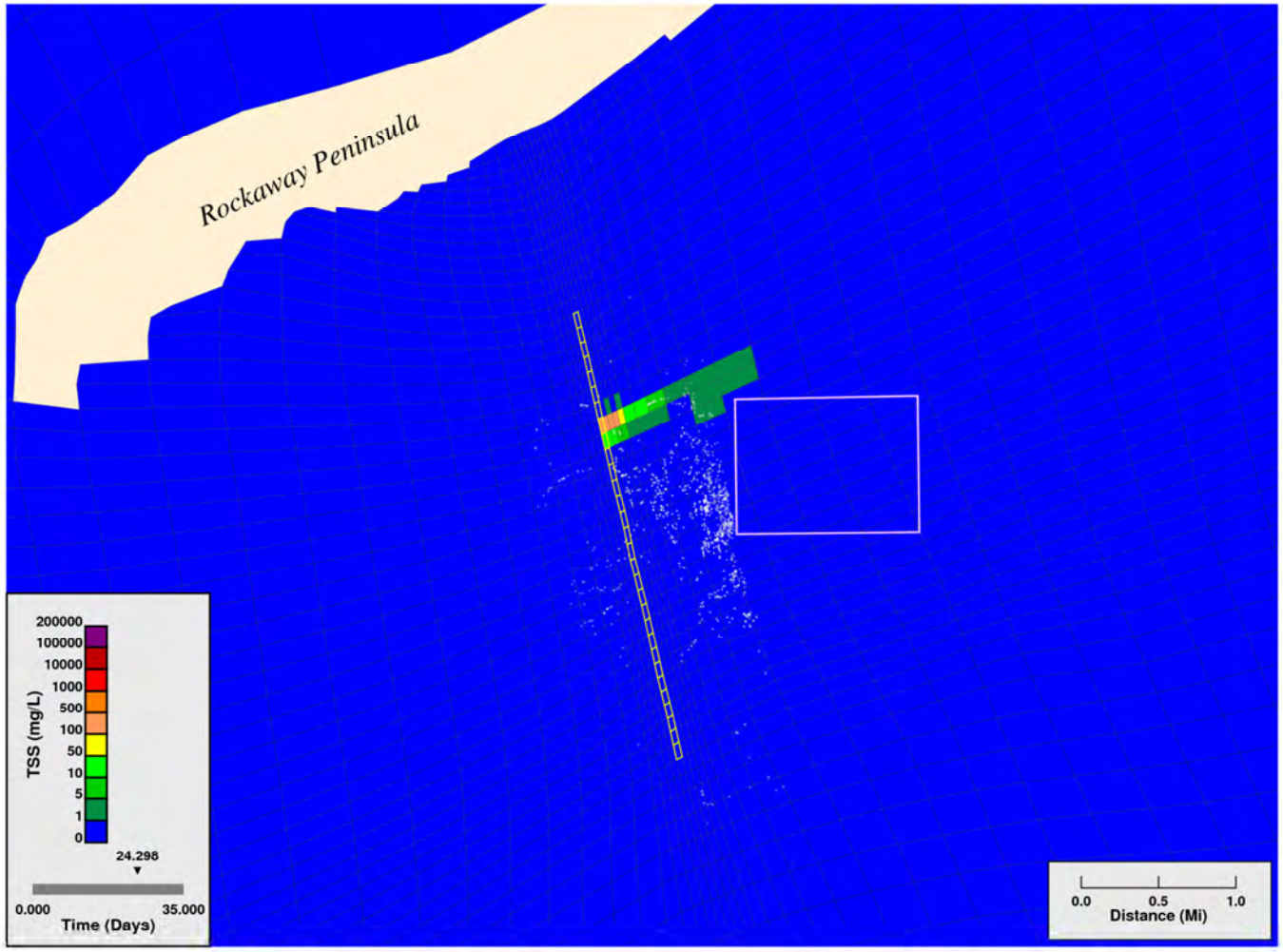

Figure 70. Mechanical trenching: simulated suspended solids near water column bottom, dredging 75% complete, rate = 4.2 m/hr.

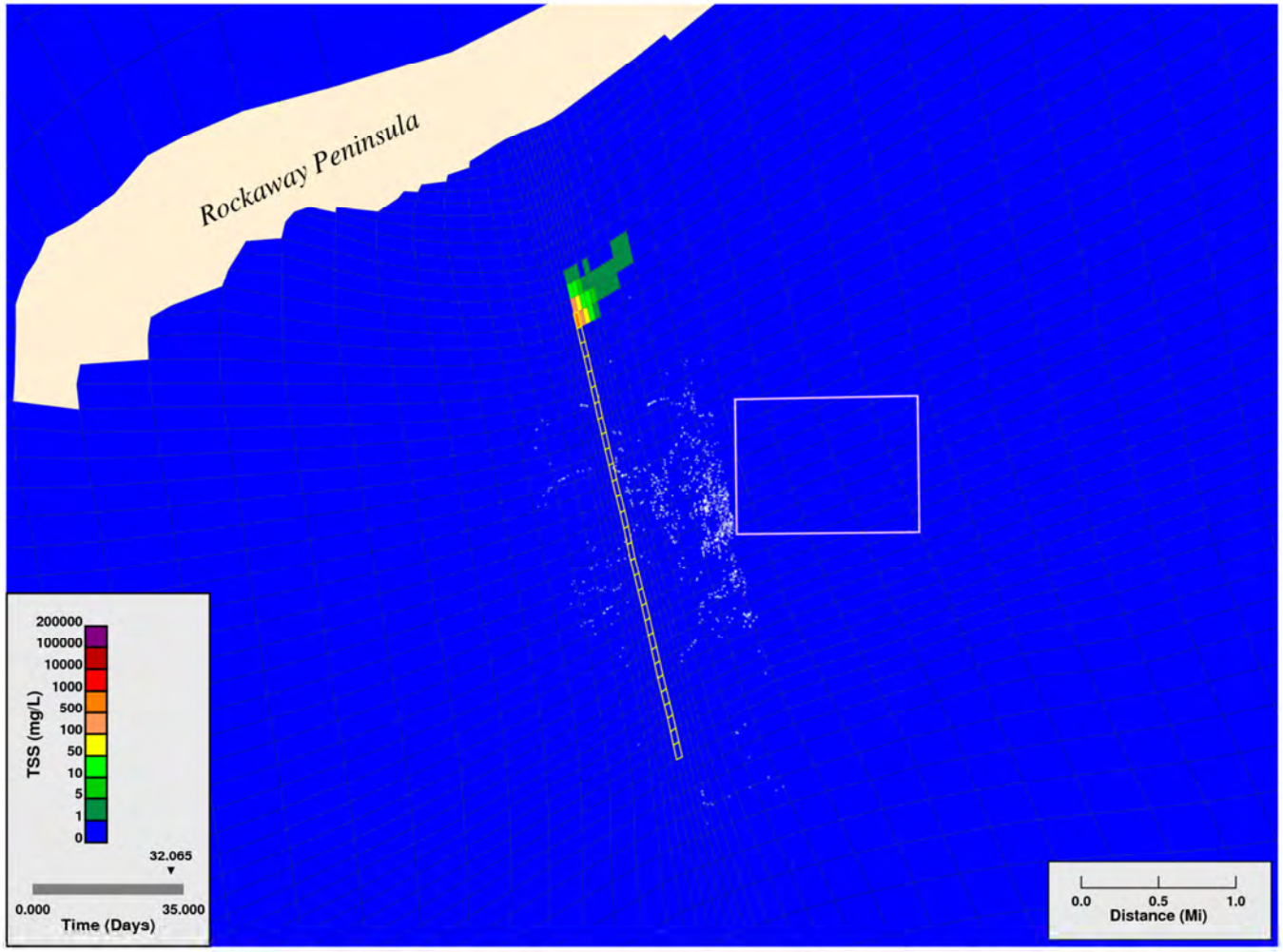

Figure 71. Mechanical trenching: simulated suspended solids near water column bottom, end of dredging, rate = 4.2 m/hr.

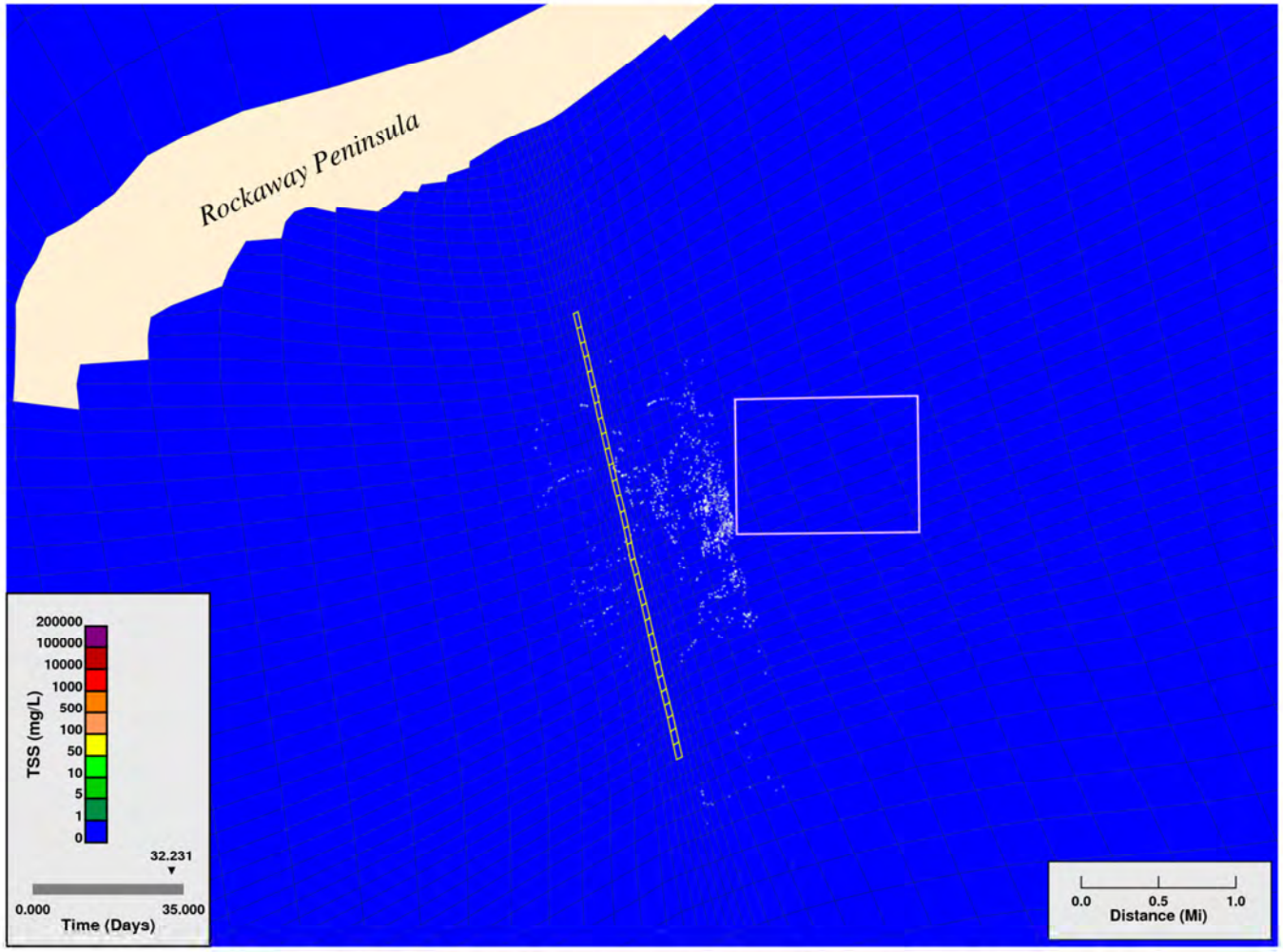

Bottom Layer Projected Solids Concentrations from Proposed Dredging, 13.8 ft/hr

Figure 72. Mechanical trenching: simulated suspended solids near water column bottom: 4 hrs after end of dredging, rate = 4.2 m/hr.

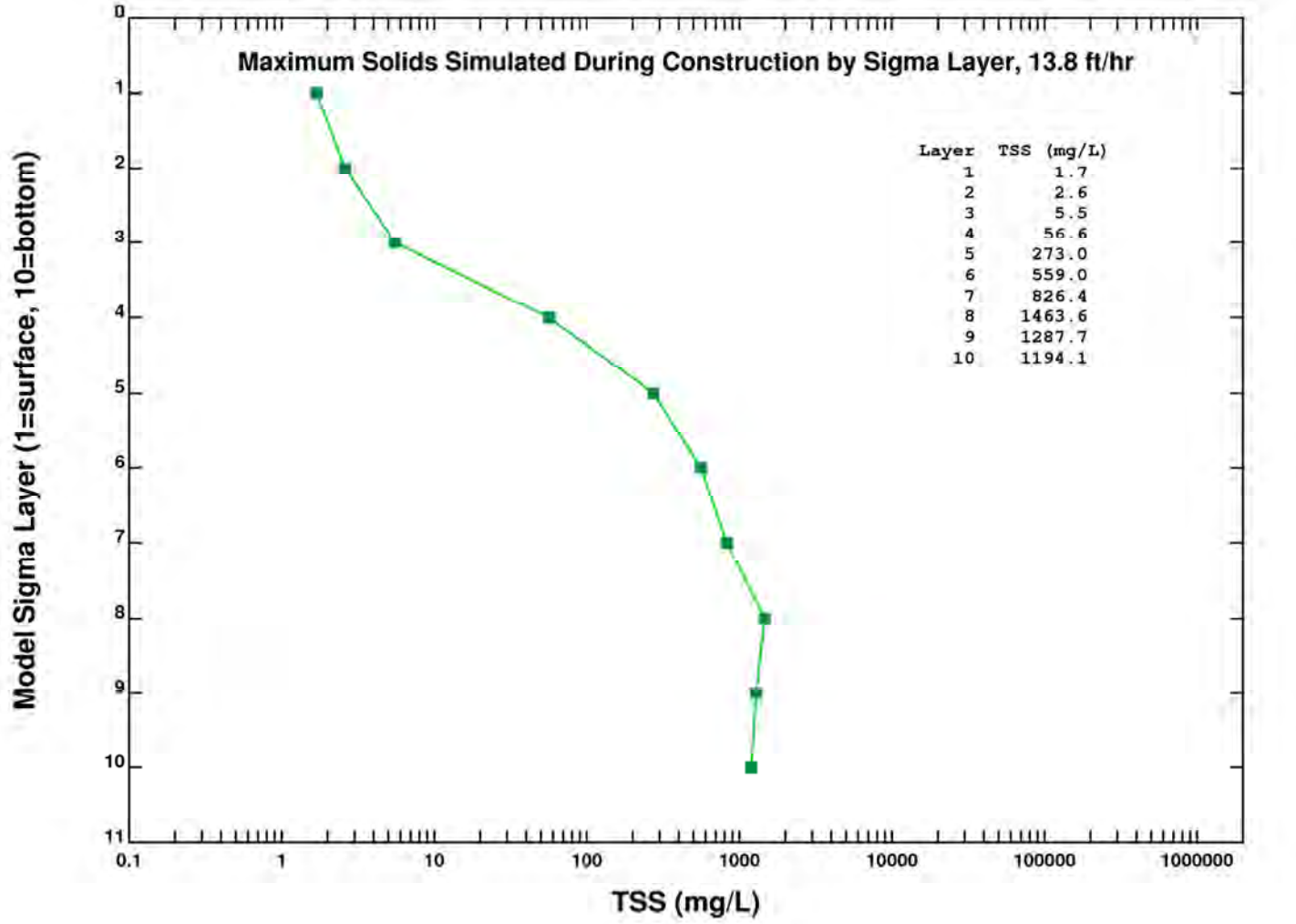

Figure 73. Mechanical trenching: maximum simulated suspended solids in each water column layer of model, rate = 4.2 m/hr.

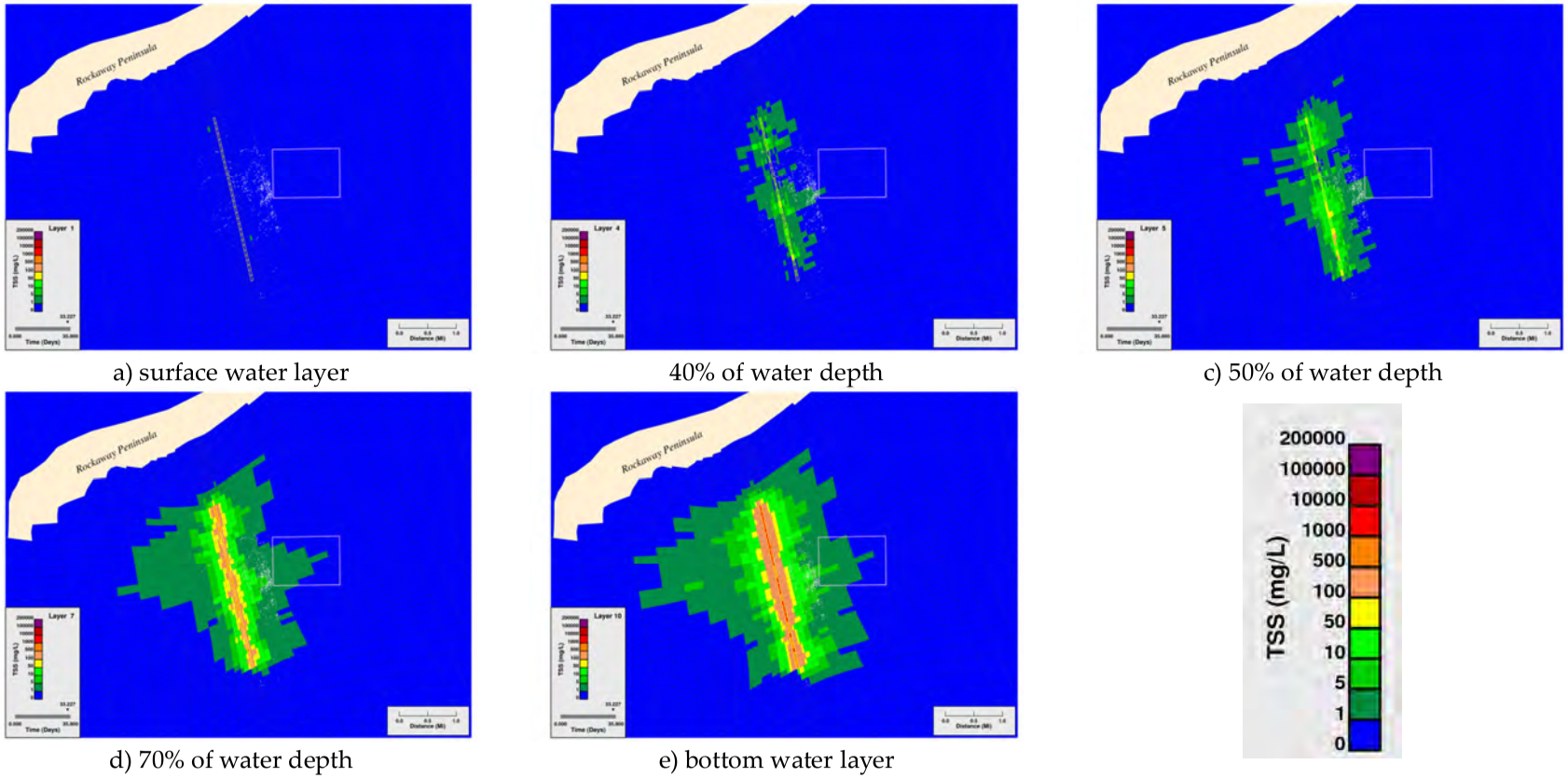

a) surface water layer

40% of water depth

c) 50% of water depth

d) 70% of water depth

e) bottom water layer

Notes: Values indicate the maximum solids concentration that occurred in each model grid at any time during the simulation. It should be noted the concentrations are elevated near the point of construction and rapidly decrease over time as a consequence of the relatively high settling velocities of sediment grains. Plumes clear the water column within 4 hours following the end of construction.

Figure 74. Mechanical trenching: maximum simulated suspended solids extent in selected water column sigma layers, rate = 4.2 m/hr.

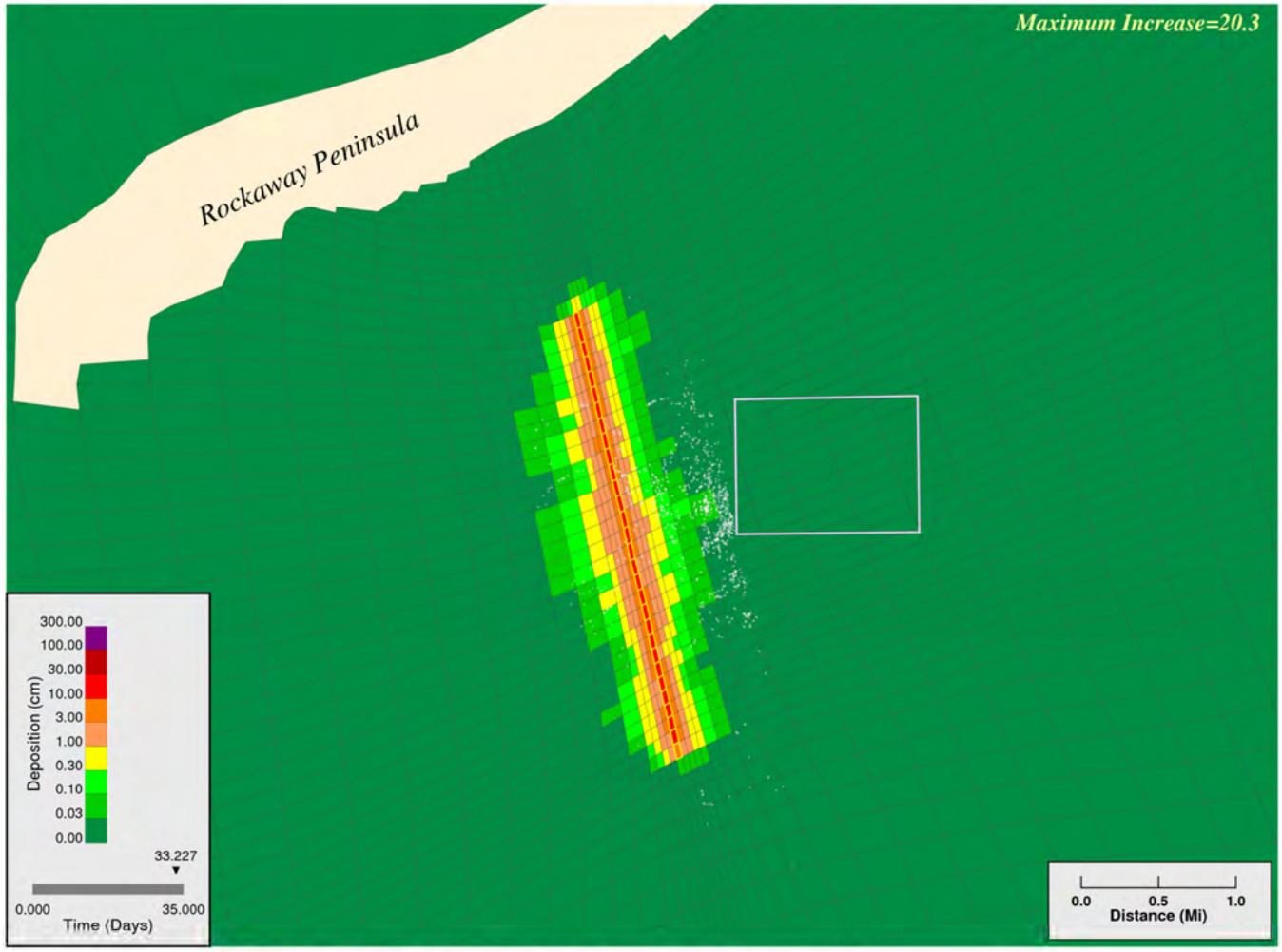

Figure 75. Mechanical trenching: simulated thickness of deposited solids on bed surface following dredging, rate = 4.2 m/hr.

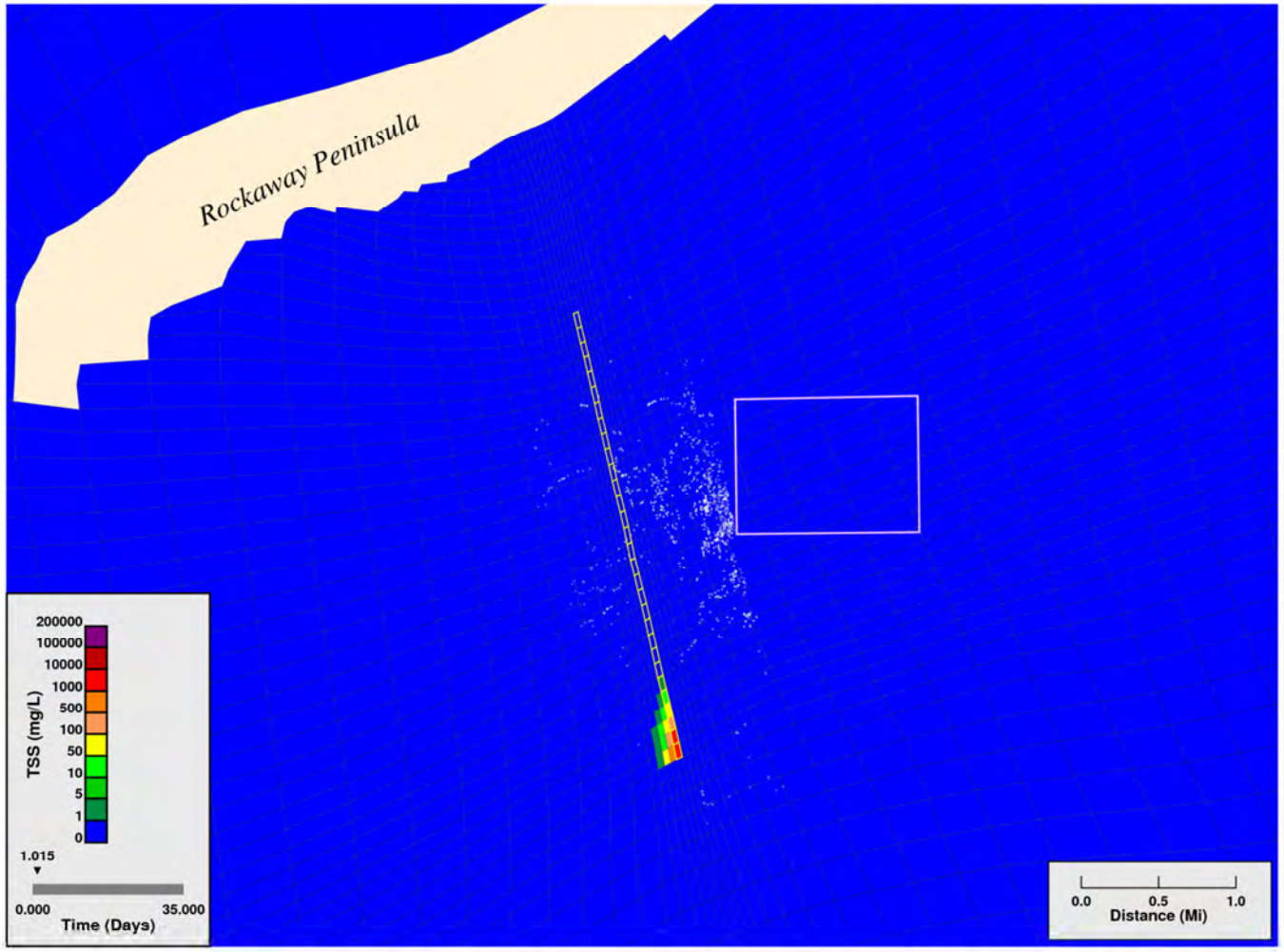

Figure 76. Hand jetting: simulated suspended solids near water column bottom, start of jetting (first 8-hour pulse).

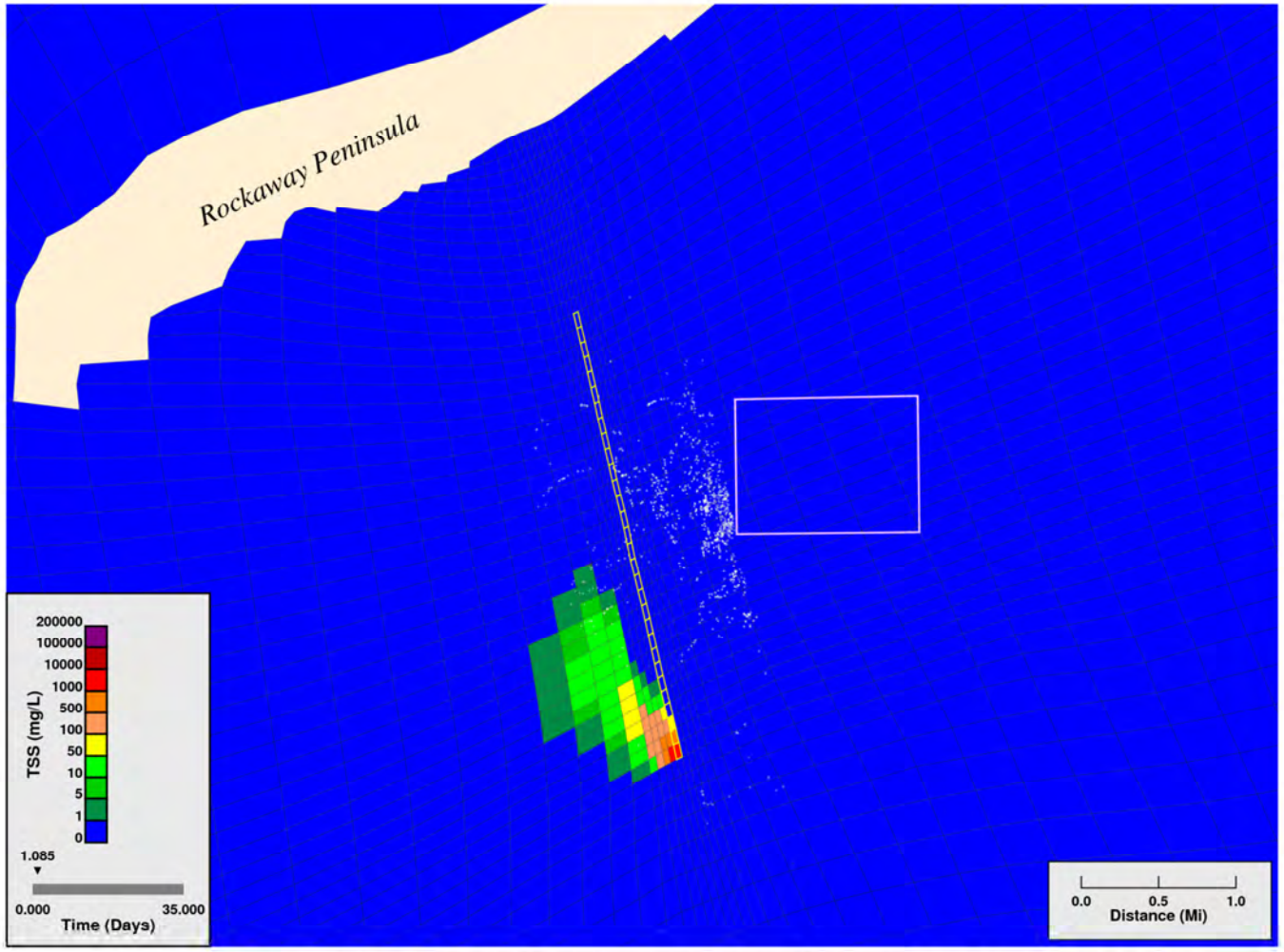

Figure 77. Hand jetting: simulated suspended solids near water column bottom, jetting 25% complete (first 8-hour pulse).

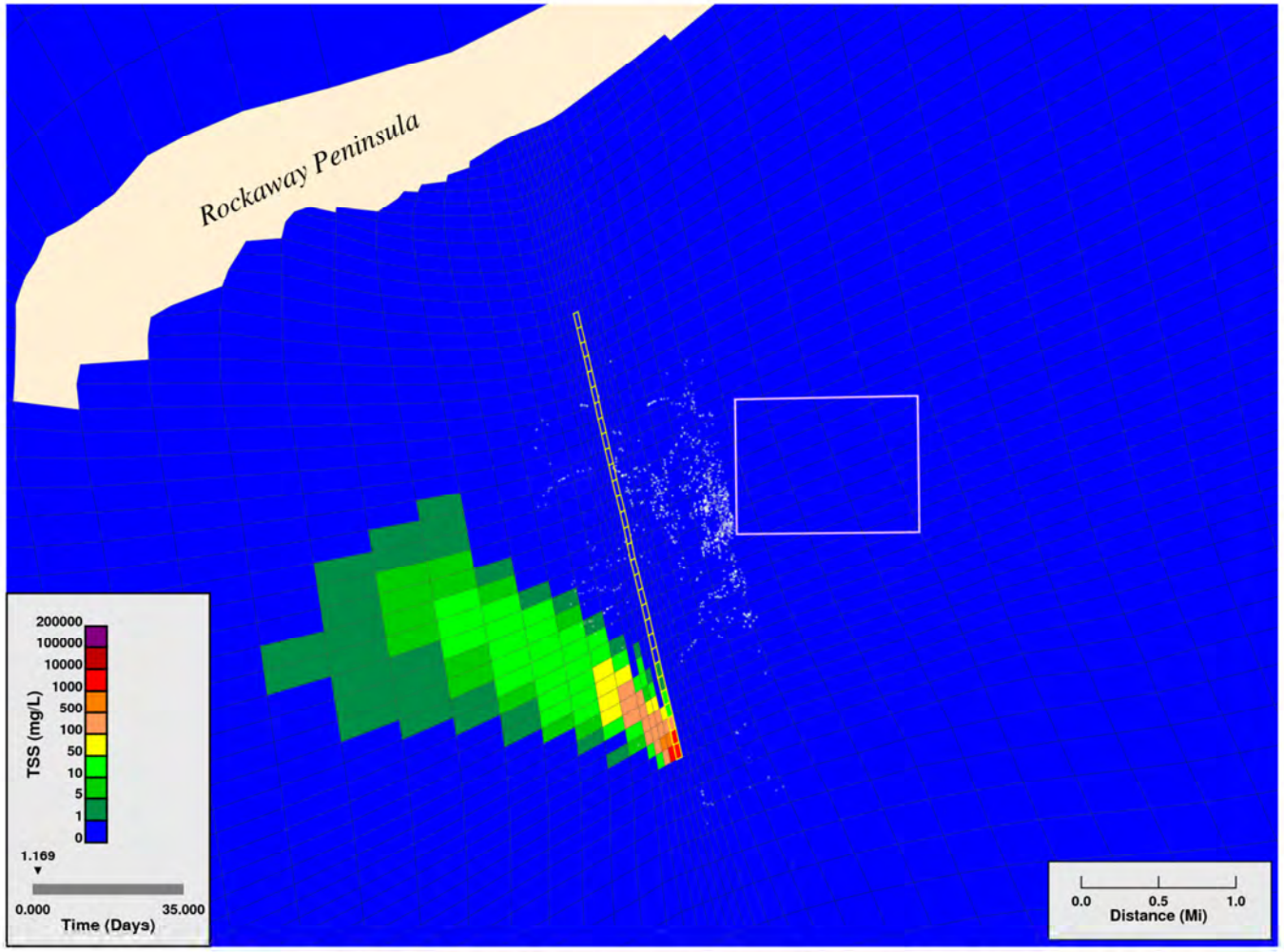

Figure 78. Hand jetting: simulated suspended solids near water column bottom, jetting 50% complete (first 8-hour pulse).

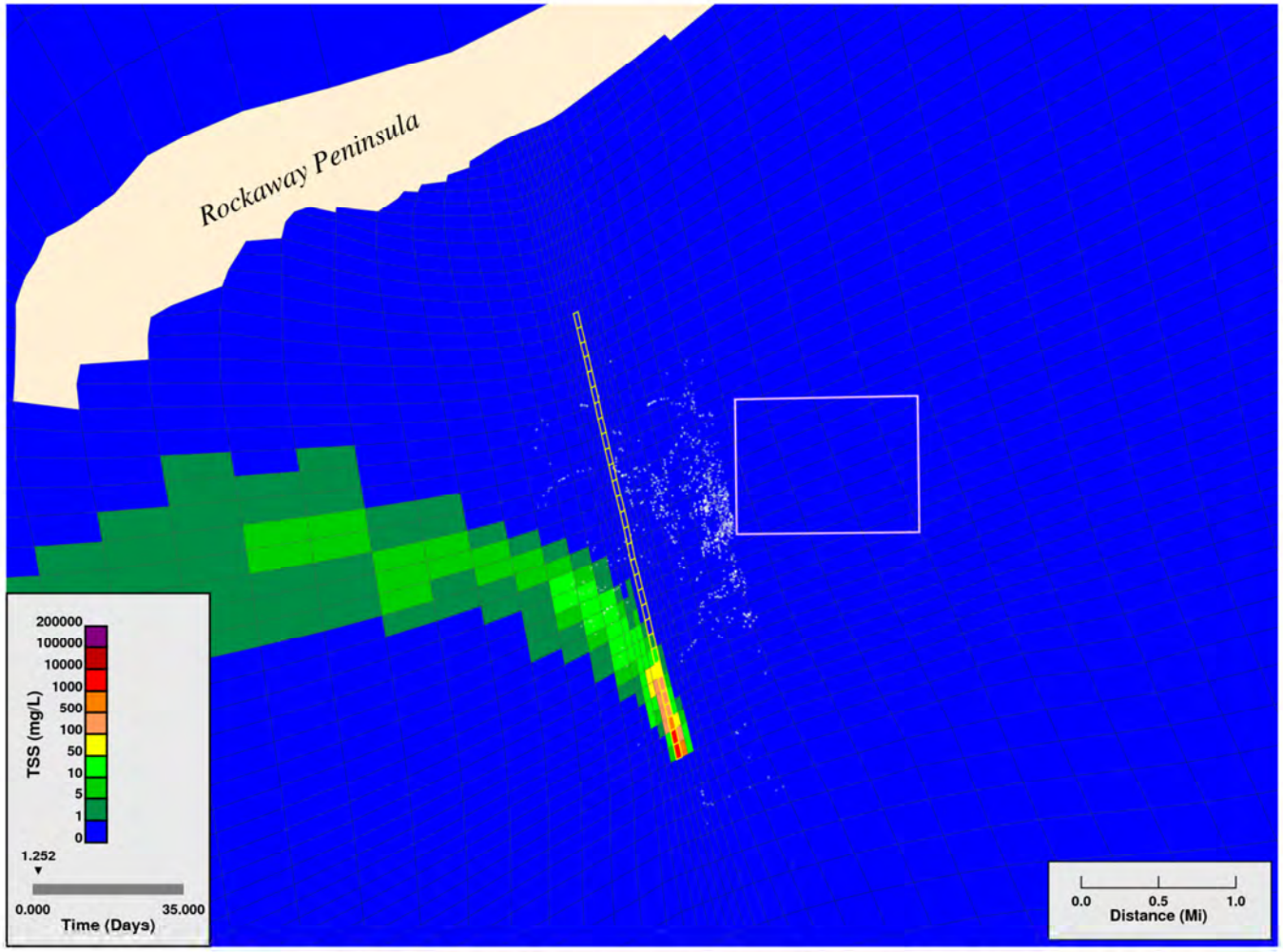

Figure 79. Hand jetting: simulated suspended solids near water column bottom, jetting 75% complete, (first 8-hour pulse).

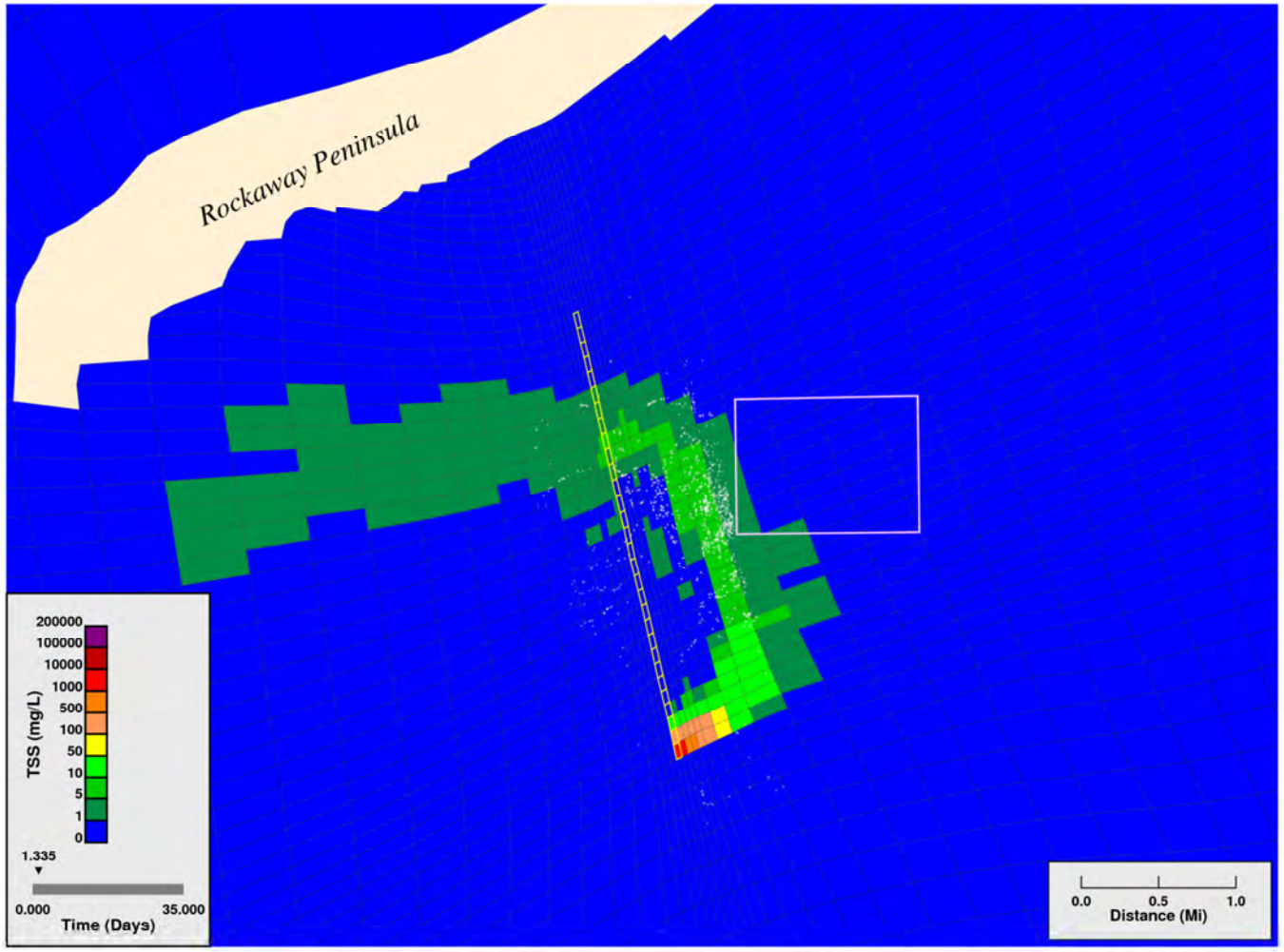

Figure 80. Hand jetting: simulated suspended solids near water column bottom, end of jetting (first 8-hour pulse).

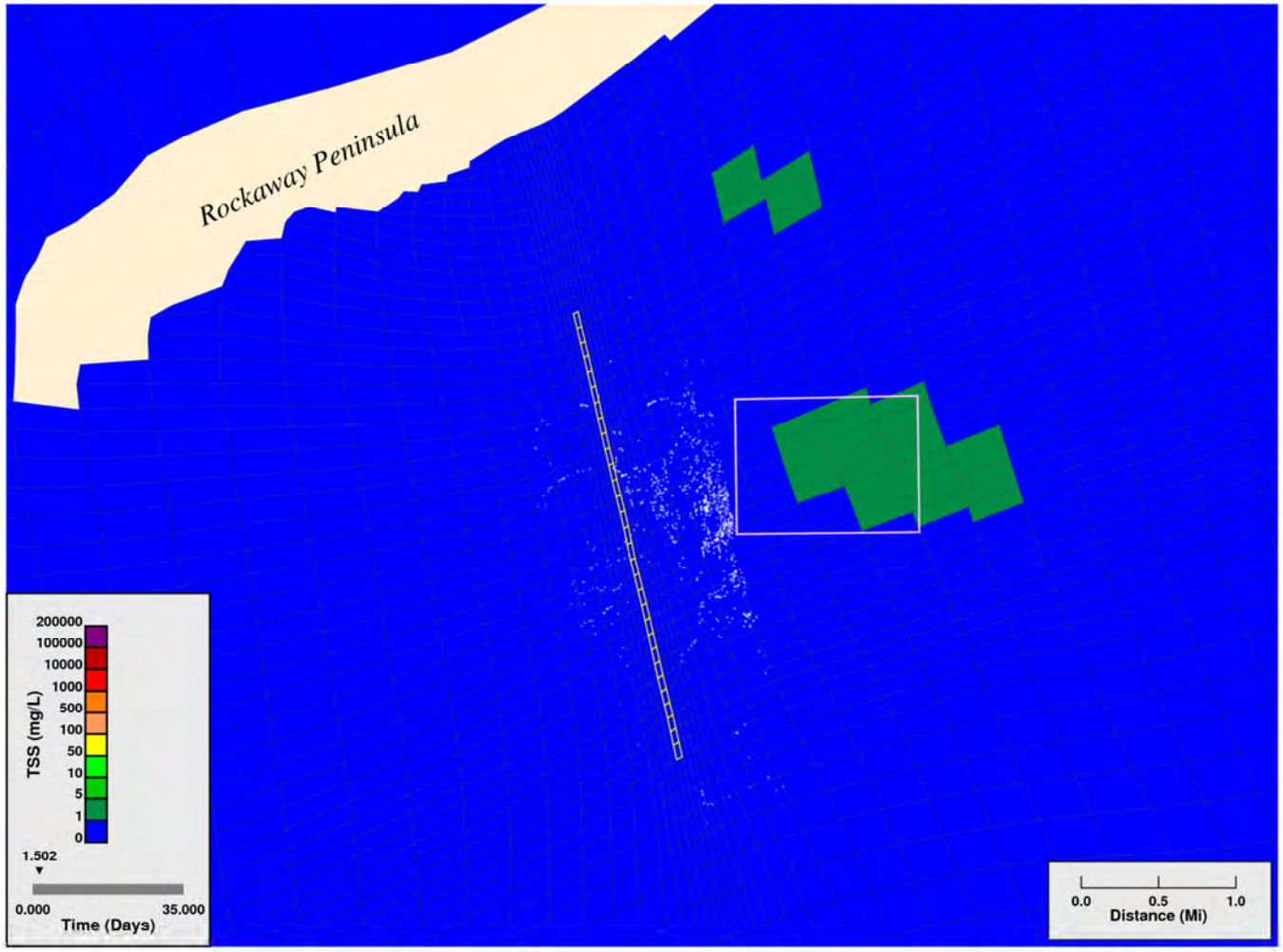

Figure 81. Hand jetting: simulated suspended solids near water column bottom: 4 hrs after end of jetting (first 8-hour pulse).

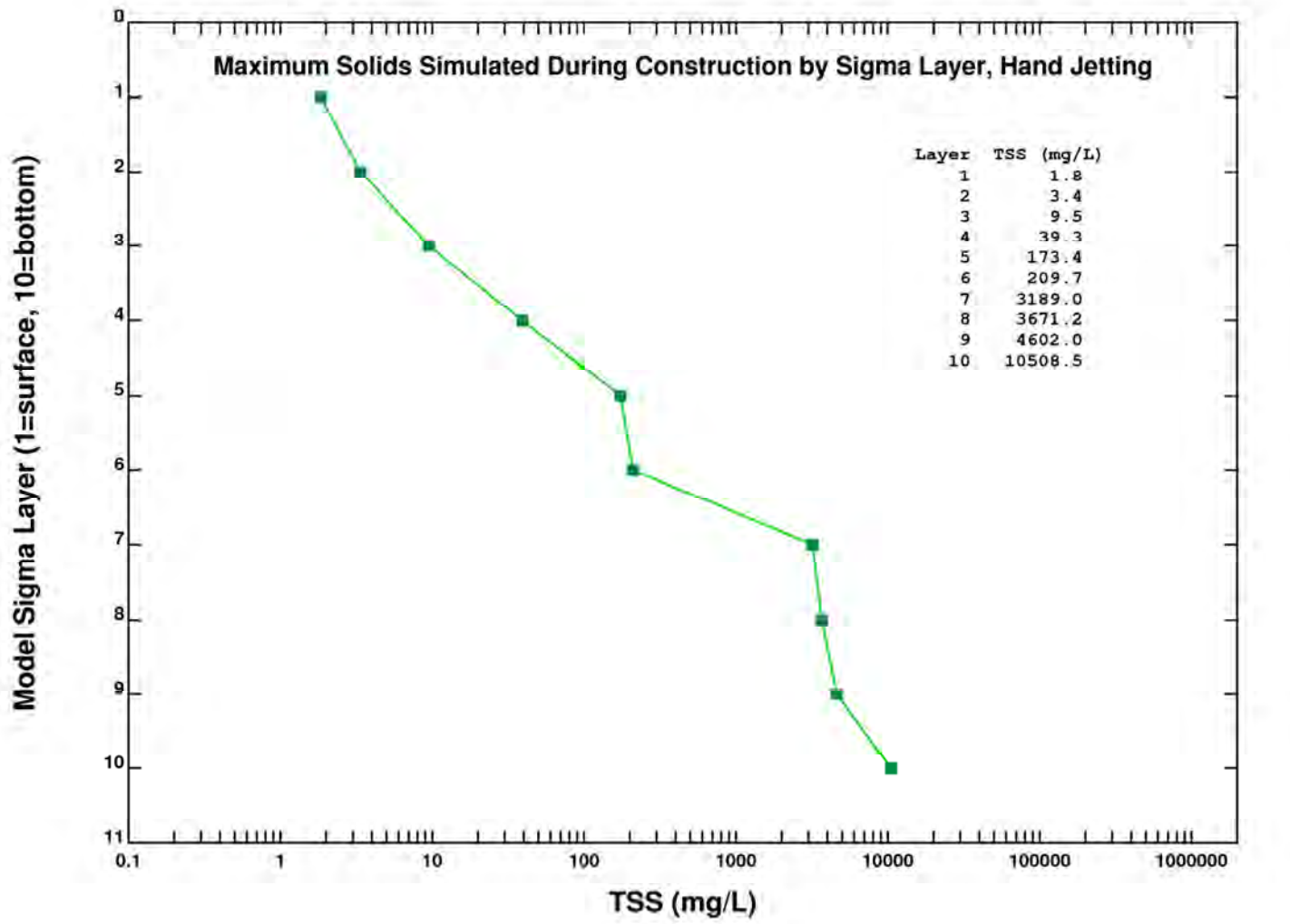

Figure 82. Hand jetting: maximum simulated suspended solids in each water column layer of model (all three pulses).

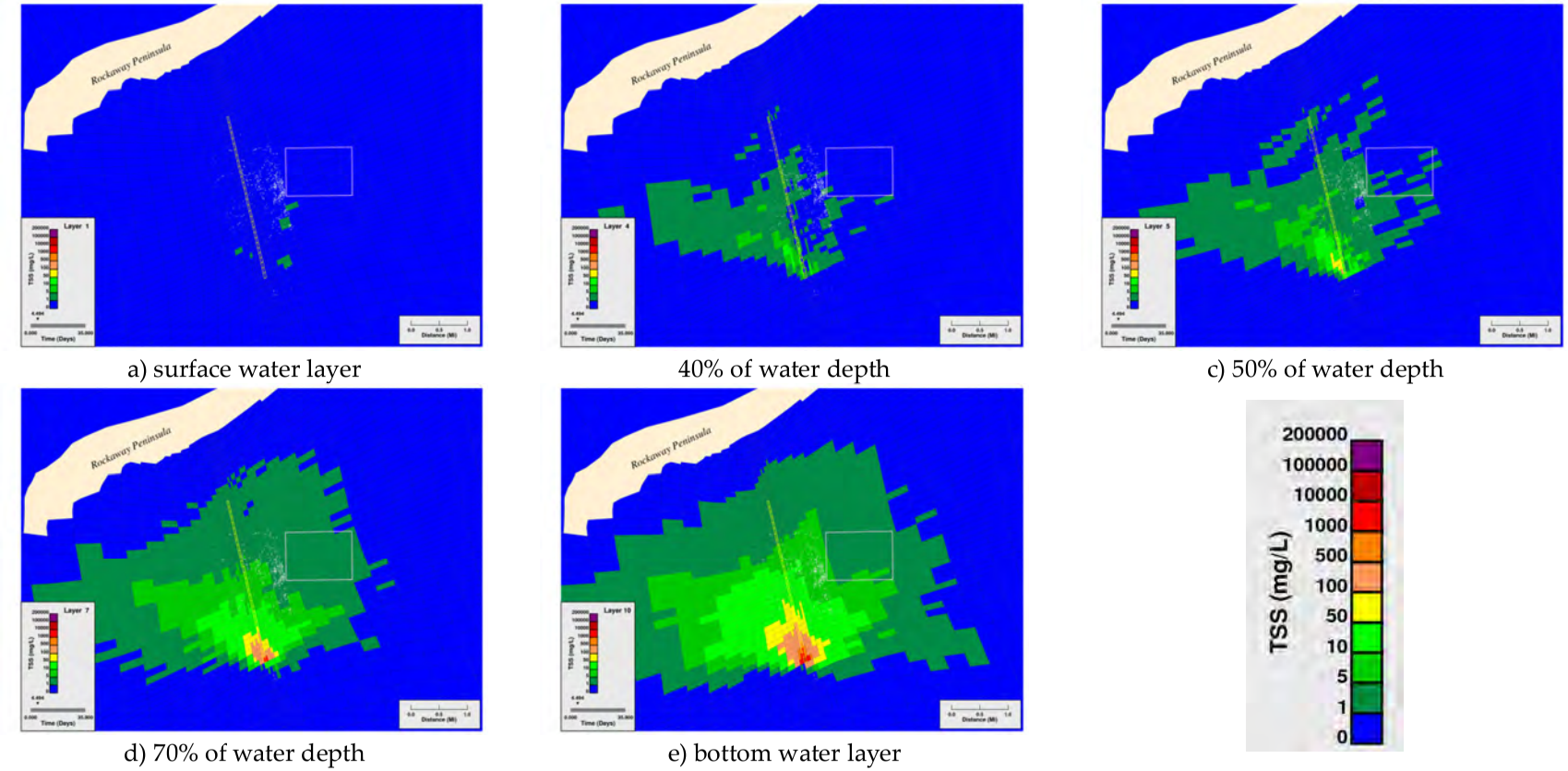

a) surface water layer

40% of water depth

c) 50% of water depth

d) 70% of water depth

e) bottom water layer

Notes: Values indicate the maximum solids concentration that occurred in each model grid at any time during the simulation. It should be noted the concentrations are elevated near the point of construction and rapidly decrease over time as a consequence of the relatively high settling velocities of sediment grains. Plumes clear the water column within 4 hours following the end of construction.

Figure 83. Hand jetting: maximum simulated suspended solids extent in selected water column sigma layers, rate = 183 m/hr.

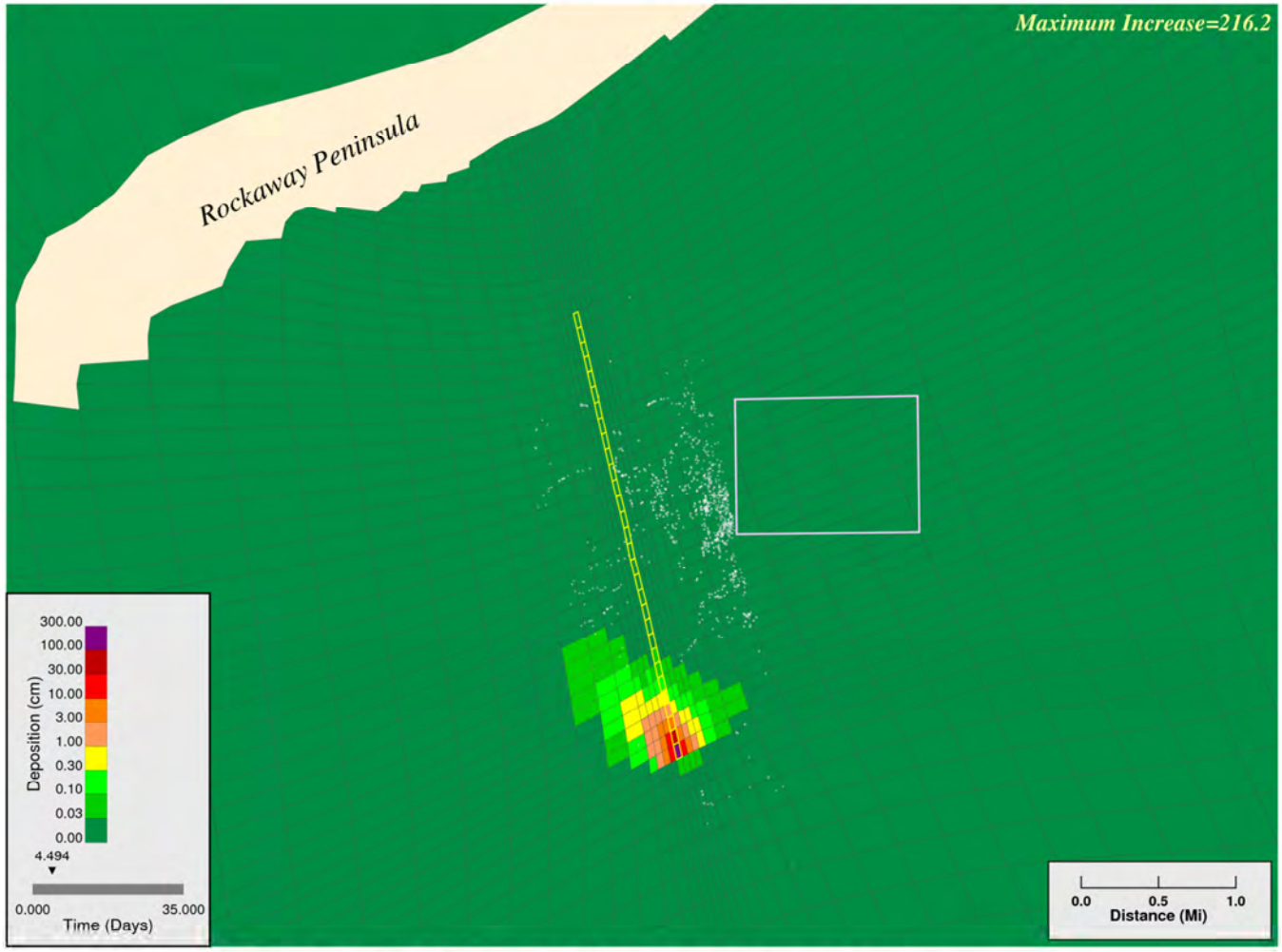

Figure 84. Hand jetting: simulated thickness of deposited solids on bed surface following jetting (after all four 8-hour pulses).

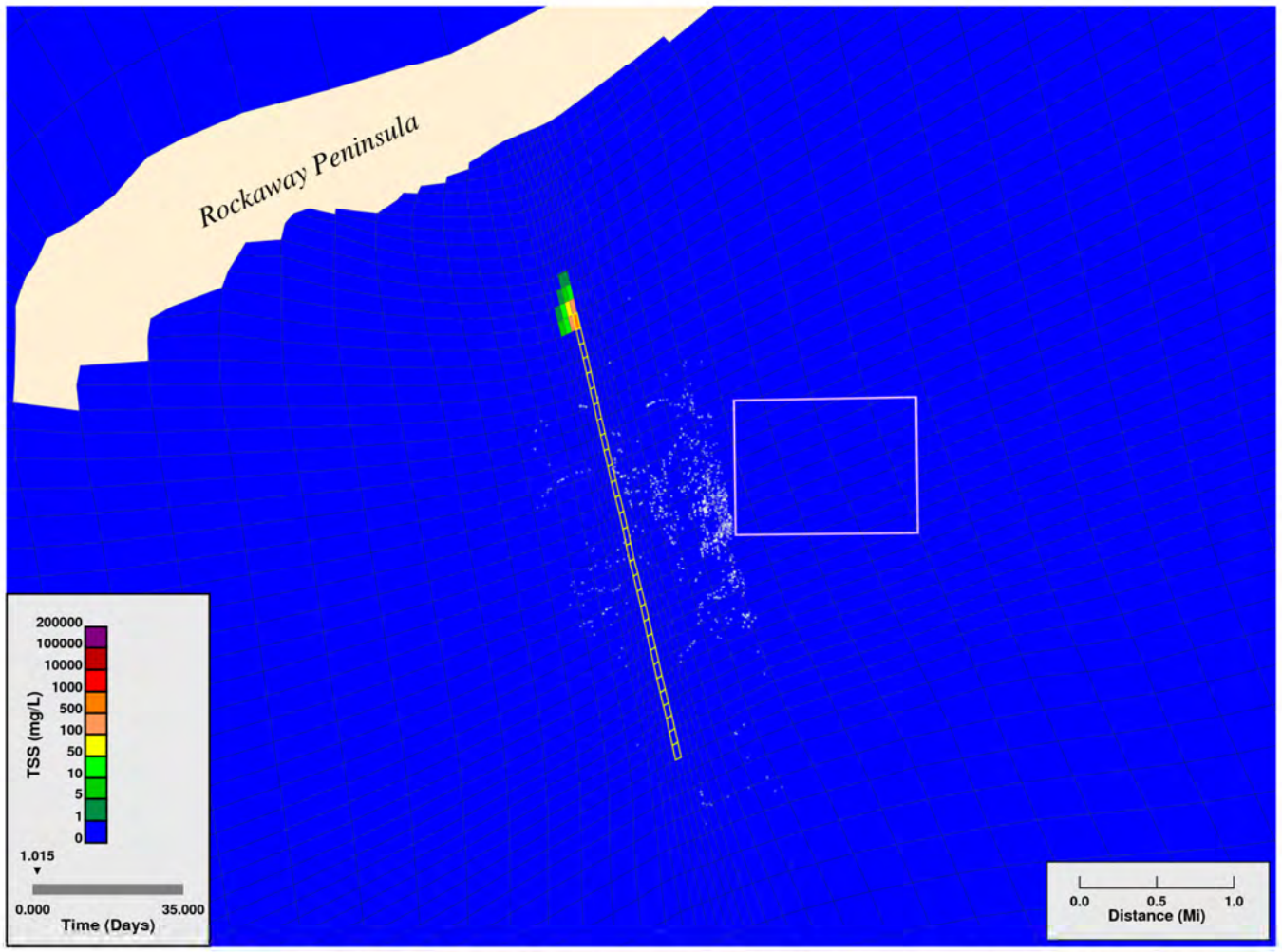

Figure 85. Pit dredging: simulated suspended solids near water column bottom, start of dredging.

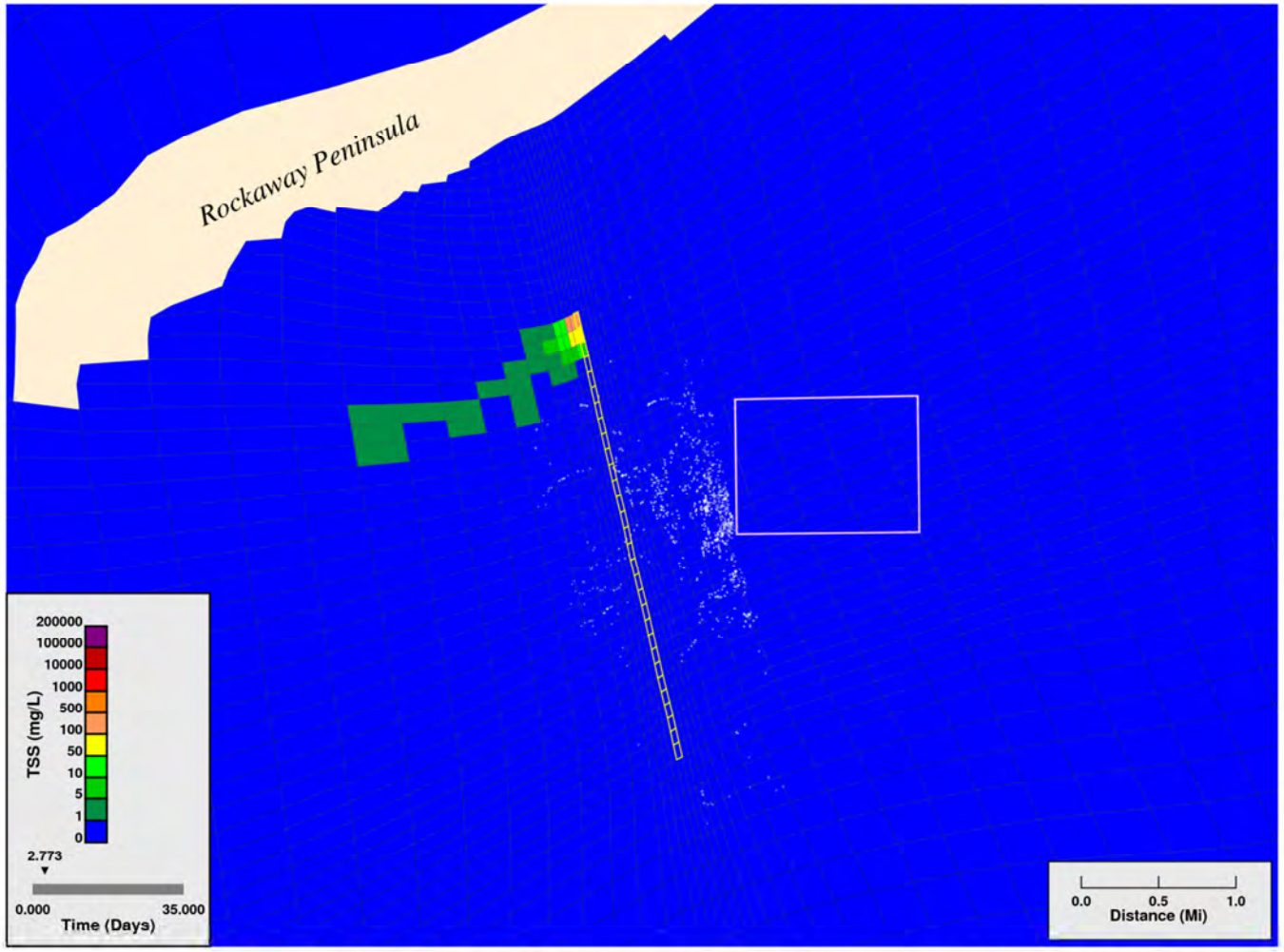

Figure 86. Pit dredging: simulated suspended solids near water column bottom, dredging 25% complete.

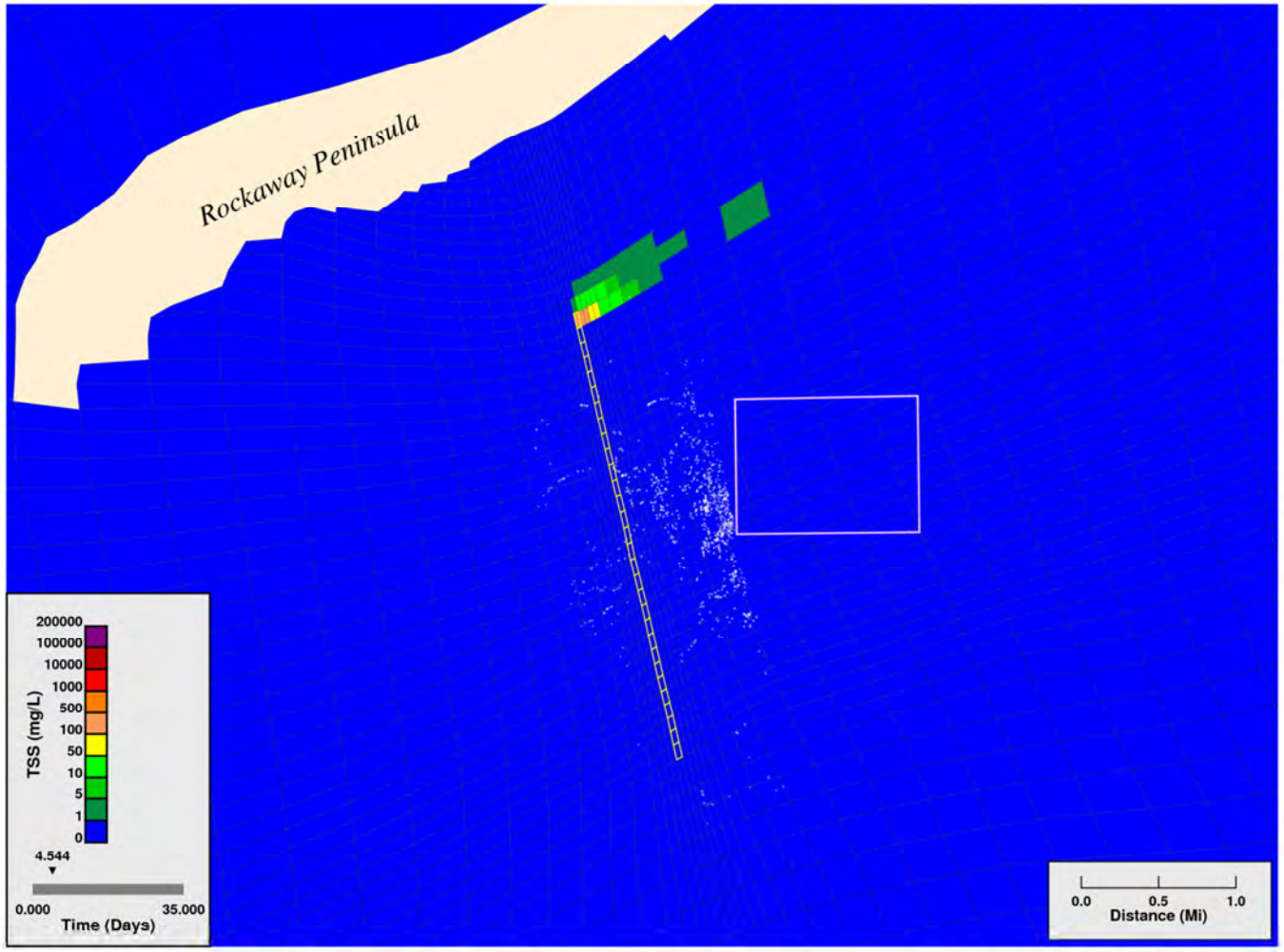

Figure 87. Pit dredging: simulated suspended solids near water column bottom, dredging 50% complete.

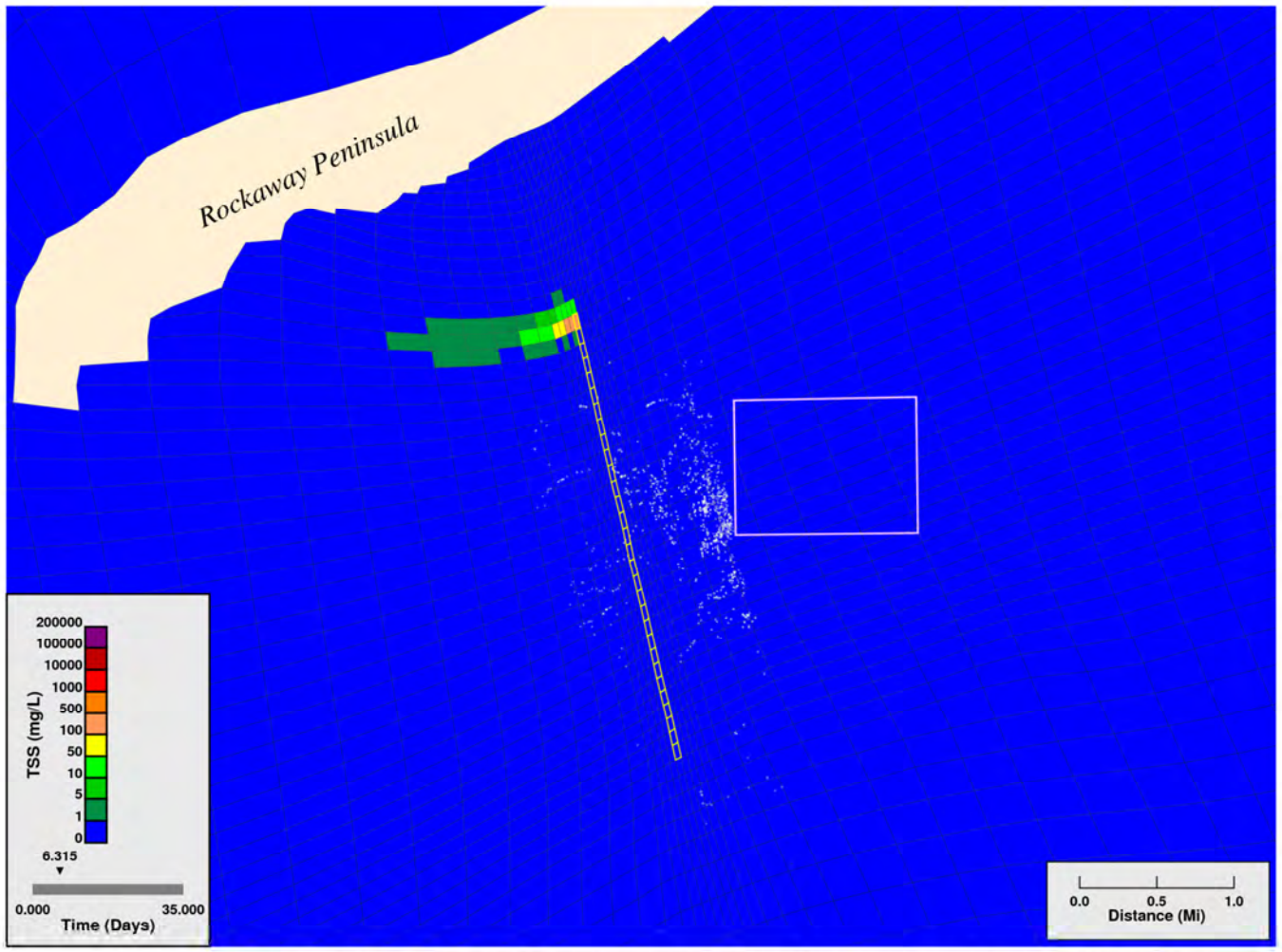

Figure 88. Pit dredging: simulated suspended solids near water column bottom, dredging 75% complete.

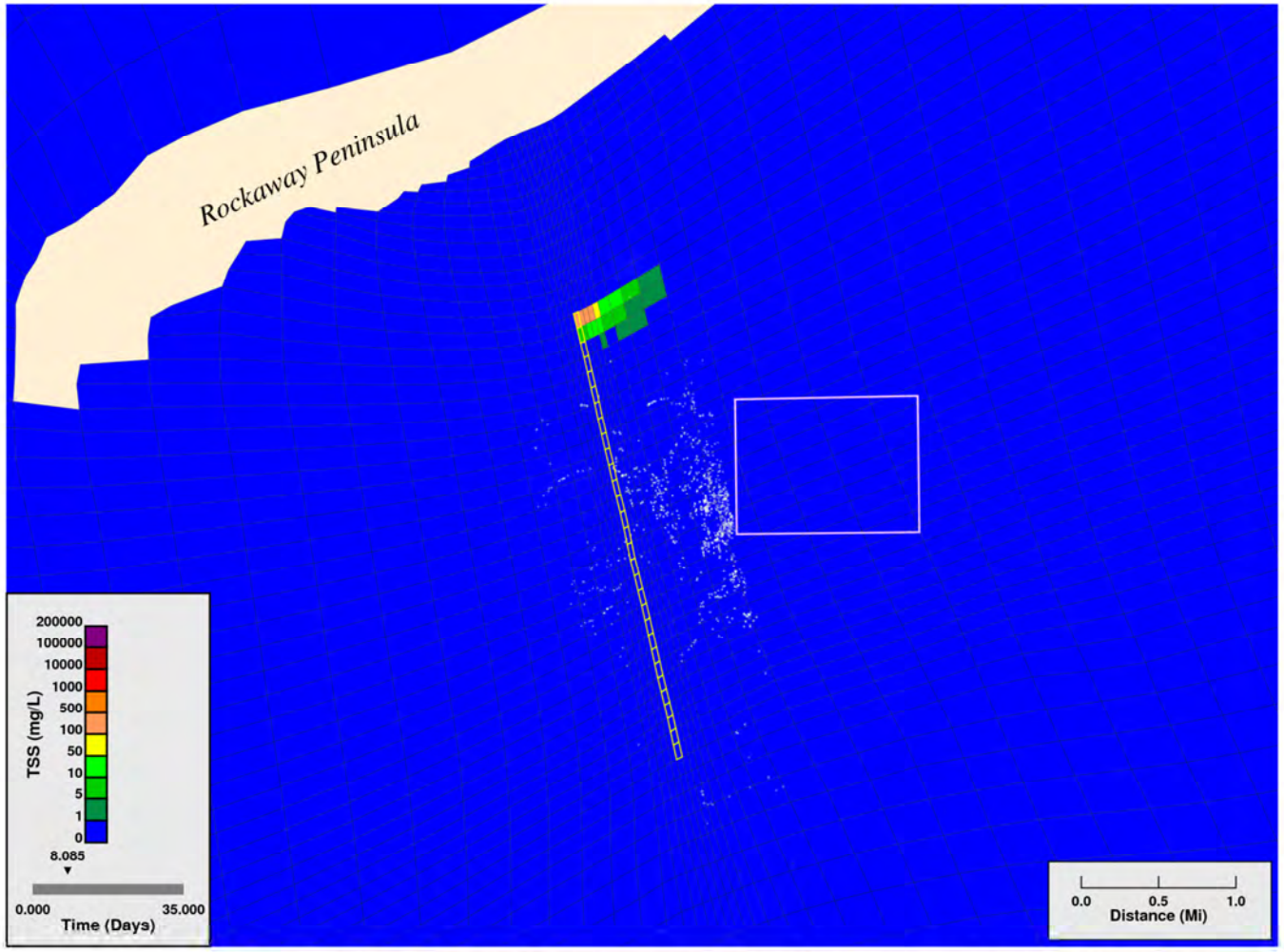

Figure 89. Pit dredging: simulated suspended solids near water column bottom, end of dredging.

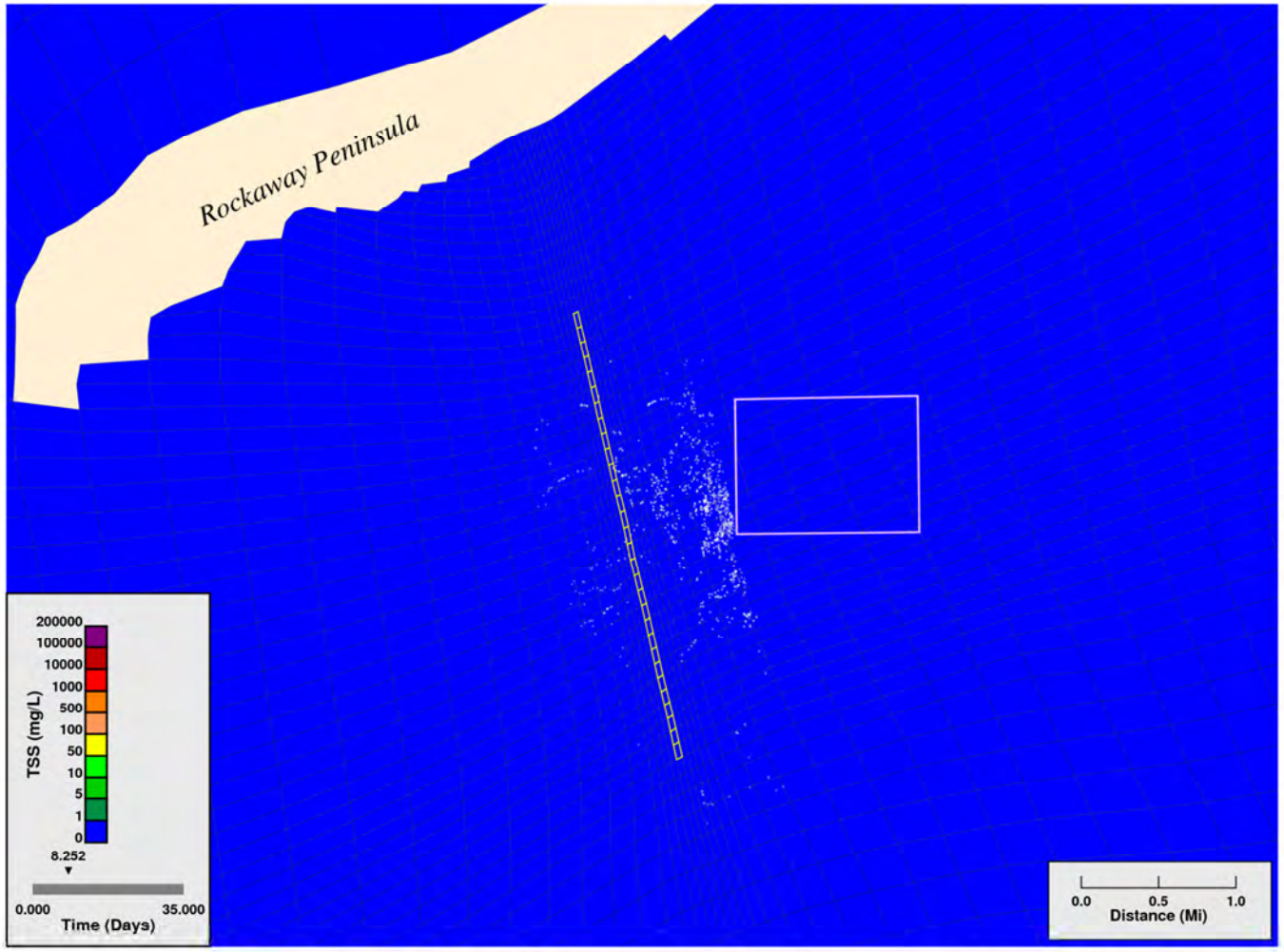

Figure 90. Pit dredging: simulated suspended solids near water column bottom: 4 hrs after end of dredging.

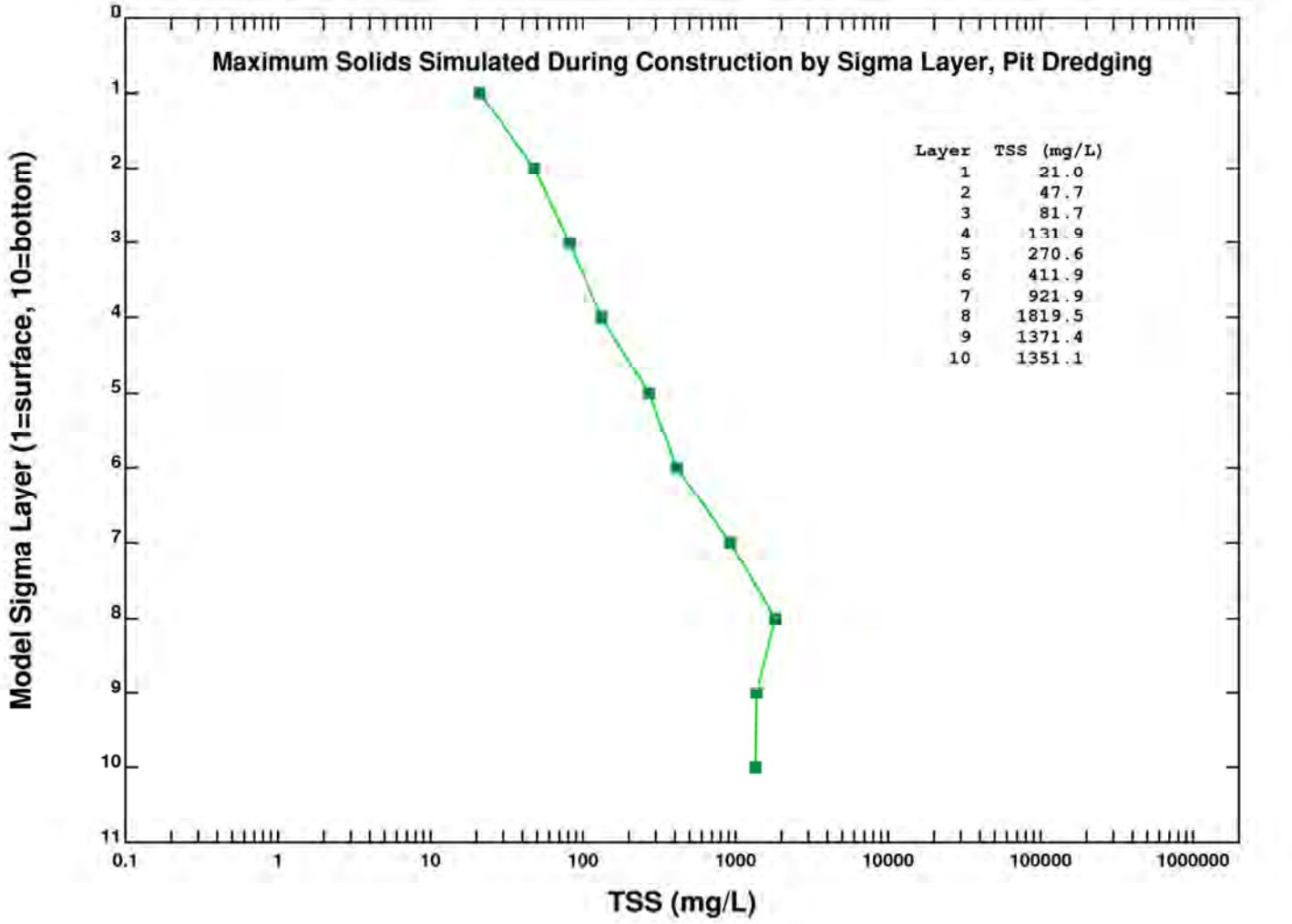

Figure 91. Pit dredging: maximum simulated suspended solids in each water column layer of model.

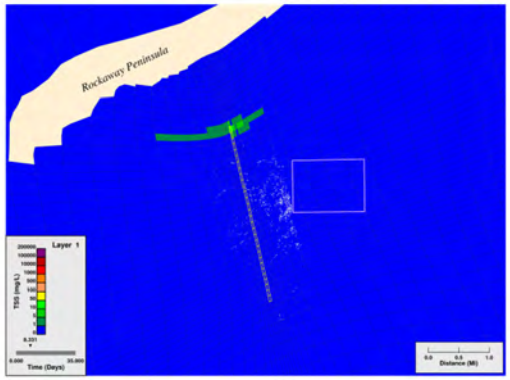

a) surface water layer

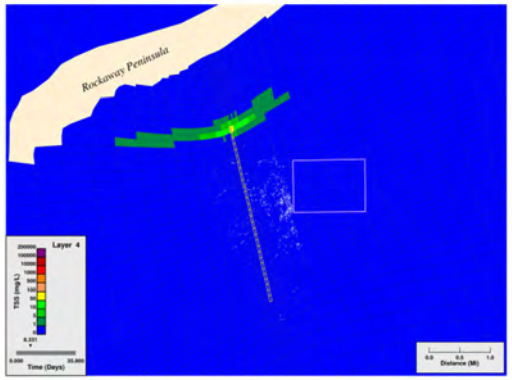

40% of water depth

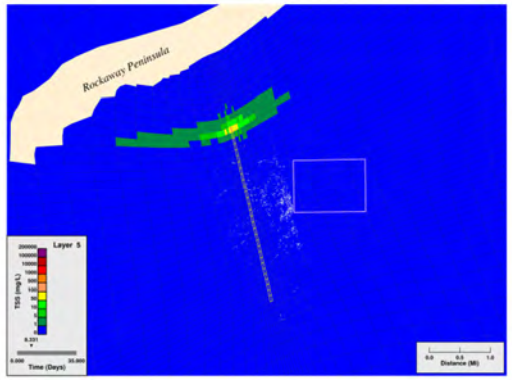

c) 50% of water depth

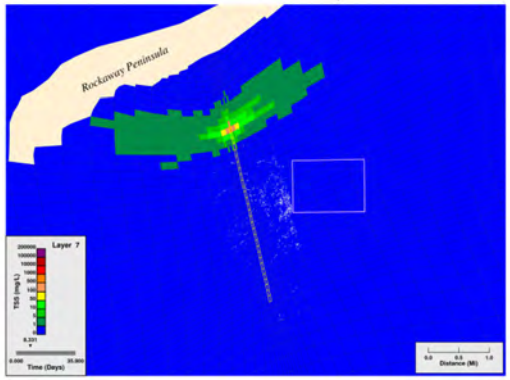

d) 70% of water depth

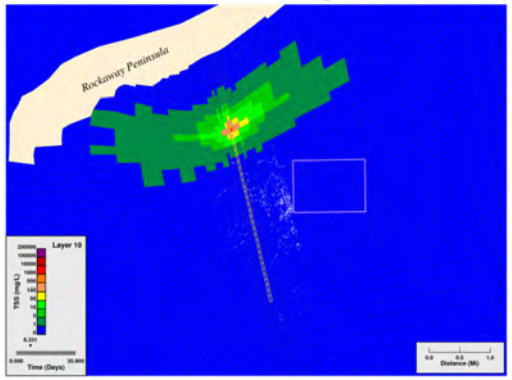

e) bottom water layer

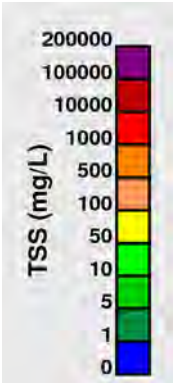

Notes: Values indicate the maximum solids concentration that occurred in each model grid at any time during the simulation. It should be noted the concentrations are elevated near the point of construction and rapidly decrease over time as a consequence of the relatively high settling velocities of sediment grains. Plumes clear the water column within 4 hours following the end of construction.

Figure 92. Pit dredging: maximum simulated suspended solids extent in selected water column sigma layers, rate = 183 m/hr.

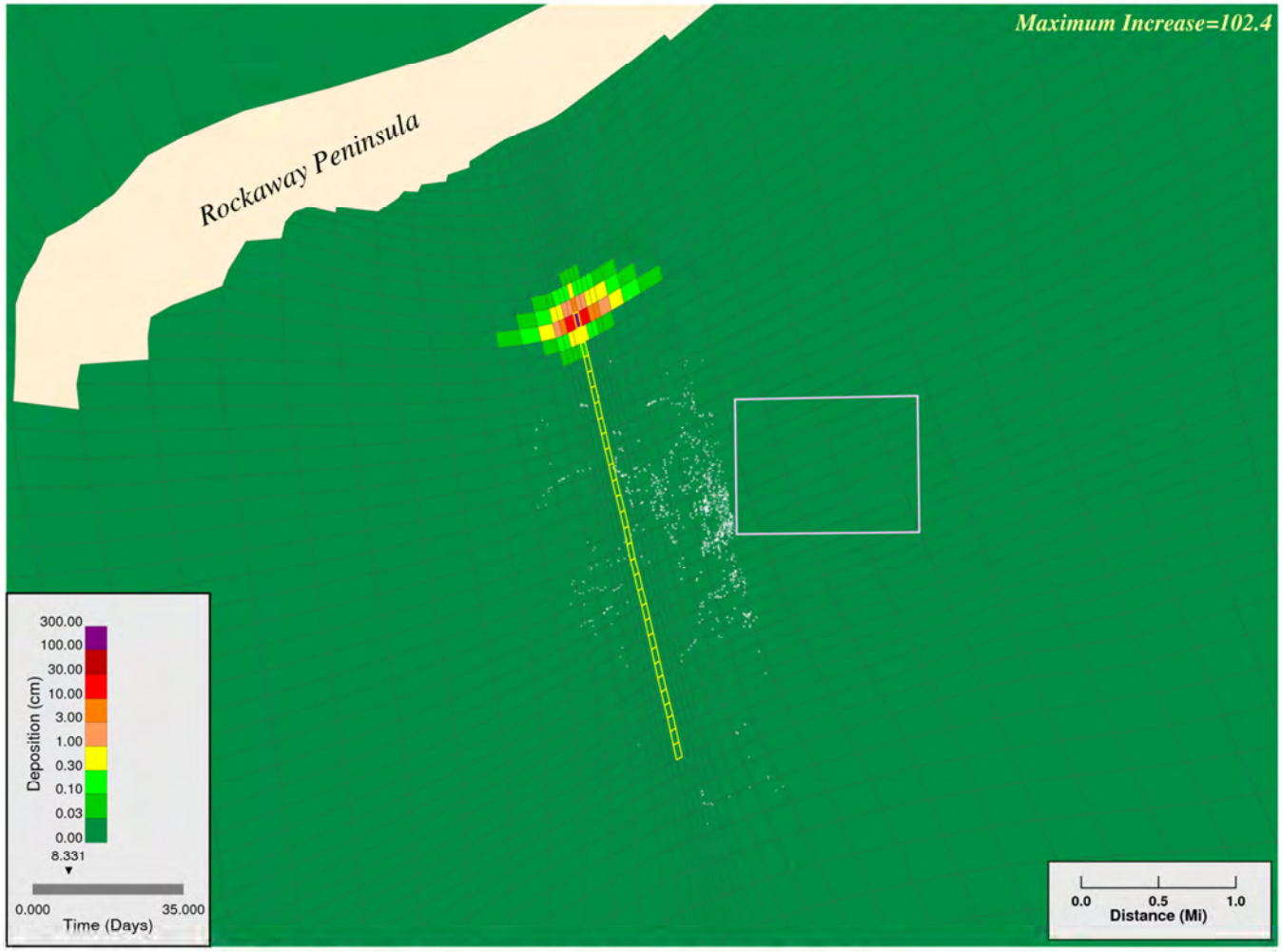

Figure 93. Pit dredging: simulated thickness of deposited solids on bed surface following dredging.

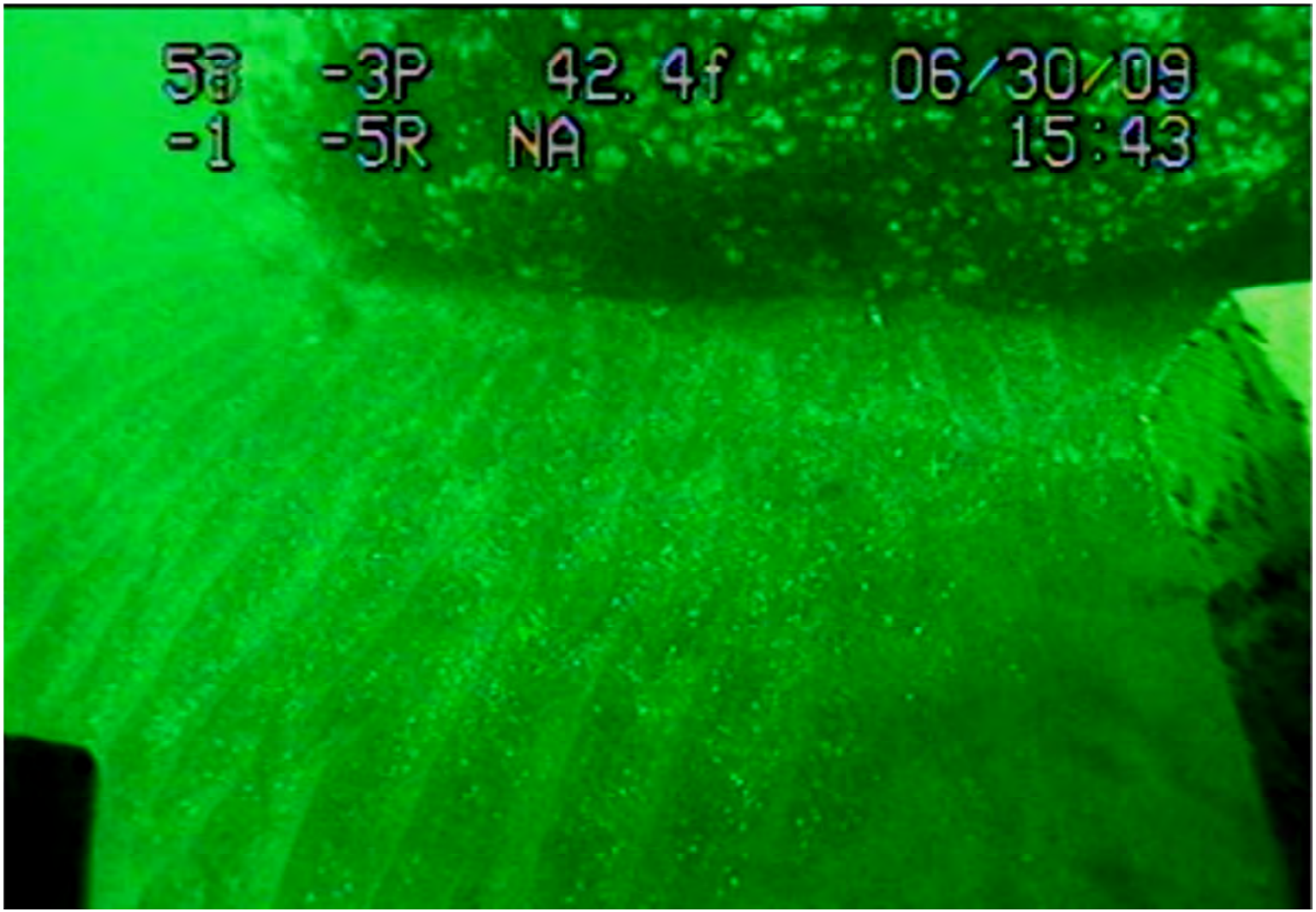

Notes: Image obtained from ROCKAWAY-20090630-154326-00clip16.wmv.

Figure 94. Image from seabed survey along pipeline route: no scour along bottom of large obstruction on seabed.

APPENDIX A. SHEAR STRESS PARTITIONING

To perform sediment transport calculations, hydrodynamic (total) shear stresses acting at the bottom of the water column need to be separated into surface drag and form drag components because individual grains on the bed surface are only subject only to the surface drag component of the total shear stress.

Total hydrodynamic shear stresses are related to eddy viscosity, velocity gradients, drag and velocities near the sediment bed:

$$\rho_w K_M \frac{\partial U}{\partial z} = \tau_b \tag{A-1}$$

$$\tau_b = \rho_w u_*^{\,2} = \rho_w C_D \left[u(z_b)\right]^2 \tag{A-2}$$

where:

ρ_w	=	density of water [M L^{-3}]
K_M	=	vertical eddy viscosity [L^2 T^{-1}]
$\frac{\partial U}{\partial z}$	=	vertical velocity gradient [T^{-1}]
τ_b	=	total (hydrodynamic) bed shear stress [M L^{-1} T^{-2}]
u_*	=	shear (friction) velocity [L T^{-1}]
$u(z_b)$	=	velocity at a height z_b above the bed [L T^{-1}]
C_D	=	coefficient of drag [dimensionless]

Eddy viscosity and velocity gradients in the water column are calculated in the hydrodynamic model. A logarithmic velocity profile is used to relate hydrodynamic roughness to water velocities in the last sigma layer of the water column and also the drag coefficient:

$$\frac{u(z_b)}{u_*} = \frac{1}{\kappa}\ln\left(\frac{z_b}{z_0}\right) \tag{A-3}$$

$$C_D = \left[\frac{1}{\kappa}\ln\left(\frac{z}{z_0}\right)\right]^{-2} \tag{A-4}$$

where:

κ = von Karman constant = 0.4 [dimensionless]

z_b = height above the bed [L]

z_o = hydrodynamic roughness height of the bed [L]

C_D = coefficient of drag [dimensionless]

The height above the bed (z_b) is set equal to one half the thickness of the bottom sigma layer in the water column of the hydrodynamic model.

To perform sediment transport calculations, total hydrodynamic bed shear stress (τ_b) must be separated (partitioned) into surface and form drag. The relationship between total bed shear stress and its components is:

$$\tau_b = \tau_g + \tau_f \tag{A-5}$$

where:

τ_b = total (hydrodynamic) bed shear stress [M L^{-1} T^{-2}]

τ_g = surface drag ("grain-related") shear stress [M L^{-1} T^{-2}]

τ_f = form drag shear stress [M L^{-1} T^{-2}]

The surface drag (grain stress) component of the total shear stress acts on particle surfaces and is iteratively calculated from total hydrodynamic bed shear stress (τ_b), total shear velocity (u_*), and an initial (first) estimate of grain roughness height:[3, 4]

$$z_{0g}^{(1)} = \frac{d_{50}}{15} \tag{A-6}$$

$$u_{*g}^{(1)} = u_* \left(\frac{\ln \frac{z_b}{z_o}}{\ln \frac{z_b}{z_{og}^{(1)}}} \right) \tag{A-7}$$

[3] Boundary roughness heights are typically expressed in terms of the Nikuradse roughness height (k_s) and is approximated as $k_s = 2\ d_{50}$. For rough turbulent flow, $z_{og} = k_s/30 = d_{50}/15$.

[4] As an expedient, the model calculates an initial estimate of grain shear stress (τ_g) from total bed shear stress (τ_b) and grain roughness height (z_{0g}) using the square of Equation (A-7). This is mathematically equivalent because $u_*^2 = \tau_b/\rho_w$ and $u_{*g}^2 = \tau_g/\rho_w$ [see Equation (A-2)].

where:

$u_{*g}^{(1)}$ = initial (first) estimate of grain stress shear velocity [L T^{-1}]

$z_{0g}^{(1)}$ = initial (first) estimate for grain roughness height [L]

d_{50} = median (i.e., 50th percentile) diameter of bulk sediment [L]

Equations (A-6) and (A-7) are applicable to hydraulically rough turbulent flow (i.e. where particles on the bed protrude beyond the boundary layer that exists in a thin layer next to the bed surface). A second estimate of grain roughness height is calculated using the approach of Winterwerp and van Kesteren (2004):

$$z_{0g}^{(2)} = \frac{0.11\nu}{u_{*g}^{(1)}} + z_{0g}^{(1)} \tag{A-8}$$

where:

ν = kinematic viscosity [L^2 T^{-1}]

$z_{0g}^{(2)}$ = second estimate for grain roughness height [L]

Equation (A-8) is applicable to transitionally rough turbulent flow. Additional iterations could be performed to allow more resolved estimates of bed roughness height (z_{0g}) to be calculated. A boundary layer Reynolds number could also be calculated to further refine bed roughness height estimates over the spectrum of hydraulically smooth, transitionally rough, and hydraulically rough turbulent flow conditions. However, for simplicity and to avoid the added computational overhead associated with additional iterations, the second estimate of bed roughness height is used to calculate a second estimate of grain stress shear velocity and the surface drag component of the total shear stress as follows:

$$u_{*g}^{(2)} = u_* \left(\frac{\ln \frac{z_b}{z_o}}{\ln \frac{z_b}{z_{og}^{(2)}}} \right) \tag{A-9}$$

$$\tau_g = \rho_w u_{*g}^{\ 2} = \rho_w \left(u_{*g}^{(2)} \right)^2 \tag{A-10}$$

where:

$u_{*g}^{(2)}$ = second (refined) estimate of grain stress shear velocity [L T^{-1}]

$z_{og}^{(2)}$ = second (refined) estimate for grain roughness height [L]

τ_g = grain stress (surface drag) component of total shear stress [M L^{-1} T^{-2}]

u_{*g} = grain stress shear velocity [L T^{-1}]

Additional adjustments to the bed shear stress partitioning process can be performed to account for the presence of bedforms. Bedform formation and decay over time alters bed roughness over time. Increasing bedform roughness causes greater form drag and reduces the surface drag component of the total shear stress. Decreasing bedform roughness results in less form drag and increases the surface drag component of total shear stress. However, for simplicity, the model code used for the Rockaway Delivery Lateral Project does not perform bed roughness adjustments to account for bedforms.

References

Winterwerp, J. C., and van Kesteren, W. G. M. 2004. *Introduction to the Physics of Cohesive Sediment in the Marine Environment*. Elsevier B.V., Amsterdam, Netherlands. 466 p.

APPENDIX B. SIMULATED SURFACE LAYER SUSPENDED SOLIDS: WORST CASE JETTING

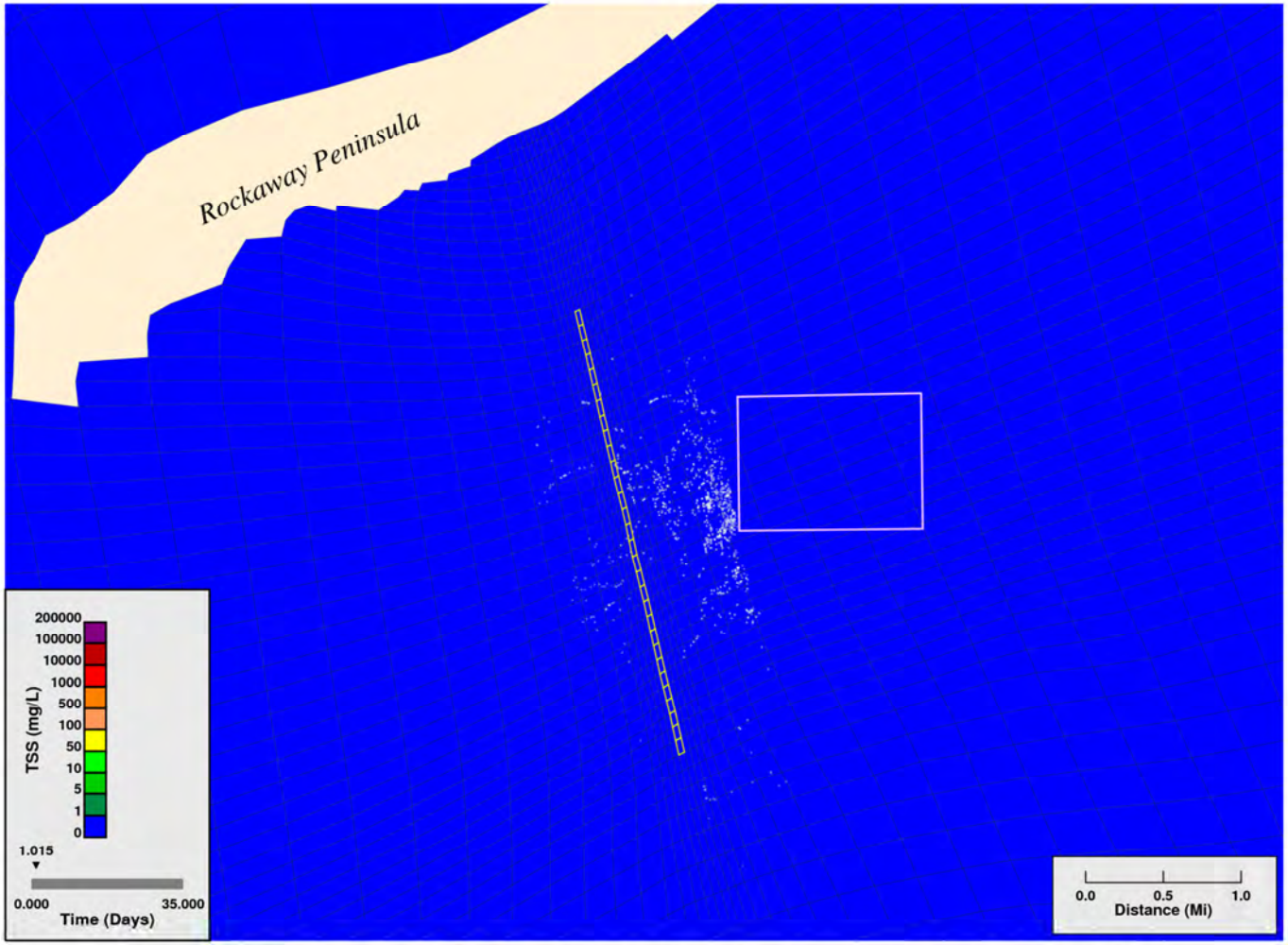

Figure B1. Worst case jetting: simulated suspended solids near water column surface, start of trenching, rate = 366 m/hr.

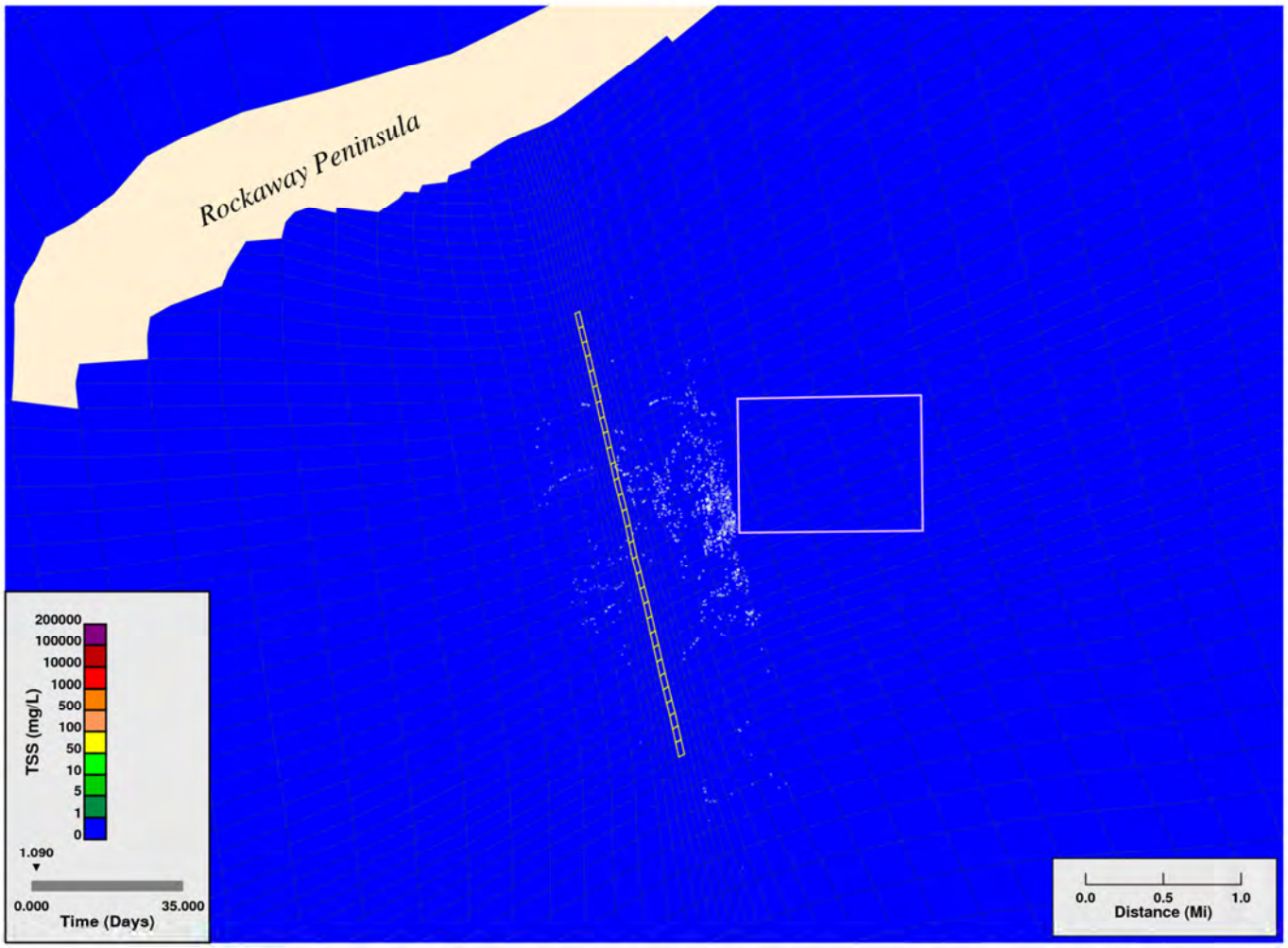

Surface Layer Projected Solids Concentrations from Proposed Dredging, 1200 ft/hr

Figure B2. Worst case jetting: simulated suspended solids near water column surface, trenching 25% complete, rate = 366 m/hr.

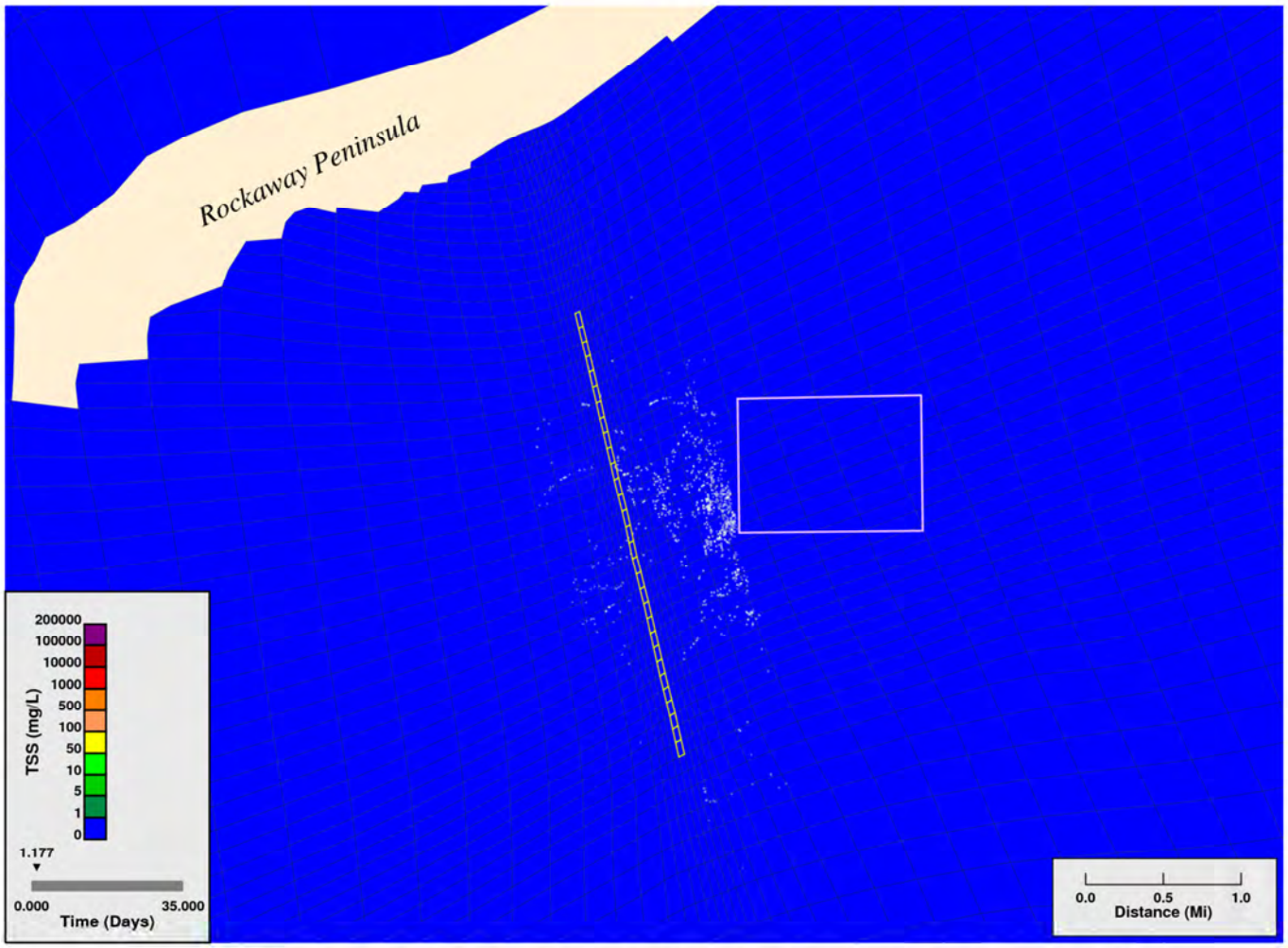

Surface Layer Projected Solids Concentrations from Proposed Dredging, 1200 ft/hr

Figure B3. Worst case jetting: simulated suspended solids near water column surface, trenching 50% complete, rate = 366 m/hr.

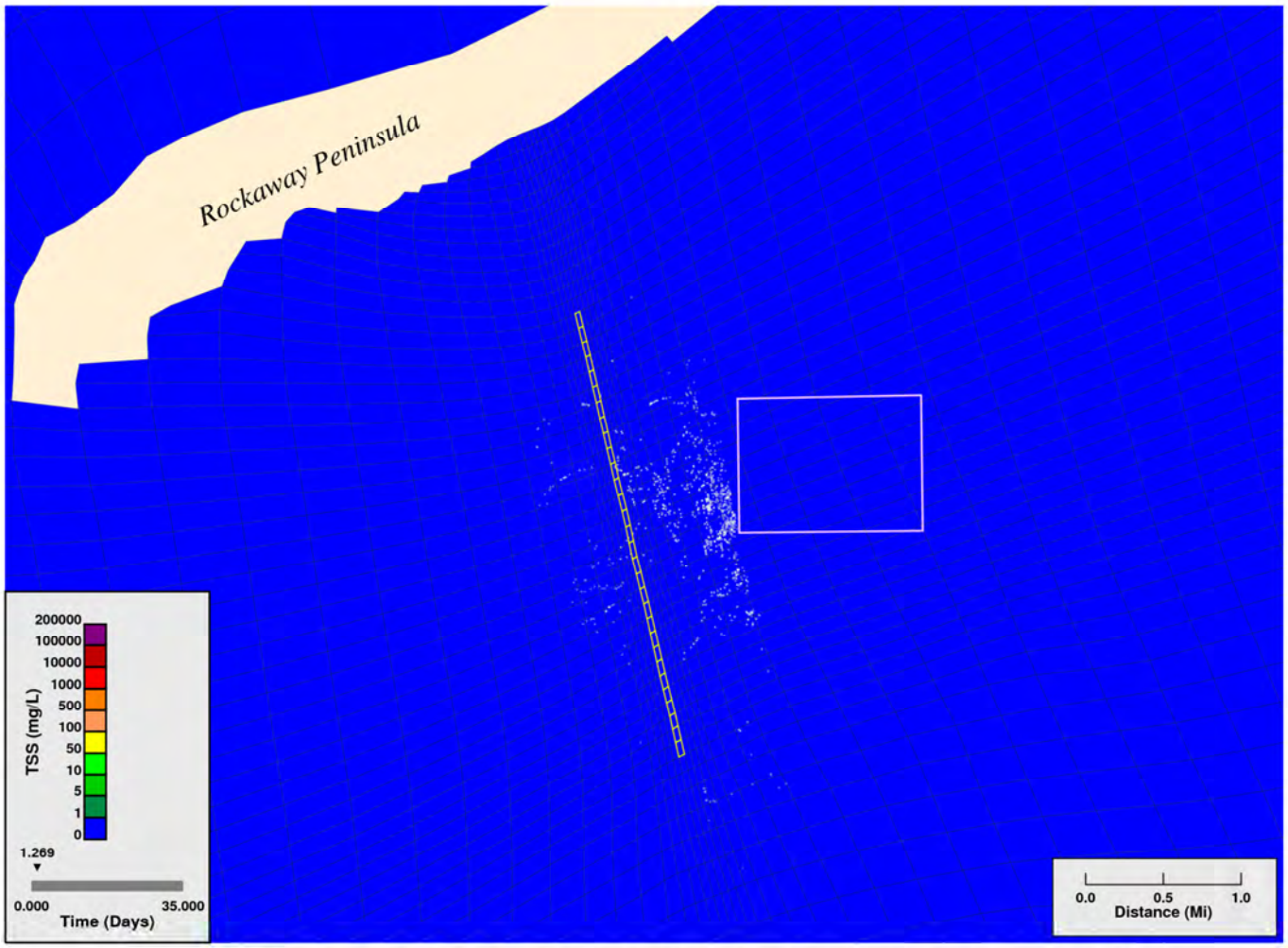

Surface Layer Projected Solids Concentrations from Proposed Dredging, 1200 ft/hr

Figure B4. Worst case jetting: simulated suspended solids near water column surface, trenching 75% complete, rate = 366 m/hr.

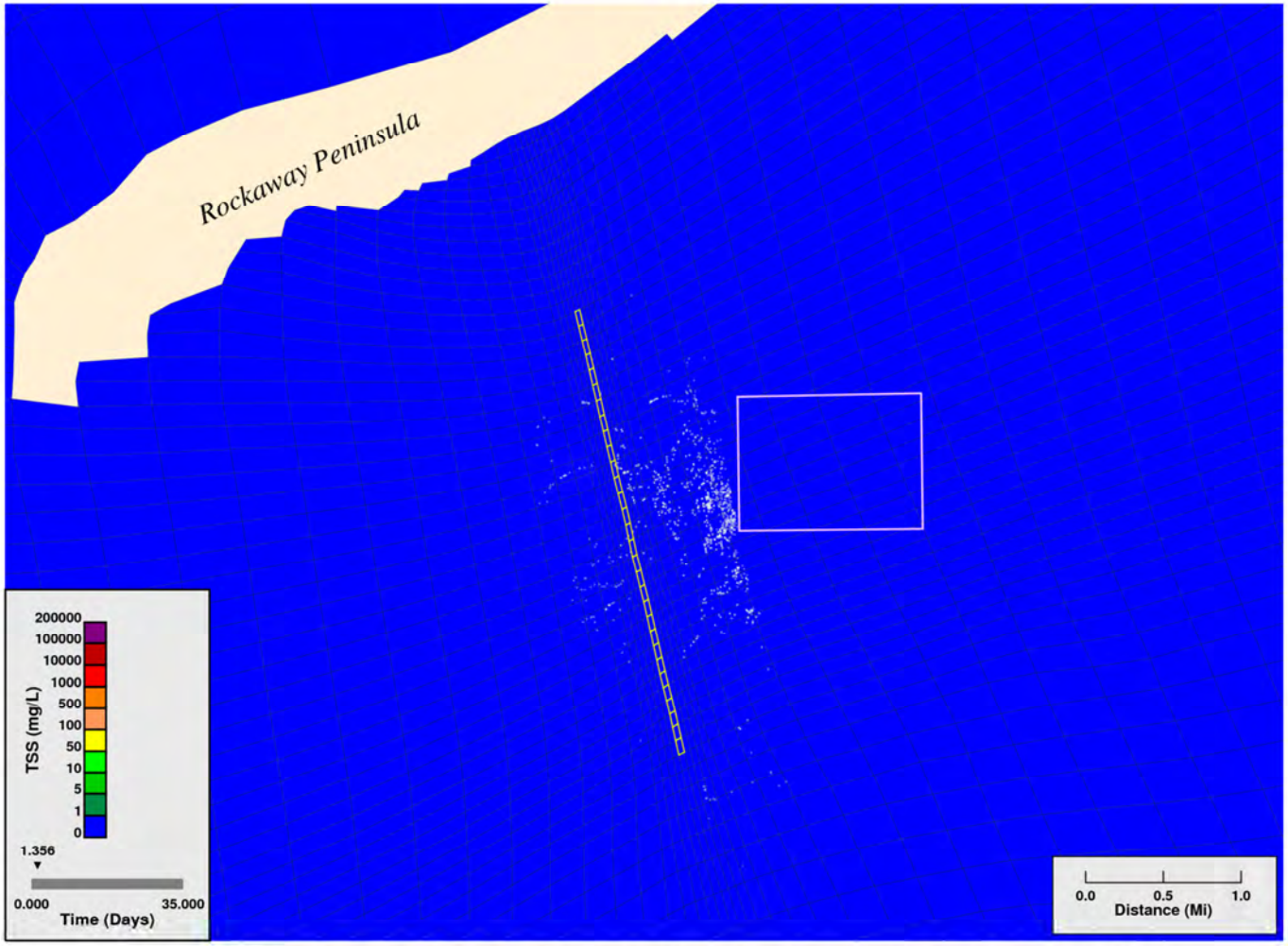

Surface Layer Projected Solids Concentrations from Proposed Dredging, 1200 ft/hr

Figure B5. Worst case jetting: simulated suspended solids near water column surface, end of trenching, rate = 366 m/hr.

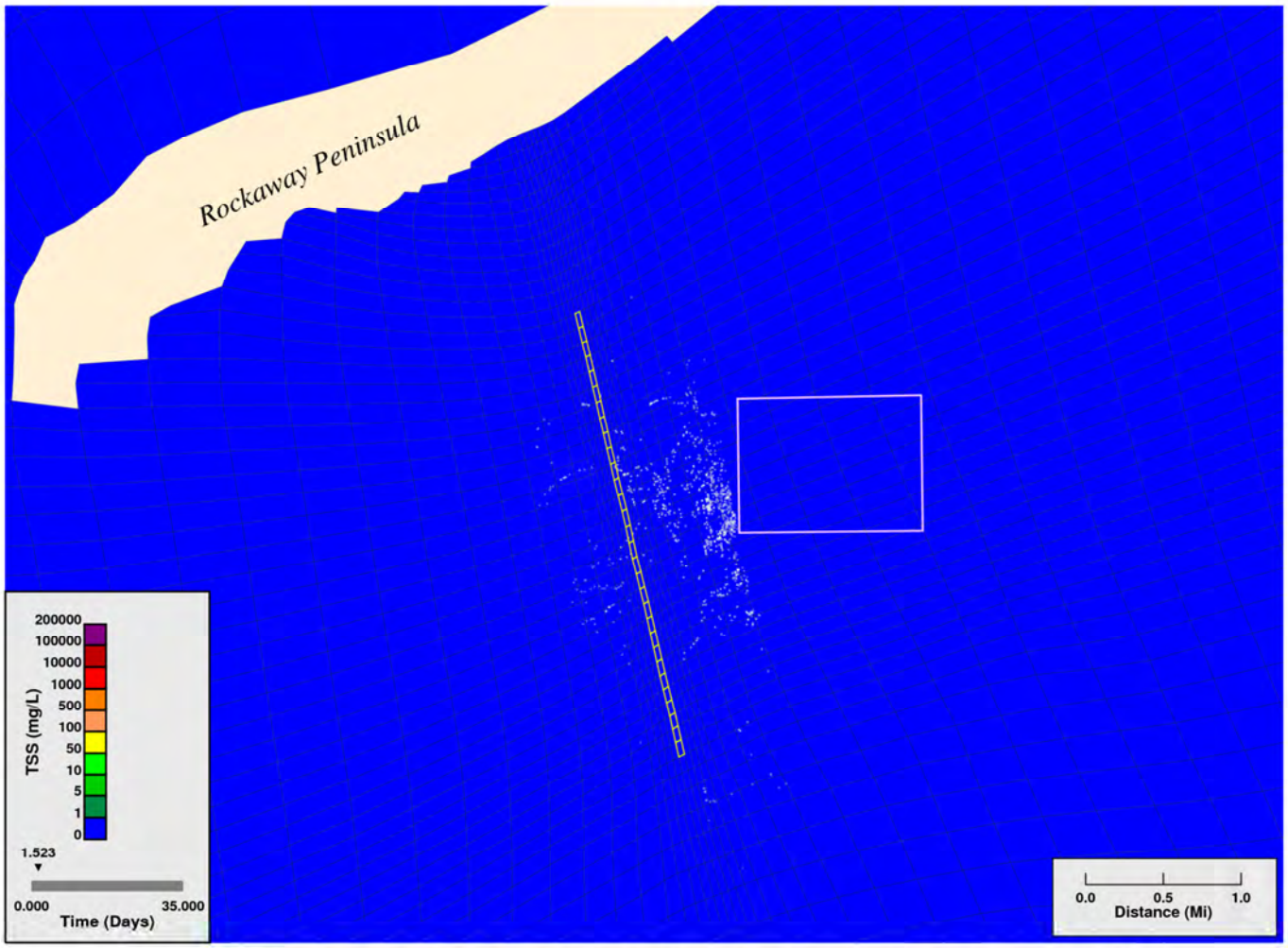

Figure B6. Worst case jetting: simulated suspended solids near water column surface, 4 hours after end of trenching, rate = 366 m/hr.

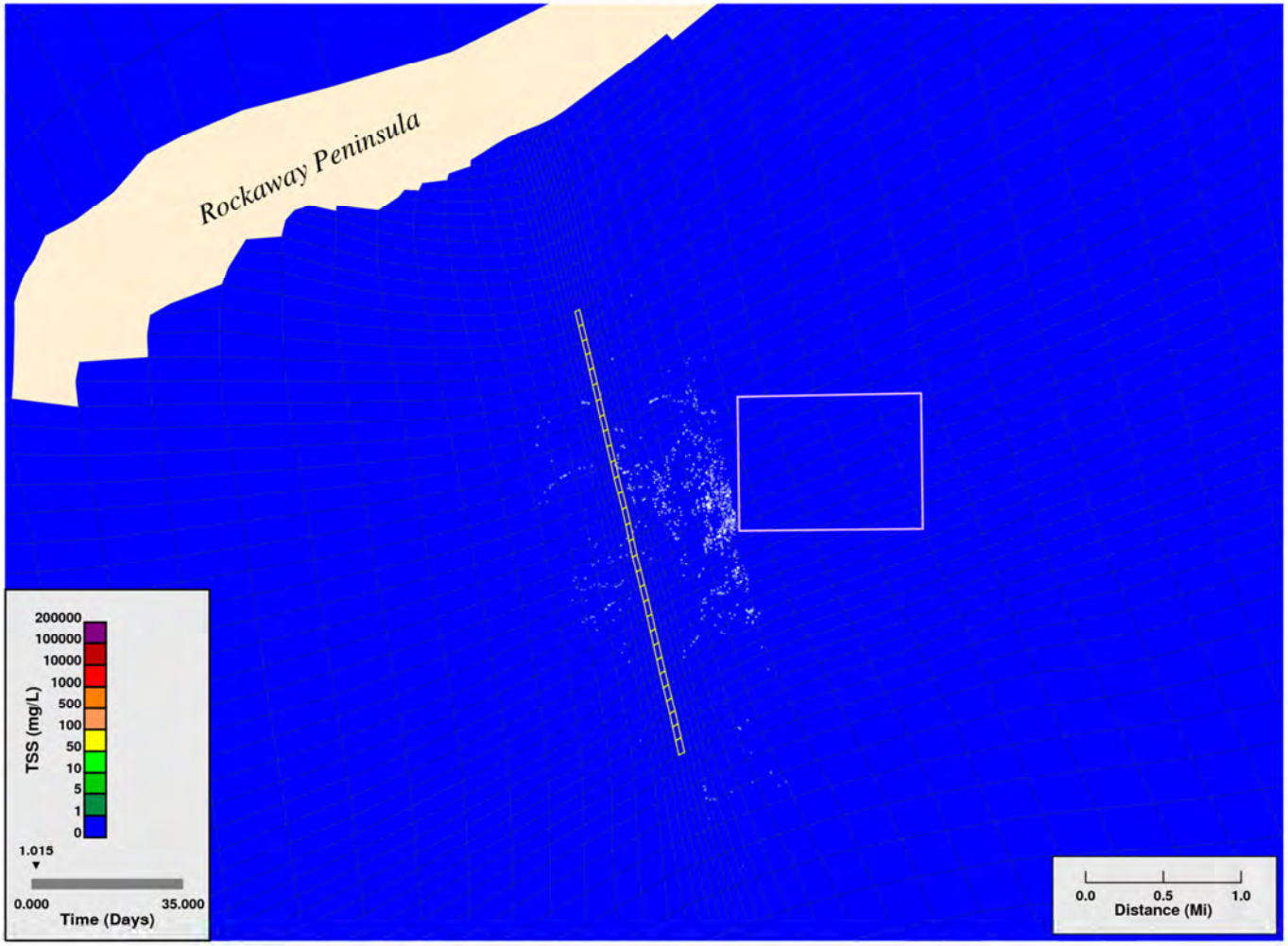

Figure B7. Worst case jetting: simulated suspended solids near water column surface, start of trenching, rate = 183 m/hr.

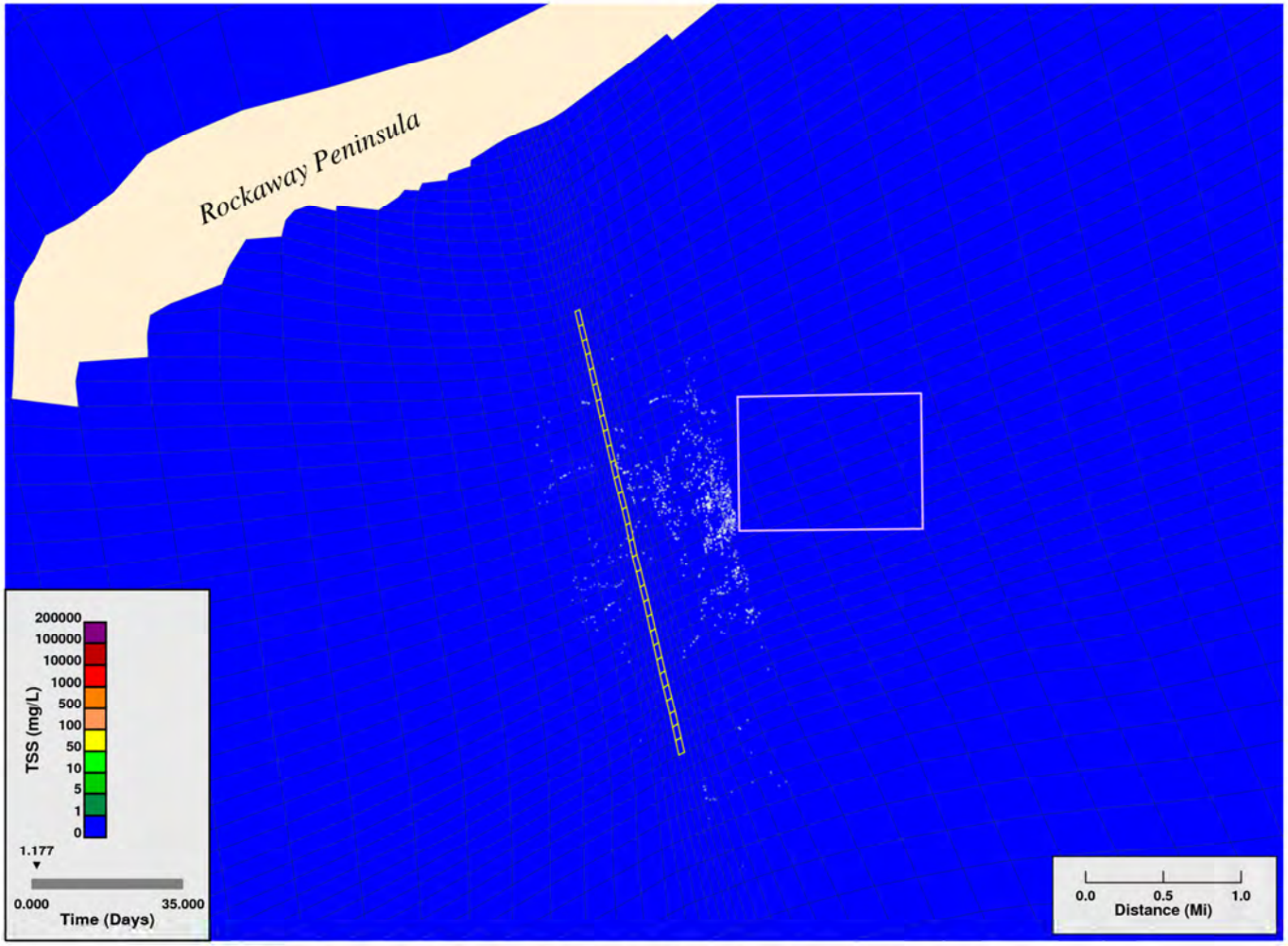

Surface Layer Projected Solids Concentrations from Proposed Dredging, 600 ft/hr

Figure B8. Worst case jetting: simulated suspended solids near water column surface, trenching 25% complete, rate = 183 m/hr.

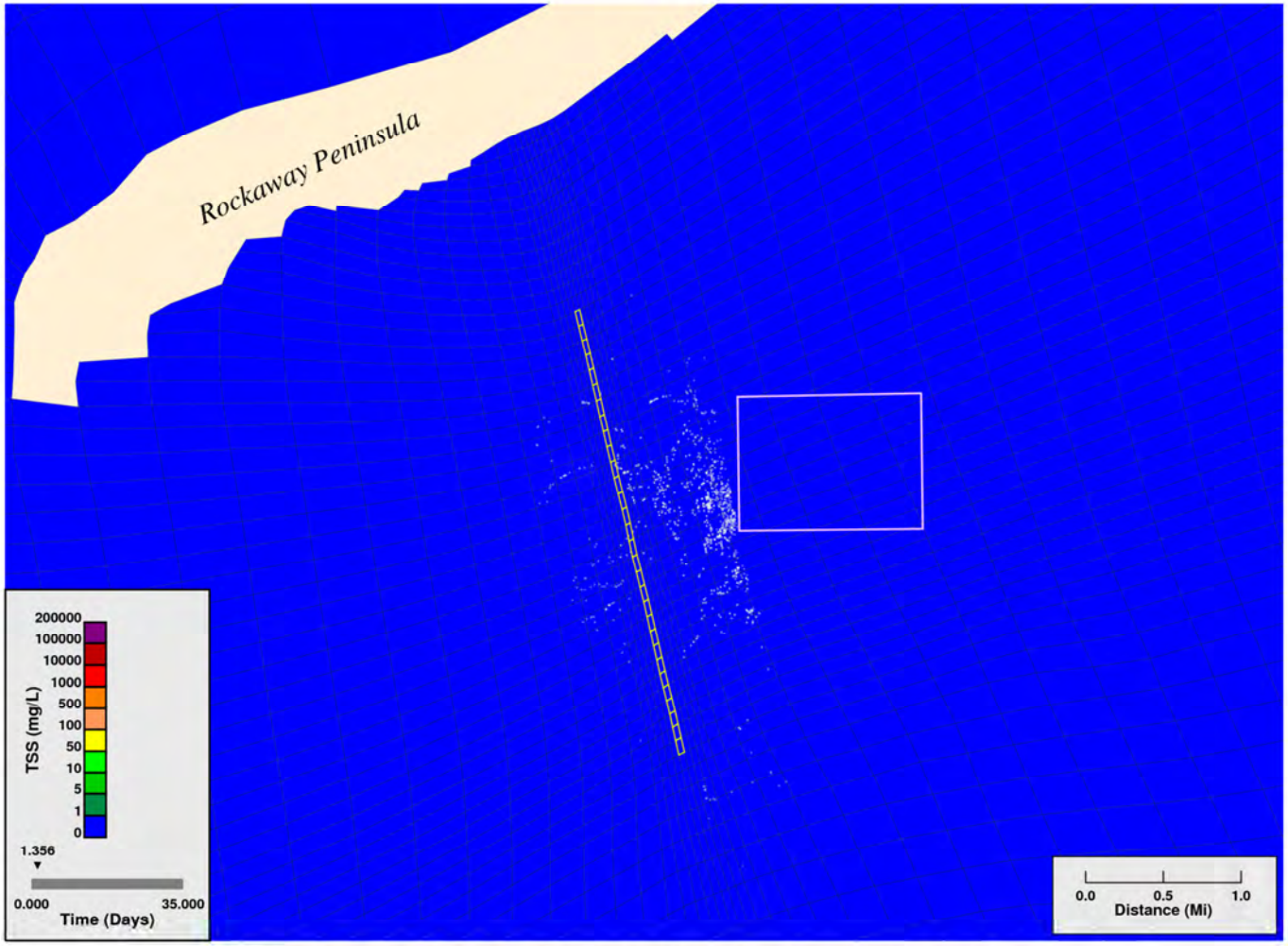

Surface Layer Projected Solids Concentrations from Proposed Dredging, 600 ft/hr

Figure B9. Worst case jetting: simulated suspended solids near water column surface, trenching 50% complete, rate = 183 m/hr.

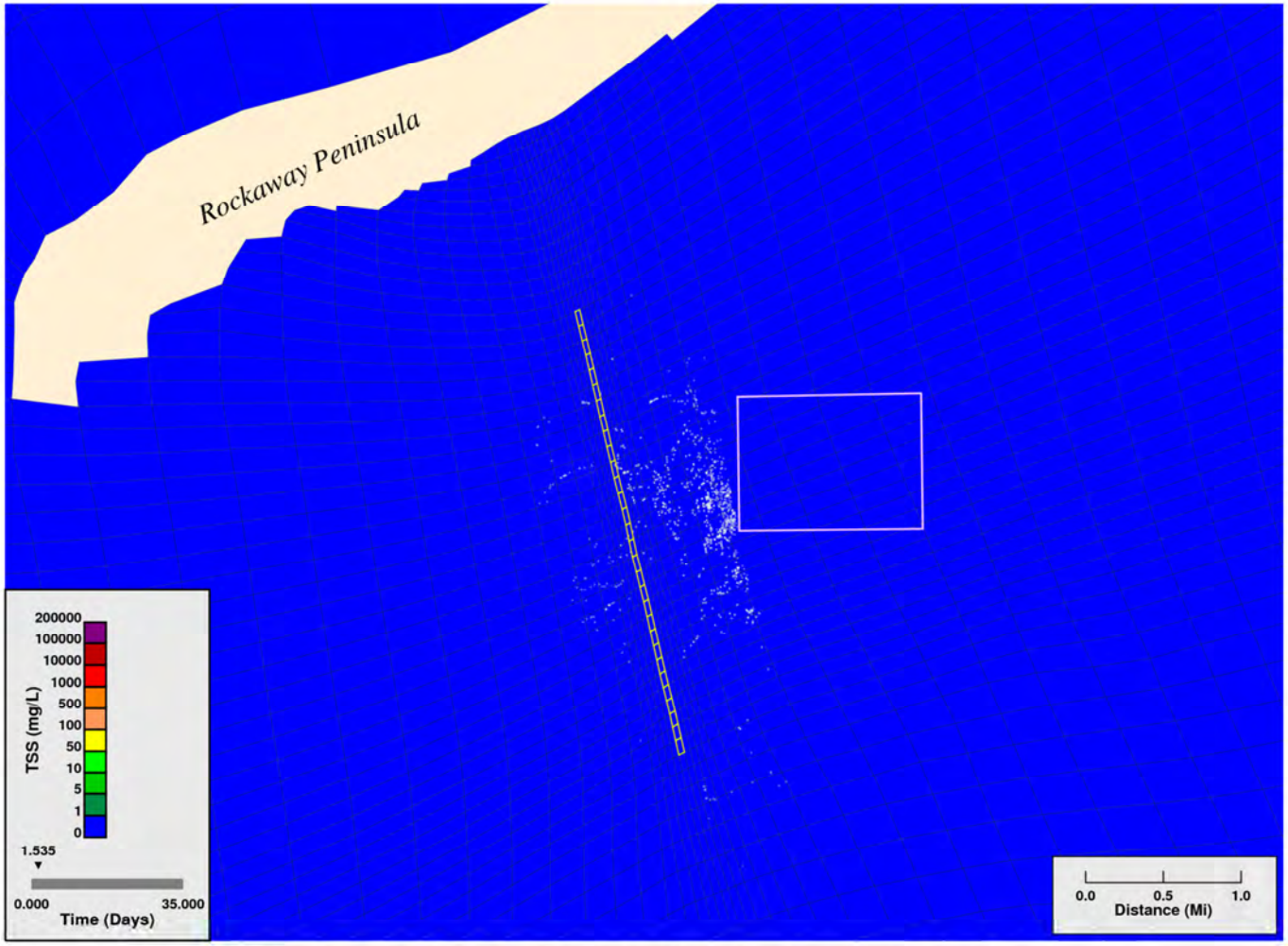

Figure B10. Worst case jetting: simulated suspended solids near water column surface, trenching 75% complete, rate = 183 m/hr.

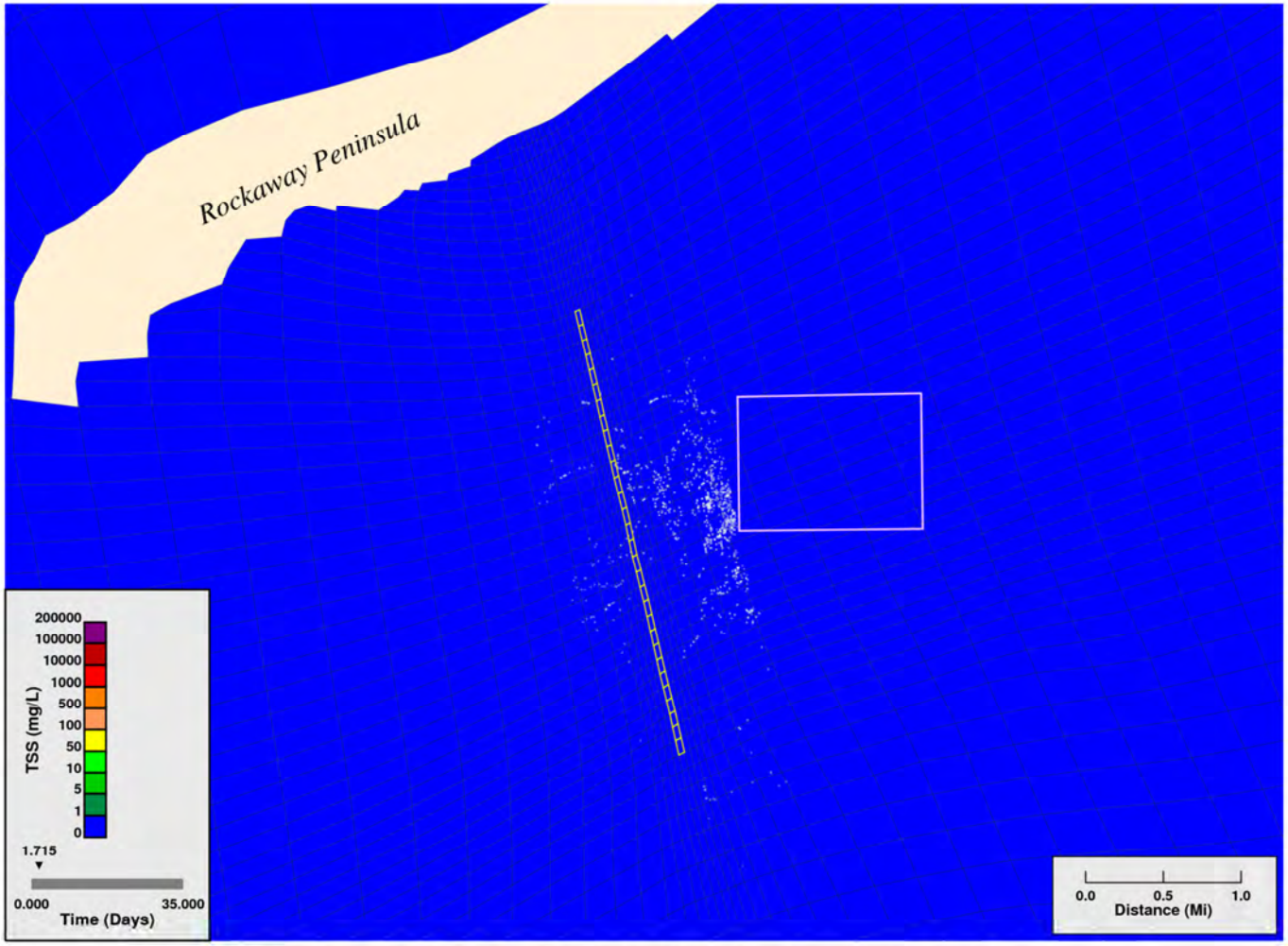

Surface Layer Projected Solids Concentrations from Proposed Dredging, 600 ft/hr

Figure B11. Worst case jetting: simulated suspended solids near water column surface, end of trenching, rate = 183 m/hr.

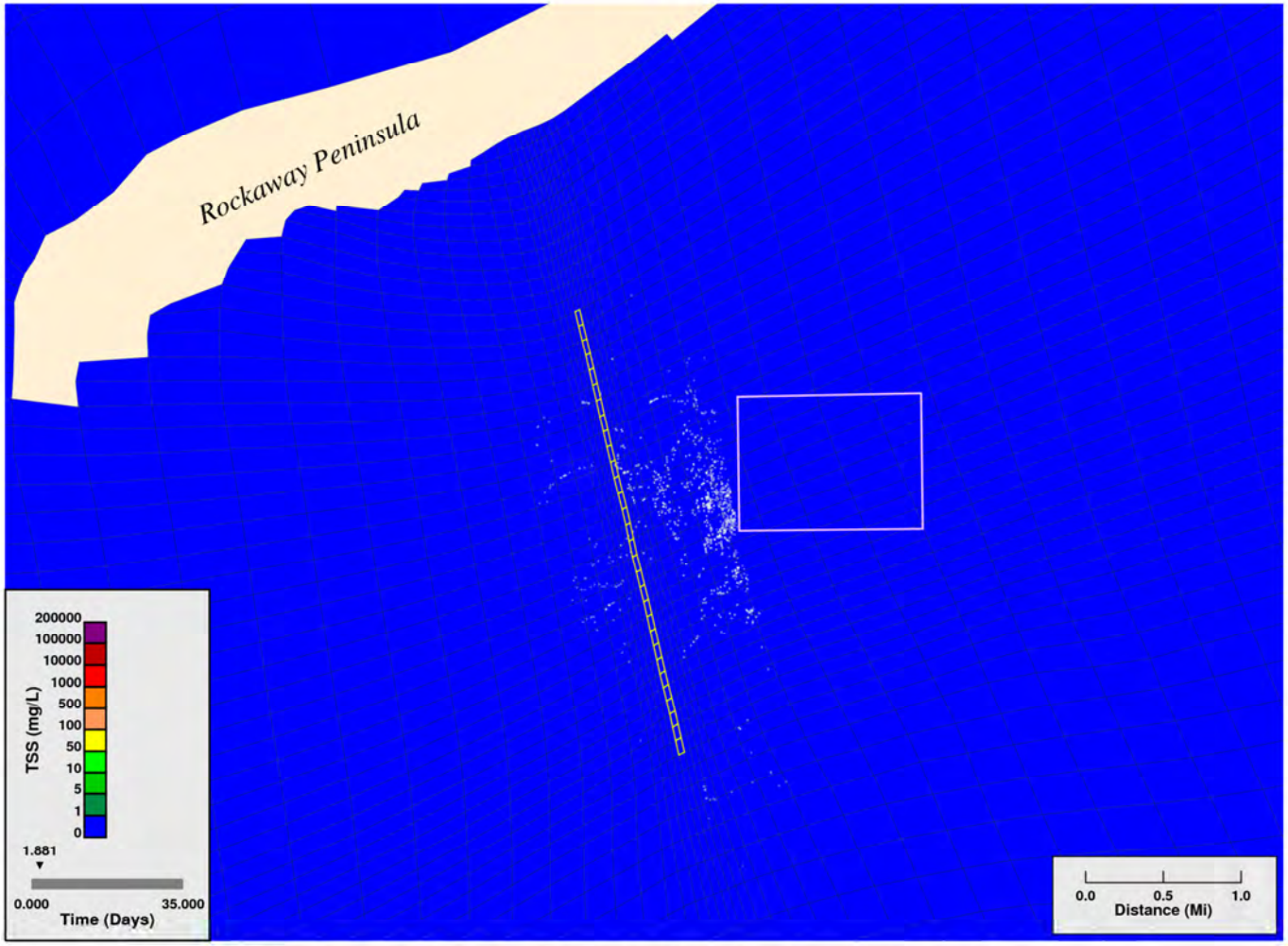

Surface Layer Projected Solids Concentrations from Proposed Dredging, 600 ft/hr

Figure B12. Worst case jetting: simulated suspended solids near water column surface, 4 hours after end of trenching, rate = 183 m/hr.

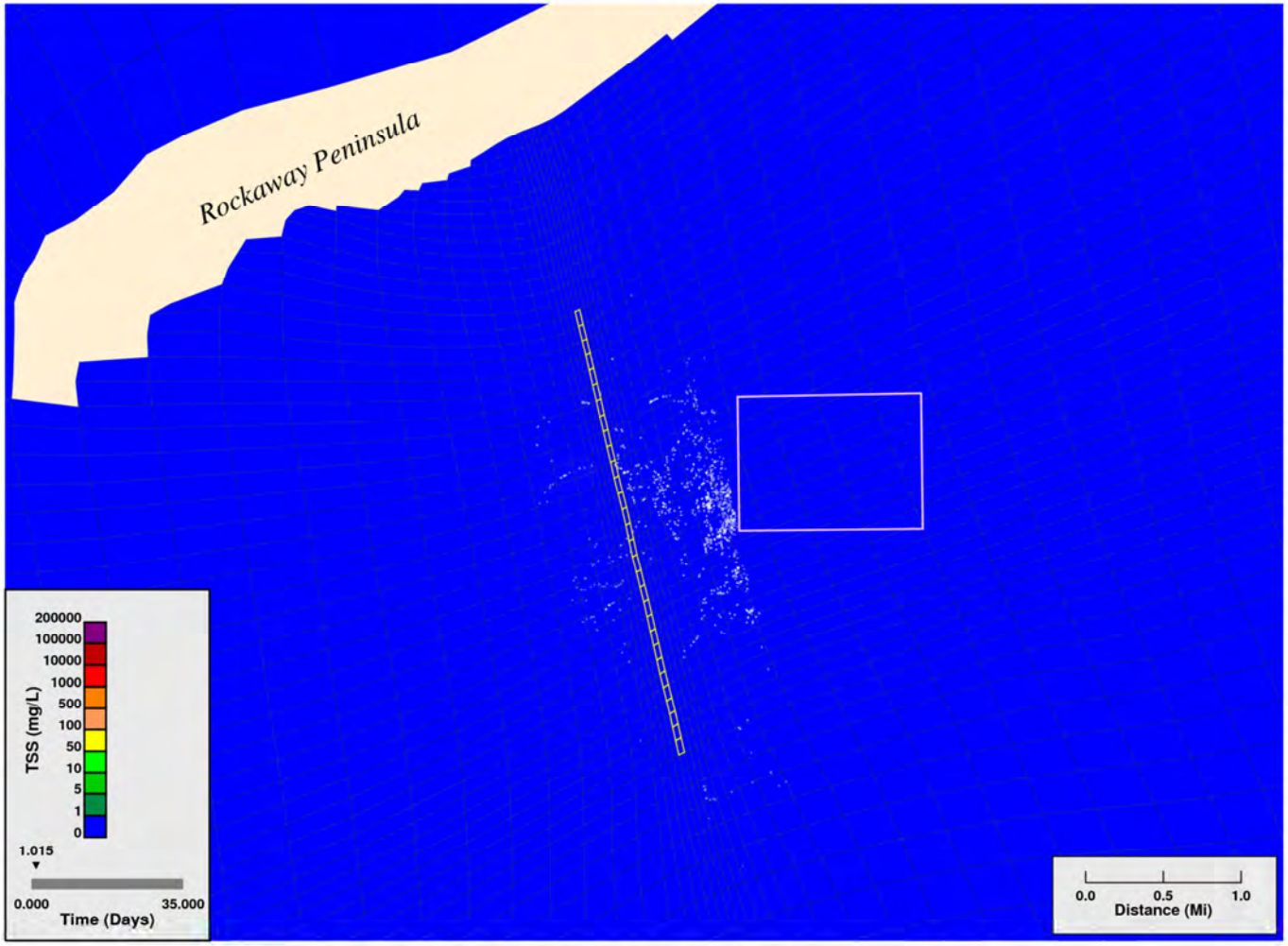

Figure B13. Worst case jetting: simulated suspended solids near water column surface, start of trenching, rate = 122 m/hr.

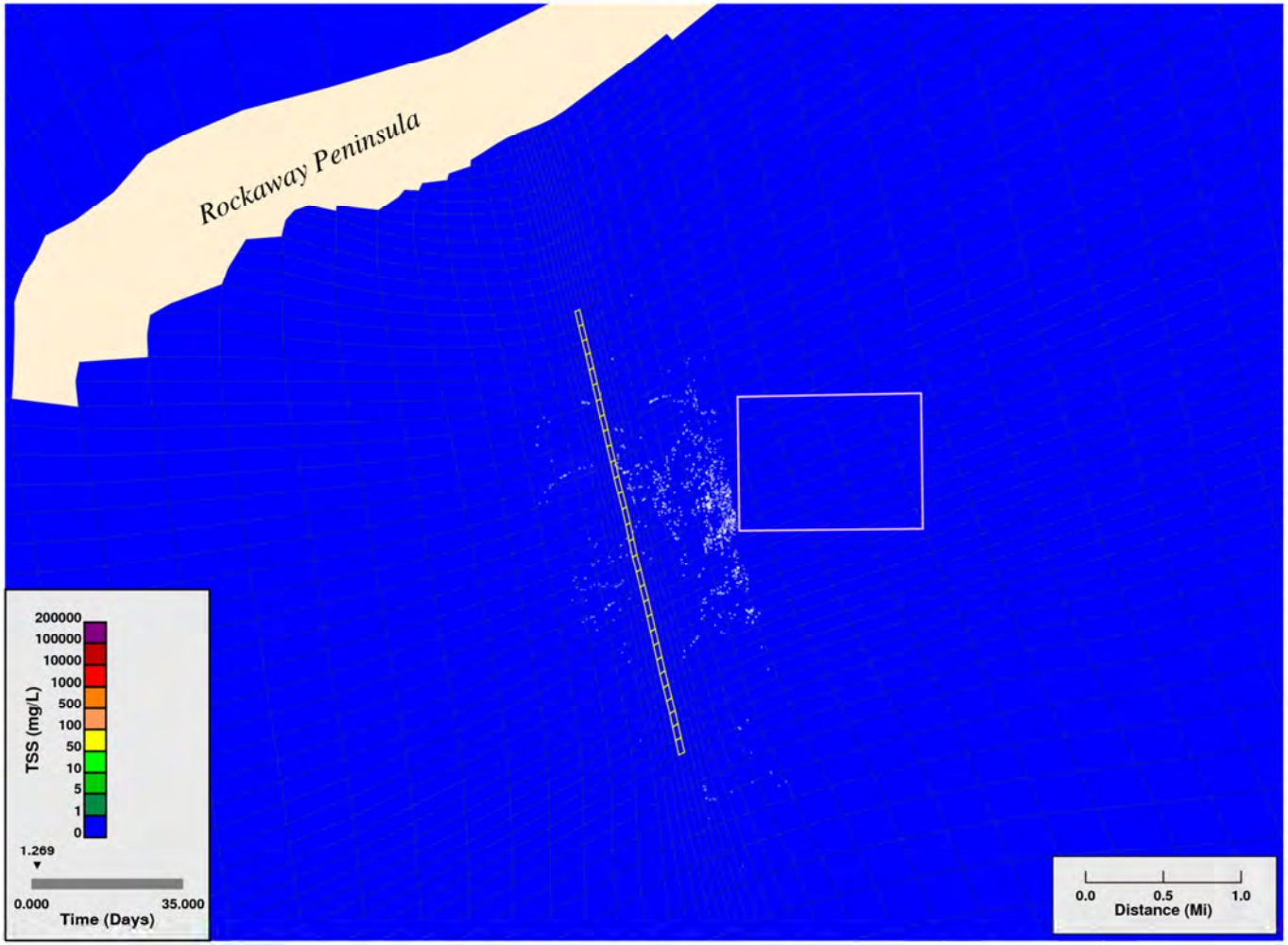

Surface Layer Projected Solids Concentrations from Proposed Dredging, 400 ft/hr

Figure B14. Worst case jetting: simulated suspended solids near water column surface, trenching 25% complete, rate = 122 m/hr.

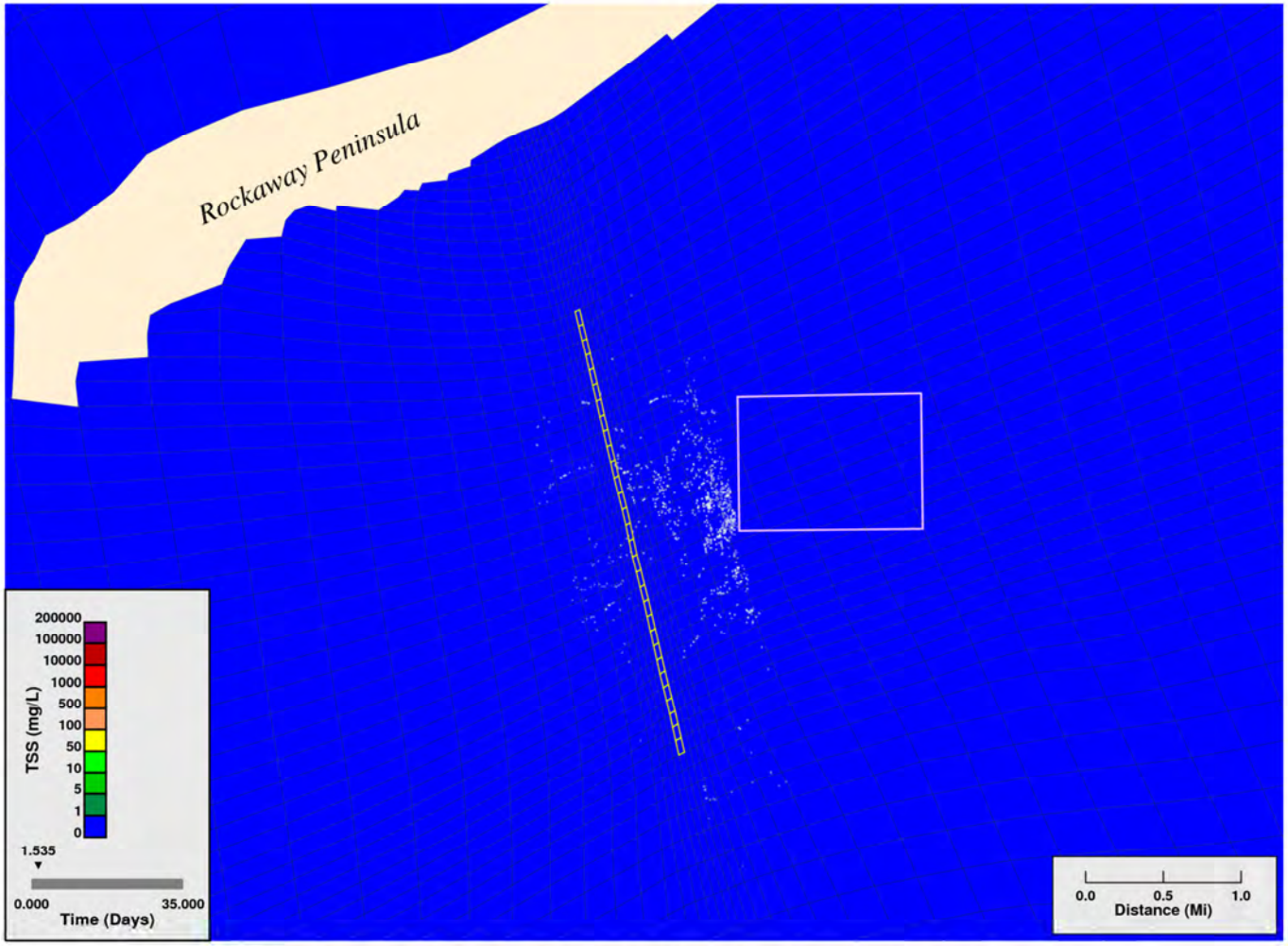

Figure B15. Worst case jetting: simulated suspended solids near water column surface, trenching 50% complete, rate = 122 m/hr.

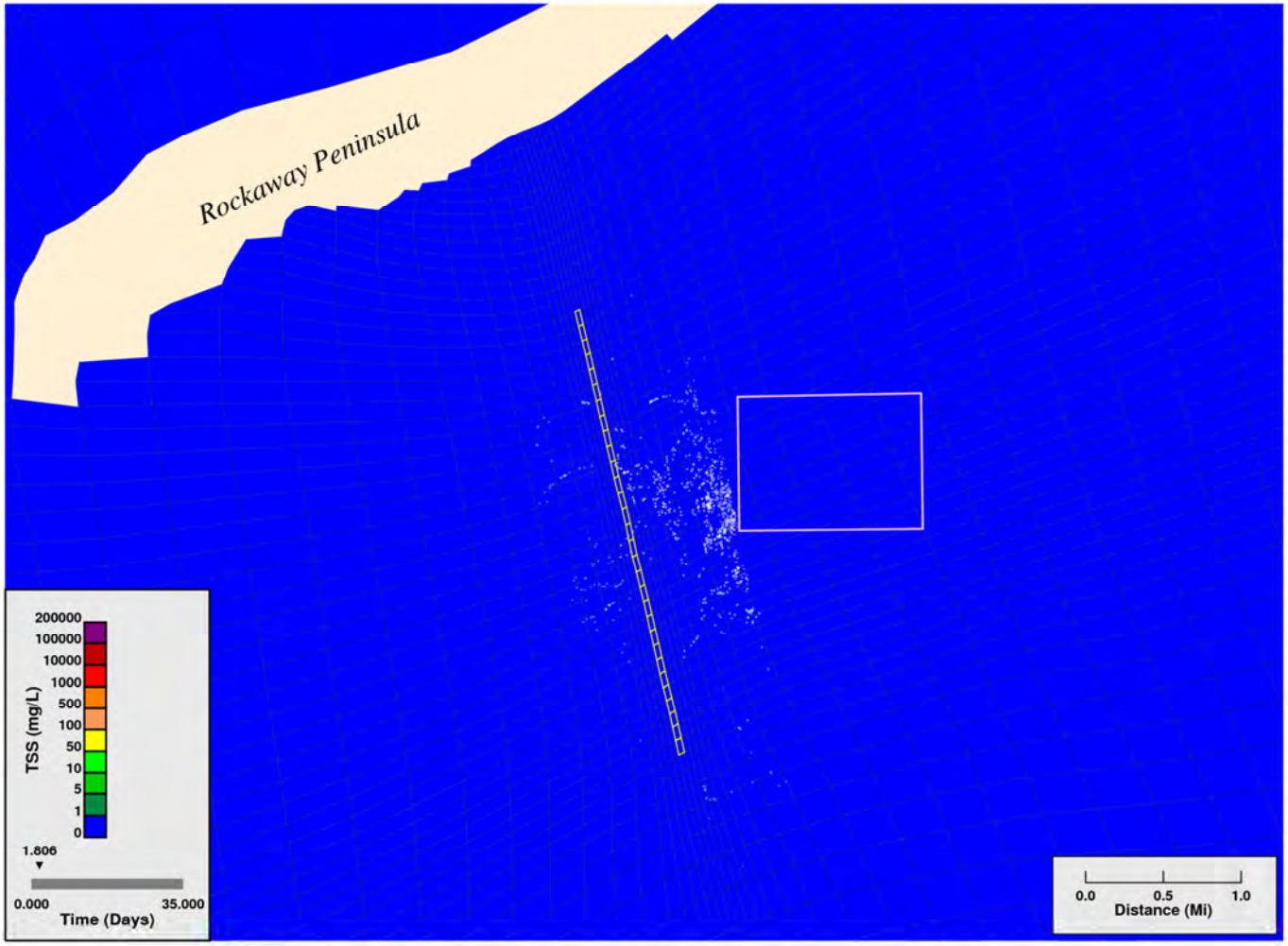

Figure B16. Worst case jetting: simulated suspended solids near water column surface, trenching 75% complete, rate = 122 m/hr.

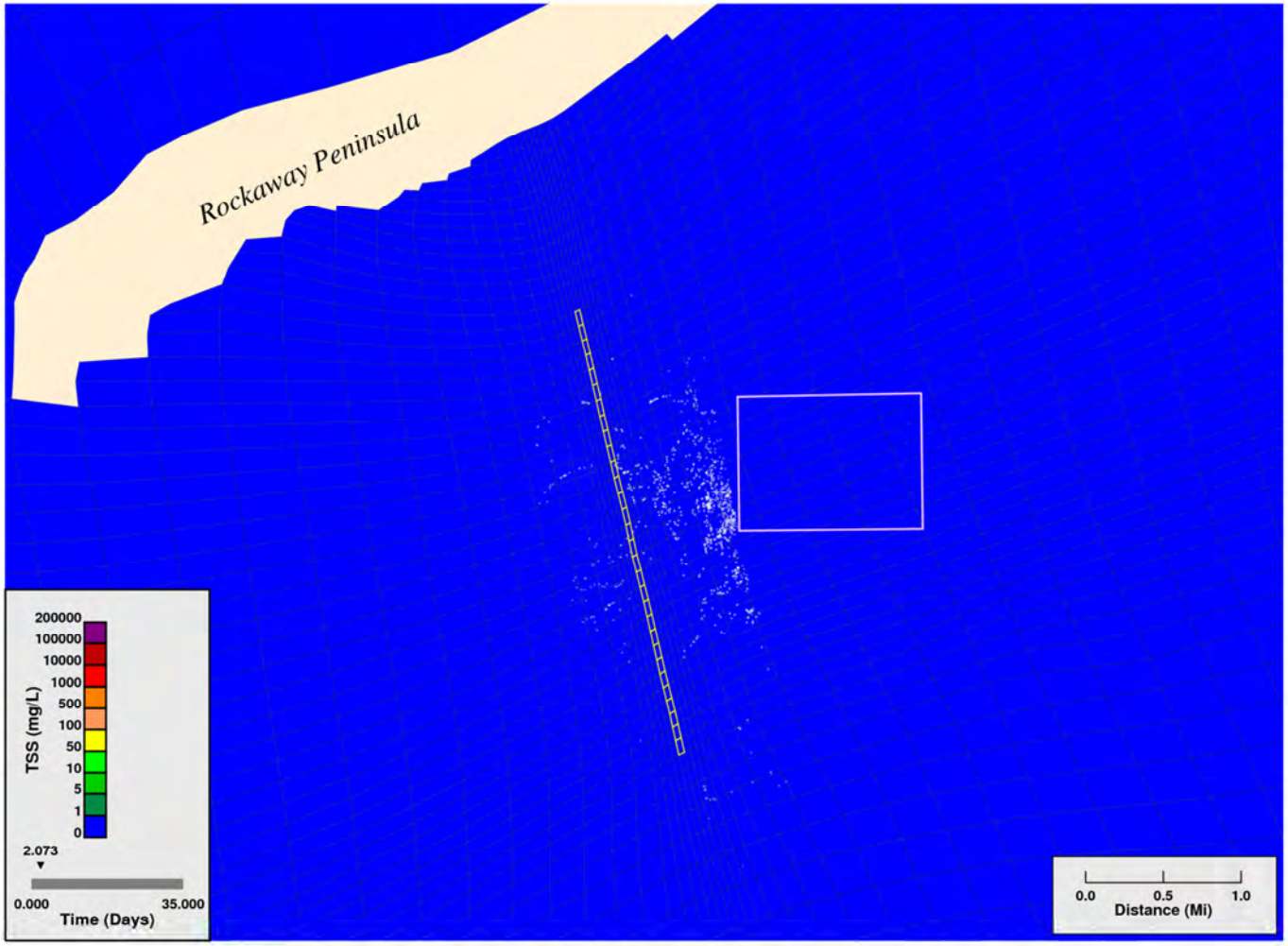

Surface Layer Projected Solids Concentrations from Proposed Dredging, 400 ft/hr

Figure B17. Worst case jetting: simulated suspended solids near water column surface, end of trenching, rate = 122 m/hr.

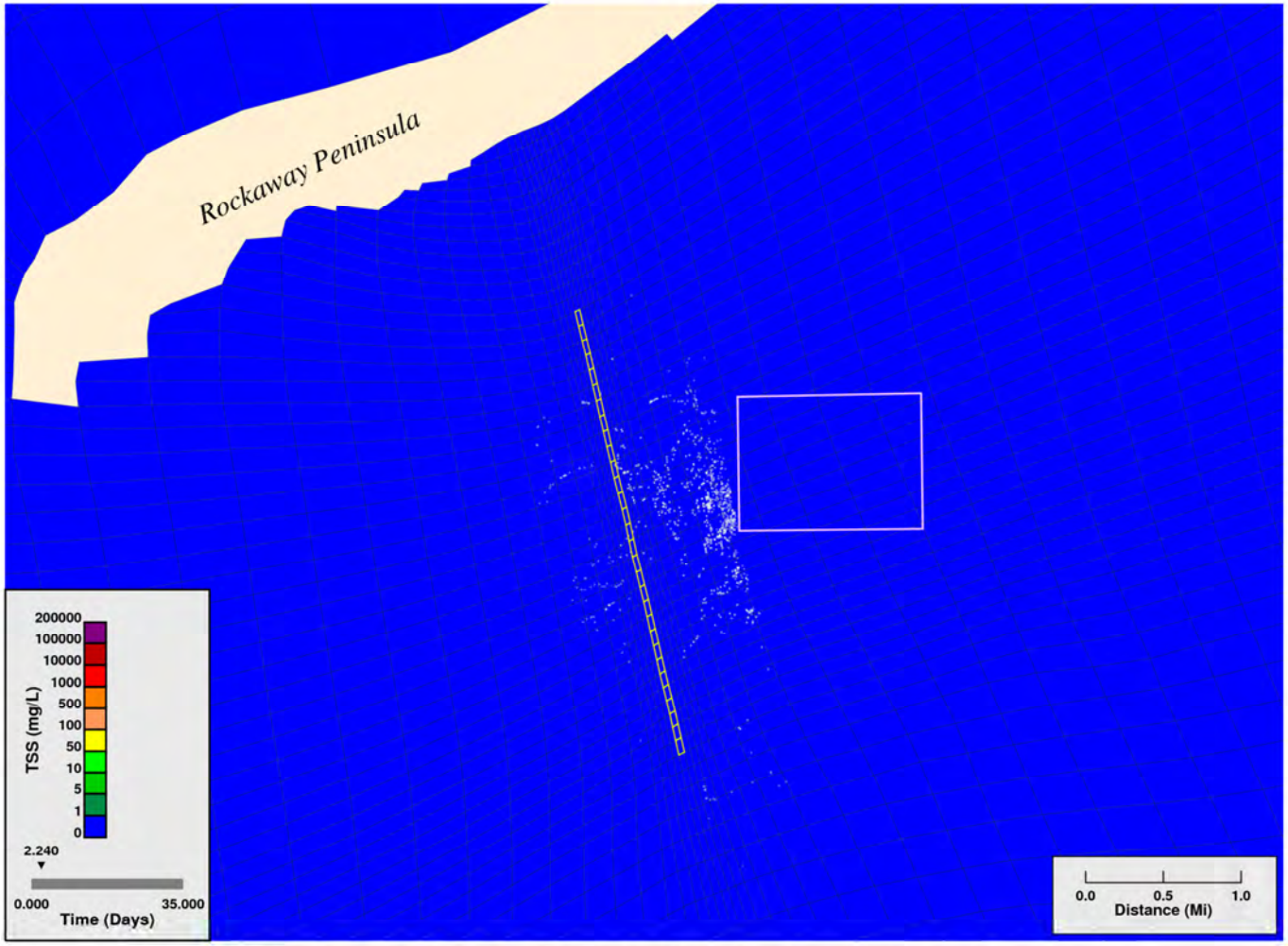

Figure B18. Worst case jetting: simulated suspended solids near water column surface, 4 hours after end of trenching, rate = 122 m/hr.

APPENDIX C. SIMULATED SURFACE LAYER SUSPENDED SOLIDS: TYPICAL JETTING

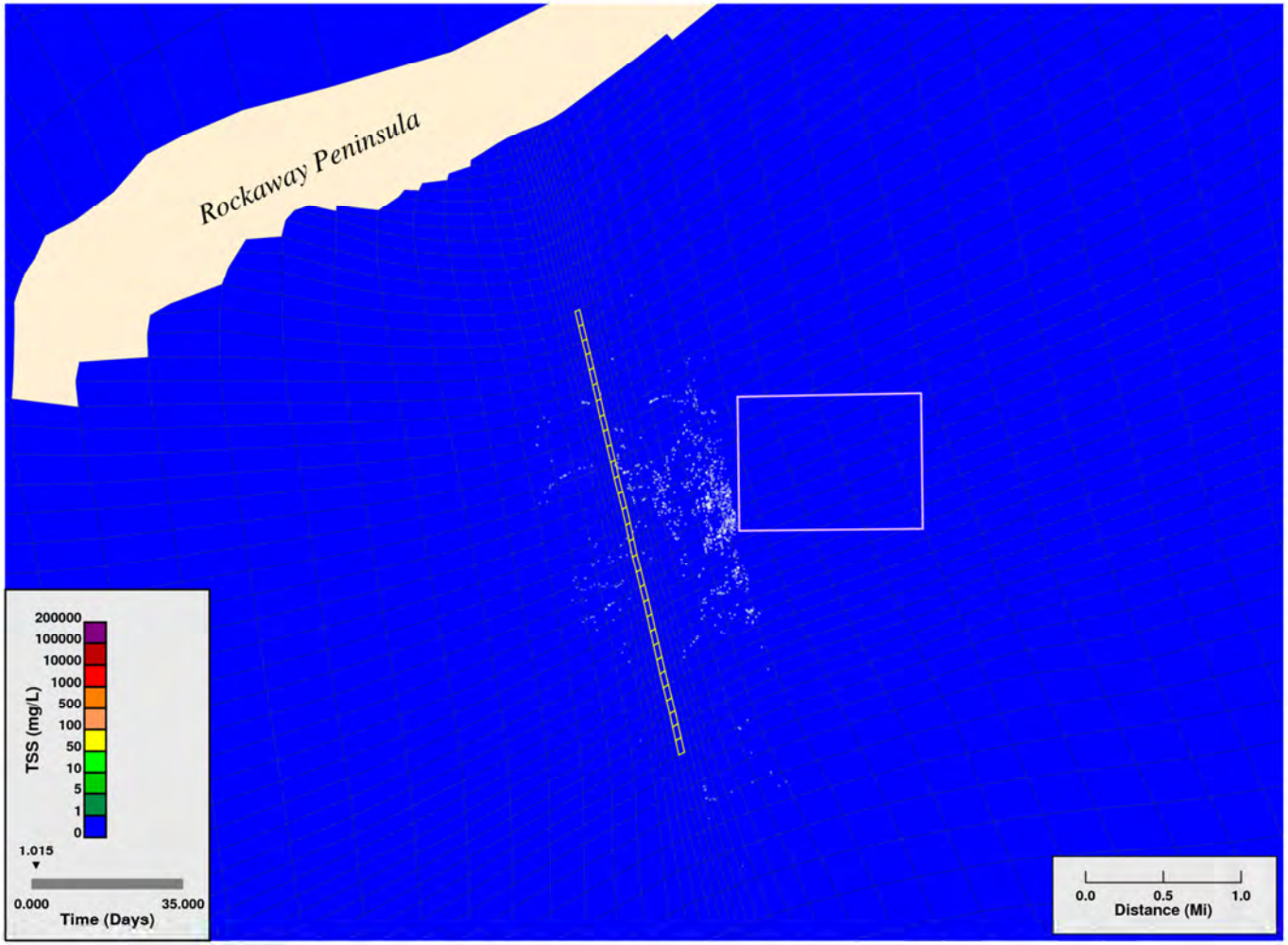

Figure C1. Typical jetting: simulated suspended solids near water column surface, start of trenching, rate = 183 m/hr.

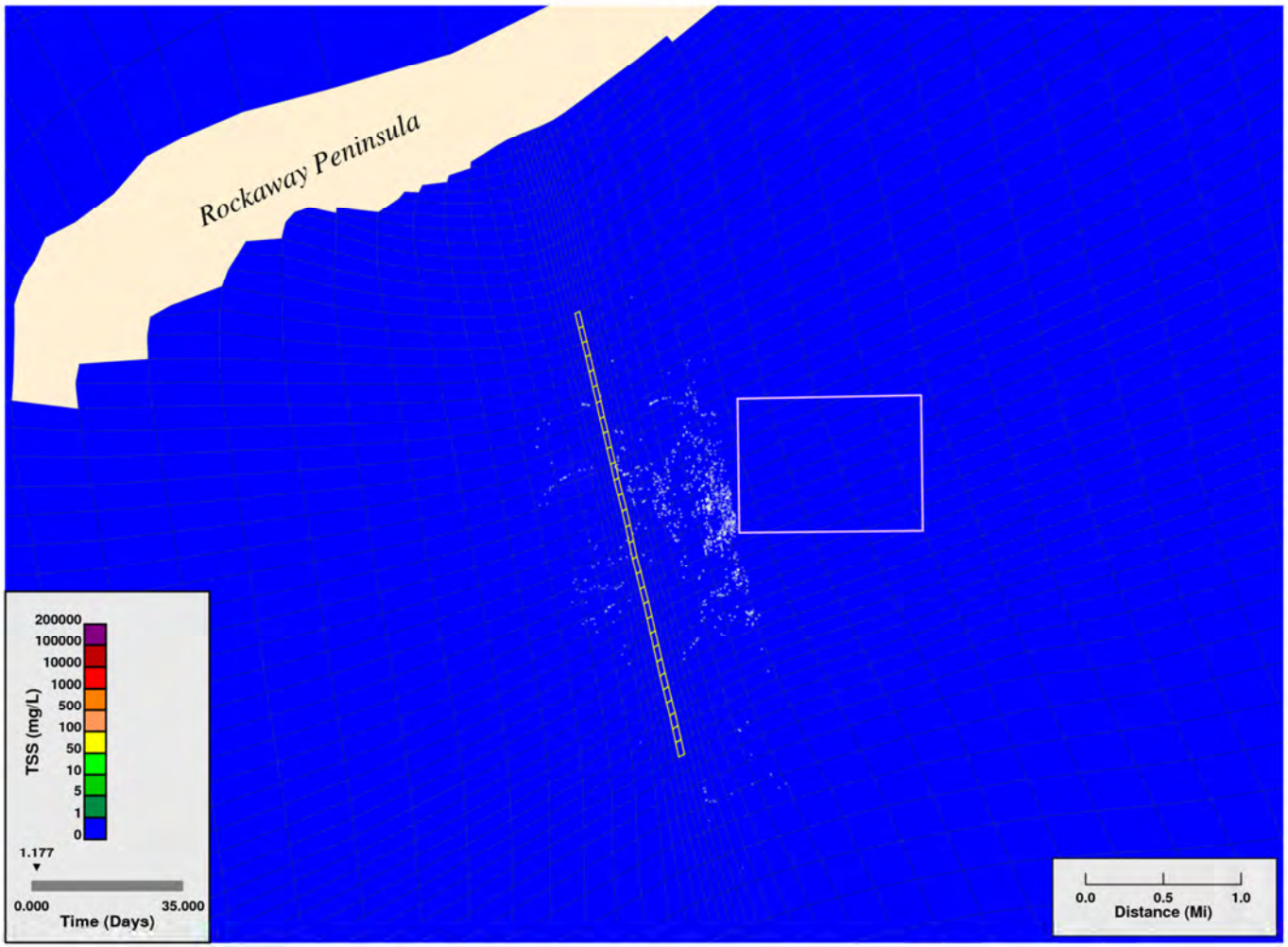

Figure C2. Typical jetting: simulated suspended solids near water column surface, trenching 25% complete, rate = 183 m/hr.

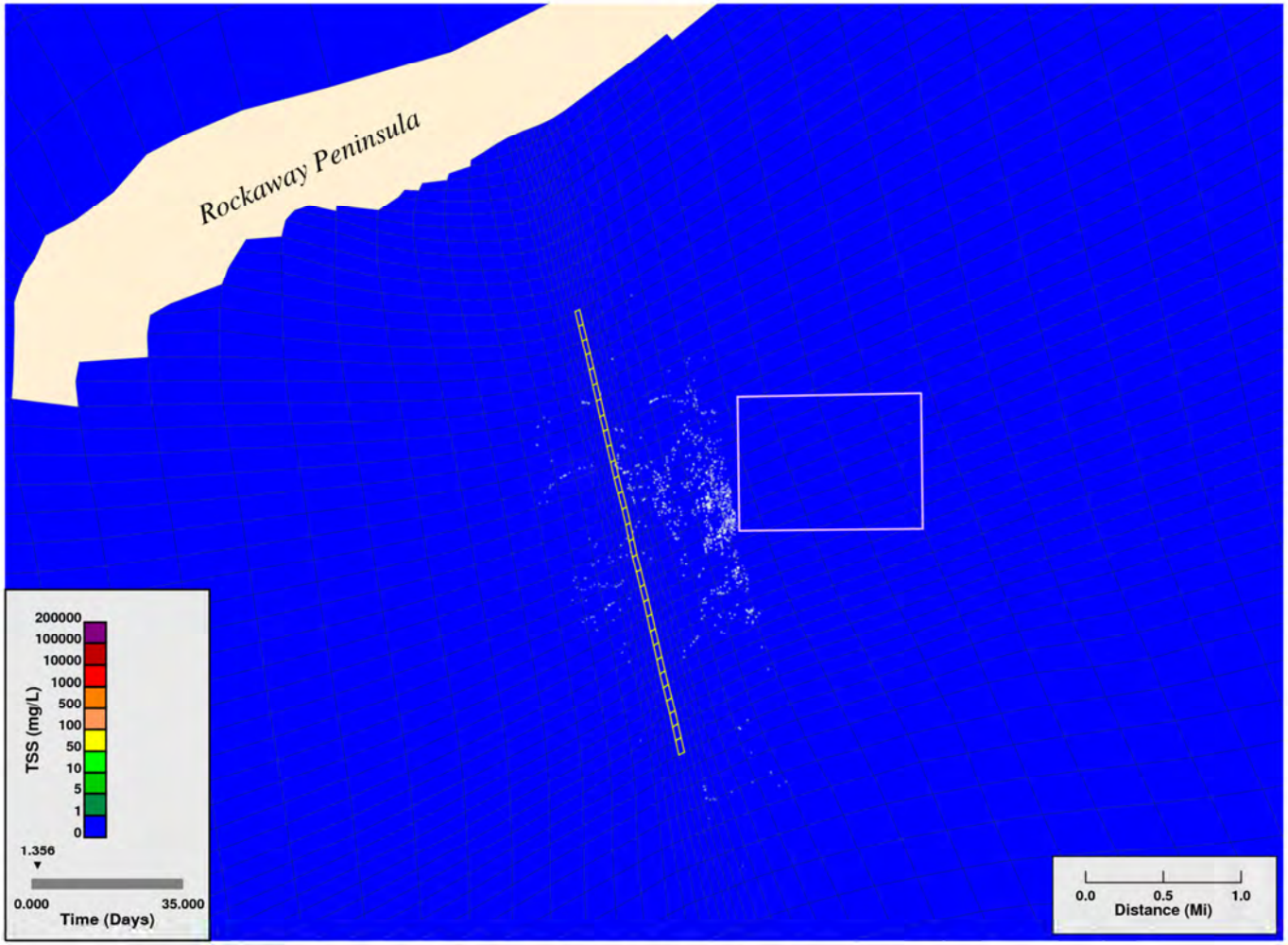

Figure C3. Typical jetting: simulated suspended solids near water column surface, trenching 50% complete, rate = 183 m/hr.

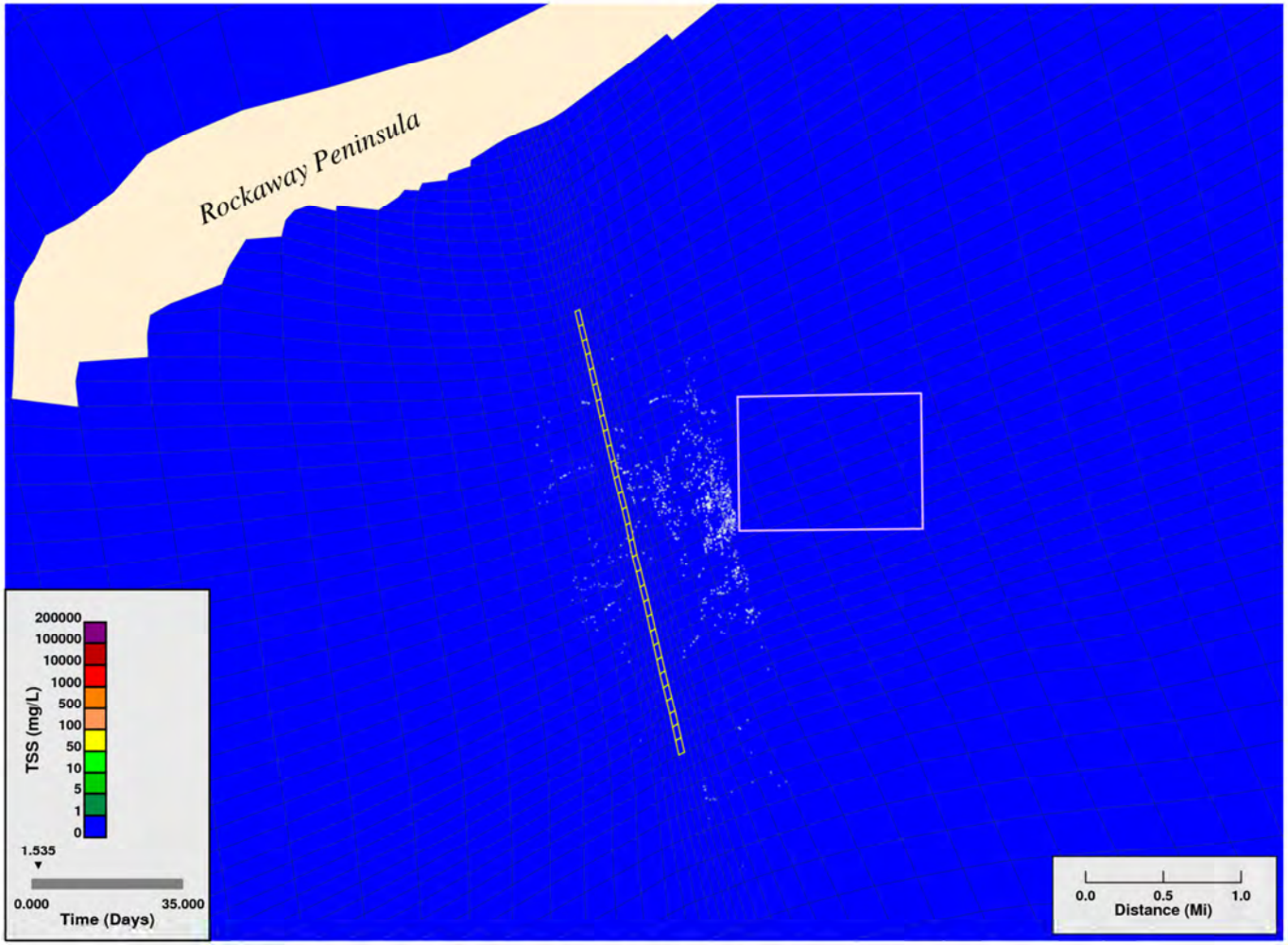

Figure C4. Typical jetting: simulated suspended solids near water column surface, trenching 75% complete, rate = 183 m/hr.

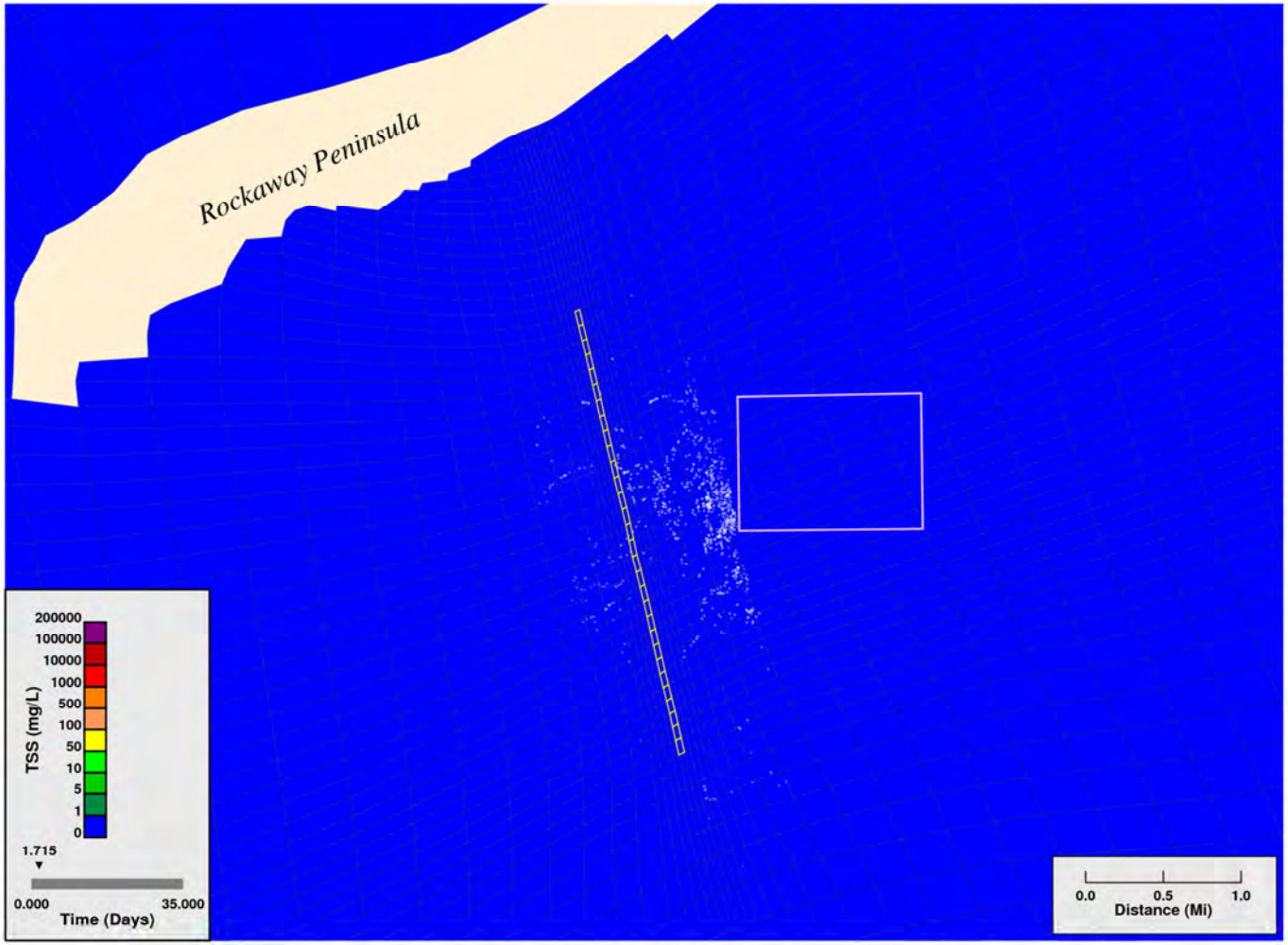

Figure C5. Typical jetting: simulated suspended solids near water column surface, end of trenching, rate = 183 m/hr.

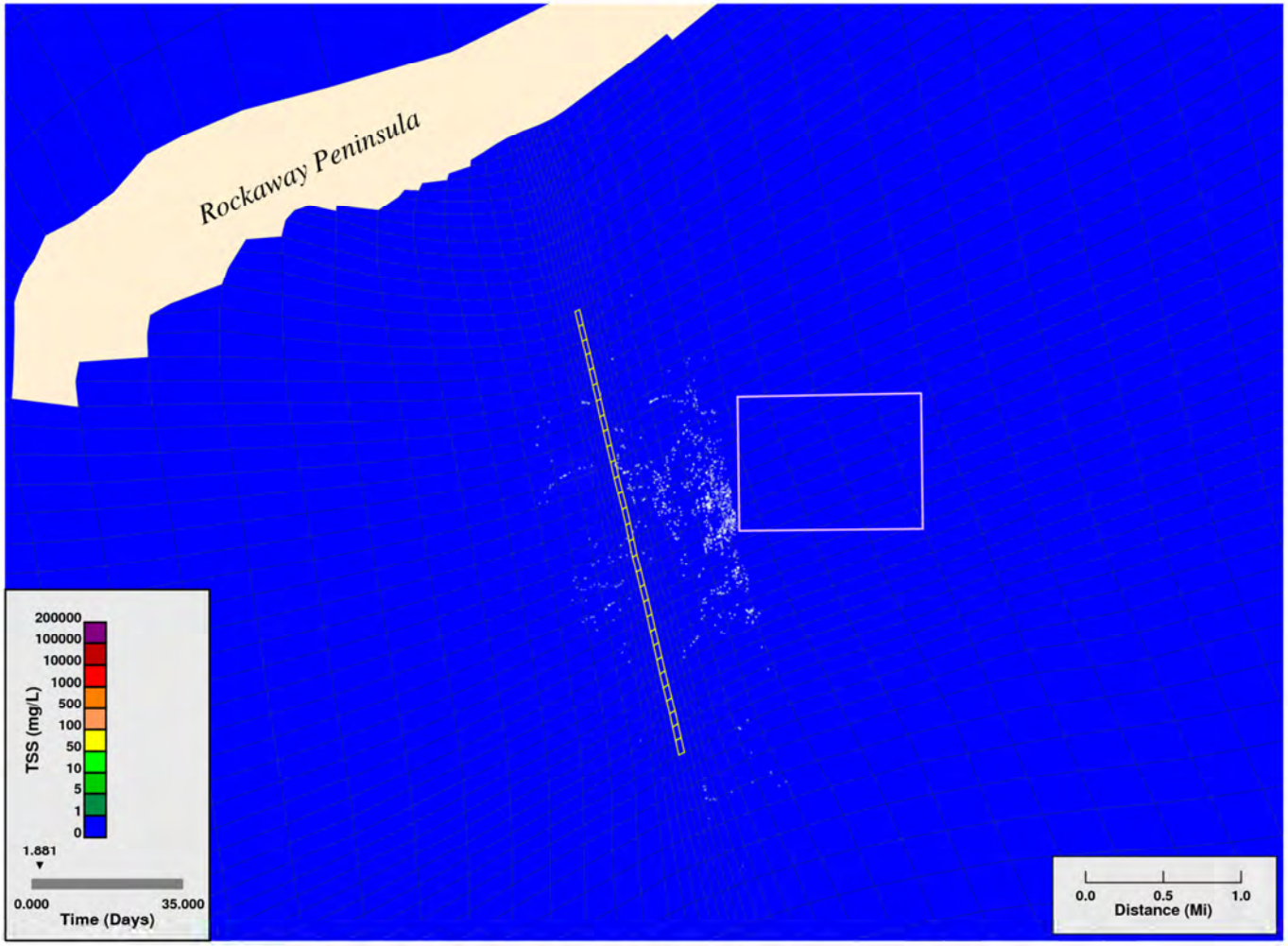

Figure C6. Typical jetting: simulated suspended solids near water column surface, 4 hours after end of trenching, rate = 183 m/hr.

APPENDIX D. SIMULATED SURFACE LAYER SUSPENDED SOLIDS: WORST CASE PLOWING

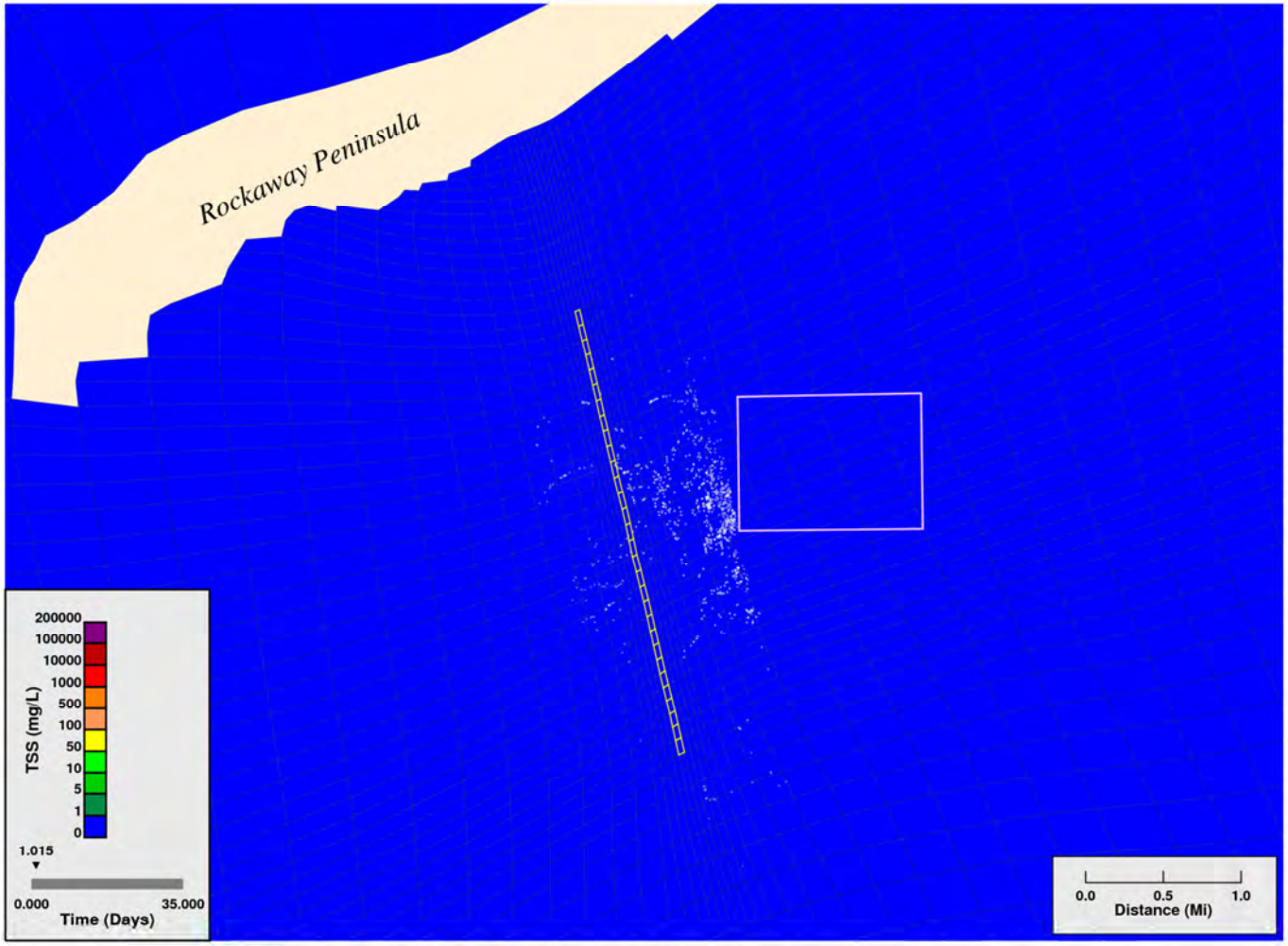

Surface Layer Projected Solids Concentrations from Proposed Dredging, 600 ft/hr

Figure D1. Worst case plowing: simulated suspended solids near water column surface, start of trenching, rate = 183 m/hr.

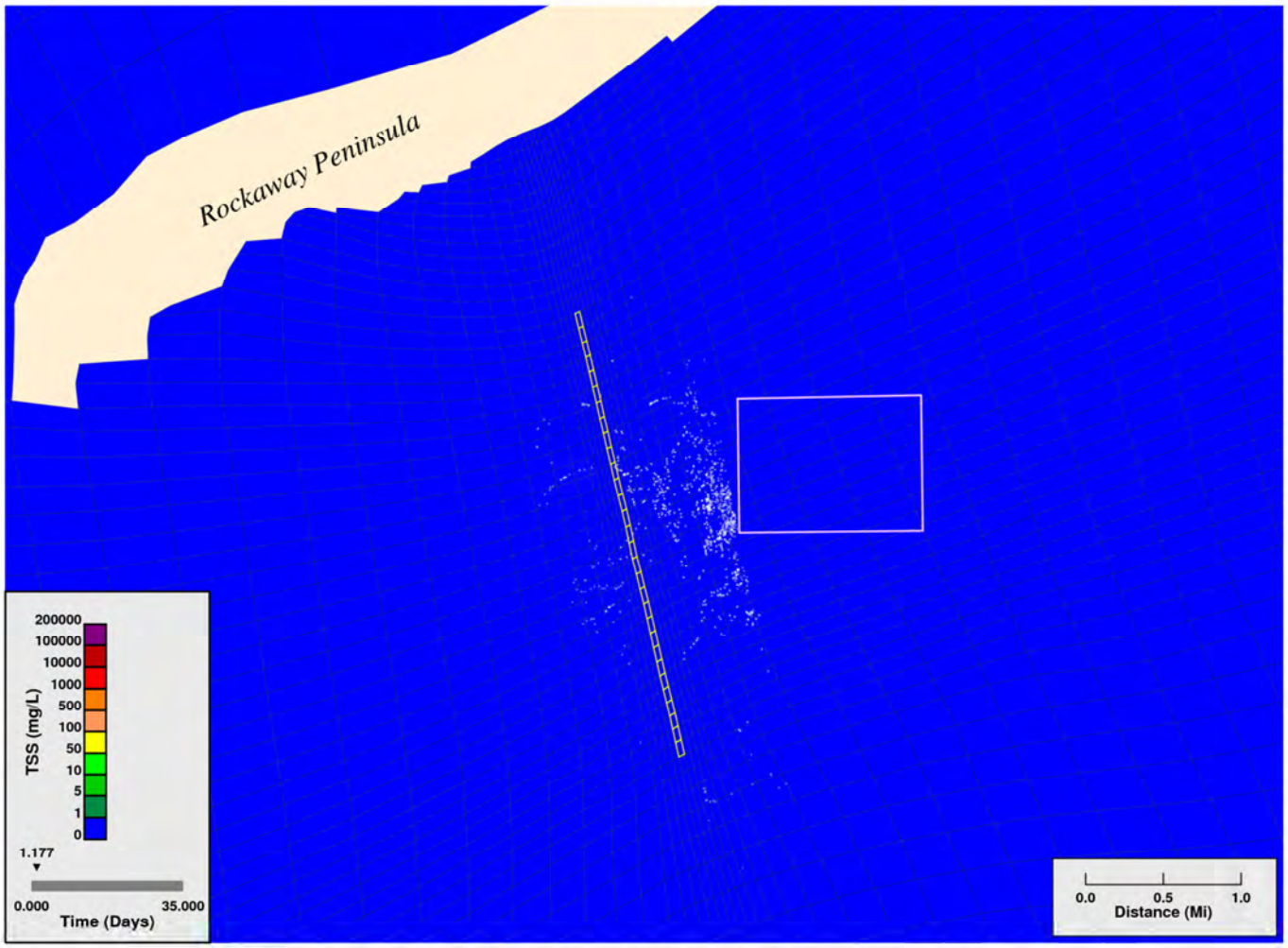

Surface Layer Projected Solids Concentrations from Proposed Dredging, 600 ft/hr

Figure D2. Worst case plowing: simulated suspended solids near water column surface, trenching 25% complete, rate = 183 m/hr.

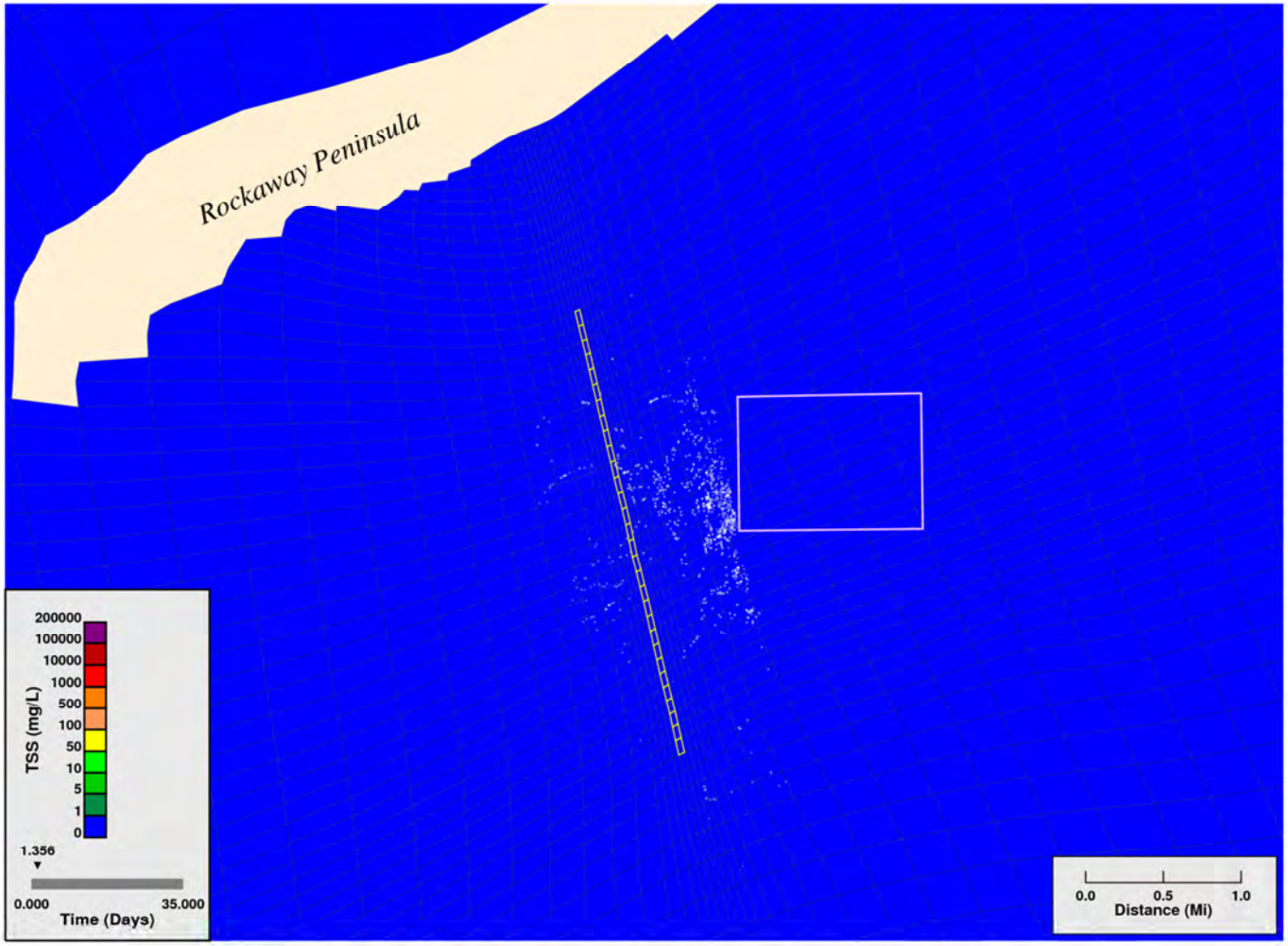

Figure D3. Worst case plowing: simulated suspended solids near water column surface, trenching 50% complete, rate = 183 m/hr.

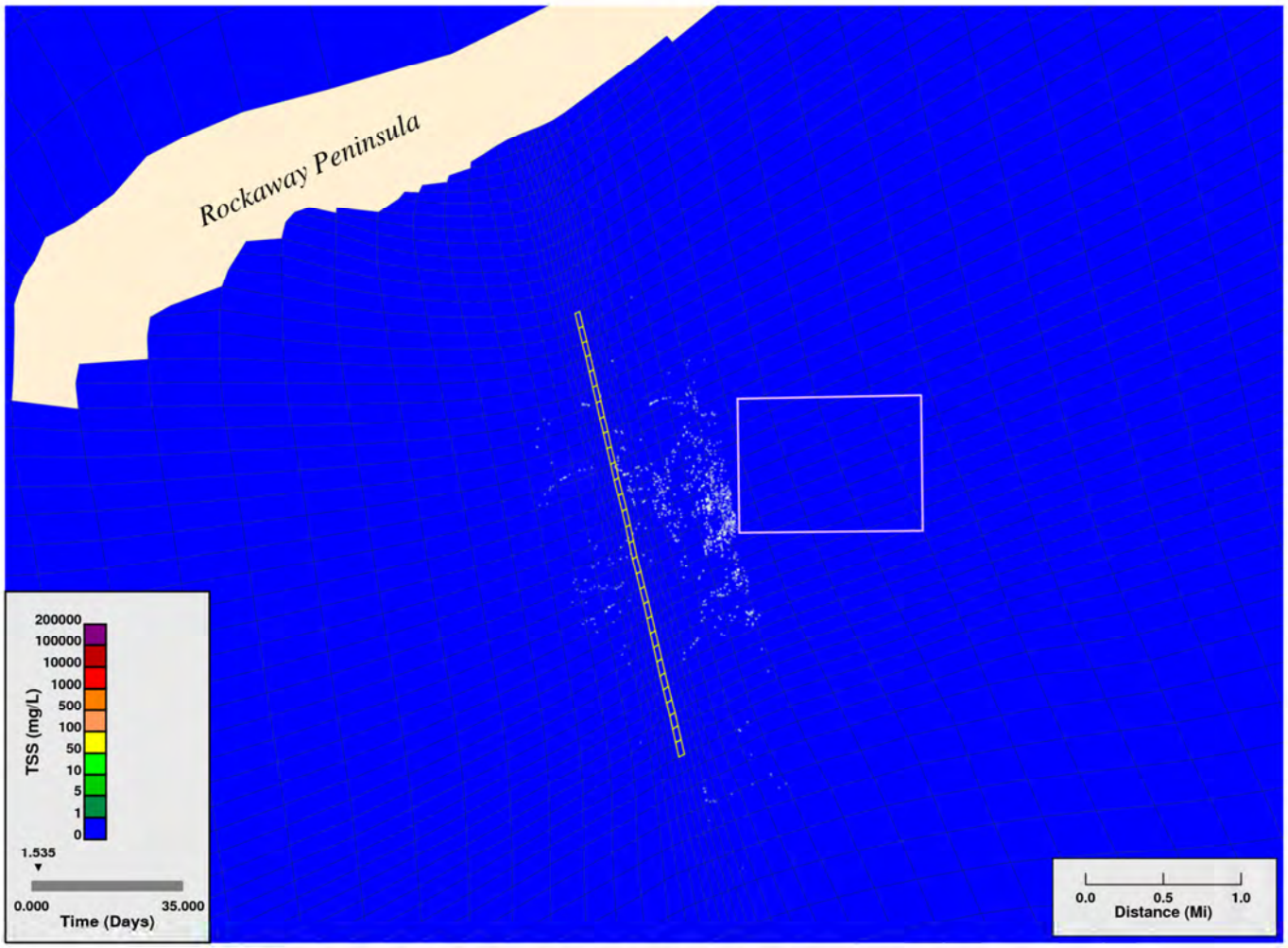

Figure D4. Worst case plowing: simulated suspended solids near water column surface, trenching 75% complete, rate = 183 m/hr.

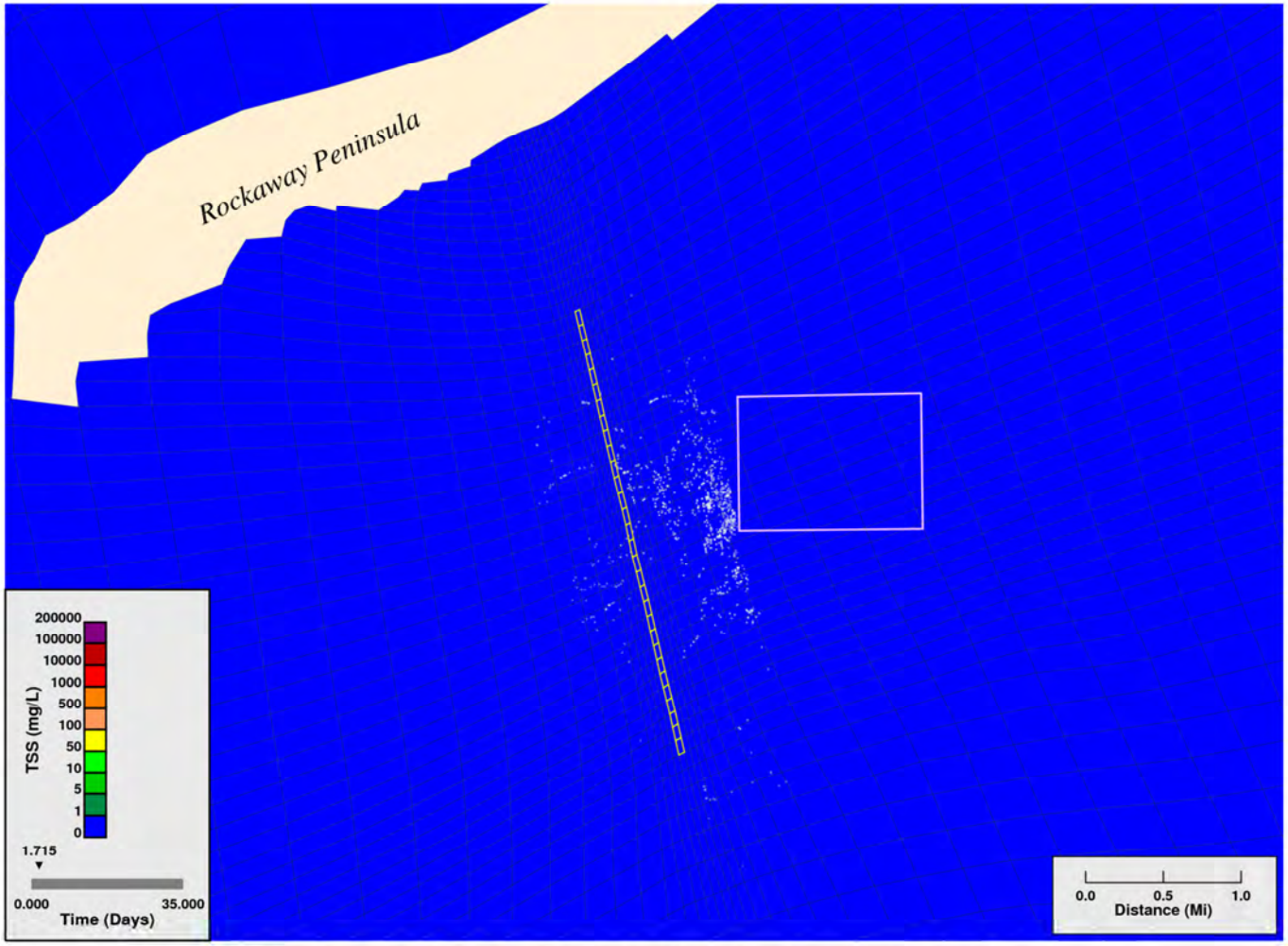

Figure D5. Worst case plowing: simulated suspended solids near water column surface, end of trenching, rate = 183 m/hr.

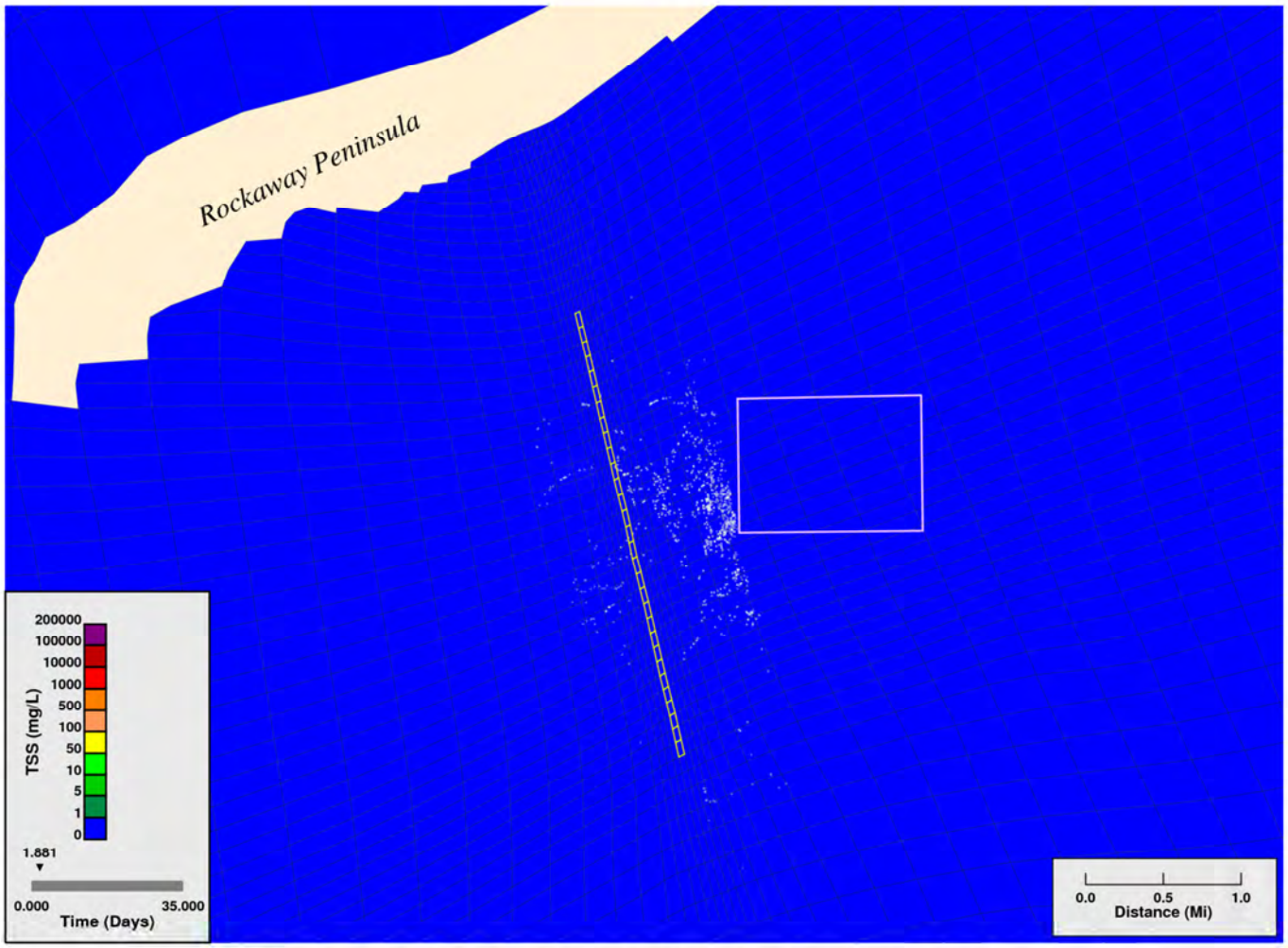

Figure D6. Worst case plowing: simulated suspended solids near water column surface, 4 hours after trenching end, rate = 183 m/hr.

APPENDIX E. SIMULATED SURFACE LAYER SUSPENDED SOLIDS: TYPICAL PLOWING

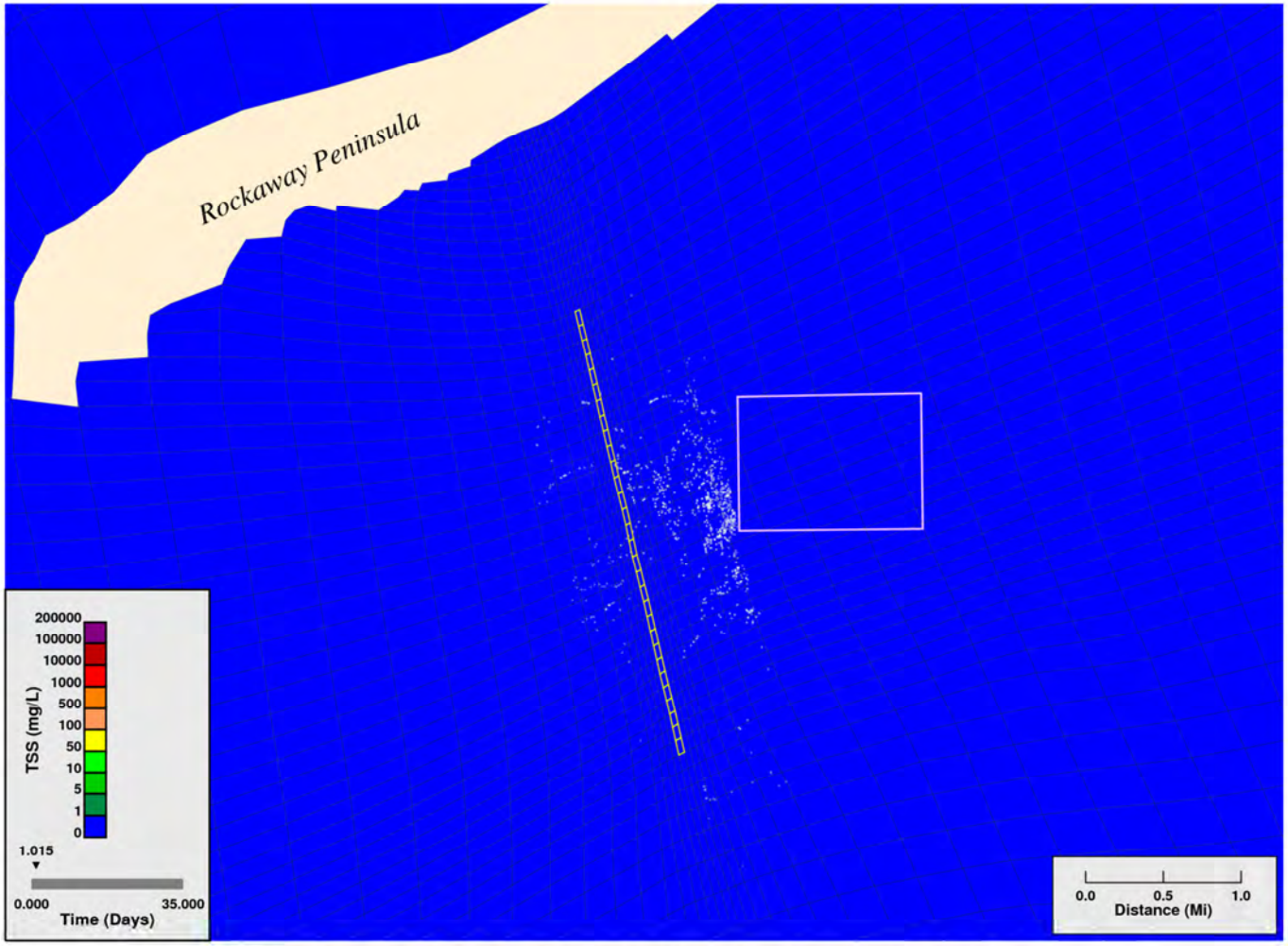

Figure E1. Typical plowing: simulated suspended solids near water column surface, start of trenching, rate = 183 m/hr.

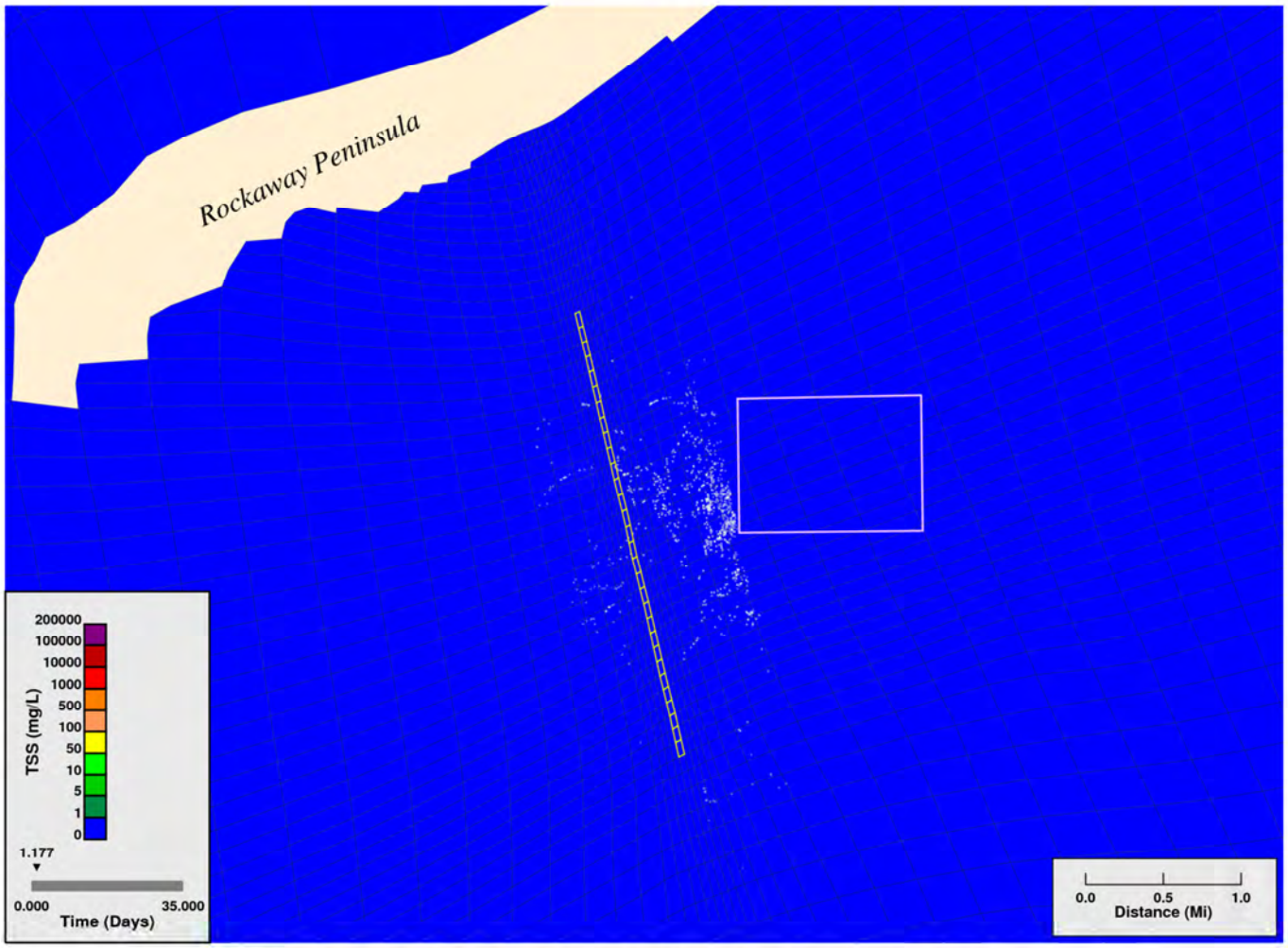

Figure E2. Typical plowing: simulated suspended solids near water column surface, trenching 25% complete, rate = 183 m/hr.

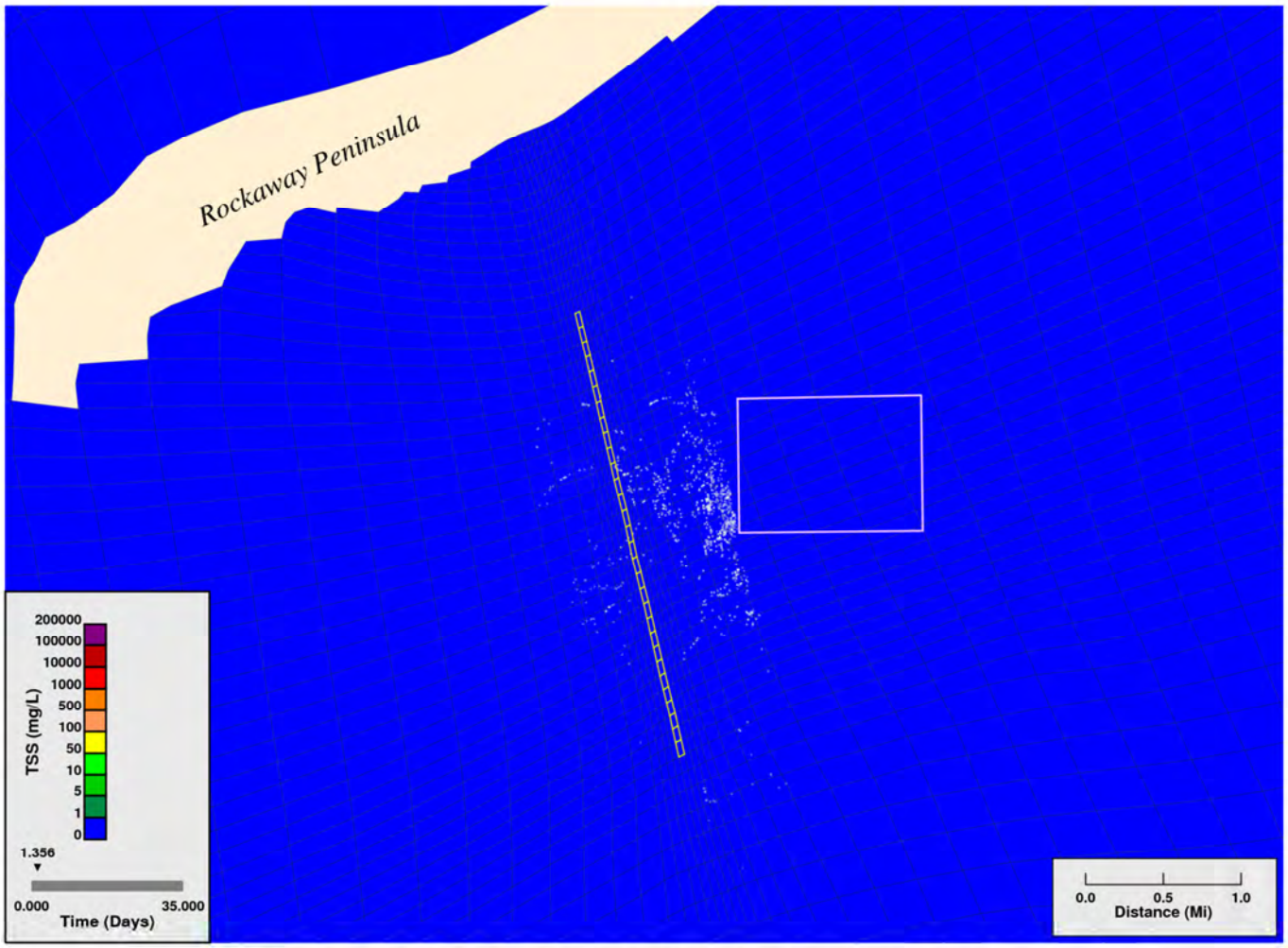

Figure E3. Typical plowing: simulated suspended solids near water column surface, trenching 50% complete, rate = 183 m/hr.

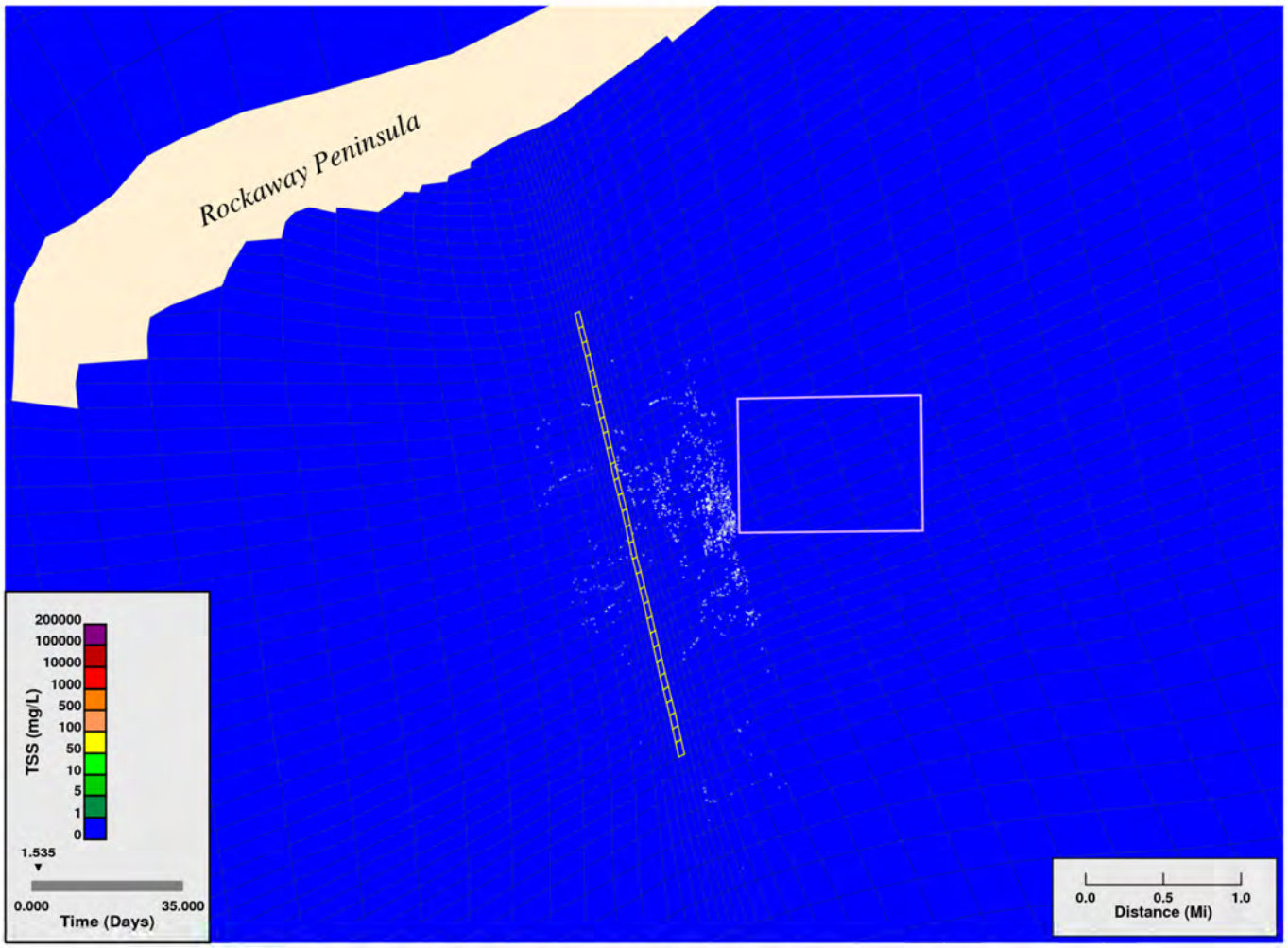

Figure E4. Typical plowing: simulated suspended solids near water column surface, trenching 75% complete, rate = 183 m/hr.

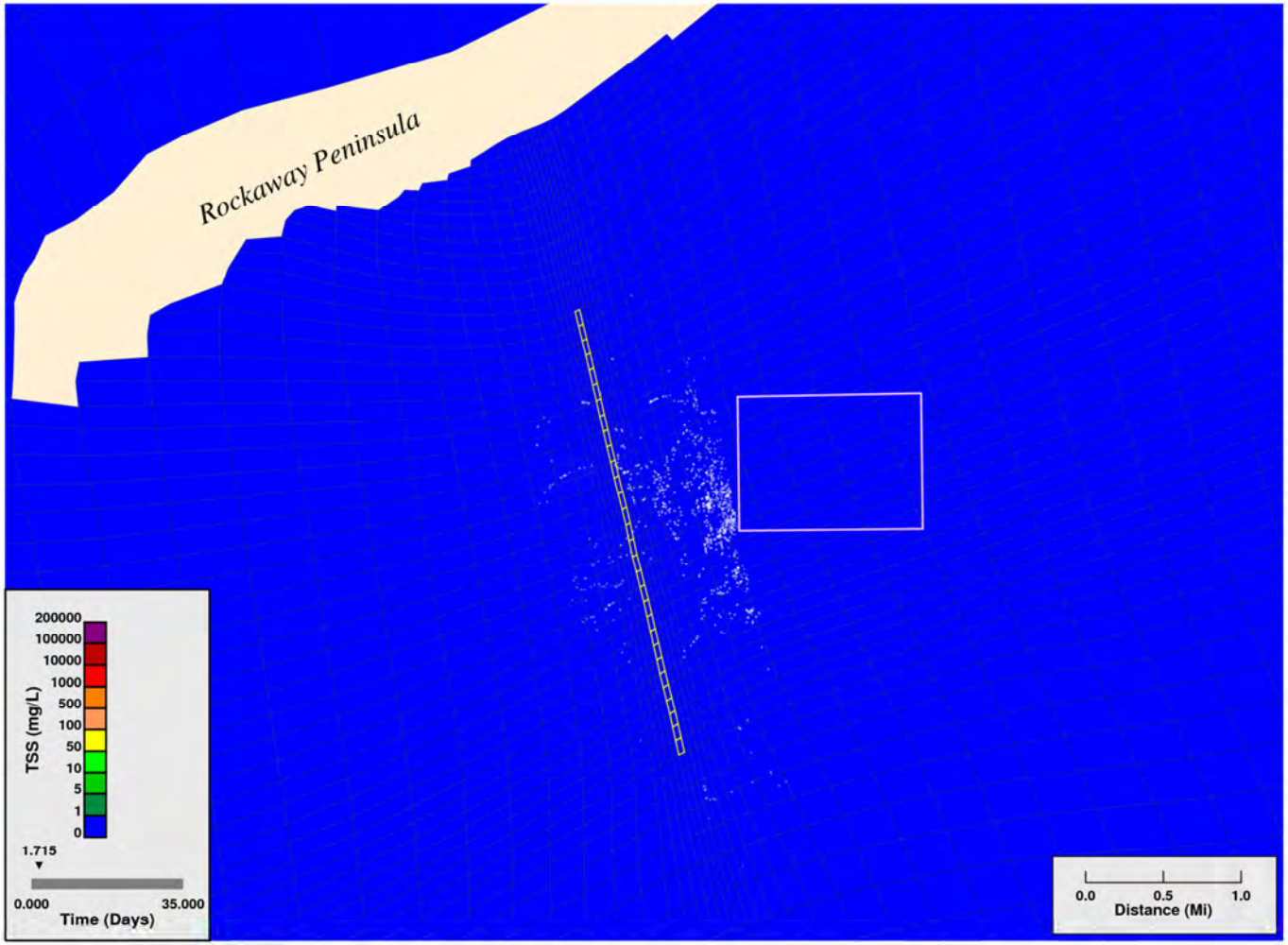

Figure E5. Typical plowing: simulated suspended solids near water column surface, end of trenching, rate = 183 m/hr.

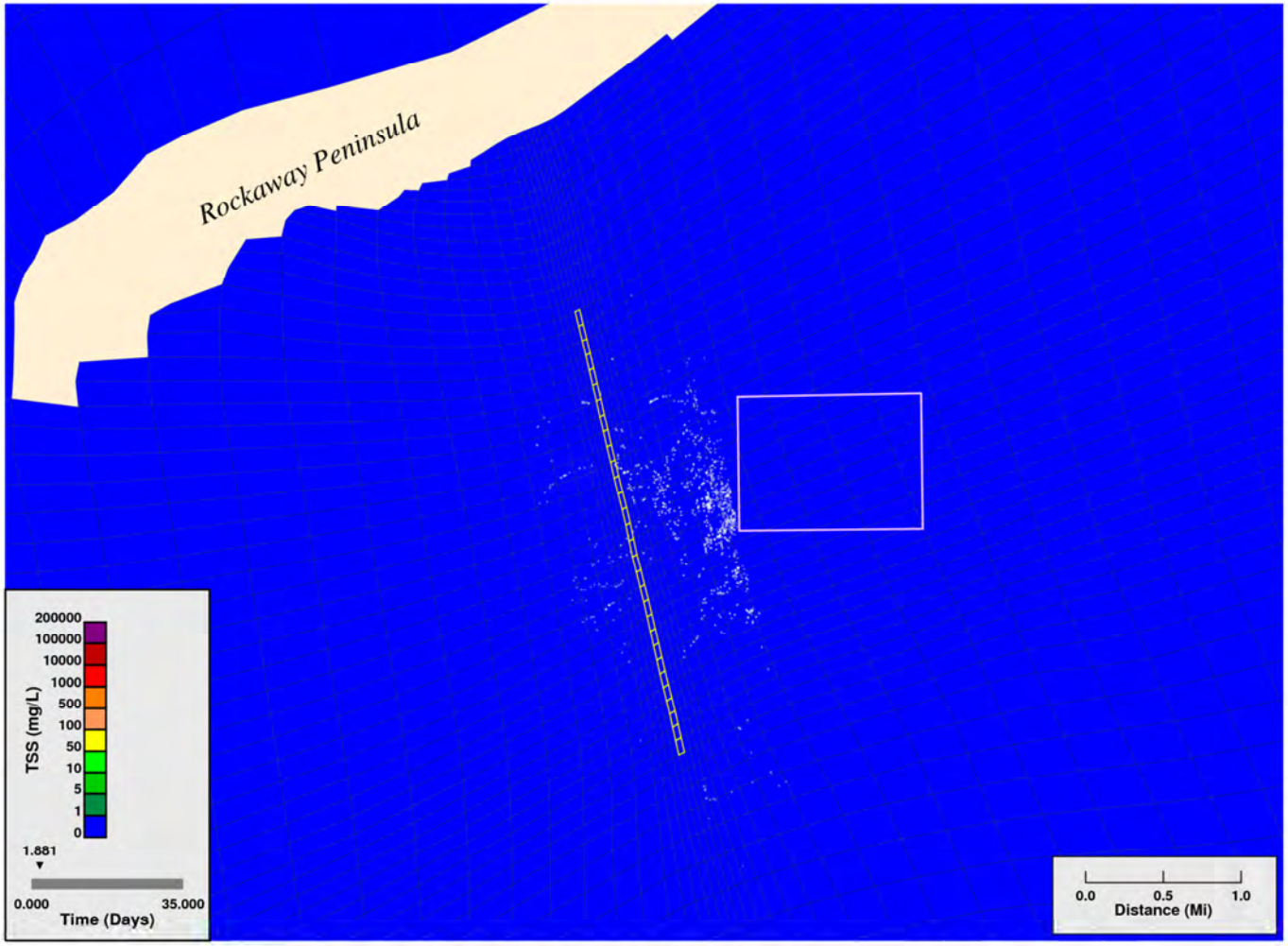

Figure E6. Typical plowing: simulated suspended solids near water column surface, 4 hours after end of trenching, rate = 183 m/hr.

APPENDIX F. SIMULATED SURFACE LAYER SUSPENDED SOLIDS: TRENCH MECHANICAL DREDGING

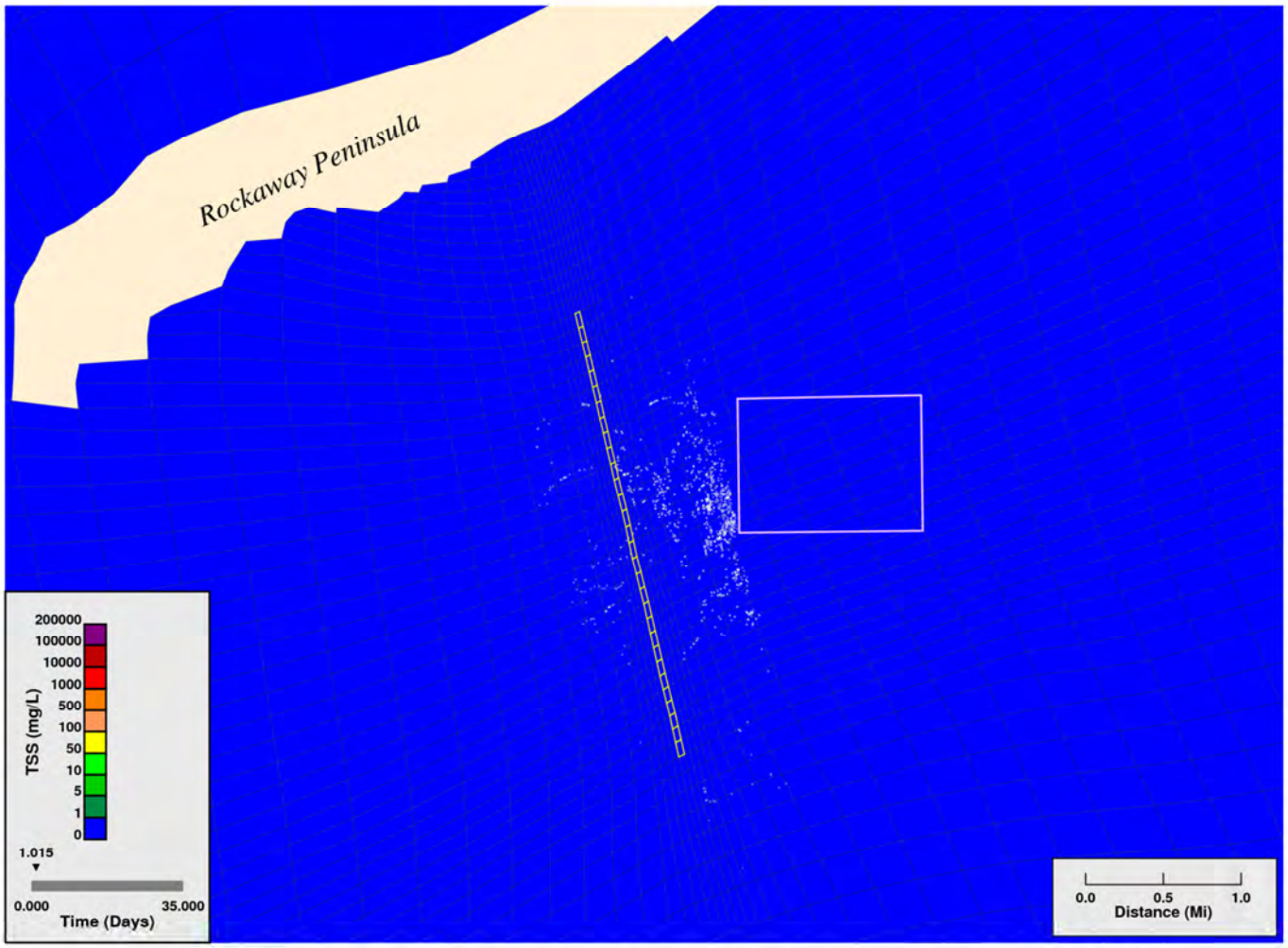

Surface Layer Projected Solids Concentrations from Proposed Dredging, 13.8 ft/hr

Figure F1. Mechanical trenching: simulated suspended solids near water column surface, start of trenching, rate = 4.2 m/hr.

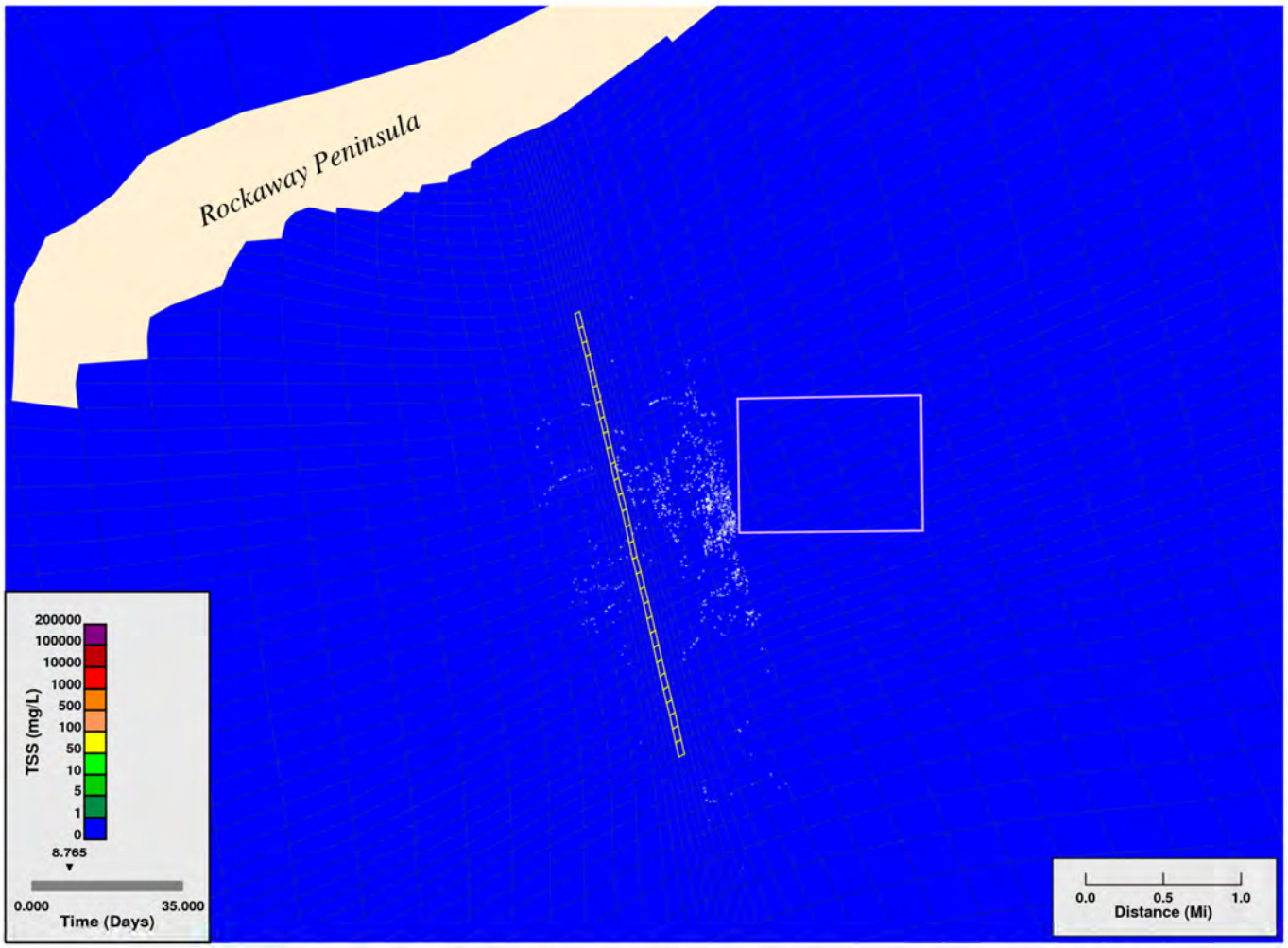

Surface Layer Projected Solids Concentrations from Proposed Dredging, 13.8 ft/hr

Figure F2. Mechanical trenching: simulated suspended solids near water column surface, trenching 25% complete, rate = 4.2 m/hr.

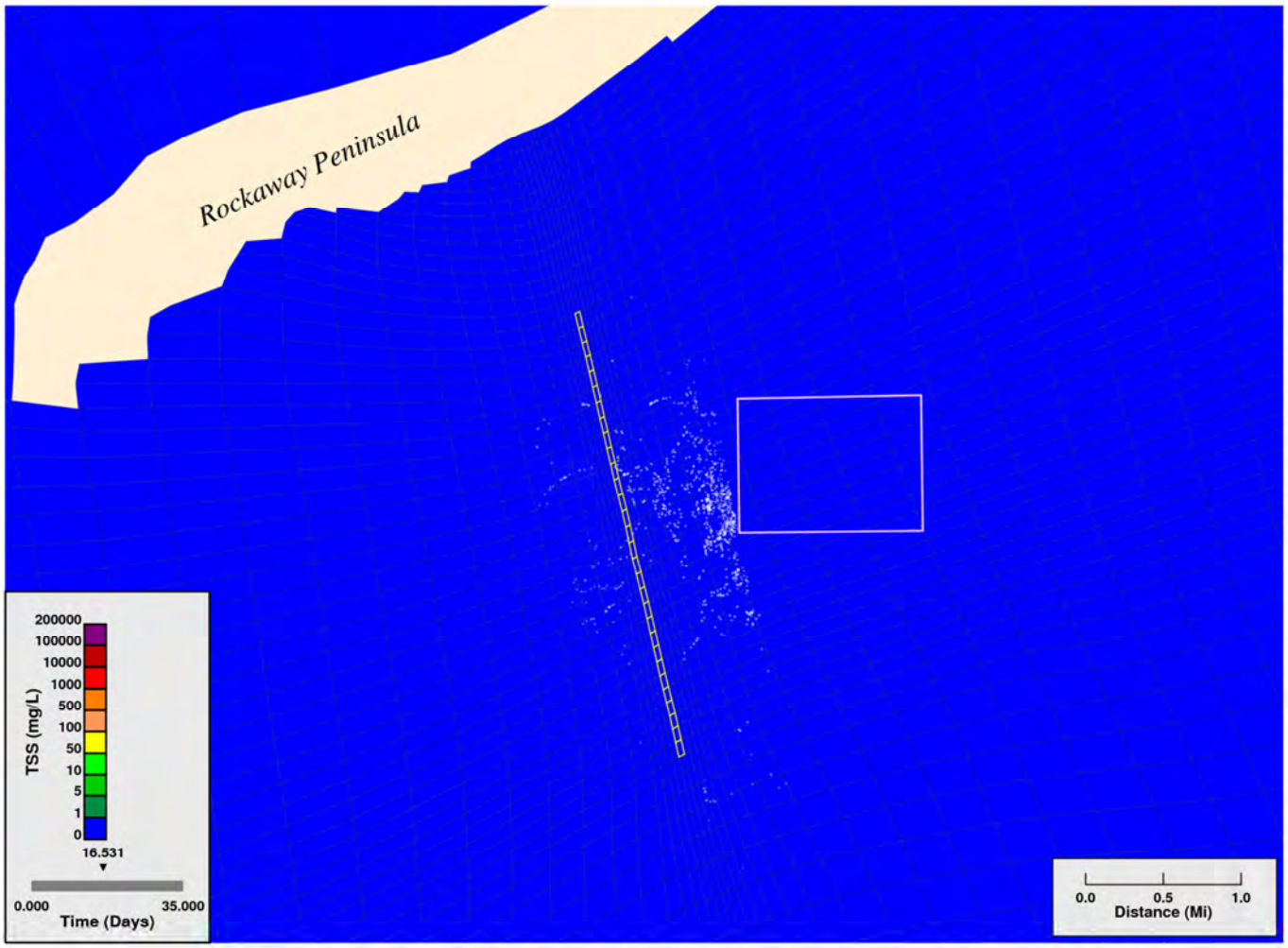

Surface Layer Projected Solids Concentrations from Proposed Dredging, 13.8 ft/hr

Figure F3. Mechanical trenching: simulated suspended solids near water column surface, trenching 50% complete, rate = 4.2 m/hr.

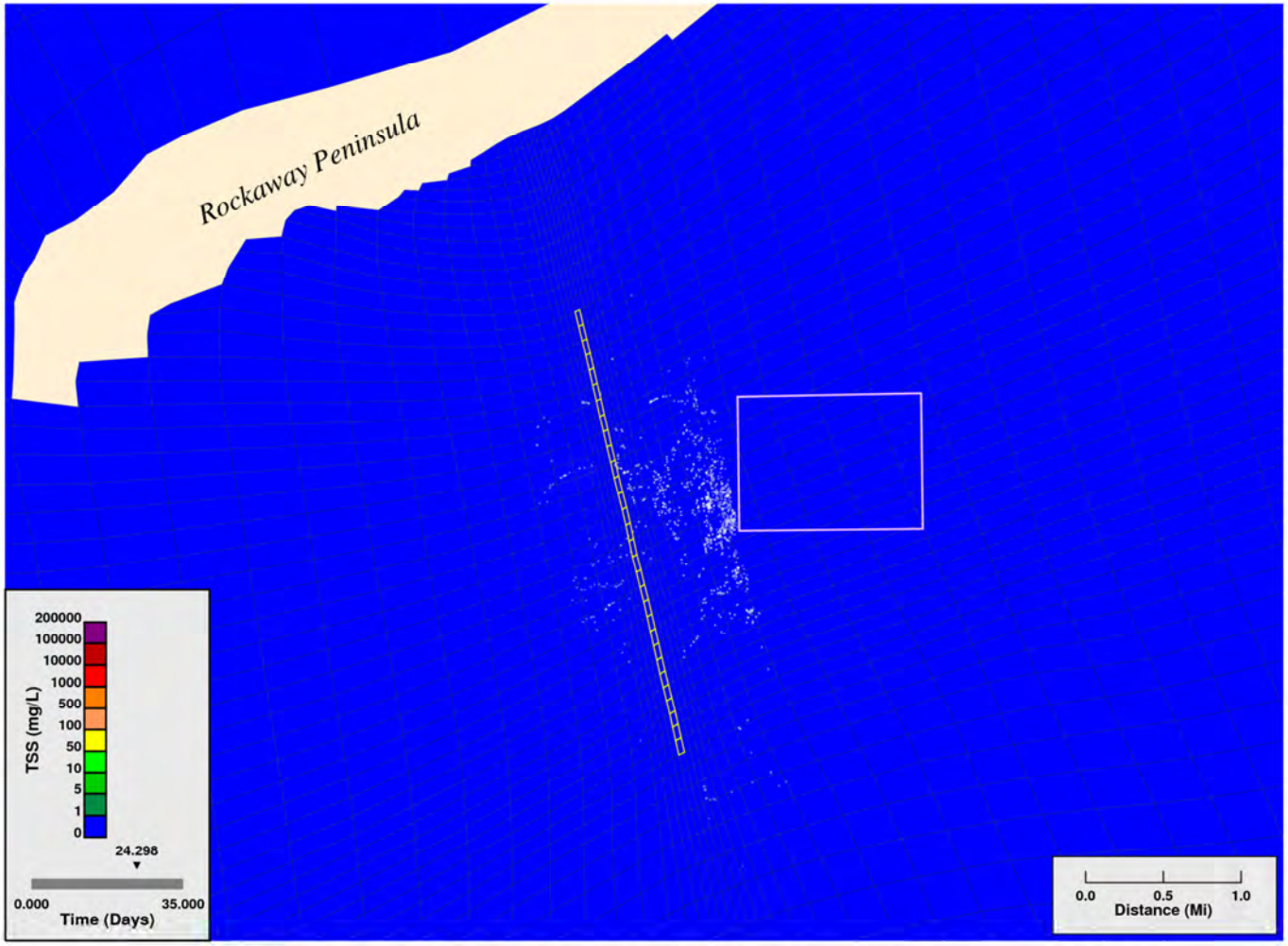

Figure F4. Mechanical trenching: simulated suspended solids near water column surface, trenching 75% complete, rate = 4.2 m/hr.

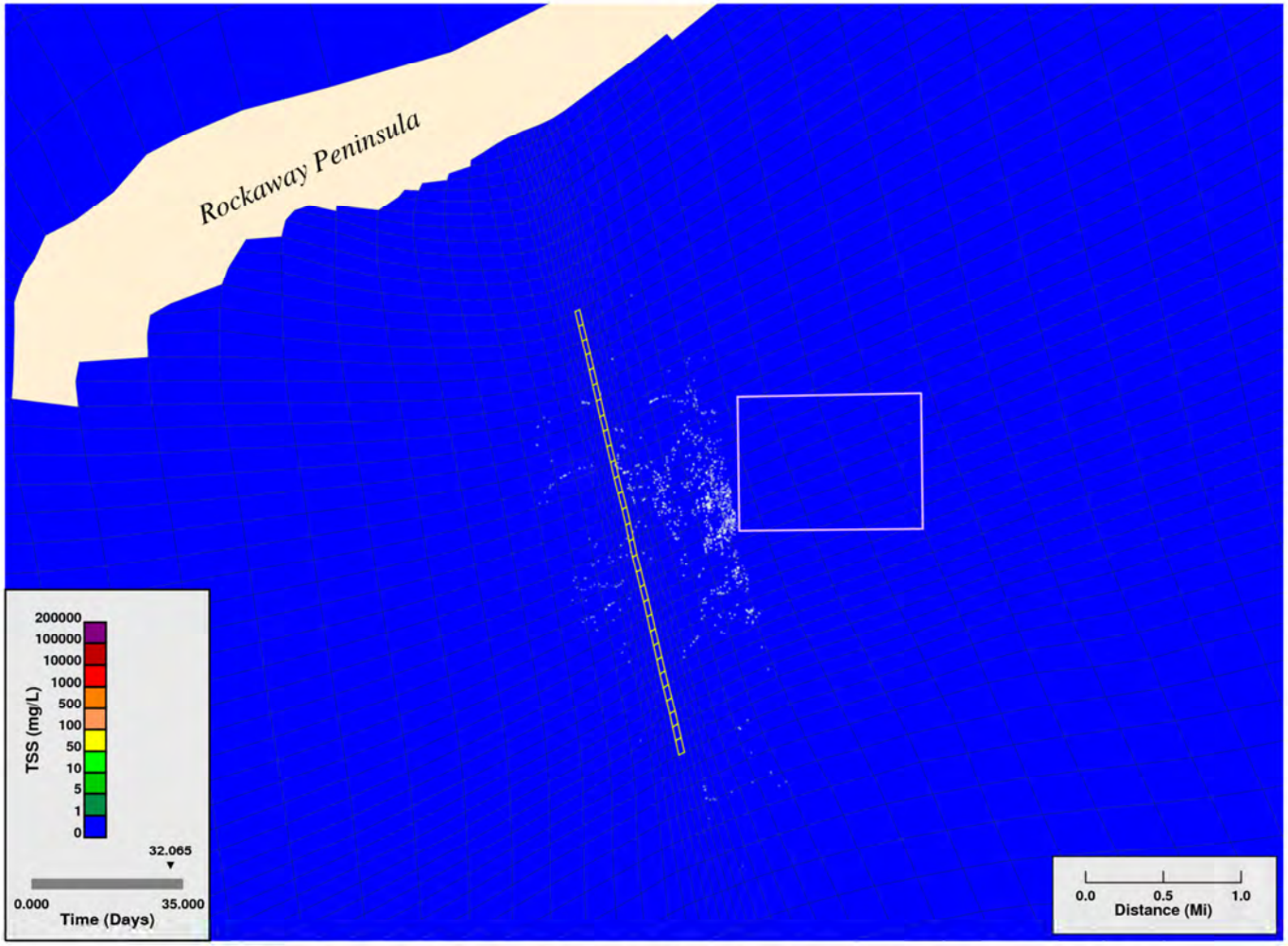

Figure F5. Mechanical trenching: simulated suspended solids near water column surface, end of trenching, rate = 4.2 m/hr.

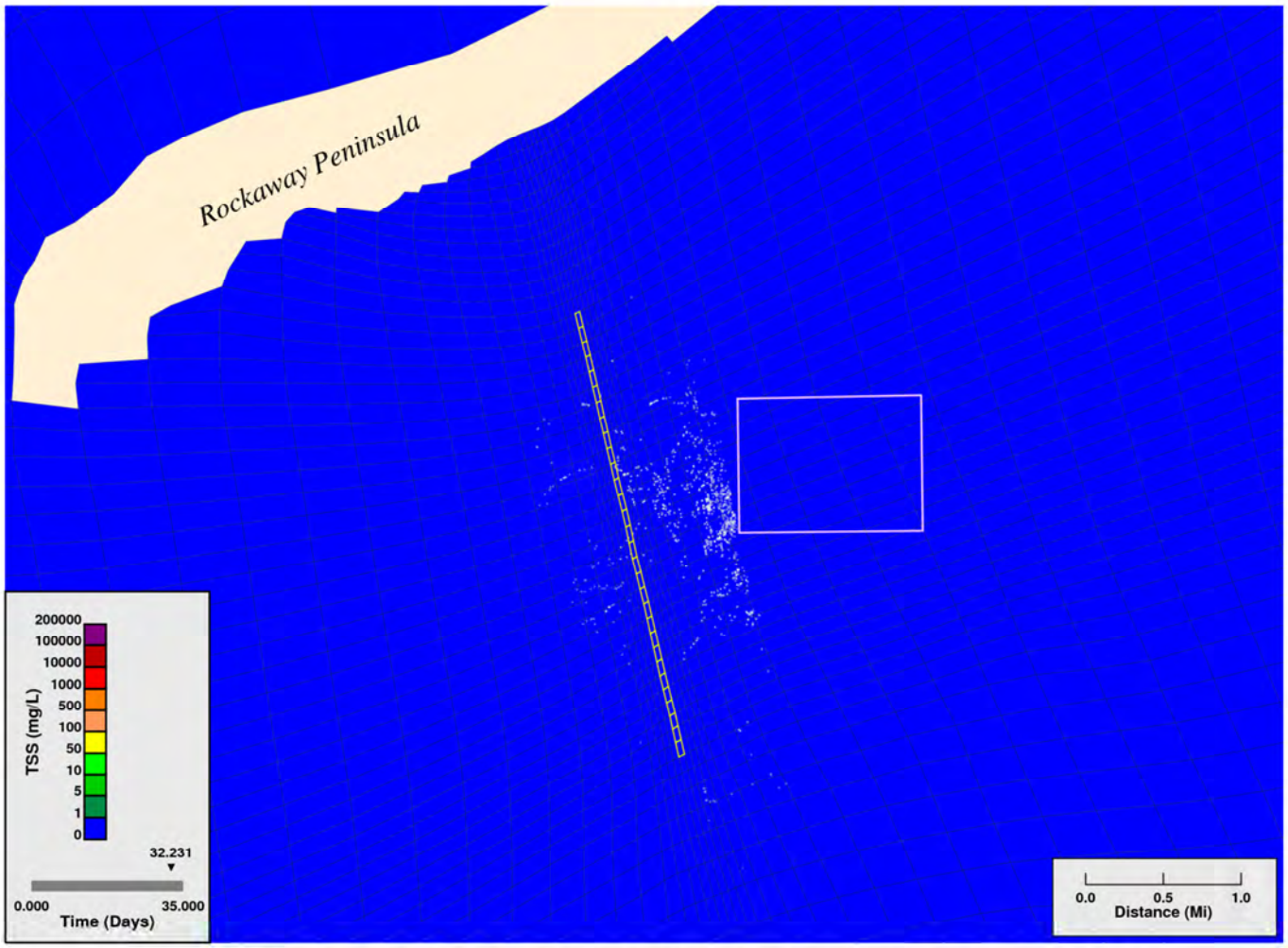

Surface Layer Projected Solids Concentrations from Proposed Dredging, 13.8 ft/hr

Figure F6. Mechanical trenching: simulated suspended solids near water column surface, 4 hours after trenching end, rate = 4.2 m/hr.

APPENDIX G. SIMULATED SURFACE LAYER SUSPENDED SOLIDS: HOT TAP HAND JETTING

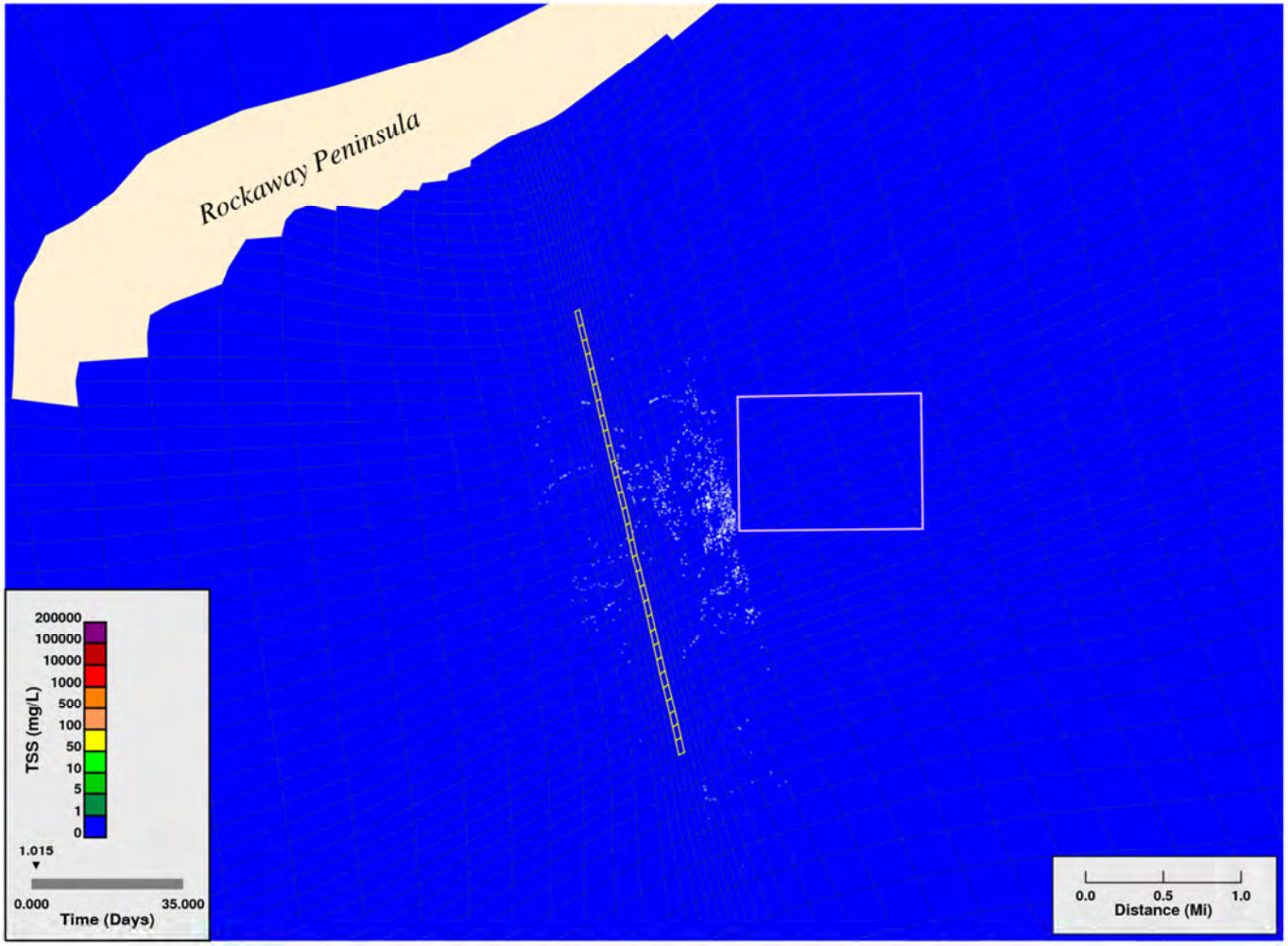

Figure G1. Hand jetting: simulated suspended solids near water column surface, start of jetting (first 8-hour pulse).

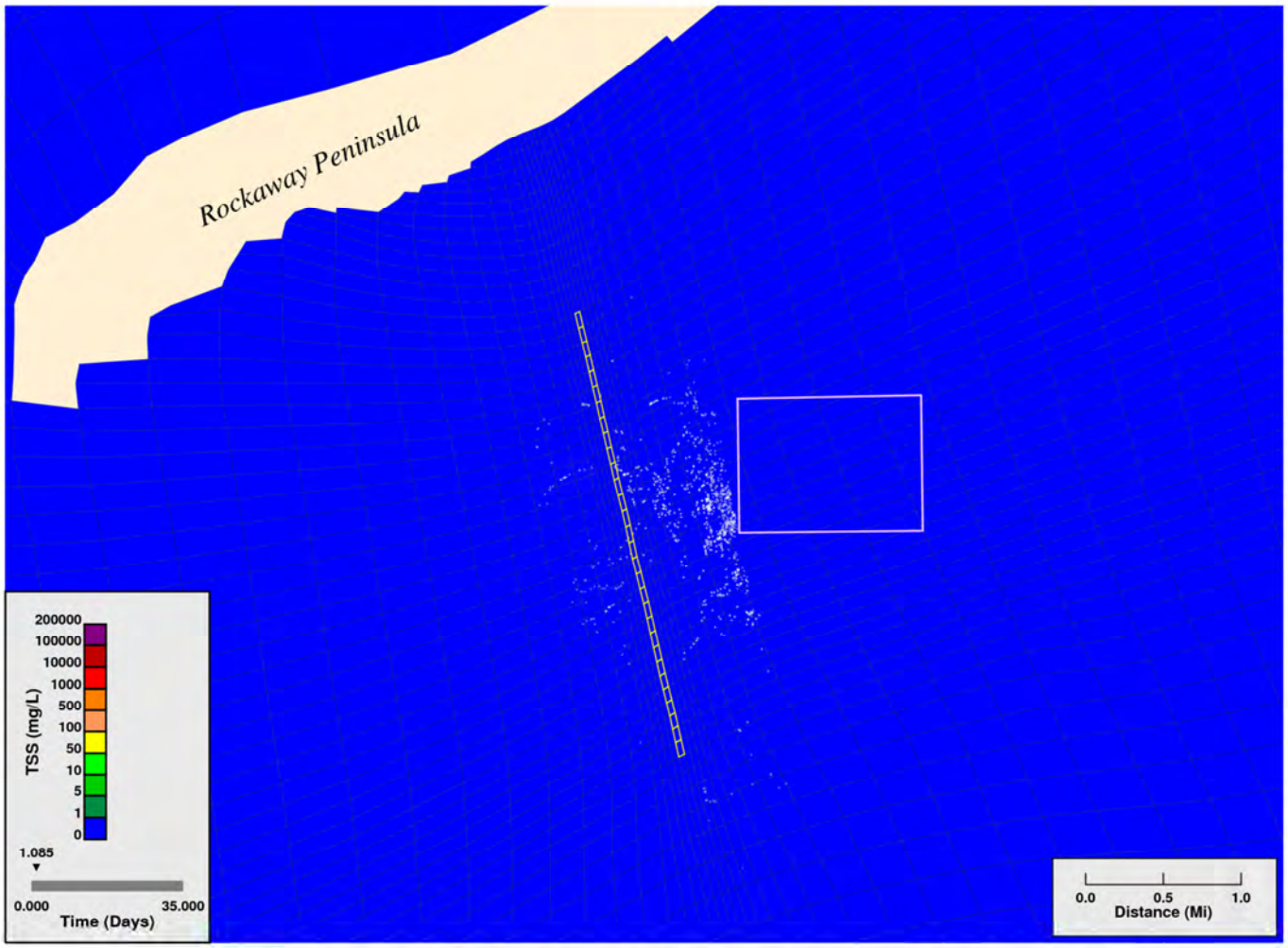

Figure G2. Hand jetting: simulated suspended solids near water column surface, jetting 25% complete (first 8-hour pulse).

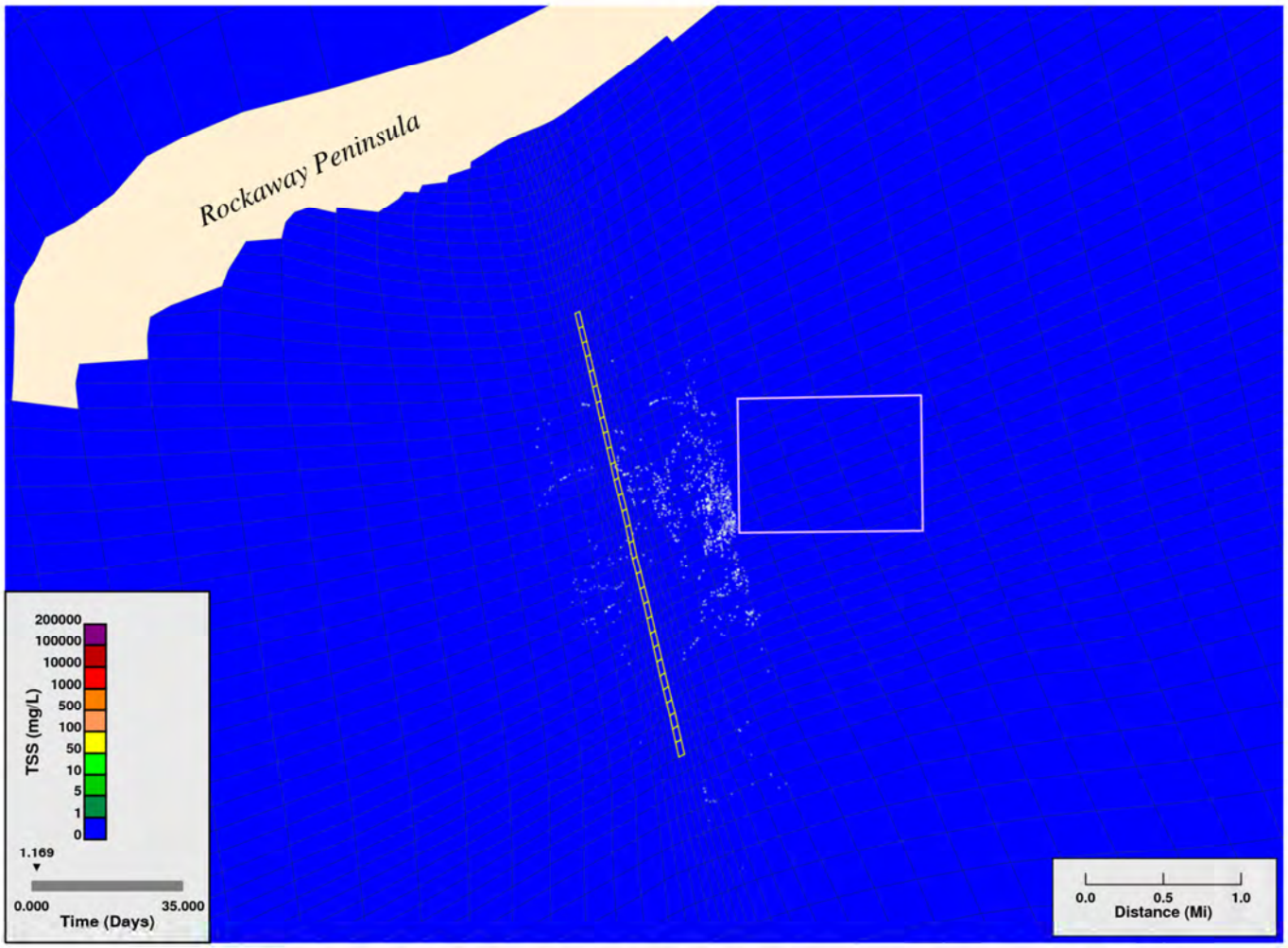

Figure G3. Hand jetting: simulated suspended solids near water column surface, jetting 50% complete (first 8-hour pulse).

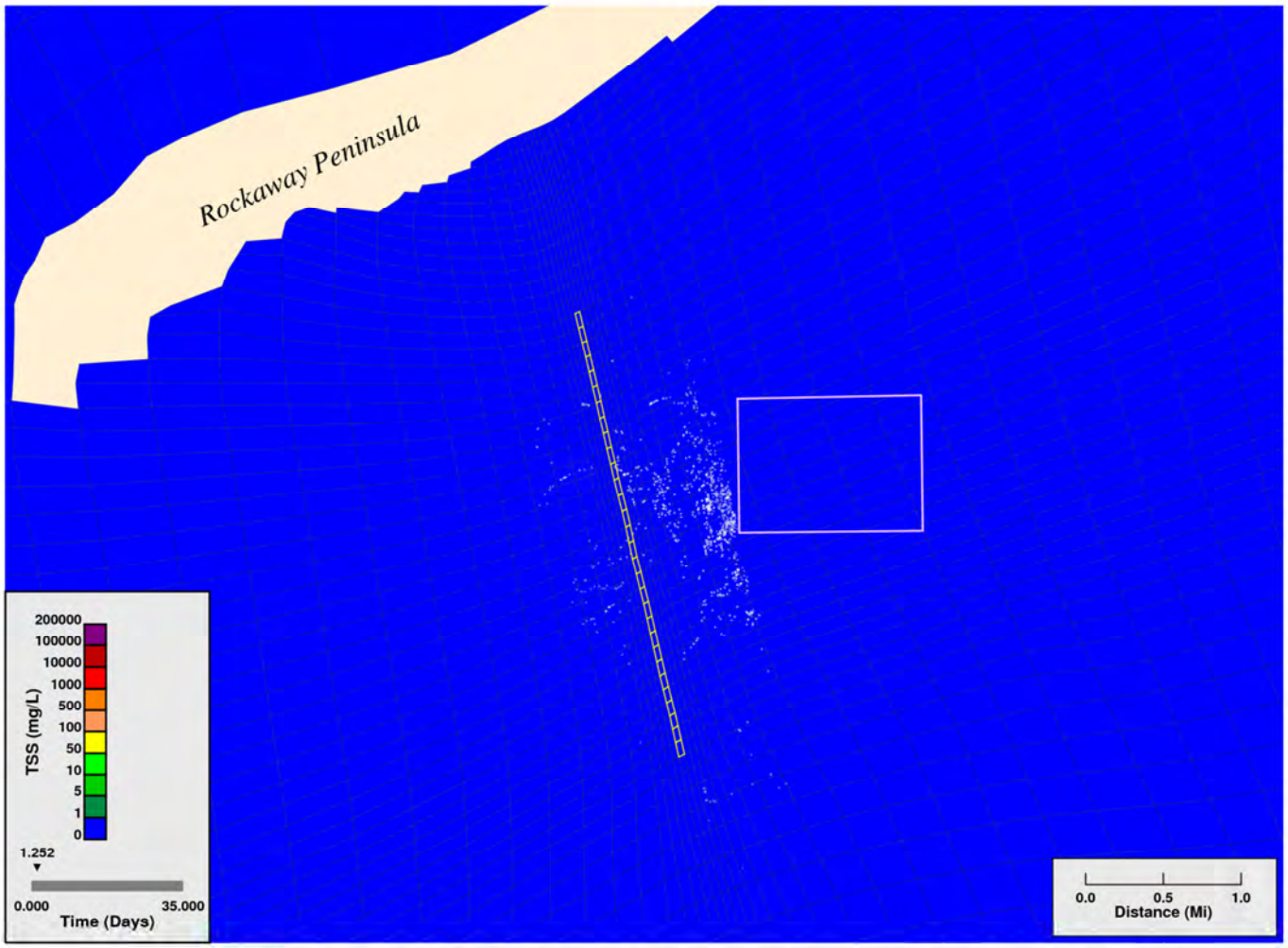

Figure G4. Hand jetting: simulated suspended solids near water column surface, jetting 75% complete (first 8-hour pulse).

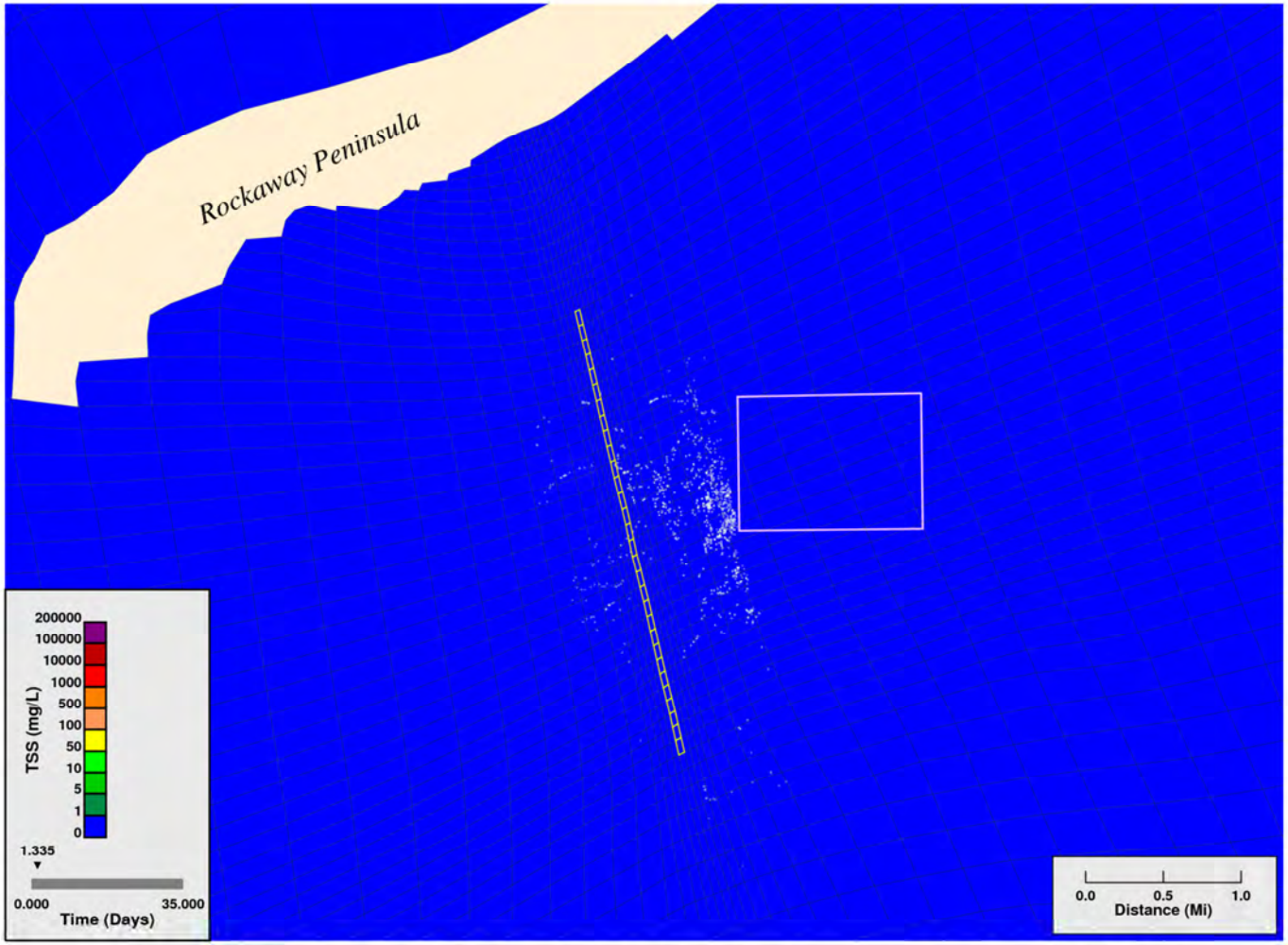

Figure G5. Hand jetting: simulated suspended solids near water column surface, end of jetting (first 8-hour pulse).

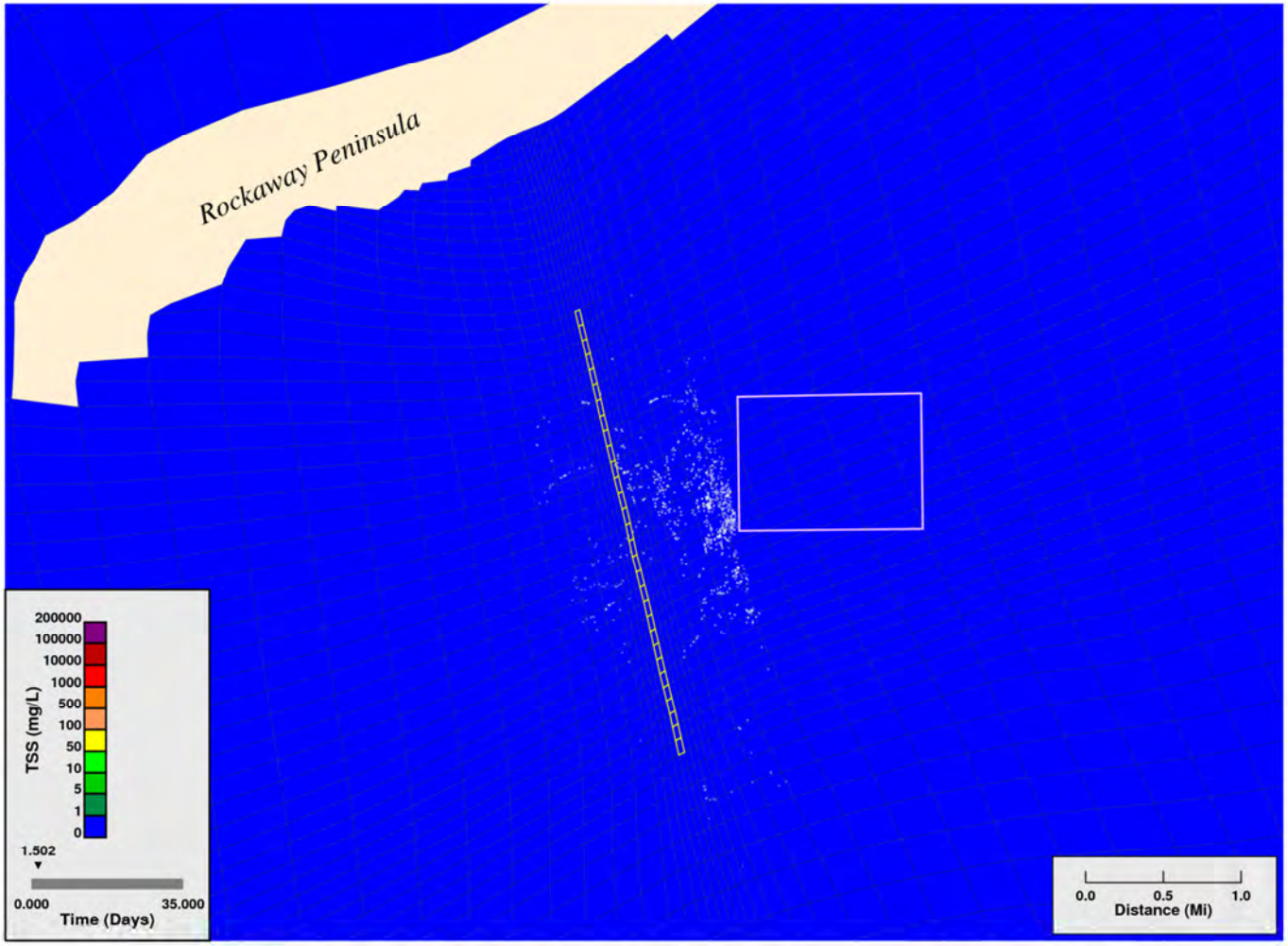

Figure G6. Hand jetting: simulated suspended solids near water column surface, 4 hours after end of jetting (first 8-hour pulse).

APPENDIX H. SIMULATED SURFACE LAYER SUSPENDED SOLIDS: HDD PIT MECHANICAL DREDGING

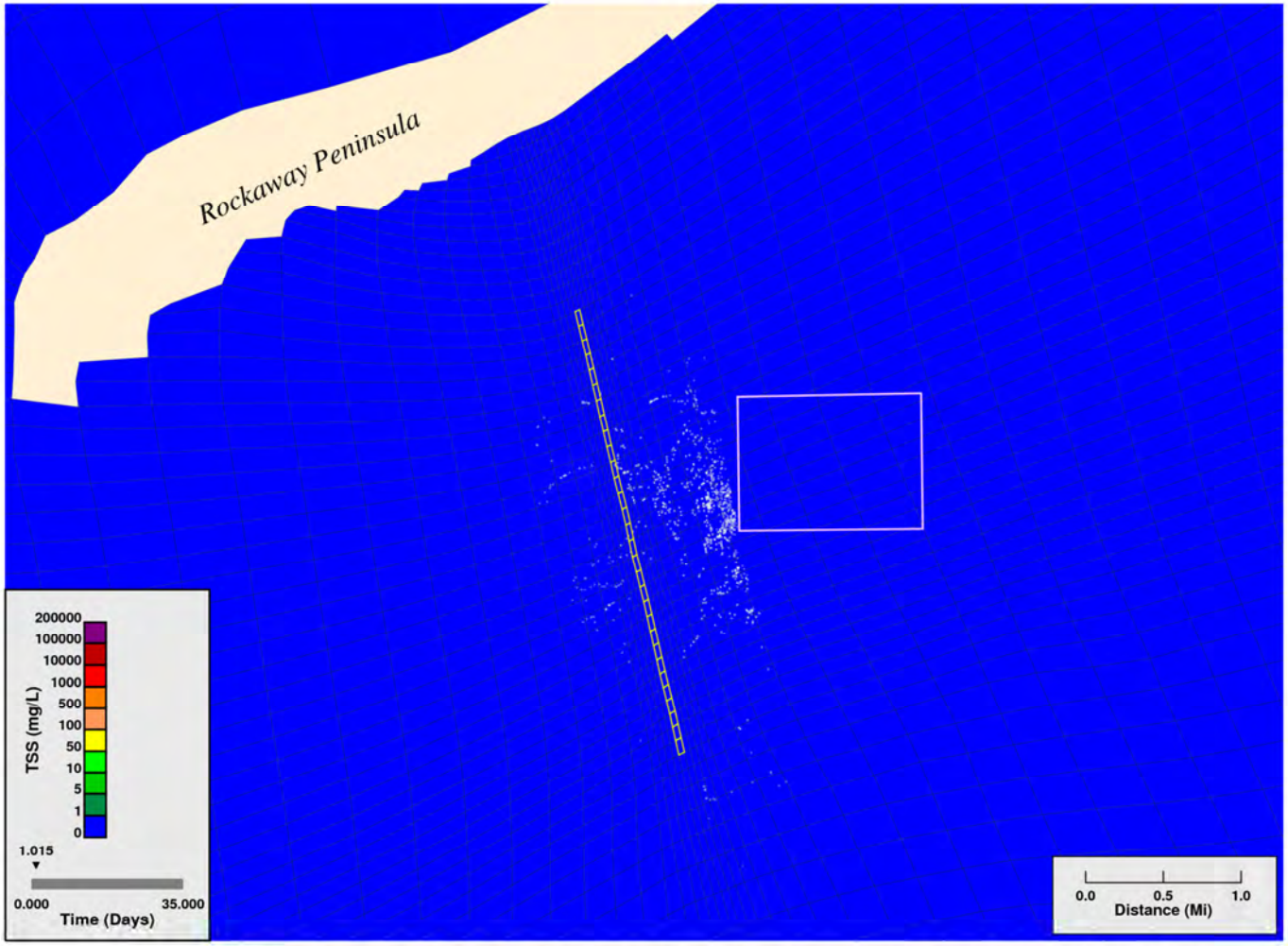

Figure H1. Pit dredging: simulated suspended solids near water column surface, start of dredging.

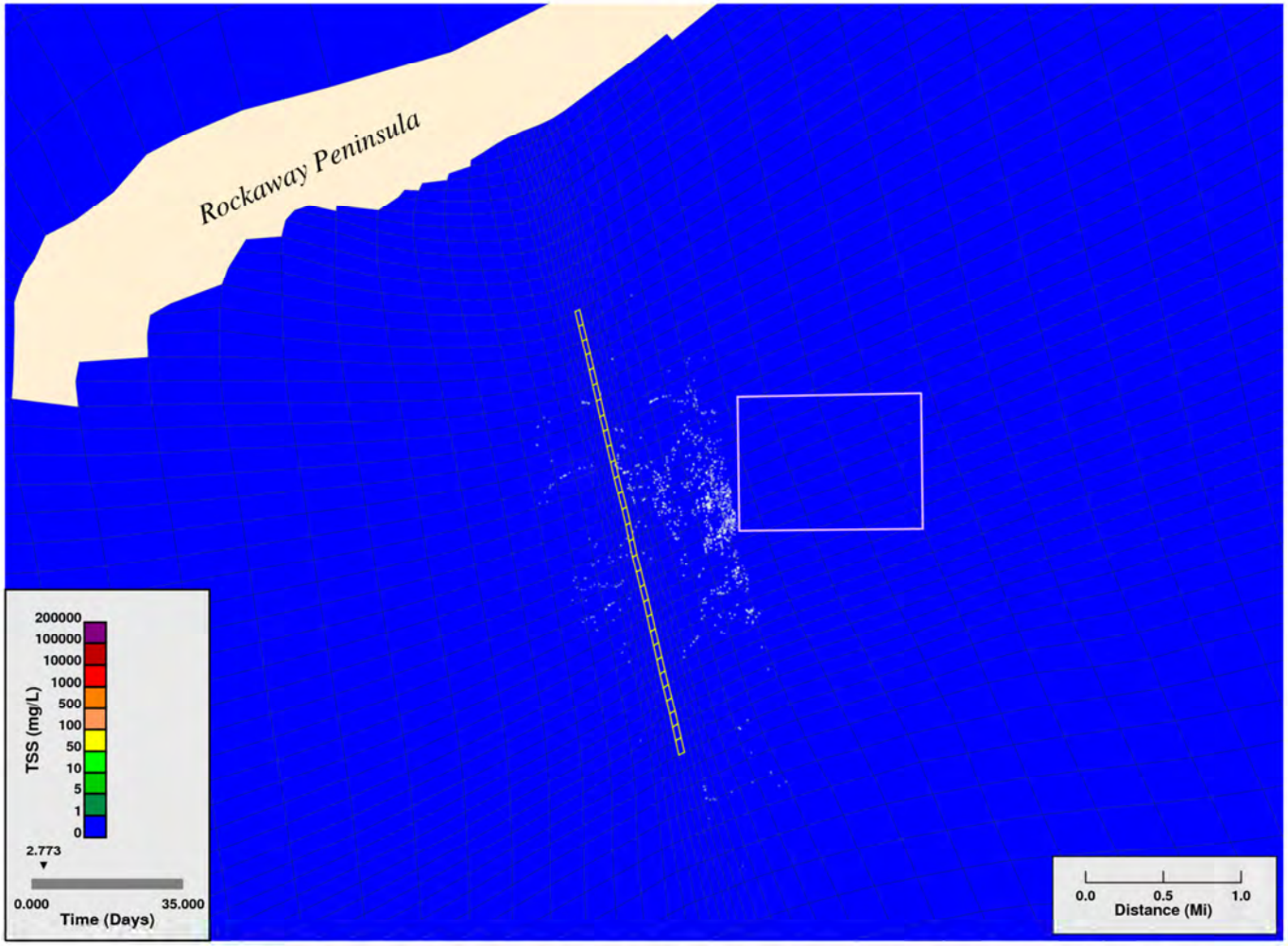

Figure H2. Pit dredging: simulated suspended solids near water column surface, dredging 25% complete.

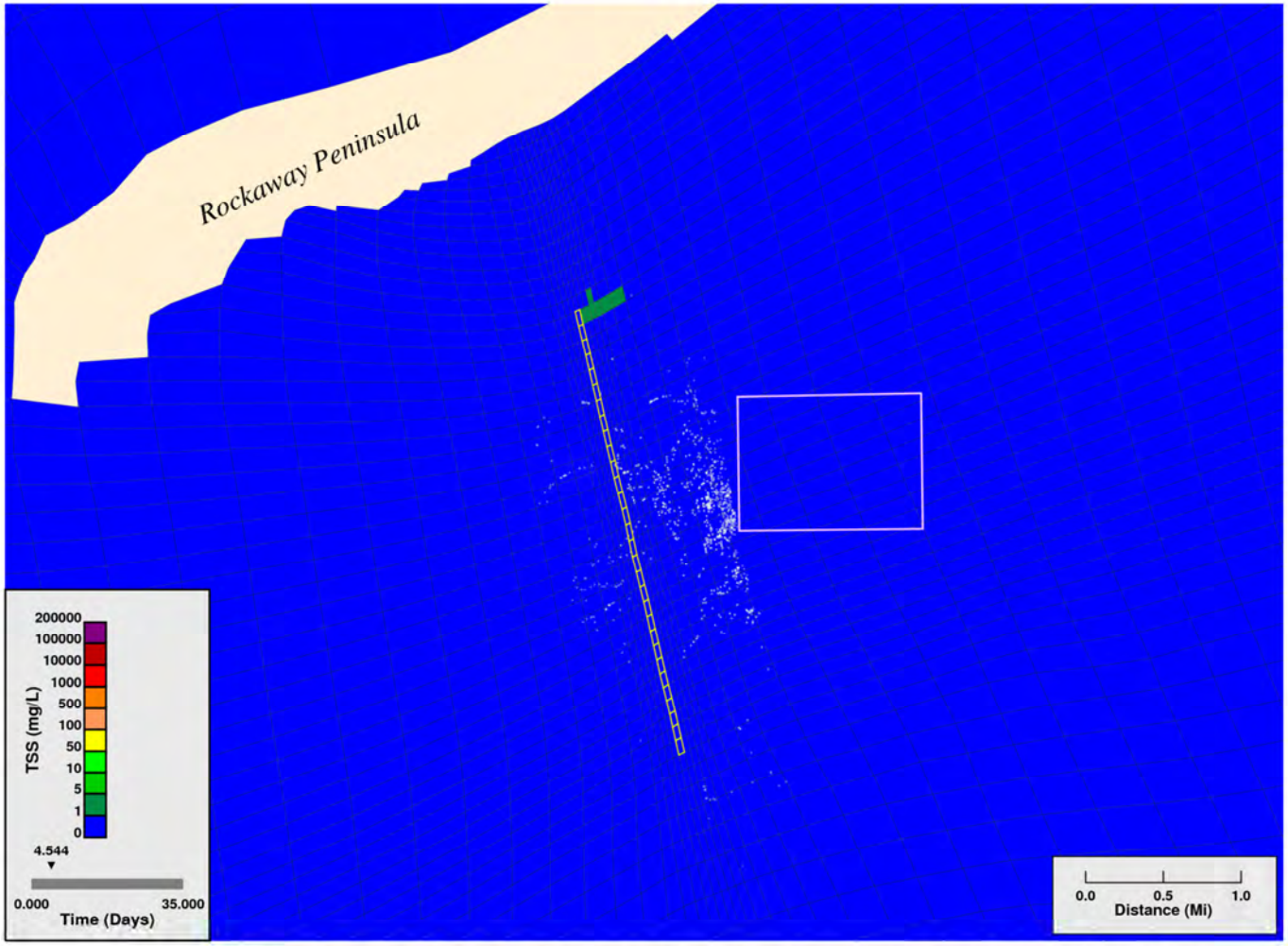

Figure H3. Pit dredging: simulated suspended solids near water column surface, dredging 50% complete.

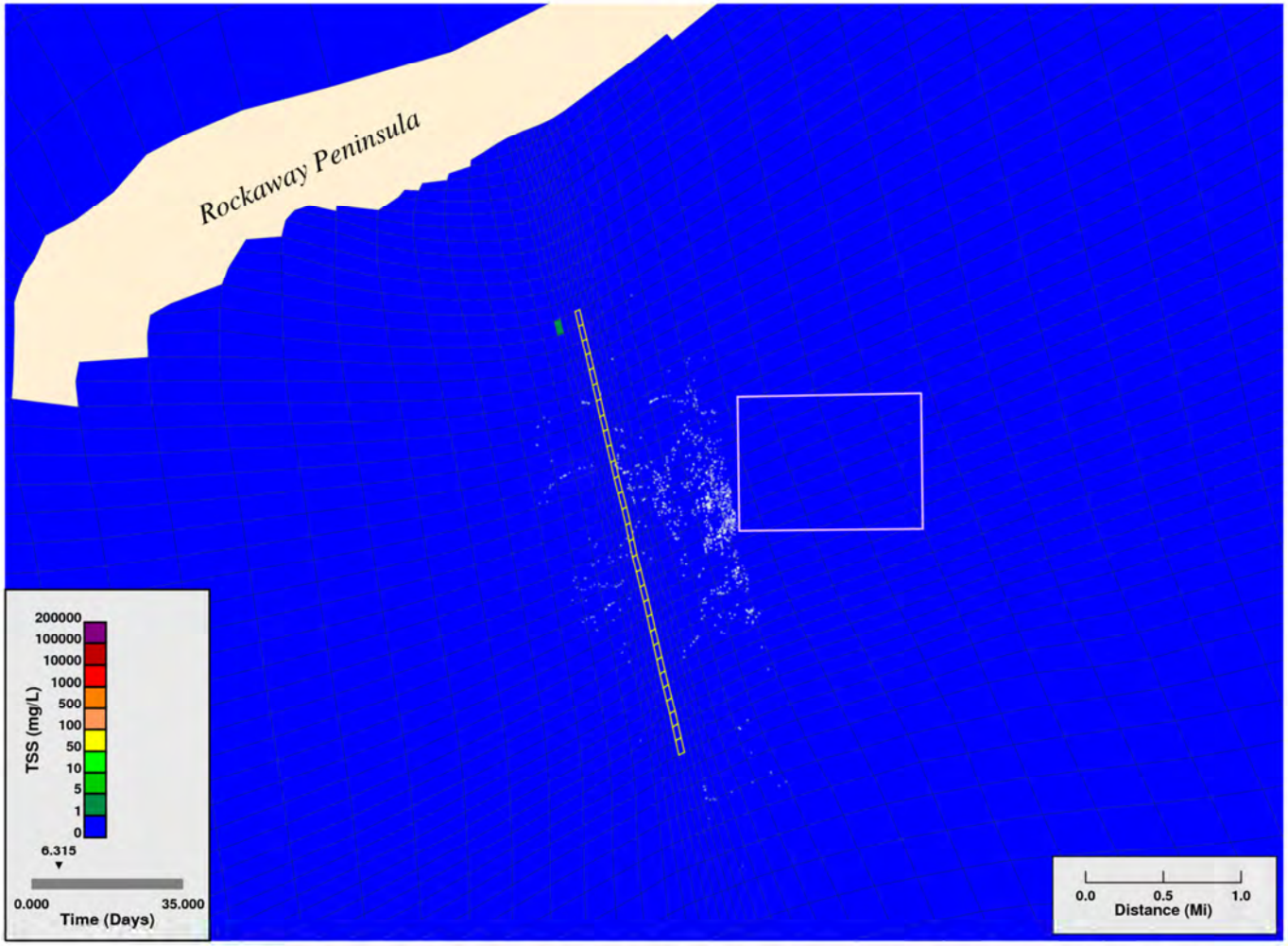

Figure H4. Pit dredging: simulated suspended solids near water column surface, dredging 75% complete.

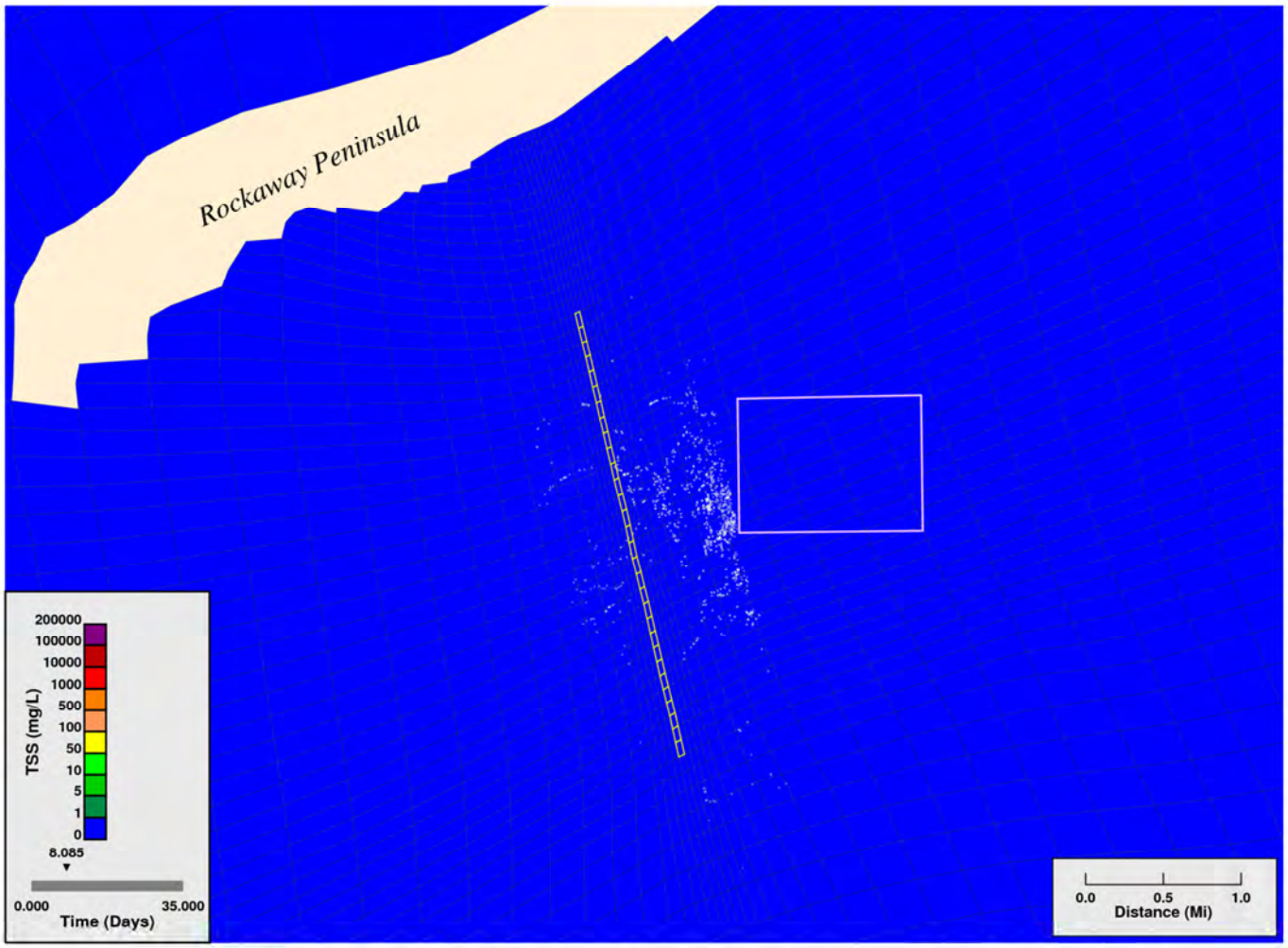

Figure H5. Pit dredging: simulated suspended solids near water column surface, end of dredging.

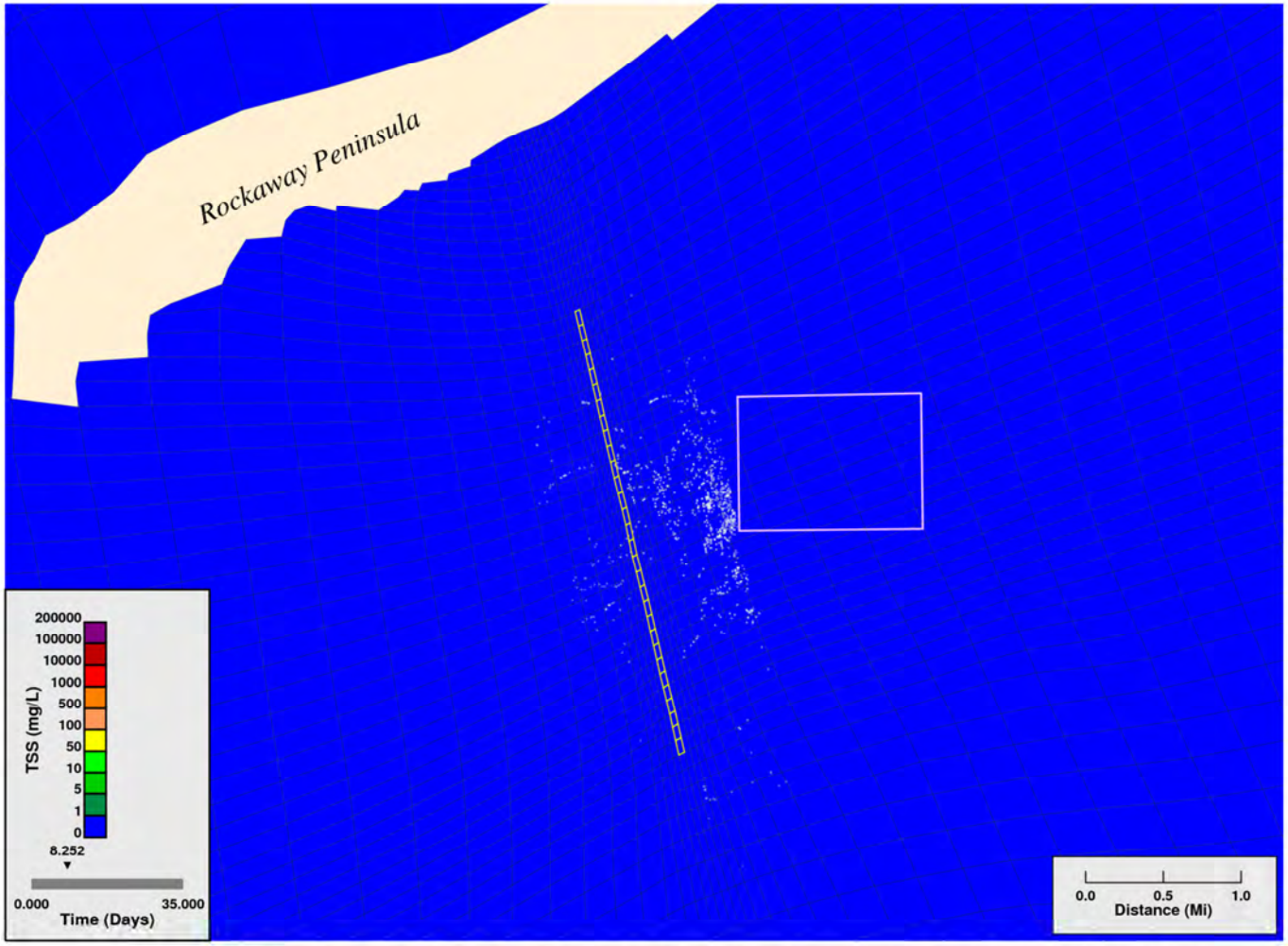

Figure H6. Pit dredging: simulated suspended solids near water column surface, 4 hours after end of dredging.